CENTRO INTERNACIONAL DE ESTUDOS
DE DOUTORAMENTO E AVANZADOS
DA USC (CIEDUS)

TESE DE DOUTORAMENTO

LONG TIME DYNAMICS OF RESONANT SYSTEMS

Anxo Fariña Biasi

ESCOLA DE DOUTORAMENTO INTERNACIONAL

PROGRAMA DE DOUTORAMENTO EN FÍSICA NUCLEAR Y DE PARTÍCULAS

SANTIAGO DE COMPOSTELA

2019

USC
UNIVERSIDADE
DE SANTIAGO
DE COMPOSTELA

DECLARACIÓN DEL AUTOR DE LA TESIS

Long Time Dynamics of Resonant Systems

D. Anxo Fariña Biasi

Presento mi tesis, siguiendo el procedimiento adecuado al Reglamento, y declaro que:

1) *La tesis abarca los resultados de la elaboración de mi trabajo.*
2) *En su caso, en la tesis se hace referencia a las colaboraciones que tuvo este trabajo.*
3) *La tesis es la versión definitiva presentada para su defensa y coincide con la versión enviada en formato electrónico.*
4) *Confirmo que la tesis no incurre en ningún tipo de plagio de otros autores ni de trabajos presentados por mí para la obtención de otros títulos.*

En Santiago de Compostela, 20 de mayo de 2019

Fdo. Anxo Fariña Biasi

USC
UNIVERSIDADE
DE SANTIAGO
DE COMPOSTELA

AUTORIZACIÓN DEL DIRECTOR / TUTOR DE LA TESIS

Long Time Dynamics of Resonant Systems

D. Javier Mas Solé

INFORMA:

Que la presente tesis, corresponde con el trabajo realizado por D. Anxo Fariña Biasi, bajo mi dirección, y autorizo su presentación, considerando que reúne los requisitos exigidos en el Reglamento de Estudios de Doctorado de la USC, y que como director de ésta no incurre en las causas de abstención establecidas en Ley 40/2015.

En Santiago de Compostela, 20 de mayo de 2019

Fdo. Javier Mas Solé

USC
UNIVERSIDADE
DE SANTIAGO
DE COMPOSTELA

"No hay viento favorable para quién no sabe a dónde se dirige."

Lucius Annaeus Seneca

"If I have seen further than others, it is by standing upon the shoulders of giants."

Isaac Newton

"It's not that I'm so smart, it's just that I stay with problems longer."

Albert Einstein

"You can't put a limit on anything. The more you dream, the farther you get."

Michael Phelps

"No es talento, es trabajo."

USC
UNIVERSIDADE
DE SANTIAGO
DE COMPOSTELA

Agradecimientos

Esta tesis no habría sido posible sin el constante apoyo de un gran número de personas. Por ello quiero dedicarles un breve homenaje.

Quiero empezar por agradecer a todas las personas que han hecho posible la formación del programa de "Ayudas para Contratos Predoctorales para la Formación de Doctores 2015" del Ministerio de Educación Cultura y Deporte, el cual ha financiado el desarrollo de esta tesis a través del proyecto FPA2014-52218-P.

También debo agradecer el trabajo realizado por las personas que están detrás del Centro de Supercomputación de Galicia (CESGA). Esta tesis se ha visto beneficiada de los servicios que ofrece.

En el ámbito académico-personal, quiero agradecer la ayuda de mi director, Javier Mas, quien me ha guiado a lo largo de esta etapa de mi carrera profesional. También quiero agradecer a Piotr Bizoń, Oleg Evnin, Ben Craps, Alexandre Serantes, Ángel Paredes, Daniele Musso, Pablo Carracedo, José Edelstein, Alfonso Vázquez y Andrzej Rostworowski, las discusiones que hemos tenido; las cuales han sido fundamentales para el desarrollo de este trabajo. Debo mencionar también a mis compañeros de doctorado: Jose, Fran, Víctor, Alejandro, Ana, David y Pedro. También quiero agradecer los consejos de Henlo y Brandon a la hora de pulir ciertos detalles de la tesis.

Entrando ya en lo personal, quiero mencionar al grupo de "Fourrrrrrier": Dani, Ana y Paloma, con quienes compartí cuatro intensos años de carrera. Con Dani he vivido prácticamente toda mi formación, desde la más elemental, hasta que tomamos especialidades distintas en el máster. Le deseo una exitosa carrera investigadora. Ana, la abeja reina del grupo, le deseo una próspera carrera de radiofísica.

En lo profundamente personal está Paloma, la persona que más de cerca ha vivido conmigo mi etapa como doctorando. Hemos compartido el inicio de nuestras carreras profesionales y ha soportado alegrías, victorias, frustraciones, tristezas y fracasos. Sin duda alguna siempre que lo he necesitado me ha ayudado, apoyado y aconsejado. Incluso debo mencionar que su ayuda ha sido fundamental en la edición de la tesis.

Finalmente, las personas más importantes, mis padres y mi hermano. A pesar de venir de familias completamente humildes, mis padres han trabajado duramente para que no nos faltase de nada; incluso ahora, cuando podemos valernos por nosotros mismos siguen haciéndonos saber que siempre van a estar apoyándonos. Con mi hermano he compartido más de 26 años, probablemente ha sido la persona que más ha influido en mi desarrollo. Al ser yo el pequeño, él ha marcado el rumbo hasta hace pocos años.

USC
UNIVERSIDADE
DE SANTIAGO
DE COMPOSTELA

Abstract

This thesis studies the long-time dynamics of resonant systems. In particular, we focus our effort on the weakly nonlinear limit models. The thesis is divided in two main branches. In the first part we study the long-time evolution of conservative systems; namely, models with conserved quantities associated with the energy, number of particles, angular momentum, etc. For this purpose, we construct an effective equation that captures the behavior of this kind of systems at long-timescales. We consider this equation with a high degree of generality as our starting point. Specifically, we will construct families of systems that admit an analytic resolution of this equation, as well as, a particular limit where we can extract useful information from the system. Once we develop the general tools, we will apply them to a large number of resonant models. Among them, we can find the Gross-Pitaevskii equation and nonlinear wave equations in anti-de Sitter spacetime.

In the second part of this thesis, we consider asymptotically anti-de Sitter geometries subject to time-periodic boundary conditions. Specifically we study two models, a scalar field in anti-de Sitter in global coordinates and purely gravitational fluctuations of the anti-de Sitter soliton. For both models time-periodic geometries perfectly synchronized with the boundary conditions will be constructed. We will also construct the phase-space of these objects, delimiting the regions of linear stability and thereafter the end states of the present instabilities will be inspected. We will find that in addition to the collapse into a black hole, there are other end states which remain regular with a long-time modulation. After that, we will show that the time-periodic geometries can be dynamically constructed from the static geometry by quenching the boundary conditions.

USC
UNIVERSIDADE
DE SANTIAGO
DE COMPOSTELA

Resumen

Esta tesis estudia la dinámica a largo tiempo de sistemas resonantes. En particular, nos hemos centrado en el límite de no linealidades débiles. La tesis está dividida en dos partes principales. En la primera parte estudiamos la evolución a largo tiempo de sistemas conservativos; es decir, modelos que presentan cargas conservadas como la energía, el número de partículas, el momento angular,... Para ello consideraremos una ecuación efectiva que captura el comportamiento del sistema a grandes escalas de tiempo. Tomaremos como punto de partida esta ecuación, manteniendo un alto grado de generalidad. Específicamente, vamos a construir familias de sistemas que admiten una resolución analítica de esta ecuación, al igual que exploraremos un límite que permitirá extraer información del sistema. Una vez hayamos desarrollado las herramientas generales, las aplicaremos a un gran número de modelos específicos. Entre ellos encontraremos la ecuación no lineal de Schrödinger u ondas no lineales sobre el espacio-tiempo de anti-de Sitter.

En la segunda parte de esta tesis, vamos a considerar geometrías asintóticamente anti-de Sitter sujetas a condiciones de frontera periódicas. Concretamente, vamos a estudiar dos modelos: un campo escalar en anti-de Sitter en coordenadas globales y fluctuaciones puramente gravitatorias del solitón de anti-de Sitter. En ambos casos construiremos geometrías que se encuentren perfectamente sincronizadas con la condiciones de frontera. También obtendremos el espacio de fases de estos objetos, delimitaremos las regiones de estabilidad lineal y estudiaremos los estados finales de las inestabilidades presentes. Veremos que a mayores del colapso a un agujero negro, existen otros posibles estados finales que desarrollan modulaciones a largo tiempo y permanecen regulares. Tras esto veremos que las geometrías periódicas en tiempo pueden ser construidas de forma dinámica partiendo de una geometría estática por medio de *quenches*.

USC
UNIVERSIDADE
DE SANTIAGO
DE COMPOSTELA

Resumo

Esta tese estuda a dinámica a longo tempo de sistemas resoantes. En particular, centrámonos no límite de non linearidades febles. A tese está dividida en dous partes principais. Na primeira parte estudamos a evolución a longo prazo de sistemas conservativos; é dicir, modelos que presentan cargas conservadas como a enerxía, o número de partículas, o momento angular,... Para iso, consideraremos unha ecuación efectiva que captura o comportamento do sistema a grandes escalas de tempo. Tomaremos como punto de partida esta ecuación, mantendo un alto grao de xeneralidade. Especificamente, imos construír familias de sistemas que admiten unha resolución analítica desta ecuación, ao igual que exploraremos un límite que permitirá extraer información do sistema. Unha vez desenroladas as ferramentas xerais, imos aplicalas a un gran número de modelos específicos. Entre eles encontraremos a ecuación non linear de Schrödinger ou ondas non lineais sobre o espazo-tempo de anti-de Sitter.

Na segunda parte desta tese, imos considerar xeometrías asintoticamente anti-de Sitter suxeitas a condicións de fronteira periódicas. Concretamente, imos estudar dous modelos: un campo escalar en anti-de Sitter en coordenadas globais e flutuacións puramente gravicionais do solitón de anti-de sitter. En ambos os casos construiremos xeometrías que estean perfectamente sincronizadas coas condicións de fronteira. Tamén obteremos o espazo de fases destes obxectos, delimitaremos as rexións de estabilidade lineal e estudaremos os estados finais das inestabilidades presentes. Veremos que a maiores do colapso a un buraco negro, existen outros posíbeis estados finais que desenrolan modulacións a longo prazo e permanecen regulares. Tras isto veremos que as xeometrías periódicas en tempo poden ser construídas de forma dinámica partindo dunha xeometría estática por medio de *quenches*.

USC
UNIVERSIDADE
DE SANTIAGO
DE COMPOSTELA

Contents

1

Introduction and Motivation

This thesis deals with the study of the weakly nonlinear regime of dynamical systems. The main focus will be set on nonlinear systems which, in the linearized approximation, exhibit a resonant spectrum. In this limit, this subclass of models provides an exciting framework where the nonlinearities do not have relevant contributions at short-timescales while they trigger nontrivial effects over long-timescales. Elucidating the long-time behavior of such systems, and illustrating our findings with particular models, will be the aim of this work.

This topic is extensive with multidisciplinary applications. It includes water waves [1], atmospheric and ocean dynamics [2, 3], solar winds [4], Bose-Einstein condensates [5], spacetimes [6], and many other physical systems (see [7] and references therein). Therefore, there are many ways to motivate the study of resonant systems. Here we will describe the particular motivation that ignited our curiosity and interest to write this thesis. The initial sparks were the Minkowski and anti-de Sitter (AdS) stability problems.

The issue of the stability of Minkowski spacetime in the presence of matter against the formation of a black hole was addressed in [8–15]. Specifically, in [8] Christodoulou proved that, if the matter consists of a free spherically symmetric massless scalar field, for small enough initial data it disperses to infinity remaining regular at any time. In contrast, in [11] Christodoulou also proved for the same model that for large initial data the scalar field collapses to form a black hole. Meanwhile, in [13] Choptuik numerically studied initial conditions placed in the neighborhood of the threshold between black hole formation and dispersion to infinity, finding critical phenomena. Finally, in [14] the collaboration between Christodoulou and Klainerman confirmed the nonlinear stability of Minkowski space under pure gravitational fluctuations.

After the issue of the nonlinear stability of Minkowski spacetime was settled, the spotlight

was focused on AdS. It was strongly motivated by the celebrated AdS/CFT (anti-de Sitter/Conformal Field Theory) correspondence proposed by Maldacena [16]. These studies were initiated in [17], again using a scalar field as the matter content. Nevertheless, the efforts were orientated toward critical phenomena around the threshold for black hole formation [17–22]. Surprisingly, it was not until several years later with the appearance of [6] by Bizoń and Rostworowski and later [23], that the question of stability of AdS spacetime was directly addressed (see [24] for a brief review). To the best of our knowledge [25] is the only exception. In [6, 23] it was conjectured that for reflective boundary conditions, despite AdS being linearly stable, it is nonlinearly unstable. For a family of initial data of amplitude ϵ, collapse would always occur in a timescale of order $1/\epsilon^2$. This discovery boosted the interest of part of the community which started to explore the deep mechanisms and consequence of this conjecture [26–60]. We must remark the main results achieved in this direction. Despite the conjecture about the instability of AdS, in [6] it was suggested that there may exist initial configurations for which the evolution remains regular, and in [26, 27] this possibility was considered in the case of purely gravitational fluctuations of AdS. After some work, families of initial conditions that evaded the instability conjecture were constructed in [28–33]. In consequence, the picture that started to shape was one where, in the space of initial conditions, there were portions where collapse was inevitable, but also "islands of stability". Since the initial work of B&R, it was clear that the full resonance of the linearized approximation played a relevant role in the conjectured instability. The advent of non-collapsing solutions demanded a refined perturbative analysis. A step forward was achieved with the introduction of the resonant system (also called Two-Time Framework or flow equations) in [34] and its development in [35, 36]. This approximation of the AdS dynamics accurately describes the slow weakly nonlinear transfer of energy between linearized modes and allows for access of the dynamics at times of order $1/\epsilon^2$ in the limit of $\epsilon \ll 1$, namely, the scale at which the black hole appears. It also provided surprises as selection rules prohibiting certain interaction channels between the linearized modes [35–38], extra conservation laws [36,39,40], dual energy cascades [40], Fermi-Pasta-Ulam-Tsingou (FPUT)-like returns of energy configurations [34] (see [61] for the original presentation of the FPUT paradox and [62] for a review), and strong numerical evidence for turbulence within the resonant system [41] (for a review, see [42]). While the bulk of these considerations have focused on the case of spherically symmetric perturbations of gravity-scalar field systems, extensions to pure gravity within squashed sphere ansatz [43] and more general perturbations outside spherical symmetry have also appeared [26, 44, 45]. Despite this incredible effort, there is not a general proof of the nonlinear instability of AdS. The only rigorous achievement for the moment consists of the Einstein-Null dust system with negative cosmological constant under the assumption of spherical symmetry [46, 47].

After this brief review of the current situation of Minkowski and AdS stabilities we must address the question: *Why are they so different?* The main difference between these two spaces consists in the existence of an effective boundary in AdS. In this situation the spatial infinity can be reached in a finite time meanwhile in Minkowski it is not possible. *Why is it a crucial difference?* As we mentioned above, the proof of the stability of Minkowski was based on the fact that perturbations generated by nonlinearities are dispersed to in-

finity; thereby they cannot be accumulated and produce a significant effect. On the other hand, in AdS the nonlinear effects are dispersed to the spatial infinity, once they reach the boundary (under appropriate boundary conditions) they are bounced, having a second opportunity to interact again. Therefore, although the nonlinear effects are initially minimal they cannot be dispersed. It produces an accumulation of small perturbations after each repetition of this mechanism, producing a significant impact if this process occurs sufficient times. Of course, this argument does not explain the gravitational collapse by itself, due to the fact that nonlinearities could be too weak to produce a divergence. A second ingredient in this issue consists of the fully resonant linearized spectrum of AdS. Even when the nonlinearities are ridiculously small, resonances provide a direct channel of interaction between modes. The fully resonant spectrum means that all modes resonate with each other producing a highly dense net of interactions in which each mode exchanges energy with all the others. The boundary and the fully resonant spectrum formed the strongest arguments in favour of the instability of AdS. Nevertheless, it is curious that the only rigorous proof we possess for a particular setup did not require making use of resonances between linear modes.

In consequence, this drastic difference between dynamical properties of Minkowski and AdS spacetimes, presumably linked to the spatial confinement and the fully resonant spectrum, was part of our motivation to explore resonant partial differential equations (PDEs), a possibility that has not gone unnoticed [63–81]. The second part of our motivation was originated by the fact that resonant equations for different systems have the same structure (assuming that they have the same resonant channel). The only difference is contained in the numerical values of couplings between modes. Due to this fact, we were interested in omitting the origin of the resonant system to study it in a general form. The procedure consisted of imposing restrictions on the structure of the interaction coefficients to extract information of validity for large classes of resonant systems.

All the discussion in relation to the stability of AdS was based on reflective boundary conditions. They isolate the system and therefore the amount of energy inside the space remains constant. Nevertheless, due to the surprises AdS was hiding, it is also interesting to explore new possibilities, for example, allowing the exchange of energy through the boundary. It can be achieved imposing time-dependent boundary conditions. Particularly, we will study time-periodic conditions consisting of a harmonic function. This choice is suitable for our interests, it prevents long-time effects coming from the boundary, leaving them for the dynamics in the bulk. Another salient property consists of the existence of time-periodic solutions (TPSs) synchronized with the boundary, they will be the central objects of our study, allowing the incursion into the nonlinear regime and its exploration. A different kind of boundary conditions was considered in [82].

Motivated by the AdS/CFT conjecture, we will consider models for this part of our study with a clear interpretation through this correspondence. It maps equilibration processes onto the dynamical evolution of a dual gravitational system (see [83] for an excellent review and [84] for more in-depth details). The holographic dictionary defines the sources of the field theory in terms of asymptotic modes of the bulk fields. Therefore, we will use this fact to control these sources through the boundary conditions, having on the

QFT side a driven system. They are isolated systems excited by an external source which is under control. As we already mentioned, in our case the boundary conditions will be time-periodic, leading our study to the realm of (holographic) periodically driven systems.

A periodic drive is one of the simplest, yet most fascinating, ways of taking a many-body quantum system out of equilibrium. The discrete time-translational invariance retained by the drive is inhered by the Hamiltonian: $H(t+T) = H(t)$ making that, observed at stroboscopic times (frames $t = nT$, $n \in \mathbb{N}$), the dynamics seems to be static. This topic, which goes under the name of Floquet engineering, has been under intense scrutiny in recent years (see [85–88] for reviews). At the same time, fundamental questions regarding the late-time behavior of periodically driven many-body quantum systems have also been thoroughly studied [89–91]. This kind of systems provide interesting phenomenology such as: synchronisation [92], modification of the band structure (e.g. *Topological insulators* [93]) or counter-intuitive effects such as the stabilisation of unstable equilibrium points of the phase-space [94–96] or time crystals [97, 98]. The most illustrative example in this context is the Kapitza's pendulum [94, 95].

At the QFT level, less is known in comparison, although remarkable results have been obtained in scalar field theories with O(N) symmetry at large N [99, 100]. Holography provides an interesting starting point to increase our knowledge about periodically driven QFTs, a possibility that has not gone unnoticed [101–108] (to the best of our knowledge [101] constitutes the first treatment of a holographic periodically driven system). These references were motivated by the study of systems driven out of equilibrium. The majority of them tried to observe how it affects the essential features of relevant systems. For example, in [101–103] holographic superconductors were considered, therein the phase diagrams were constructed, and the dependence of the superconducting transition temperature with the parameters of the drive was studied. Meanwhile in [104] the authors checked if the properties of a holographic Weyl semimetal are preserved or destroyed under the action of a rotating electric field. Using a similar setup [106] studies how the phase diagram strongly depends on the amplitude and frequency of the electric field; the system behaves as an insulator or a conductor for certain combinations of these values. On the other hand, the models of [105, 107] are less sophisticated than the previous ones. They consist of a scalar field in an asymptotically-AdS geometry. Nevertheless, they take advantage of this fact to consider more complicated nonlinear effects. In [101–104, 106, 108] the backreaction of the metrics was not considered, only the probe limits were studied. In contrast, in [105] the first contribution for the backreaction was computed and in [107] the full effects were taken into account. A constant in all these studies is the fact that the states are thermal from the beginning due to the geometries have a horizon and therefore the system has a temperature. This fact radically differentiates us from the other studies of periodically driven holographic systems. In our case, the initial geometries will not contain a horizon and the backreaction of the metric will be considered. If the dynamics leads the initial conditions to a gravitational collapse is an interesting question for our setups.

This thesis is organized as follows. The content in chapter 2 is of purely mathematical style. It tries to condense the common formal structures and properties that are shared by

the particular examples to be addressed later. It contains technical details which require a significant effort to be properly assimilated and they could deviate the attention from the main results of this thesis, which are contained in chapters 3 and 4. The reader can safely chose to skip this chapter in a first reading, and look back for rigorous results when necessary. In chapter 3, we explore resonant models. Particularly, we shall focus on their weakly nonlinear limit where the resonant system can be derived. It will be studied in a general form, and we will see that after imposing certain constraints, we obtain large families of resonant systems admitting an analytic treatment. After the presentation of these results, we will display specific models with a resonant system which can be studied through the techniques we have developed. In chapter 4, motivated by holography, we restrict our study of bounded systems to only asymptotically-AdS solutions of Einstein's equations. We impose boundary conditions which allow the exchange of energy through the boundary. Specifically, we shall consider two models subject to time-periodic conditions: a free spherically symmetric massless scalar field in AdS and pure gravitational fluctuations of the AdS-soliton. Chapter 5 contains a global view and discussion of the results presented in this thesis. In particular, there is a section dedicated to future extensions of the content of this thesis. After the summary and outlook, a number of technical resultas have been relegated to the Appendices.

USC
UNIVERSIDADE
DE SANTIAGO
DE COMPOSTELA

2

Background, Methods and Techniques

2.1 Structure of the Problem

Our main goal consists in improving our understanding of the weakly nonlinear limit of systems displaying a fully resonant linearized spectrum on bounded domains (these concepts will be introduced through this section). Therefore, we will avoid excessively elaborated models, which could blur our analysis by complicating the isolation of effects associated with the properties we want to study. In consequence, the typical models we are going to consider in this thesis consists of a scalar field in different geometries, although systems as the Nonlinear Schrödinger equation (NLSE) or the cubic Szegö equation will also be considered.

We are mainly interested in systems which can be reduced to the form:

$$u_{tt}(t,x) - \mathcal{L}u(t,x) = \epsilon\, \mathcal{F}_N\left[u(t,x),\epsilon\right], \qquad \mathcal{L} = \frac{1}{\mu(x)}\partial_x\left(p(x)\partial_x\right) + q(x), \tag{2.1.1}$$

in the weakly nonlinear limit; namely, $\epsilon\|\mathcal{F}_N\| \ll \|u\|, \|u_{tt}\|, \|\mathcal{L}u\|$, with $\|\ \|$ denoting the appropriate norm. The domain is $(t,x) \in \mathbb{R}\times[x_i,x_f]$, $\mu(x), p(x) > 0$ and $\mu(x), p(x), p'(x), q(x)$ are smooth functions on (x_i,x_f), ϵ is the coupling of the nonlinearities and $\mathcal{F}_N$ is a polynomial in $u(t,x)$ and its derivatives, where the lowest order of the nonlinearities is N and the coefficients are functions of x[1]. We also establish that in this regime $\mathcal{F}_N$ can be

[1] In some situations $\mathcal{F}_N$ also contains integrals of some of its terms.

expanded as

$$\mathcal{F}_N\left[u(t,x),\epsilon\right]=\sum_{n=0}^{\infty}\epsilon^n\mathcal{F}^{(N+n)}\left[u(t,x)\right], \tag{2.1.2}$$

where $\mathcal{F}^{(k)}\left[u(t,x)\right]$ are nonlinear terms of order k.

The weakly nonlinear regime can be achieved by using the different scaling between the linear and nonlinear terms in relation to the amplitude of the solution, $\|u\|$. In consequence, we can relate ϵ with this amplitude by performing the rescaling $u\to\epsilon^{1/N}u$ and taking ϵ small enough to guarantee that in this regime the original system is suitable reduced to (2.1.1). Nevertheless, for particular physical systems the weakly nonlinear limit can be engineered by external methods. An example is the NLSE in the context of Bose-Einstein condensates (BEC). As we will briefly comment in section 3.3.2, in this case the couplings of the nonlinear terms depend on the strength of interactions between atoms, which can be reduced using special experimental protocols (Feshbach resonance [109]). Hence, respecting the range of validity of these protocols, we can directly consider the weakly nonlinear regime identifying ϵ with this quantity.

As we will see in section 2.2, the utility of this approximation is based on the fact that the *reduced equation*,

$$u_{0,tt}(t,x)-\mathcal{L}u_0(t,x)=0, \tag{2.1.3}$$

is simpler than the nonlinear equation. In many situations, solutions $u_0(t,x)$ can be obtained analytically, providing a starting point to extend these solutions to the nonlinear regime. Equation (2.1.3) can be solved by the standard method of separation of variables, leading to the Sturm-Liouville problem

$$\omega^2\psi(x)+\mathcal{L}\psi(x)=0, \tag{2.1.4}$$

where ω^2 is the eigenvalue associated with the eigenfunction ψ. We will refer to the full set of $\{\omega_n\}$ as the linearized spectrum[2] of (2.1.1).

In this thesis we will restrict our study to Sturm-Liouville operators $\mathcal{L}$ which, under appropriate boundary conditions, the spectrum is real $\omega_n\in\mathbb{R}\ \forall n\in\mathbb{N}$, property that will be assumed from now on. This condition is required to guarantee the linear stability of (2.1.1). Thereby the growth of u_0 is bounded and the weakly nonlinear regime is preserved at short-time scales; only at long times, nonlinear effects may show important effects. In chapter 3 the boundary conditions will be such that the operator $\mathcal{L}$ is self-adjoint on $L^2\left([x_i,x_f],\mu(x)dx\right)$, with $\mu(x)$ given in (2.1.1). Therefore, the inner product of this Hilbert space is give by

$$\langle f,g\rangle=\int_{x_i}^{x_f}ds\mu(s)f(s)g(s), \tag{2.1.5}$$

and the set of eigenfunctions $\{\psi_n(x)\}$ forms an orthogonal basis

$$\langle\psi_n,\psi_m\rangle=N_{n,m}\delta_{n,m}. \tag{2.1.6}$$

[2]On occasions we will omit "linearized".

Therefore, we can normalize the eigenfunctions as $e_n = \psi_n/\sqrt{N_{nn}}$ to obtain a orthonormal basis $\{e_n(x)\}$ that we will denominated *eigenbasis*. Hence, the solution of (2.1.3) is written in terms of a linear combination of these modes,

$$u_0(t,x) = \sum_{n=0}^{\infty} \left(\alpha_n e^{i\omega_n t} + \beta_n e^{-i\omega_n t}\right) e_n(x), \tag{2.1.7}$$

with $\alpha_n, \beta_n \in \mathbb{C}$. On the other hand, in chapter 4 we will consider boundary conditions which provide, in addition to these normalizable modes, a non-normalizable mode ($\langle h_0, h_0\rangle$ being unbounded) denoted by $h_0(x)$. When this mode is present in the problem we will denote its eigenvalue by ω_0 and the spectrum of normalizable modes by $\{\Omega_n\}$. On this occasion, solutions of the reduced equation becomes

$$u_0(t,x) = \left(\tilde{\alpha} e^{i\omega_0 t} + \tilde{\beta} e^{-i\omega_0 t}\right) h_0(x) + \sum_{n=0}^{\infty} \left(\alpha_n e^{i\Omega_n t} + \beta_n e^{-i\Omega_n t}\right) e_n(x), \tag{2.1.8}$$

with $\tilde{\alpha}, \tilde{\beta}, \alpha_n, \beta_n \in \mathbb{C}$.

At the nonlinear level, for infinitesimally small values of the coupling ϵ in (2.1.1), we expect the nonlinear terms to be sub-dominant at least at times of order $t \sim 1/\epsilon$. For certain classes of spectra the nonlinear effects become relevant at this timescale. We will explain in section 2.2 methods to take into account these effects, which are consequence of a *fully resonant spectrum*. It is characterized by the fact that it provides solutions to the following relations [110],

$$\sum_{n=0}^{\infty} a_n \omega_n = 0, \quad \sum_{n=0}^{\infty} a_n^2 \neq 0, \qquad \text{with} \quad a_n \in \mathbb{Z}. \tag{2.1.9}$$

Each set of $\{a_n\}$ satisfying these relations is denominated *resonant channel*. In particular, if $\omega_n \in \mathbb{Q}\ \forall n$, there are integer numbers a_n which satisfy the condition.

We will see in section 2.2 that for our nonlinear problem (2.1.1), the only relevant resonant channels have the form

$$\pm\,\omega_{n_1} \pm \omega_{n_2} \pm \ldots \pm \omega_{n_{N+1}} = 0, \tag{2.1.10}$$

where N is identified with the lowest order of nonlinear terms, $\mathcal{F}_N$. We will show in chapter 3, that indeed, a number of important results can be obtained for a generic system whose resonance condition is like this.

In order to satisfy (2.1.10) we are particularly interested in systems with a spectrum of the form

$$\omega_n = an + b, \qquad a, b \in \mathbb{R}^+, \tag{2.1.11}$$

as well as in odd powers of nonlinear terms. Note the relevance of working with odd powers; under these assumptions there is always a resonant channel like (2.1.10) independently of a, b. It consists of the same number of positive and negative signs. In this specific channel the constant term vanishes and a is factored out, therefore, (2.1.10) is

reduced tho the same expression substituting $\omega_{n_i} \to n_i$. Following this argument, additional channels are present only for special values of a, b, which we will discuss in section 2.2. In particular, in this thesis we are going to focus on the most common situation, cubic nonlinearities ($N = 3$).

2.2 Perturbative Methods

In this section we are going to summarize the perturbation methods required in this thesis. The behavior of several physical systems is characterized by a dominant motion which is slightly altered under the presence of small disturbances. Typically, this kind of systems can be studied through standard perturbative techniques, which add small corrections to the main motion. Nevertheless, in some situations, although the disturbances are extremely small they have a cumulative effect. It means that after enough time they have a contribution which could drastically modify the behavior of the system, which is not suitably captured by naive perturbative techniques.

We are going to present two illustrative examples. They have analytic solutions allowing a direct comparison with perturbative solutions. The first example belongs to the context of periodic solutions:

$$\frac{d^2y}{dt^2}(t) + (1+\epsilon)^2 y(t) = 0, \quad y(0) = 1, \quad \frac{dy}{dt}(0) = 0, \tag{2.2.1}$$

where $\alpha, \epsilon \in \mathbb{R}$. This equation has an analytic solution of the form

$$y(t) = \cos((1+\epsilon)t), \tag{2.2.2}$$

which it is clearly $2\pi/(1+\epsilon)$-periodic. We can expand the solution in powers of ϵ as

$$y(t) = \sum_{n=0}^{\infty} \epsilon^n y_n(t). \tag{2.2.3}$$

Assuming that $0 < \epsilon \ll 1$ and $y_n(t)$ remain bounded, equation (2.2.1) is decoupled in powers of ϵ which lead to an iterative resolution order by order,

$$\frac{d^2y_0}{dt^2}(t) + y_0 = 0 \tag{2.2.4}$$

$$\frac{d^2y_1}{dt^2}(t) + y_1 = -2y_0 \tag{2.2.5}$$

$$\frac{d^2y_2}{dt^2}(t) + y_2 = -2y_1 - y_0 \tag{2.2.6}$$

This protocol leads to an approximated solution $\tilde{y}_N$ which is truncated at order N in ϵ. At second order it has the form

$$\tilde{y}_2 = \cos t - \epsilon t \sin t - \frac{1}{2}\epsilon^2 t^2 \cos t. \tag{2.2.7}$$

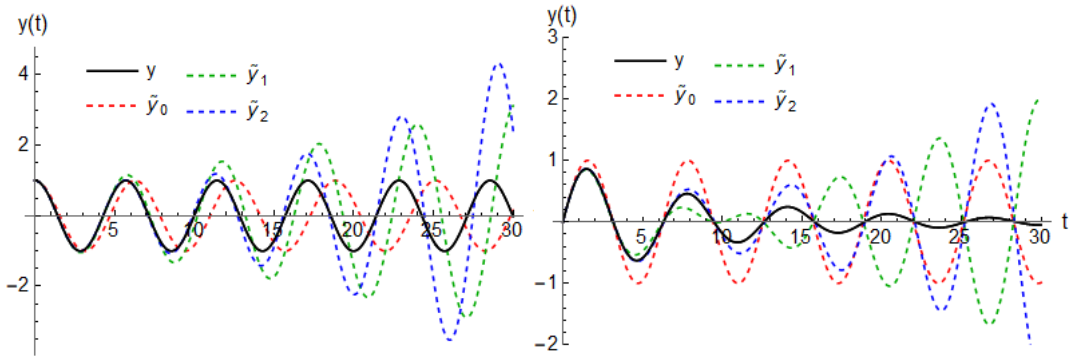

(a) $\ddot{y} + (1+\epsilon)^2 y = 0$ (b) $\ddot{y} + 2\epsilon\dot{y} + y = 0$

Figure 2.1: Analytic solutions and their perturbative expansions in powers of ϵ until order 2. For these examples we have used $\epsilon = 0.1$

We observe that $\tilde{y}_2$ is not a periodic solution, in contrast with the analytic solution (2.2.2). Nevertheless the problematic part comes from the presence of continuously growing terms $t\sin t$, $t^2\cos t$, which invalidate the assumptions that $y_n(t)$ are bounded and that equation (2.2.1) can be decoupled in powers of ϵ at times $t \sim 1/\epsilon$. These kind of terms are denominated *secular terms*. They are defined as terms which become unbounded as $t \to \infty$, and are consequence that the RHSs of (2.2.5) and (2.2.6) contain solutions of the homogeneous equation (2.2.4). Fig. 2.1 illustrates this discussion.

The second example consists of an equation where the solution evolves in two different scales of time: an oscillatory motion with a slowly decreasing amplitude (assuming $\epsilon \ll 1$). The equation has the form

$$\frac{d^2y}{dt^2}(t) + 2\epsilon\frac{dy}{dt}(t) + y = 0, \quad y(0) = 0, \quad \frac{dy}{dt}(0) = 1, \tag{2.2.8}$$

and the analytic solution is

$$y(t) = \frac{e^{-\epsilon t}}{\sqrt{1-\epsilon^2}}\sin\left(\sqrt{1-\epsilon^2}t\right). \tag{2.2.9}$$

Following the same procedure as in the previous example we obtain an approximated solution in powers of ϵ,

$$\tilde{y}_2 = \sin t - \epsilon t\sin t + \frac{1}{2}\epsilon^2\left(\sin t - t\cos t + t^2\sin t\right). \tag{2.2.10}$$

We observe that secular terms are also present in this example; but in addition to the ones coming from the oscillatory motion, there are also terms coming from the slow evolution in time of the amplitude. Fig. 2.1 shows as these perturbative expansions are not suitable at times $t \sim 1/\epsilon$.

From these examples we observe that secular terms are a consequence of the truncated expansion in powers of ϵ. There are sophisticated methods developed to avoid these

spurious terms, they do not completely expand the solution in powers of ϵ. Instead, they only expand specific parts of the dependence on ϵ. In the case of problems with solutions evolving at a single timescale the required protocol is the Poincaré-Lindstedt method. It will be briefly presented in the next subsection and used in section 2.3 to construct time-periodic solutions for our particular models of chapter 4. The two main methods which take into account evolutions at different timescales are the method of multi-scales and the method of averaging. These methods allow an extension of the validity of perturbative solutions in presence of different scales of time to $\mathcal{O}(1/\epsilon)$, and errors are estimated at times $\mathcal{O}(1/\epsilon^2)$. The versions of the methods we are going to present here approximate the exact solution of an ODE as

$$y(t) \sim y_0(t, \epsilon t) + \epsilon y_1(t, \epsilon t) + \epsilon^2 y_2(t, \epsilon t) + ... \tag{2.2.11}$$

The additional argument is introduced to denote that the expansion in powers of ϵ avoids terms with a dependence ϵt. The term $y_0(t, \epsilon t)$ is called *first approximation* due to the fact that it contains information of ϵ instead of the leading terms in standard perturbation methods which consists of the solution of the *reduced equation* ($\epsilon = 0$). In the next sections we are going to introduce basic ideas and the protocols to obtain the *first approximation* for both methods. This approximation properly describes the solution of the problem at times $\mathcal{O}(1/\epsilon)$; for this reason, remaining at this level will be enough for our future purposes. As we will see, the methods follow different philosophies, having crucial differences from the core. Nevertheless, despite this fact they report the same result for the *first approximation*, while beyond this correction they can differ.

2.2.1 Poincaré-Lindstedt Method

The Poincaré-Lindstedt method is a perturbative protocol focused on solutions with a single timescale; for example time-periodic solutions. We are going to introduce the basic ideas through the example of an oscillatory equation of the form

$$\frac{d^2y}{dt^2} + k^2 y = \epsilon f\left(t, y, \frac{dy}{dt}, \epsilon\right), \tag{2.2.12}$$

where f is either independent of t or periodic in t. Excellent and rigorous descriptions of the method can be found in [110, 111]. The explicit application to models of our interest can be found in section 2.3.

As we have already seen in the example (2.2.1), if the frequency of oscillations depends on ϵ, expanding the solution in powers of ϵ introduces secular terms which invalidate the perturbative approach at $t \sim 1/\epsilon$. For this reason, the key idea of the method consists of expanding independently the frequency and $y(t)$ omitting contributions from the frequency. This process can be understood as an arbitrary change of variable depending on ϵ, which will be determined imposing the condition that the solution must remain bounded (removing secular terms). This new variable is denominated *strained time* and has the form

$$t^+ = \nu(\epsilon)t. \tag{2.2.13}$$

Equation (2.2.12) in terms of this variable becomes

$$\nu(\epsilon)^2 \frac{d^2y}{(dt^+)^2} + k^2 y = \epsilon f\left(\frac{t^+}{\nu}, y, \nu\frac{dy}{dt^+}, \epsilon\right). \tag{2.2.14}$$

Now, we can expand the solution $y(t^+)$ in powers of ϵ

$$y(t^+) = \sum_{n=0}^{\infty} \epsilon^n y_n(t^+), \tag{2.2.15}$$

as well as

$$\nu(\epsilon) = \sum_{n=0}^{\infty} \epsilon^n \nu_n. \tag{2.2.16}$$

Taking $0 < \epsilon \ll 1$ we can decouple (2.2.14) in powers of ϵ

$$\frac{d^2y_0}{(dt^+)^2} + k^2 y_0 = 0, \tag{2.2.17}$$

$$\frac{d^2y_1}{(dt^+)^2} + k^2 y_1 = \epsilon f\left(t^+, y_0, \frac{dy_0}{dt^+}, \epsilon\right) - 2\nu_1 \frac{d^2y_0}{(dt^+)^2}, \tag{2.2.18}$$

where we have set $\nu_0 = 1$ and higher powers are obtained by following the same expansion. It is the moment to fix part of the freedoms introduced with the change of variable (2.2.13). Secular terms are consequence of the presence of solutions of the homogeneous equation on the RHS of (2.2.18); in consequence, we can adjust ν_1 to remove these terms, leaving a bounded solution. Following this process we observe that the determination of the coefficient ν_{k+1} requires the previous resolution of $\nu_1, \ldots, \nu_k$, $y_0(t^+), \ldots, y_k(t^+)$ and the equation for $y_{k+1}(t^+)$. Once these variables are introduced in the equation for $y_{k+1}(t^+)$ ν_{k+1} is determined by removing secular terms from the RHS.

On some occasions, the number of freedoms is not enough for the complete cancellation of secular terms. It can be produced by a failure in our supposition that solutions only evolve at a single timescale, and more sophisticated methods are required. An example of this situation is equation (2.2.8). If we use the strained time $t^+ = \sqrt{1-\epsilon^2}t$, we can observe that the solution (2.2.9) expanded in powers of ϵ as in (2.2.15) still contains secular terms. It is a consequence of cumulative effects which become relevant at long-timescales $t \sim 1/\epsilon$. To deal with this kind of problems we introduce the method of multi-scales and the averaging method in the next sections.

2.2.2 The Method of Multi-Scales

The method of multi-scales can be presented in multiple forms which can be found in [110, 111]. Through this thesis only one version will be presented and used. The key idea consists in decoupling two different timescales: t ("fast time" acting at a short-timescale) and $\tau = \epsilon t$ ("slow time" acting at a long-timescale), and using the introduced freedom to remove secular terms.

Allow us to introduce the method through an example, a second order ODE of the form:

$$y_{tt}(t) + k^2 y(t) = \epsilon f(y, y_t), \qquad y(0) = \alpha,\ y_t(0) = \beta. \tag{2.2.19}$$

As we said in the introduction, this method approaches the solution as

$$y(t) \sim y_0(t,\tau) + \epsilon y_1(t,\tau) + \epsilon^2 y_2(t,\tau) + ... \tag{2.2.20}$$

Due to the treatment of t and τ as independent variables, a freedom is introduced and must be compensated order by order to approach the solution of the problem. $y_0(t,\tau)$ cannot be completely determined until this freedom is removed through the explicit equation of $y_1(t,\tau)$. The same happens in subsequent orders, $y_n(t,\tau)$ is fully determined when the equation for $y_{n+1}(t,\tau)$ is explicitly written using the solutions $y_{0,\dots,n-1}$. The procedure consists of calculating the first and second derivatives of $y_n(t,\tau)$ using ϵt instead of τ, after that we rewrite any ϵt as the independent variable τ:

$$\frac{d}{dt} y_n(t,\tau) = \left(\frac{\partial}{\partial t} + \epsilon \frac{\partial}{\partial \tau}\right) y_n(t,\tau). \tag{2.2.21}$$

$$\frac{d^2}{dt^2} y_n(t,\tau) = \left(\frac{\partial^2}{\partial t^2} + \epsilon^2 \frac{\partial^2}{\partial \tau^2} + 2\epsilon \frac{\partial^2}{\partial t \partial \tau}\right) y_n(t,\tau). \tag{2.2.22}$$

Introducing these expressions in (2.2.19) and gathering the terms of the same order we obtain a system of equations for y_n. Remaining at first order it takes the form

$$y_{0,tt} + k^2 y_0 = 0 \qquad y_0(0,0) = \alpha,\ y_{0,t}(0,0) = \beta \tag{2.2.23}$$

$$y_{1,tt} + k^2 y_1 = f(y_0, y_{0,t}) - 2y_{0,t\tau} \qquad y_1(0,0) = 0,\ y_{1,t}(0,0) = -y_{0,\tau} \tag{2.2.24}$$

They are currently partial differential equations, therefore the solution of (2.2.23) is

$$y_0(t,\tau) = A(\tau)\cos(kt) + B(\tau)\sin(kt) \qquad A(0) = \alpha,\ B(0) = \beta/k. \tag{2.2.25}$$

The determination of $A(\tau)$ and $B(\tau)$ comes by imposing that the approach to the solution becomes uniformly valid in intervals of time $\mathcal{O}(1/\epsilon)$ (at least). This consideration requires that the series must be uniformly ordered ($\epsilon^n y_n \ll \epsilon^{n+1} y_{n+1}\ \forall n$) on this interval and the coefficients must be bounded. τ is bounded on this interval; in consequence, the so-called τ-secular terms are allowed while it is not the case of t-secular terms which must be eliminated. Substituting (2.2.25) in (2.2.24) we obtain

$$y_{1,tt} + k^2 y_1 = f\left(A(\tau)\cos(kt) + B(\tau)\sin(kt), -kA(\tau)\sin(kt) + kB(\tau)\cos(ky)\right)$$

$$+ 2kA'(\tau)\sin(kt) - 2kB'(\tau)\cos(kt). \tag{2.2.26}$$

As function f is $2\pi/k$-periodic in t, the RHS of this equation can be expanded in a Fourier series. Thereby y_1 will be free of t-secular terms if and only if the coefficients of $\sin(kt)$ and $\cos(kt)$ are zero. This condition leads to

$$\frac{dA}{d\tau} \equiv P(A,B) = \\ -\frac{k}{2\pi}\int_0^{2\pi/k} f\left(A(\tau)\cos(kt) + B(\tau)\sin(kt), -kA(\tau)\sin(kt) + kB(\tau)\cos(ky)\right)\sin(kt)dt \tag{2.2.27}$$

$$\frac{dB}{d\tau} \equiv Q(A,B) = \\ \frac{k}{2\pi}\int_0^{2\pi/k} f\left(A(\tau)\cos(kt) + B(\tau)\sin(kt), -kA(\tau)\sin(kt) + kB(\tau)\cos(ky)\right)\cos(kt)dt \tag{2.2.28}$$

After the integrations, $P(A,B)$ and $Q(A,B)$ become functions of A and B which can be determined by solving the equations (2.2.27)-(2.2.28). After that the *first approximation*, $y_0(t,\tau)$, is completely determined.

After the introduction of the basic ideas of the method through an example based on ODEs, the point of view will be focused on the kind of problems treated in this thesis chapter 3. Here we are going to show how to apply the method of multi-scales to a problem of the form (2.1.1). In particular, we will work with boundary conditions which restrict the linear modes of the problem to to normalizable modes with a real linearized spectrum $\{\omega_n\}$ of the form $\omega_n = an + b$ with $a, b \in \mathbb{R}^+$. In consequence, modes form the eigenbasis $\{e_n\}$ with inner product defined in (2.1.6).

To apply the method of multi-scales to (2.1.1), we have to consider first that the solution is approximated by

$$u(t,x) \approx u_0(t,\tau,x) + \epsilon u_1(t,\tau,x) + ... \tag{2.2.29}$$

where $\tau = \epsilon t$ is the "slow time". Following with the procedure $u_0(t,\tau,x)$, the *first approximation*, is the solution of the *reduced equation* (2.1.3) where the constants of integration are functions of the "slow time", τ. Hence

$$u_0(t,\tau,x) = \sum_{n=0}^{\infty} \alpha_n(\tau)e_n(x)e^{iw_n t}, \tag{2.2.30}$$

where $\alpha_n \in \mathbb{C}$. Note that we should have considered the full complex function

$$u(t,\tau,x) = \sum_{n=0}^{\infty} \left(\alpha_n(\tau)e^{iw_n t} + \beta_n(\tau)e^{-iw_n t}\right) e_n(x), \tag{2.2.31}$$

where $\alpha_n, \beta_n \in \mathbb{C}$, which also contains the particular case of a real function ($\beta_n = \bar{\alpha_n}$). Nevertheless, to clarify the process we have decided to set negative exponents to zero. Of course, it can be checked that it is a consistent truncation of the problem.

The following step consists of writing the equation for $u_1(t,\tau,x)$:

$$u_{1,tt}(t,\tau,x) - \mathcal{L}u_1(t,\tau,x) = \ \mathcal{F}_N\left[u_0(t,\tau,x),0\right] - 2u_{0,t\tau}(t,\tau,x). \tag{2.2.32}$$

At this point the freedom introduced when τ was decoupled from t is used to eliminate solution for the *reduced equation* on the RHS of (2.2.32) to prevent secular terms. This condition is satisfied if projections of the RHS on $\{e_n(x)e^{iw_nt}\}$ are zero. It leads to

$$iw_n\frac{d\alpha_n}{d\tau} = \frac{1}{2T}\int_0^T ds e^{-iw_ns}\left\langle e_n(x), \mathcal{F}_N\left[u_0(s,\tau,x),0\right]\right\rangle, \tag{2.2.33}$$

where $\langle\ ,\ \rangle$ is the inner product (2.1.6), and T is the common period of modes. Note that we are supposing a spectrum of the form $\omega_n = an+b$ with $a,b\in\mathbb{R}$; in consequence, the period of each mode is $T_n = 2\pi/(an+b)$. If $a,b\in\mathbb{Q}$ we can always find a period T for the full set of modes. Writing a,b as $a=a_1/a_2$ and $b=b_1/b_2$ with $a_1,a_2,b_1,b_2\in\mathbb{Z}$ we observe that the common period is $T = 2\pi a_2b_2$. If a_2,b_2 are large numbers, we only require taking a smaller ϵ such that the relation $T \ll 1/\epsilon$ is satisfied. The problem happens when $c = b/a \in \mathbb{I}$ such that T does not exists. In this case we can apply a "heuristic" approximation[3].

Specifically, we will treat cubic nonlinear terms which satisfy

$$\mathcal{F}_3\left[u_0(t,\tau,x),0\right] = \tag{2.2.34}$$

$$+\sum_{m=0}^{\infty}\sum_{k=0}^{\infty}\sum_{l=0}^{\infty}\mathcal{G}_1\left[e_m,e_k,e_k\right]\bar{\alpha}_m\alpha_k\alpha_l e^{i(\omega_k+\omega_l-\omega_m)t} + \sum_{m=0}^{\infty}\sum_{k=0}^{\infty}\sum_{l=0}^{\infty}\mathcal{G}_2\left[e_m,e_k,e_k\right]\bar{\alpha}_m\alpha_k\bar{\alpha}_l e^{i(\omega_k-\omega_l-\omega_m)t}$$

$$+\sum_{m=0}^{\infty}\sum_{k=0}^{\infty}\sum_{l=0}^{\infty}\mathcal{G}_3\left[e_m,e_k,e_k\right]\alpha_m\alpha_k\alpha_l e^{i(\omega_k+\omega_l+\omega_m)t} + \sum_{m=0}^{\infty}\sum_{k=0}^{\infty}\sum_{l=0}^{\infty}\mathcal{G}_4\left[e_m,e_k,e_k\right]\bar{\alpha}_m\bar{\alpha}_k\bar{\alpha}_l e^{-i(\omega_k+\omega_l+\omega_m)t}$$

Then, through the definition of the *interaction coefficients*

$$C_{nmkl} \equiv \frac{1}{2}\left\langle e_n, \mathcal{G}_1\left[e_m,e_k,e_l\right]\right\rangle, \qquad U_{nmkl} \equiv \frac{1}{2}\left\langle e_n, \mathcal{G}_2\left[e_m,e_k,e_l\right]\right\rangle, \tag{2.2.35}$$

$$Q_{nmkl} \equiv \frac{1}{2}\left\langle e_n, \mathcal{G}_3\left[e_m,e_k,e_l\right]\right\rangle, \qquad P_{nmkl} \equiv \frac{1}{2}\left\langle e_n, \mathcal{G}_4\left[e_m,e_k,e_l\right]\right\rangle, \tag{2.2.36}$$

the resulting system takes the form

$$i\omega_n\frac{d\alpha_n}{d\tau} = \tag{2.2.37}$$

[3]We approximate the irrational number c with rational numbers by truncating it up to a number s of decimals. First, we take $q\in\mathbb{Z}$ and $s\in\mathbb{N}$ such that $c = \frac{q}{10^s} + \frac{(c10^s-q)}{10^s} \approx \frac{q}{10^s} + \mathcal{O}(10^{-s})$. In consequence we have $\omega_n = a(n+c) \approx a\,(n+q10^{-s}) + a\mathcal{O}(10^{-s})$. Nevertheless, if we set the common period to $T = 2\pi 10^s/a$, the error in our approximation becomes of order one and it does not work. To avoid this problem we must seek s,q such that $q,10^s$ have a large greatest common divisor denoted by Q =GCD$[q,10^s]$. Therefore using $T = 2\pi\frac{10^s}{aQ}$ the error in our estimations will be $\mathcal{O}(1/Q)$. For example, taking $c=\sqrt{2}$ and setting $s=45$ we obtain q such that $Q=15625$; in consequence we have a deviation of $\sim 10^{-4}$.

$$\sum_{m=0}^{\infty}\sum_{k=0}^{\infty}\sum_{l=0}^{\infty} C_{nmkl}\bar{\alpha}_m\alpha_k\alpha_l \left\langle e^{i(\omega_k+\omega_l-\omega_m-\omega_n)t}\right\rangle_t + \sum_{m=0}^{\infty}\sum_{k=0}^{\infty}\sum_{l=0}^{\infty} U_{nmkl}\bar{\alpha}_m\alpha_k\bar{\alpha}_l \left\langle e^{i(\omega_k-\omega_l-\omega_m-\omega_n)t}\right\rangle_t$$

$$+\sum_{m=0}^{\infty}\sum_{k=0}^{\infty}\sum_{l=0}^{\infty} Q_{nmkl}\alpha_m\alpha_k\alpha_l \left\langle e^{i(\omega_k+\omega_l+\omega_m-\omega_n)t}\right\rangle_t, + \sum_{m=0}^{\infty}\sum_{k=0}^{\infty}\sum_{l=0}^{\infty} P_{nmkl}\bar{\alpha}_m\bar{\alpha}_k\bar{\alpha}_l \left\langle e^{-i(\omega_k+\omega_l+\omega_m+\omega_n)t}\right\rangle_t,$$

where $\langle\ \rangle_t$ denotes the time averaging. Here we observe the crucial introduction of the fully resonant spectrum. If the exponents are different from zero the time averaging through a period make them vanish. Nevertheless, if there is a resonance of the form $\omega_n = \pm\omega_k \pm \omega_l \pm \omega_m$, at these particular combinations of modes $\{n, m, k, l\}$, exponents are zero, contributing to the interaction between modes.

As we have already commented in section 2.1 and above, we will deal with systems with a linearized spectrum: $\omega_n = an + b$, with $a, b \in \mathbb{R}^+$, $n \in \mathbb{N}$. In this case the resonant channels appear by combining modes:

$$\omega_n = \omega_k + \omega_l - \omega_m \quad \Rightarrow \quad n = k + l - m \tag{2.2.38}$$

$$\omega_n = \omega_k - \omega_l - \omega_m \quad \Rightarrow \quad n = k - l - m - \frac{2b}{a} \tag{2.2.39}$$

$$\omega_n = \omega_k + \omega_l + \omega_m \quad \Rightarrow \quad n = k + l + m + \frac{2b}{a} \tag{2.2.40}$$

$$\omega_n = -\omega_k - \omega_l - \omega_m \quad \Rightarrow \quad n = -(k + l + m) - \frac{4b}{a} \tag{2.2.41}$$

We observe that the first channel is present independently of a, b while the last one is not satisfied for $a, b > 0$, and the other two require that $2b/a \in \mathbb{N}$. This kind of spectrum leads to the denominated *resonant system*

$$i\omega_n\frac{d\alpha_n}{d\tau} = \sum_{m=0}^{\infty}\sum_{k=0}^{\infty}\sum_{l=0}^{\infty}\delta_{n+m,k+l}C_{nmkl}\bar{\alpha}_m\alpha_k\alpha_l \tag{2.2.42}$$

$$+\sum_{m=0}^{\infty}\sum_{k=0}^{\infty}\sum_{l=0}^{\infty}\delta_{n,k-l-2b/a}U_{nmkl}\bar{\alpha}_m\alpha_k\bar{\alpha}_l + \sum_{m=0}^{\infty}\sum_{k=0}^{\infty}\sum_{l=0}^{\infty}\delta_{n,k+l+2b/a}Q_{nmkl}\alpha_m\alpha_k\alpha_l,$$

where $\delta_{i,j}$ is the Kronecker-delta to restrict the interactions to the resonant channels. From this expression we obtain the conclusion that non-resonant terms are suppressed, only resonant channels govern the time evolutions of the coefficients α_n at timescales of ϵt.

Models considered in this thesis only enjoy the first resonant channel, $n + m = k + l$, because the interaction terms do not provide the other channels ($\mathcal{G}_2 = \mathcal{G}_3 = 0$) or despite being present, the interaction coefficients vanish ($Q_{nmkl} = U_{nmkl} = 0$). The resulting system of equations will take the form

$$i\omega_n\frac{d\alpha_n}{d\tau} = \sum_{m=0}^{\infty}\sum_{k=0}^{n+m} C_{nmk(n+m-k)}\bar{\alpha}_m\alpha_k\alpha_{(n+m-k)}. \tag{2.2.43}$$

Then the *first approximation* is complete once this system of equations is solved and the solution for the full problem (2.1.1) is well approximated at timescales of $\mathcal{O}(1/\epsilon)$. As we can see, an analytic resolution of the resonant system (2.2.43) seems to be a formidable task due to the infinite couplings for each mode. Even the numerical resolution of this problem is not satisfactory in some situations. We will leave deep details of this equation for chapter 3.

2.2.3 The Method of Averaging

In this section, we are going to introduce the second strategy developed to obtain approximated solutions for systems of differential equations, which take into account evolutions at different timescales. It is known as the method of averaging and can be presented in multiple versions. We shall present the *first approximation* here, which is enough for our future treatments. Further details can be found in [110, 111].

We are going to start explaining the basic ideas of the method using a system of ODEs. After that, it will be applied to the kind of systems of our interest. The version of the method we present here requires that the system of differential equations can be written in the, so called, *periodic standard form*. That is

$$\dot{\mathbf{x}}(t) = \epsilon\, \mathbf{f}(\mathbf{x}, \mathbf{t}, \epsilon) = \epsilon\, \mathbf{f}_1(\mathbf{x}, t) + \epsilon^2\, \mathbf{f}_2(\mathbf{x}, t) + ..., \tag{2.2.44}$$

where $\mathbf{x}$ is a d-dimensional vector of unknown functions of t, ϵ a small parameter and $\mathbf{f}$ a d-dimensional vector of functions of $\mathbf{x}, t, \epsilon$ which are T-periodic in time and T is independent of ϵ. Note that any period T can be set to 2π through a time rescaling, thereby we will consider $T = 2\pi$.

In order to obtain an autonomous system, we are going to consider a change of variables known as *near-identity transformation*,

$$\mathbf{x} = \mathbf{y} + \epsilon\, \mathbf{u}(\mathbf{y}, t, \epsilon). \tag{2.2.45}$$

The name comes from the fact that this transformation reduces to the identity for $\epsilon = 0$. We require that $\mathbf{u}$ is also 2π-periodic in time and that it can be expanded in Taylor series in powers of ϵ, $\mathbf{u} = \mathbf{u}_1 + \epsilon\mathbf{u}_2 + ...$ Equation (2.2.44) can be rewritten as

$$\dot{\mathbf{y}}(t) = \epsilon\, \mathbf{g}_1(\mathbf{y}, t) + \epsilon^2 \mathbf{g}_2(\mathbf{y}, t) + ... \tag{2.2.46}$$

For our interest it is sufficient to just consider the first order in ϵ, such that

$$\mathbf{x} = \mathbf{y} + \epsilon\, \mathbf{u}_1(\mathbf{y}, t) + \mathcal{O}(\epsilon^2), \tag{2.2.47}$$
$$\dot{\mathbf{x}} = \epsilon\, \mathbf{f}_1(\mathbf{x}, t) + \mathcal{O}(\epsilon^2), \tag{2.2.48}$$
$$\dot{\mathbf{y}} = \epsilon\, \mathbf{g}_1(\mathbf{y}, t) + \mathcal{O}(\epsilon^2). \tag{2.2.49}$$

Combining these equations and remaining at first order in ϵ, we obtain the relation

$$\frac{\partial \mathbf{u}_1}{\partial t}(\mathbf{y}, t) = \mathbf{f}_1(\mathbf{y}, t) - \mathbf{g}_1(\mathbf{y}). \tag{2.2.50}$$

Note that at this order $\mathbf{f}_1(\mathbf{y},t) = \mathbf{f}_1(\mathbf{x},t)$. In order to obtain an autonomous system through the change of variables (2.2.45), $\mathbf{g}_1(\mathbf{y},t)$ is imposed to be independent of time, hence integrating (2.2.50) and using that $\mathbf{u}_1$ is 2π-periodic the next expression must be satisfied

$$\mathbf{g}_1(\mathbf{y}) = \frac{1}{2\pi}\int_0^{2\pi} \mathbf{f}_1(\mathbf{y},s)ds. \tag{2.2.51}$$

Hence, the autonomous system we obtain consists of the averaging of $\mathbf{f}_1(\mathbf{x},t)$ through a period

$$\dot{\mathbf{y}} = \epsilon\bar{\mathbf{f}}_1(\mathbf{y}) + \mathcal{O}(\epsilon^2), \tag{2.2.52}$$

where we have defined $\bar{\mathbf{f}}_1(\mathbf{y}) \equiv \mathbf{g}_1(\mathbf{y})$ given in (2.2.51). Therefore, using $\mathbf{z}$ to denote the first order of $\mathbf{y}$, the *averaging system* is constructed from the original one, (2.2.44), as

$$\frac{d\mathbf{z}}{d\tau} = \bar{\mathbf{f}}(\mathbf{z}), \tag{2.2.53}$$

where the "slow-time", $\tau \equiv \epsilon t$, has been introduced as well as the definition

$$\bar{\mathbf{f}}(\mathbf{z}) \equiv \frac{1}{2\pi}\int_0^{2\pi} \mathbf{f}(\mathbf{z},s,0)ds. \tag{2.2.54}$$

In [110] we can find a theorem which says that the difference between solutions for (2.2.44) and (2.2.53) remains bounded at order ϵ at times $1/\epsilon$. Specifically, the exact solution is approximated as

$$\mathbf{x}(t,\epsilon) = \mathbf{z}(\epsilon t) + \mathcal{O}(\epsilon), \qquad \text{for } 0 \le t \le c/\epsilon, \tag{2.2.55}$$

where $0 < c \ll 1/\epsilon$. Note that to compute $\mathbf{z}$ we do not require a previous determination of $\mathbf{u}_1$, reducing the requirements to obtain the *first approximation*.

In the realm of PDEs, the theory of the method of averaging is also applicable. Therefore we are going to describe its application to models of our interest through their representative (2.1.1). First, equation (2.1.1) must be written in the *periodic standard form*. For this purpose the solution is expanded in terms of the eigenbasis $\{e_n\}$

$$u(t,x) = \sum_{n=0}^{\infty} c_n(t)e_n(x). \tag{2.2.56}$$

Introducing (2.2.56) in the equation and projecting on each mode, the LHS is decoupled leaving the infinite system of ODEs

$$\ddot{c}_n(t) + \omega_n^2 c_n(t) = \epsilon\left\langle e_n, \mathcal{F}_N\left[\sum_{j=0}^{\infty} c_j(t)e_j(x), \epsilon\right]\right\rangle. \tag{2.2.57}$$

Now we perform the change of variables using the variation of constants (2.2.57)

$$\begin{aligned} u(t,x) &= \sum_{n=0}^{\infty} \alpha_n(t)e^{iw_n t}e_n(x), \\ u_t(t,x) &= iw_n\sum_{n=0}^{\infty} \alpha_n(t)e^{iw_n t}e_n(x), \end{aligned} \tag{2.2.58}$$

where $\alpha_n \in \mathbb{C}$. Note that in favour of a clear explanation we have set solutions for the homogeneous equation with negative frequency to zero. Their inclusion is straightforward and can be checked that our choice is a consistent truncation. The differential equation for each $\dot{\alpha}_n$ is obtained by differentiating the combination

$$\alpha_n = \frac{1}{2}\left(c_n + \frac{\dot{c}_n}{i\omega_n}\right), \tag{2.2.59}$$

and using (2.2.57):

$$2i\omega_n \frac{d\alpha_n}{dt} = \epsilon \left\langle e_n, \mathcal{F}_N \left[\sum_{j=0}^{\infty} \alpha_j(t) e^{iw_j t} e_j(x), \epsilon\right]\right\rangle e^{-i\omega_n t}. \tag{2.2.60}$$

Hence, equation (2.1.1) written in terms $\{\alpha_n\}$ becomes the *periodic standard form* (2.2.44). We are now prepare to apply the method of averaging. Following the steps described above the solution for (2.2.57) is approximated by the averaged system (2.2.53)-(2.2.54), which in this case becomes

$$2i\omega_n \frac{d\alpha_n}{d\tau} = \frac{1}{T}\int_0^T ds \left\langle e_n, \mathcal{F}_N \left[\sum_{j=0}^{\infty} \alpha_j(\tau) e^{iw_j s} e_j(x), 0\right]\right\rangle e^{-i\omega_n s}, \tag{2.2.61}$$

with $\tau \equiv \epsilon t$ and T is the common period of modes. Note that we have reached the same result as (2.2.33). Therefore all the incoming results will be the same. Nevertheless for completeness of this section and to avoid a break in the understanding of the method we shall repeat the derivations.

In order to go beyond the current step, we are going to introduce the typical structure of the nonlinear terms we are going to consider. We will focus our attention on cubic nonlinearities which satisfy

$$\mathcal{F}_3 \left[\sum_{n=0}^{\infty} \alpha_n(\tau) e^{iw_n s} e_n(x), 0\right] = \tag{2.2.62}$$

$$\sum_{m=0}^{\infty}\sum_{k=0}^{\infty}\sum_{l=0}^{\infty} \mathcal{G}_1\left[e_m, e_k, e_k\right] \bar{\alpha}_m \alpha_k \alpha_l e^{i(\omega_k+\omega_l-\omega_m)t} + \sum_{m=0}^{\infty}\sum_{k=0}^{\infty}\sum_{l=0}^{\infty} \mathcal{G}_2\left[e_m, e_k, e_k\right] \bar{\alpha}_m \alpha_k \bar{\alpha}_l e^{i(\omega_k-\omega_l-\omega_m)t}$$

$$+ \sum_{m=0}^{\infty}\sum_{k=0}^{\infty}\sum_{l=0}^{\infty} \mathcal{G}_3\left[e_m, e_k, e_k\right] \alpha_m \alpha_k \alpha_l e^{i(\omega_k+\omega_l+\omega_m)t} + \sum_{m=0}^{\infty}\sum_{k=0}^{\infty}\sum_{l=0}^{\infty} \mathcal{G}_4\left[e_m, e_k, e_k\right] \bar{\alpha}_m \bar{\alpha}_k \bar{\alpha}_l e^{-i(\omega_k+\omega_l+\omega_m)t}.$$

Defining the *interaction coefficients* as

$$C_{nmkl} \equiv \tfrac{1}{2}\left\langle e_n, \mathcal{G}_1\left[e_m, e_k, e_l\right]\right\rangle, \quad U_{nmkl} \equiv \frac{1}{2}\left\langle e_n, \mathcal{G}_2\left[e_m, e_k, e_l\right]\right\rangle, \tag{2.2.63}$$

$$Q_{nmkl} \equiv \tfrac{1}{2}\left\langle e_n, \mathcal{G}_3\left[e_m, e_k, e_l\right]\right\rangle, \quad P_{nmkl} \equiv \frac{1}{2}\left\langle e_n, \mathcal{G}_4\left[e_m, e_k, e_l\right]\right\rangle, \tag{2.2.64}$$

the *averaging system* takes the form

$$i\omega_n \frac{d\alpha_n}{d\tau} = \tag{2.2.65}$$

$$\sum_{m=0}^{\infty}\sum_{k=0}^{\infty}\sum_{l=0}^{\infty} C_{nmkl}\bar{\alpha}_m\alpha_k\alpha_l \left\langle e^{i(\omega_k+\omega_l-\omega_m-\omega_n)t}\right\rangle_t + \sum_{m=0}^{\infty}\sum_{k=0}^{\infty}\sum_{l=0}^{\infty} U_{nmkl}\bar{\alpha}_m\alpha_k\bar{\alpha}_l \left\langle e^{i(\omega_k-\omega_l-\omega_m-\omega_n)t}\right\rangle_t$$

$$+\sum_{m=0}^{\infty}\sum_{k=0}^{\infty}\sum_{l=0}^{\infty} Q_{nmkl}\alpha_m\alpha_k\alpha_l \left\langle e^{i(\omega_k+\omega_l+\omega_m-\omega_n)t}\right\rangle_t + \sum_{m=0}^{\infty}\sum_{k=0}^{\infty}\sum_{l=0}^{\infty} P_{nmkl}\bar{\alpha}_m\bar{\alpha}_k\bar{\alpha}_l \left\langle e^{-i(\omega_k+\omega_l+\omega_m+\omega_n)t}\right\rangle_t,$$

where $\langle\ \rangle_t$ denotes the time averaging. Here we observe the crucial introduction of the fully resonant spectrum. If the exponents are different from zero the time averaging through a period makes them vanish. Nevertheless, if there is a resonance of the form $\omega_n = \pm\omega_k \pm \omega_l \pm \omega_m$, at these particular values the exponents are zero providing a contribution for the interactions between these modes. In conclusion, non-resonant terms are suppressed by the averaging, only the resonant channels remain.

The models we are going to consider in chapter 3 have a linearized spectrum: $\omega_n = an + b$, with $a, b \in \mathbb{R}^+$, $n \in \mathbb{N}$. In this case all these channels can be present by the combination of modes:

$$\omega_n = \omega_k + \omega_l - \omega_m \ \Rightarrow\ n = k + l - m \tag{2.2.66}$$

$$\omega_n = \omega_k - \omega_l - \omega_m \ \Rightarrow\ n = k - l - m - \frac{2b}{a} \tag{2.2.67}$$

$$\omega_n = \omega_k + \omega_l + \omega_m \ \Rightarrow\ n = k + l + m + \frac{2b}{a} \tag{2.2.68}$$

$$\omega_n = -\omega_k - \omega_l - \omega_m \ \Rightarrow\ n = -(k + l + m) - \frac{4b}{a} \tag{2.2.69}$$

We observe that the first channel is present independently of a, b while the last one is not satisfied if $a, b > 0$, and the other two require that $2b/a \in \mathbb{N}$. This kind of spectrum leads to the *averaged system*

$$i\omega_n \frac{d\alpha_n}{d\tau} = \sum_{m=0}^{\infty}\sum_{k=0}^{\infty}\sum_{l=0}^{\infty} \delta_{n+m,k+l} C_{nmkl}\bar{\alpha}_m\alpha_k\alpha_l \tag{2.2.70}$$

$$+\sum_{m=0}^{\infty}\sum_{k=0}^{\infty}\sum_{l=0}^{\infty} \delta_{n,k-l-2b/a} U_{nmkl}\bar{\alpha}_m\alpha_k\bar{\alpha}_l + \sum_{m=0}^{\infty}\sum_{k=0}^{\infty}\sum_{l=0}^{\infty} \delta_{n,k+l+2b/a} Q_{nmkl}\alpha_m\alpha_k\alpha_l,$$

where $\delta_{i,j}$ is the Kronecker-delta to restrict the interactions to the resonant channels. Models considered in this thesis only enjoy the first resonant channel, $n + m = k + l$, because the interaction terms do not provide the other channels ($\mathcal{G}_2 = \mathcal{G}_3 = 0$) or despite being present, the interaction coefficients vanish ($Q_{nmkl} = U_{nmkl} = 0$). The resulting system of equations will take the form

$$i\omega_n \frac{d\alpha_n}{d\tau} = \sum_{m=0}^{\infty}\sum_{k=0}^{n+m} C_{nmk(n+m-k)}\bar{\alpha}_m\alpha_k\alpha_{(n+m-k)}. \tag{2.2.71}$$

Then the *first approximation* is complete once this system of equations is solved, and the solution for the full problem (2.1.1) is well approximated at timescales of $\mathcal{O}(1/\epsilon)$. As we can see, an analytic resolution of the resonant system (2.2.43) seems to be a formidable task due to the infinite couplings for each mode. Even the numerical resolution of this problem is not satisfactory in some situations. We will leave the deep details of this equation for chapter 3.

Note that the reduced system of equations we have obtained with the application of the method of multi-scales (2.2.43) and the method of averaging (2.2.71) are exactly the same, as was explained in the introduction of the section. Nevertheless, the philosophy is drastically different. In the method of multi-scales we split the short and long timescales by introducing a new freedom which is used to eliminate secular terms for the short time scale. In contrast, the method of averaging does not pursue the resummation of secular terms, instead of it, the method averages the evolutions at short time scales to be focused on the relevant contributions preserved after a period.

2.3 Time-Periodic Solutions: Construction and Stability

In this section we will describe the methods used to construct TPSs and their linear modes in chapter 4. The first one was developed in [28] and improved in [112], in the context of a massless scalar field in global AdS. In [82] and [113] the method was extended to a driven massless scalar field in global AdS and in [114] was applied to gravitational fluctuations of the AdS soliton. In the case of the method used to study the linear stability of TPSs, it was developed in [113] and also applied in [114].

2.3.1 Time-Periodic Solutions

In this case, we are interested in time-periodic solutions of the full system of equation instead of being restricted to the weakly nonlinear regime described in section 2.1. In consequence, we are going to present the structure of the full problem, and in the following sections, the specific application of the Poincaré-Lindstedt method to obtain these solutions (making use of the weakly nonlinear limit) as well as a numerical resolution of the full system of equations. For this purpose, we shall describe a general example which contains the particular models studied in chapter 4. The problem consists of

$$\mathbf{z}_t = \mathcal{F}\left[\mathbf{z}\right], \qquad (t,x) \in [0,\infty) \times [x_i, x_f], \tag{2.3.1}$$

with $-\infty < x_i < x_f < \infty$ and $\mathcal{F}$ is a 2×1 matrix where its components are smooth functions of x, $\mathbf{z}$ and its spatial derivatives. The unknown $\mathbf{z}$ is composed as

$$\mathbf{z} = \begin{pmatrix} u \\ v \end{pmatrix}, \qquad \text{with } v = u_t/F(\mathbf{z}) \tag{2.3.2}$$

being also $F(\mathbf{z})$ and its derivatives smooth functions of $\mathbf{z}$. The basic idea of the method consists of constructing TPSs as fluctuations of a known static solution $\mathbf{z}_s$ (it will consists of a spacetime such as: AdS or the AdS soliton), namely

$$\mathcal{F}[\mathbf{z}_s] = 0. \tag{2.3.3}$$

Taking fluctuations of this background

$$\mathbf{z} = \mathbf{z}_s + \epsilon\, \tilde{\mathbf{z}}, \tag{2.3.4}$$

substituting $v = u_t/F(\mathbf{z})$ and linearising in $\epsilon \ll 1$ ($\|\tilde{\mathbf{z}}\| \sim 1$), the system of equations is reduced to

$$\tilde{u}_{tt} - \mathcal{L}\tilde{u} = 0, \tag{2.3.5}$$

where it is a linear equation of the form (2.1.3), and the operator $\mathcal{L}$ is defined in (2.1.1). As we explained in section 2.1, for homogeneous Dirichlet boundary conditions

$$u(t, x_i) = u(t, x_f) = 0, \tag{2.3.6}$$

the linear modes of the problem form the eigenbasis $\{e_n(x)\}$. Remember that we use e_n and h_n to denote normalizable and non-normalizable modes respectively. Additionally, we will denote in this section and in chapter 4 the spectrum of normalizable modes as $\{\Omega_n\}$ and assume the linear stability of the background (the static solution $\mathbf{z}_s$), namely $\Omega_n^2 \geq 0$. Therefore, the general solution of (2.3.5) subject to (2.3.6) can be written as a linear combination of modes,

$$\tilde{u}(t, x) = \sum_{n=0}^{\infty} a_n \cos(\Omega_n t + \phi_n) e_n(x), \tag{2.3.7}$$

with $\{a_n\}$ and $\{\phi_n\}$ being constants, amplitudes and phases respectively, determined by the initial conditions $\tilde{u}(0, x)$ and $\tilde{u}_t(0, x)$.

Finally, we are also interested in solutions for (2.3.1) subject to inhomogeneous boundary conditions of the form

$$u(t, x_i) = u(t, x_f) = \epsilon\rho \cos(\omega t). \tag{2.3.8}$$

Note that they contain the homogeneous conditions (2.3.6) for the particular case $\rho = 0$. The situation $\rho \neq 0$ is more complicated due to the fact that solutions of (2.3.5) contain a non-normalizable mode h_0. For this reason, the general solution takes the form

$$\tilde{u}(t, x) = \tilde{a} \cos(\omega_0 t) h_0(x) + \sum_{n=0}^{\infty} a_n \cos(\Omega_n t + \phi_n) e_n(x), \tag{2.3.9}$$

where e_n are the solutions for homogeneous boundary conditions, a_n, ϕ_n are determined with the initial conditions $\tilde{u}(0, x), \tilde{u}_t(0, x)$ and $\tilde{a} = \epsilon\rho/h_0(x_f)$. We continue assuming the linear stability of the background subject to (2.3.8), thereby $\omega_0^2, \Omega_n^2 \geq 0$. The presence of h_0 disallows the projection of $\tilde{u}$ in the eigenbasis $\{e_n\}$.

2.3.1.1 Perturbative Construction

Now, we are going to apply the Poincaré-Lindstedt method to our problem. The static solutions consist of spacetimes for which $u_s = v_s = 0$; therefore their fluctuations will be calculated using the Poincaré-Lindstedt method through the expansion

$$u(t,x) = \sum_{j=1}^{\infty} \epsilon^j \tilde{u}_j(t,x), \qquad v(t,x) = \sum_{j=1}^{\infty} \epsilon^j \tilde{v}_n(t,x), \qquad \omega = \omega^{(0)} + \sum_{j=1}^{\infty} \epsilon^j \omega^{(j)}. \quad (2.3.10)$$

After introducing (2.3.10) in the EOMs (2.3.1) and defining $\tau \equiv \omega t$, the resulting equation at order j becomes

$$(\omega^{(0)})^2 \tilde{u}_{j,\tau\tau} - \mathcal{L}\tilde{u}_j = S_j(u_k, v_k, \omega^{(k)}), \quad (2.3.11)$$

with S_j denoting all the nonlinear terms at order ϵ^j which is formed by lower order terms, $k < j$. Note that equation (2.3.5) is the first order equation and therefore $S_1 = 0$. The structure of (2.3.11) allows an iterative resolution order by order: $j = 1, 2, 3, ...$

In this section we will seek TPSs subject to homogeneous boundary conditions (2.3.6). The protocol starts by considering a single mode solution of (2.3.5) subject to (2.3.6), namely

$$u_1(\tau, x) = a_1 \cos(\tau) e_n(x), \quad (2.3.12)$$

with $w^{(0)} = \Omega_n$. Introducing it in (2.3.11) for $j = 2$ the first nonlinear equation takes the form

$$(w^{(0)})^2 u_{2,\tau\tau} - \mathcal{L}\tilde{u}_2 = S_2(u_1, v_1, w^{(1)}). \quad (2.3.13)$$

At this order, the solution can suffer secular terms if S_j contains a solution of the homogeneous equation. For this reason, the freedoms $w^{(j)}$ were introduced to be adjusted such that secular terms are removed. The internal structure of $S_2(u_1, v_1)$ allows rewriting this function as

$$S_2(u_1, v_1, \omega^{(1)}) = S_{2,0}(x) + S_{2,1}(x)\cos(\tau) + S_{2,2}(x)\cos(2\tau). \quad (2.3.14)$$

In this situation the freedom $w^{(1)}$ is fixed by imposing that the RHS is free of mode n, that is

$$\langle S_{2,1}, e_n \rangle = 0. \quad (2.3.15)$$

A special situation happens if the homogeneous equation has a mode h_m such that $\Omega_m = 2\Omega_n$ and the projection $\langle S_{2,2}, e_m \rangle$ is different from zero. It would mean that the ansatz (2.3.12) does not contain enough freedom to remove all the emergent secular terms. If it is the case, the ansatz (2.3.12) must be improved. Fortunately, the expansion is safe for our backgrounds.

This process of removing secular terms must be repeated order by order taking into account that for our systems S_j satisfies

$$S_j(x, \tau) = \sum_{k=0}^{j} S_{j,k}(x)\cos(k\tau). \quad (2.3.16)$$

This fact allows extracting the content in Fourier modes in (2.3.10) (as long as the secular terms can be removed)

$$u(t,x) = \epsilon \cos(\tau) e_n(x) + \sum_{j=2}^{\infty} \sum_{k=0}^{j} \epsilon^j \cos(k\tau) \tilde{u}_{j,k}(x), \tag{2.3.17}$$

$$v(t,x) = -\epsilon\ \Omega_n \sin(\tau) e_n(x) + \sum_{j=2}^{\infty} \sum_{k=1}^{j} \epsilon^j \sin(k\tau) \tilde{v}_{j,k}(x), \tag{2.3.18}$$

$$\omega = \Omega_n + \sum_{j=1}^{\infty} \epsilon^j \omega^{(j)}. \tag{2.3.19}$$

The described protocol to construct TPSs was based on homogeneous boundary conditions (2.3.6). In chapter 4 we shall also be interested in TPSs with inhomogeneous conditions (2.3.8). As we explained in the introduction of this section, this situation is more complicated due to the presence of non-normalizable modes. Nevertheless, let us suppose that starting with

$$u_1(t,x) = a_1 \cos(\tau) h_0(x), \qquad \tau \equiv \omega t, \tag{2.3.20}$$

the expansion (2.3.10) is free of secular terms; namely, the set of $\{w^{(j)}\}$ allows removing these terms. This assumption also reports the content in Fourier modes of TPSs subject to inhomogeneous boundary conditions (2.3.6). In this situation, the structure of S_j is the same as in (2.3.16) and therefore the expansion (2.3.17)-(2.3.19) is hypothetically valid such that

$$u(t,x) = \epsilon \cos(\tau) h_0(x) + \sum_{j=2}^{\infty} \sum_{k=0}^{j} \epsilon^j \cos(k\tau) \tilde{u}_{j,k}(x), \tag{2.3.21}$$

$$v(t,x) = -\epsilon\ \omega_0 \sin(\tau) h_0(x) + \sum_{j=2}^{\infty} \sum_{k=1}^{j} \epsilon^j \sin(k\tau) \tilde{v}_{j,k}(x), \tag{2.3.22}$$

$$\omega = \omega_0 + \sum_{j=1}^{\infty} \epsilon^j \omega^{(j)}. \tag{2.3.23}$$

Due to the inconvenience of the non-orthogonality of $h_0(x)$, and the fact that they cannot be properly expanded in the eigenbasis $\{e_n\}$; TPSs with inhomogeneous boundary conditions will be only calculated numerically based on the structure inferred in this section.

2.3.1.2 Numerical Construction

In this section we will describe the numerical method used to obtain TPSs. In contrast with the analysis performed in the previous section, this construction allows extending the solutions beyond the perturbative regime. The first step consists of the extraction of the content in Fourier modes of TPSs. The structure (2.3.17)-(2.3.19) was rigorously

derived for TPSs satisfying homogeneous boundary conditions (2.3.6) making use of the orthogonality properties of the eigenbasis $\{e_n\}$. For inhomogeneous conditions (2.3.8) the same structure, (2.3.21)-(2.3.23), was obtained under the assumption that a similar perturbative expansion is free of secular terms. Therefore, the ansatz we are going to present is the same for both situation,

$$u(\tau,x)=\sum_{n=0}^{\infty}\cos(n\tau)\hat{u}_n(x),\qquad v(\tau,x)=\sum_{n=1}^{\infty}\sin(n\tau)\hat{v}_n(x). \tag{2.3.24}$$

where $\tau=\omega t$.

For a proper explanation of this section we are going to report more information about the structure of the system of equations (2.3.1). We assume that the EOMs have the form ($\dot{}\equiv\partial_t$ and $'\equiv\partial_x$)

$$\dot{u}(t,x)=F(t,x)v(t,x) \tag{2.3.25}$$

$$\dot{v}(t,x)=\frac{1}{\mu(x)}\left[F(t,x)\left(c_{v,1}(x)+c_{v,2}(x)u'(t,x)\right)\right]' \tag{2.3.26}$$

$$F'(t,x)=c_F(x)\left(e^{-\delta(t,x)}-F(t,x)\right) \tag{2.3.27}$$

$$\delta'(t,x)=c_{\delta,1}(x)u'(t,x)+c_{\delta,2}(x)(u'(t,x))^2+c_{\delta,3}(x)v(t,x)^2 \tag{2.3.28}$$

where $\mu, c_{v,1}, c_{v,2}, c_F, c_{\delta,1}, c_{\delta,1}, c_{\delta,1}$ and their derivatives are smooth functions on the domain (the regularity of u, v, F, δ at the excluded points is obtained through asymptotic expansions). The domain has the form $(t,x)\in[0,\infty)\times[-x_f,x_f]$, and the next functions are symmetric at $x=0$: $u(t,-x)=u(t,x)$, $v(t,-x)=v(t,x)$, $F(t,-x)=F(t,x)$ and $\delta(t,-x)=\delta(t,x)$. F and δ can be (almost) determined from u and v through (2.3.27)-(2.3.28); there is a freedom consisting of the constant of integration coming from (2.3.28). In this thesis we will set this constant to satisfy $\delta(t,x_f)=0$. This choice simplifies the boundary conditions due to $F(t,x_f)=1$,

$$u(t,x_f)=\rho\cos(\omega t),\qquad v(t,x_f)=-\rho\omega\sin(\omega t). \tag{2.3.29}$$

The numerical approach to this problem will be done using the polynomial pseudospectral method developed in [112]. The idea consists of solving the EOMs (2.3.25)-(2.3.28) on selected points of t and x called *collocation point*. Nevertheless, as ω is not known we will use $\tau=\omega t$ instead of t to guarantee that the initial election of *collocation points* is always valid. The natural basis to write a periodic solution is the Fourier basis while, if we do not have additional information for this choice, the optical election is the basis of Chebyshev polynomials [115]. Therefore the set of *collocation points* for τ and x will be associated with Fourier modes and Chebyshev polynomials respectively,

$$\tau_k=\pi\frac{k-1/2}{2K+1},\qquad x_i=x_f\cos\left(\frac{i\pi}{2N+1}\right), \tag{2.3.30}$$

with $k=1,2,...,K$ and $i=0,1,...,N$. The ansatz (2.3.24), evaluated at these points takes the form

$$u(\tau_k,x_i)=\sum_{n=0}^{\infty}\cos(n\tau_k)\hat{u}_{n,i},\qquad v(\tau_k,x_i)=\sum_{n=1}^{\infty}\sin(n\tau_k)\hat{v}_{n,i}, \tag{2.3.31}$$

where $\hat{u}_{n,i} \equiv \hat{u}_n(x_i)$ and $\hat{v}_{n,i} \equiv \hat{v}_n(x_i)$. Note that the point x_0 corresponds with the boundary x_f and therefore $\hat{u}_{n,0}$ and $\hat{v}_{n,0}$ are determined with the boundary conditions (2.3.29), such that

$$\hat{u}_{n,0} = \rho\delta_{n,1} \qquad \hat{v}_{n,0} = -\rho\omega\delta_{n,1}. \tag{2.3.32}$$

Introducing (2.3.31) in the system of equations (2.3.25)-(2.3.28), we obtain two equations for each couple of collocation points (τ_k, x_i), namely the total number of equations is $2NK$ (taking into account that F and δ are completely determined by u, v and $\delta(t, x_f) = 0$). Due to this fact, the number of unknowns is reduced through the truncation of (2.3.31), such that

$$u(\tau_k, x_i) = \sum_{n=0}^{K-1} \cos(n\tau_k)\hat{u}_{n,i}, \qquad v(\tau_k, x_i) = \sum_{n=0}^{K-1} \sin(n\tau_k)\hat{v}_{n,i}. \tag{2.3.33}$$

This truncation leaves $2NK+1$ unknowns: $\{\hat{u}_{n,i}, \hat{v}_{n,i}\}$ and ω, because we consider ρ fixed (the opposite situation can also be implemented). To close the system of equations with $2NK + 1$ unknowns, an additional equation is required. In this situation we decided to use

$$u(0, 0) = \rho_0, \tag{2.3.34}$$

where ρ_0 is a fixed parameter.

Once equations (2.3.25)-(2.3.28) and (2.3.34) are properly adapted to the grid of *collocation points*, as is explained in appendix A.1, and the ansatz (2.3.33) introduced, we finally have a nonlinear system of $2NK + 1$ equations with $2NK + 1$ unknowns. The resolution of this system is done through the Newton-Raphson method. This iterative resolution requires an initial seed close enough to the solution to guarantee the convergence. For this reason, we start seeking TPSs close to single linear modes. Namely $\rho_0 \ll 1, \rho = \rho_0 h_0(x_f)/h_0(0)$ (or $\rho = 0$) and

$$\hat{u}_{1,i} = \rho_0, \qquad \hat{v}_{1,i} = -\omega_0 \frac{h_0(x_i)}{h_0(0)}, \qquad \hat{u}_{n,i} = \hat{v}_{n,i} = 0 \ \forall n \neq 1 \tag{2.3.35}$$

and $\omega = \omega_n$. After the convergence to a TPS, we slightly modify ρ_0, ρ or both and use the previous TPS as the seed for the new one.

The protocol described until this point works properly for small ρ_0; nevertheless, we have observed that the convergence of the Newton-Raphson method can be significantly improved extracting from $\hat{u}_{n,i}, \hat{v}_{n,i}$ some terms of their asymptotic expansion close to the boundary. For the models displayed in chapter 4, after imposing $\delta(t, x_f) = 0$ the expansions for regular functions have the form

$$\begin{aligned} u(t, x) &= u_0(t) + u_2(t)\xi^2 + u_3(t)\xi^3 + \mathcal{O}(\xi^4), \\ v(t, x) &= v_0(t) + v_2(t)\xi^2 + v_3(t)\xi^3 + \mathcal{O}(\xi^4), \end{aligned} \tag{2.3.36}$$

with $\xi = (x - x_f)$. In this case $v_0(t), u_2(t), v_2(t)$ are completely determined by $u_0(t)$, and therefore, for the boundary conditions. The first unknowns appear at $u_3(t), v_3(t)$, which require initial conditions to be determined. Therefore, rewriting u, v as

$$u(t, x) = R_u(x)\psi(t, x) + S_u(t, x), \qquad v(t, x) = R_v(x)\eta(t, x) + S_v(t, x), \tag{2.3.37}$$

with the definitions

$$R_v(x) = R_u(x) = \cos^2\left(\frac{\pi}{2}\frac{x}{x_f}\right), \tag{2.3.38}$$

$$S_u(t,x) = u_0(t) + u_2(t)\left(\frac{2}{\pi}x_f\right)^2\cos^2\left(\frac{\pi}{2}\frac{x}{x_f}\right), \tag{2.3.39}$$

$$S_v(t,x) = v_0(t) + v_2(t)\left(\frac{2}{\pi}x_f\right)^2\cos^2\left(\frac{\pi}{2}\frac{x}{x_f}\right), \tag{2.3.40}$$

the new variables have a linear behavior close to the boundary,

$$\psi(t,x) = \left(\frac{2}{\pi}x_f\right)^2 u_3(t)\xi + \mathcal{O}(\xi^2), \tag{2.3.41}$$

$$\eta(t,x) = \left(\frac{2}{\pi}x_f\right)^2 v_3(t)\xi + \mathcal{O}(\xi^2), \tag{2.3.42}$$

which ease the convergence of the method. The ansatz (2.3.31) is also rewritten in terms of the new variables

$$u(\tau_k,x_i) = R_{u,i}\sum_{n=0}^{\infty}\cos(n\tau_k)\hat{\psi}_{n,i} + S_{u,k,i}, \qquad v(\tau_k,x_i) = R_{v,i}\sum_{n=1}^{\infty}\sin(n\tau_k)\hat{\eta}_{n,i} + S_{v,k,i}, \tag{2.3.43}$$

with $R_{u,i} \equiv R_u(x_i), R_{v,i} \equiv R_v(x_i), S_{u,i,k} \equiv S_u(\tau_k,x_i), S_{v,i,k} \equiv S_v(\tau_k,x_i)$ and boundary conditions $\hat{\psi}_{n,0} = \hat{\eta}_{n,0} = 0$. We must remark that this new ansatz, with the definitions (2.3.38)-(2.3.40), slows down the computation of TPSs. For our purpose, the best relation time/convergence was obtained with the elimination of the spatial dependence in $S_{u,v}$ such that

$$R_v(x) = R_u(x) = \cos\left(\frac{\pi}{2}\frac{x}{x_f}\right), \qquad S_u(t,x) = u_0(t), \qquad S_v(t,x) = v_0(t). \tag{2.3.44}$$

Note that to clarify the explanation, we have described the method applied in problems with asymptotic expansion of the form (2.3.36). Nevertheless, there are problems with the first independent terms at ξ^{Δ_-} and ξ^{Δ_+}, playing the role of u_0 and u_3 in our explanation. For example, in the case of a massive scalar field in AdS_4 the relevant powers are $\Delta_\pm = \frac{3}{2}\pm\sqrt{\left(\frac{3}{2}\right)^2+m^2}$. For these problems, TPSs can also be targeted by imposing the condition $u_{\Delta_-}(t) = \rho\cos(\omega t)$ and using a transformation of the form (2.3.37) with the appropriate functions $R_{u,v}$ and $S_{u,v}$.

2.3.2 Floquet Theory and Linear Stability

2.3.2.1 Floquet Theory

The mathematical theory of differential equations with periodic coefficients is known as Floquet theory or on some occasions Floquet-Bloch theory. It is well established [116–120] and is of great interest in some physical contexts as quantum mechanics [92,93], hydrodynamics [121, 122] or elasticity theory [123, 124]. Floquet developed the theory to solve ODEs with periodic coefficients [116] while Bloch, in the context of solid state physics, extended the results to 3-dimensional systems with discrete translation symmetry in each spatial direction (periodic crystal lattice) [117]. For ODEs the main result consists of the following theorem:

Floquet-Lyapunov theorem [120]: *Consider a system of ODEs with periodic coefficients of the form*

$$\frac{d\mathbf{u}(t)}{dt} = A(t)\mathbf{u}(t), \tag{2.3.45}$$

where $A(t)$ is a T-periodic $N \times N$ matrix and $\mathbf{u}(t)$ are N unknown functions of time. Then, the solution for (2.3.45) *is any linear combination of the following functions*

$$\mathbf{u}_n(t) = e^{i\lambda_n t} \sum_{k=0}^{N} t^k \mathbf{a}_{n,k}(t), \tag{2.3.46}$$

where $n = 1, 2, \ldots, N$; and for each n, $\mathbf{a}_{n,k}(t)$ are N, T-periodic functions of time and the exponent $\lambda_n \in \mathbb{C}$.

In literature solutions (2.3.46) are known as *Floquet modes* and λ_n as *Floquet exponents*.

A useful application of the Floquet theory is the study of linear stability of periodic solutions. Suppose a function $u(t, \mathbf{x})$ defined in the domain $(t, \mathbf{x}) \in \mathbb{R}^{d+1}$ and governed by a nonlinear PDE with coefficients depending only on $\mathbf{x}$. Allow also that the equation has a TPS, $u_p(t+T, \mathbf{x}) = u_p(t, \mathbf{x})$. This equation does not belong to the class of problems covered by the Floquet theory; nevertheless, considering fluctuations around u_p,

$$u(t, \mathbf{x}) = u_p(t, \mathbf{x}) + \epsilon \tilde{u}(t, \mathbf{x}), \tag{2.3.47}$$

and linearising for $\epsilon \ll 1$ the remaining operator $\mathcal{L}$, is linear with periodic coefficients in time

$$\mathcal{L}(t, \mathbf{x})\tilde{u}(t, \mathbf{x}) = 0, \qquad \mathcal{L}(t + T, \mathbf{x}) = \mathcal{L}(t, \mathbf{x}). \tag{2.3.48}$$

Hence the Floquet theory reports the structure of linear perturbations

$$\tilde{u}(t, \mathbf{x}) = e^{i\lambda t} \sum_{k=0}^{\infty} t^k a_k(t, \mathbf{x}), \tag{2.3.49}$$

where $a_k(t, \mathbf{x})$ are T-periodic functions of time, which can be expanded in Fourier modes

$$a_k(t, \mathbf{x}) = \sum_{n=0}^{\infty} c_{k,n}(\mathbf{x}) \cos(n\omega t) + \sum_{n=1}^{\infty} s_{k,n}(\mathbf{x}) \sin(n\omega t) \tag{2.3.50}$$

with $\omega = 2\pi/T$. Terms with $k > 0$ are the so-called secular terms, which reflect that the perturbative expansion (2.3.47) is too naive, claiming for a more sophisticated method (Poincaré-Lindstedt method). Therefore, if the perturbative expansion is well defined on an interval of $\mathcal{O}(1/\epsilon)$ the ansatz for linear fluctuations is free of secular terms,

$$\tilde{u}(t, \mathbf{x}) = e^{i\lambda t} \left(\sum_{n=0}^{\infty} c_n(\mathbf{x}) \cos(n\omega t) + \sum_{n=1}^{\infty} s_n(\mathbf{x}) \sin(n\omega t) \right). \tag{2.3.51}$$

Note that this derivation also contains the case of static solutions ($\omega = 0$).

The ansatz (2.3.51) provides a criterion for the stability of TPSs in times of $\mathcal{O}(1/\epsilon)$, based on the full set of *Floquet exponents* $\{\lambda_n\}$:

- $\lambda_n \in \mathbb{R}\ \forall n$: the fluctuation $\tilde{u}$ remains bounded in time; in consequence, the TPS u_p is linearly stable.
- Exists k such that $\mathrm{Im}(\lambda_k) \neq 0$: this situation requires a deeper study
  - If $\mathrm{Im}(\lambda_k) > 0\ \forall k$ such that $\mathrm{Im}(\lambda_k) \neq 0$, these *Floquet modes* have an exponential decay, therefore the TPS is linearly stable.
  - If for at least a single k, $\mathrm{Im}(\lambda_k) < 0$, this *Floquet mode* has an exponential growth, and therefore, the TPS is linearly unstable.

2.3.2.2 Numerical Construction of Floquet Modes

In this section we will explain the method used in chapter 4 to study the linear stability of TPSs. The philosophy of the method is very similar to the construction of TPSs. In that case, we started calculating fluctuations around a static solution to infer the structure of Fourier modes of TPSs. It allowed for the construction of an ansatz to perform a numerical resolution of the full system of equation. In contrast, in this situation the background will be periodic; therefore, the Floquet theory described above can be used to obtain the ansatz for linear perturbations. Finally, using the same numerical methodology as for TPS we will solve the ansatz.

First, we consider small fluctuations around a TPS $(u_p, v_p, F_p, \delta_p)$:

$$\begin{aligned} u(t,x) &= u_p(t,x) + \epsilon\tilde{u}(t,x), \\ v(t,x) &= v_p(t,x) + \epsilon\tilde{v}(t,x), \\ F(t,x) &= F_p(t,x) + \epsilon\tilde{F}(t,x), \\ \delta(t,x) &= \delta_p(t,x) + \epsilon\tilde{\delta}(t,x), \end{aligned} \tag{2.3.52}$$

with $\epsilon \ll 1$. Introducing (2.3.52) in the EOMs (2.3.25)-(2.3.28) and linearising in ϵ, the resulting equations for linear fluctuations are

$$\dot{\tilde{u}} = \tilde{F} v_p + F_p \tilde{v}, \tag{2.3.53}$$

$$\dot{\tilde{v}} = \frac{1}{\mu}\left[\left(c_{v,1} + c_{v,2} u_p'\right)\tilde{F} + c_{v,2} F_p \tilde{u}'\right]', \tag{2.3.54}$$

$$\tilde{F}' = -c_F\left(\tilde{\delta} e^{-\delta_p} + \tilde{F}\right), \tag{2.3.55}$$

$$\tilde{\delta}' = \left(c_{\delta,1} + 2c_{\delta,2} u_p'\right)\tilde{u}' + 2c_{\delta,3} v_p \tilde{v}. \tag{2.3.56}$$

This system of equations has time-periodic coefficients $(u_p, v_p, F_p, \delta_p)$, and therefore the Floquet theory can be applied. We will consider an ansatz as (2.3.51) for linear perturbations,

$$\begin{aligned}
\tilde{u}(t,x) &= e^{i\lambda t}\left(\sum_{n=0}^{\infty} \tilde{u}_n^{(1)}(x)\cos(n\omega t) + \sum_{n=1}^{\infty} \tilde{u}_n^{(2)}(x)\sin(n\omega t)\right), \\
\tilde{v}(t,x) &= e^{i\lambda t}\left(\sum_{n=1}^{\infty} \tilde{v}_n^{(1)}(x)\sin(n\omega t) + \sum_{n=0}^{\infty} \tilde{v}_n^{(2)}(x)\cos(n\omega t)\right),
\end{aligned} \tag{2.3.57}$$

where ω is the frequency of the TPS and λ, $\{\tilde{u}_n^{(1)}\}, \{\tilde{u}_n^{(2)}\}, \{\tilde{v}_n^{(1)}\}, \{\tilde{v}_n^{(2)}\}$ must be determined. Introducing (2.3.57) in (2.3.53)-(2.3.56) we observe that solutions come in pairs $\left(\pm\lambda, \tilde{u}_n^{(1)}, \tilde{v}_n^{(1)}, \pm\tilde{u}_n^{(2)}, \pm\tilde{v}_n^{(2)}\right)$. Therefore, based on the discussion made in section 2.3.2.1, if a solution for (2.3.53)-(2.3.56) exists such that $\mathrm{Im}(\lambda) \neq 0$, the TPS is unstable, while it is linearly stable if all the solutions satisfy $\lambda \in \mathbb{R}$. Note that the combination of solutions with $\pm\lambda$ also allows constructing real perturbations: $\tilde{u}, \tilde{v} \in \mathbb{R}$.

The ansatz (2.3.57) is an exponential times a $2\pi/\omega$-periodic solution. We observe that once it is introduced in (2.3.53)-(2.3.56), the exponential can be factorized from both sides and the problem is reduced to find a TPS. Therefore, the method to obtain numerically TPSs described in section 2.3.1.2 can be applied under minor modifications. In this situation ω is already known, thereby, the unknowns are $\tilde{u}_n^{(1)}, \tilde{u}_n^{(2)}, \tilde{v}_n^{(1)}, \tilde{v}_n^{(2)}$ and λ. The time is rescaled as $\tau = \omega t$, the *collocation points* are chosen as in (2.3.30), the ansatz evaluated on them and truncated as

$$\begin{aligned}
\tilde{u}(\tau_k, x_i) &= e^{i\lambda/\omega\tau}\left(\sum_{n=0}^{K-1} \tilde{u}_{n,i}^{(1)}\cos(n\tau_k) + \sum_{n=0}^{K-1} \tilde{u}_{n,i}^{(2)}\sin(n\tau)\right), \\
\tilde{v}(\tau_k, x_i) &= e^{i\lambda/\omega\tau}\left(\sum_{n=0}^{K-1} \tilde{v}_{n,i}^{(1)}\sin(n\tau) + \sum_{n=0}^{K-1} \tilde{v}_{n,i}^{(2)}\cos(n\tau)\right),
\end{aligned} \tag{2.3.58}$$

where $\tilde{u}_{n,i}^{(1)} \equiv \tilde{u}_n^{(1)}(x_i), \tilde{u}_{n,i}^{(2)} \equiv \tilde{u}_n^{(2)}(x_i), \tilde{v}_{n,i}^{(1)} \equiv \tilde{v}_n^{(1)}(x_i), \tilde{v}_{n,i}^{(2)} \equiv \tilde{v}_n^{(2)}(x_i)$. In our case, we are interested in perturbations that do not modify the boundary conditions of the original TPS. Then, fluctuations must vanish at the boundary, in consequence, $\tilde{u}_{n,0}^{(1)} = \tilde{u}_{n,0}^{(2)} = \tilde{v}_{n,0}^{(1)} = \tilde{v}_{n,0}^{(2)} = 0$. The number of unknowns is $4NK + 1$, $\{\tilde{u}_{n,i}^{(1)}, \tilde{u}_{n,i}^{(2)}, \tilde{v}_{n,i}^{(1)}, \tilde{v}_{n,i}^{(2)}\}$ and λ, while

the number of equations at each couple of *collocation points* (τ_k, x_i) is four, after using the independence of cosine and sine. The total number of equations is $4NK$ and an additional condition must be introduced

$$\tilde{u}(0,0) = 1. \tag{2.3.59}$$

Note that in this situation the system of equations (2.3.53)-(2.3.56) is linear in $\tilde{u}$ and $\tilde{v}$, in consequence, $\tilde{u}(0,0)$ can be chosen arbitrarily (excluding 0).

Finally, after writing the $4NK+1$ equations in the discrete form on the *collocation points* (see appendix A.1) and imposing the appropriate boundary conditions, the problem is solved with the Newton-Raphson method.

We must remark that in particular situations, the ansatz (2.3.57) can be too naive, and an extension to (2.3.49) is required, or a more sophisticated perturbative expansions as the Poincaré-Lindstedt method. The next section reports some intuition about this fact.

2.3.2.3 Secular Terms and Zero-Modes

In this section we are going to present analytic results in relation to linear modes of TPSs. In particular, we will show that on some occasions the ansatz (2.3.57) is not suitable, and also the existence of zero-modes ($\lambda = 0$) for specific TPSs. For this purpose, we require an analytic structure of TPSs. Then we are going to suppose that they allow a perturbative series of the form

$$u_p(t,x,\epsilon) = \sum_{n=0}^{\infty} \cos(n\omega t) \sum_{k=0}^{\infty} u_{n,k}(x)\epsilon^k = \sum_{n=0}^{\infty} \cos(n\omega t) u_n(x,\epsilon), \tag{2.3.60}$$

$$v_p(t,x,\epsilon) = \sum_{n=1}^{\infty} \sin(n\omega t) \sum_{k=0}^{\infty} v_{n,k}(x)\epsilon^k = \sum_{n=1}^{\infty} \sin(n\omega t) v_n(x,\epsilon), \tag{2.3.61}$$

$$\omega(\epsilon) = \sum_{k=0}^{\infty} \epsilon^k \omega^{(k)}, \tag{2.3.62}$$

where u_p, v_p denote the functions of a TPS. Note that the perturbative structure for TPSs with homogeneous boundary conditions (2.3.17)-(2.3.19) is a particular case of this proposal. For inhomogeneous boundary conditions we argued that the structure (2.3.21)-(2.3.23) should be valid and is also covered by (2.3.60)-(2.3.62). Based on this analytic structure two propositions can be formulated.

Proposition 2.1: *Suppose a family of TPSs given by* (2.3.60)-(2.3.62). *Then two solutions:* $\epsilon, \epsilon' = \epsilon(1+\delta)$, *arbitrarily close* ($\delta << 1$), *satisfy at first order in* δ

$$u_p(t,x,\epsilon') - u_p(t,x,\epsilon) = (\tilde{u}(t,x,\epsilon) + t\hat{u}(t,x,\epsilon))\,\delta + \mathcal{O}(\delta^2) \tag{2.3.63}$$

$$v_p(t,x,\epsilon') - v_p(t,x,\epsilon) = (\tilde{v}(t,x,\epsilon) + t\hat{v}(t,x,\epsilon))\,\delta + \mathcal{O}(\delta^2) \tag{2.3.64}$$

where $\tilde{u}, \tilde{v}$ *satisfy* (2.3.57) *with* $\lambda = 0$, *and* $\hat{u}, \hat{v}$ *are bounded* $2\pi/\omega$*-periodic functions.*

This proposition must be analyzed carefully. If we are considering families of TPSs bifurcating from a linear mode with inhomogeneous boundary conditions, as is our current situation, solutions for ϵ, ϵ' do not have the same value at the boundary and their difference also has inhomogeneous boundary conditions. Therefore, at first order this difference is a linear perturbation that modifies the boundary. As we are excluding this kind of linear fluctuations from our analysis of the previous section, this secular term is not present and the ansatz (2.3.57) remains valid. It is not the situation for $\rho = 0$, the homogeneous conditions are transferred to the linear perturbation which has a secular term. This fact prevents us to talk about the linear stability of these TPSs. Nevertheless, this particular mode does not trigger an instability[4]. In consequence, we will omit this mode when we discuss the linear stability of TPSs with $\rho = 0$.

Proposition 2.2: *Suppose two families of TPSs:* $(u_{p,1}, v_{p,1}, \omega_1)$, $(u_{p,2}, v_{p,2}, \omega_2)$ *satisfying* (2.3.60)-(2.3.62) *with boundary conditions*

$$u_{p,1,2}(t, x_f, \epsilon) = \epsilon\rho_{1,2}\cos(\omega_{1,2}(\epsilon)t), \tag{2.3.65}$$

$$v_{p,1,2}(t, x_f, \epsilon) = -\epsilon\omega_{1,2}(\epsilon)\rho_{1,2}\cos(\omega_{1,2}(\epsilon)t), \tag{2.3.66}$$

which are arbitrarily close $\rho_2 = \rho_1(1+\delta)$, *with* $|\delta| \ll 1$. *Also consider that there exists* ρ_1, ϵ *such that*

$$\omega_2\left(\frac{\epsilon}{1+\delta}\right) = \omega_1(\epsilon) + \delta^2\tilde{\omega}(\epsilon) + \mathcal{O}(\delta^3), \tag{2.3.67}$$

$$u_{p,2}\left(t, x, \frac{\epsilon}{1+\delta}\right) = u_{p,1}\left(t, x, \epsilon\right) + \delta\ \tilde{u}(t, x, \epsilon) + \mathcal{O}(\delta^2), \tag{2.3.68}$$

$$v_{p,2}\left(t, x, \frac{\epsilon}{1+\delta}\right) = v_{p,1}\left(t, x, \epsilon\right) + \delta\ \tilde{v}(t, x, \epsilon) + \mathcal{O}(\delta^2), \tag{2.3.69}$$

with $\tilde{\omega}, \tilde{b} \neq 0$. *Then, they have a zero-mode with homogeneous boundary conditions, namely a linear perturbation* (2.3.57) *with* $\lambda = 0$.

Analyzing the implications of this proposition, we observe that the predicted zero-mode belongs to the class of linear perturbations we are considering. The question now consists of clarifying which TPSs satisfy the particular conditions (2.3.67)-(2.3.68). First, we observe that $b_{p,2}(0, x_f, \epsilon/(1+\delta))$ and $b_{p,1}(t, x, \epsilon)$ have the same amplitude at the boundary with different frequency. Second, we have

$$\begin{cases} \omega_2 > \omega_1 & \text{if } \tilde{\omega} > 0,\ |\delta| \ll 1 \\ \omega_2 < \omega_1 & \text{if } \tilde{\omega} < 0,\ |\delta| \ll 1 \end{cases} \tag{2.3.70}$$

[4]As consequence of the presence of this particular mode, TPSs are not stable in the strict sense; nevertheless, if there are no additional instabilities, TPSs are stable in the sense of oscillatory solutions. This fact is illustrated with a basic example. Suppose that an ODE admits a continuous family of solutions of the form $s(t, \delta) = \cos((1+\delta)t)$, where $\delta \in \mathbb{R}$ is determined by the initial conditions. These solutions have a linear modes of the form $\tilde{s}(t, \delta) = -t\sin((1+\delta)t)$ as our solutions. In this case, the difference $|s(t, \delta) - s(t, 0)|$ cannot be arbitrary small at any time when $\delta \ll 1$; nevertheless, we can obtain a period $T(\delta)$ which guarantees that $|s(nT(\delta), \delta) - s(nT(\delta), 0)| = 0$ for $n = 0, 1, 2, \ldots$

Therefore, we conclude that the zero-mode appears in curves formed by TPSs with the same amplitude at the boundary, at points where the frequency has a local extrema (commonly denominated turning-point). In chapter 4 we will observe as these zero-modes at turning-points of the frequency form a threshold between stable and unstable TPSs.

Finally, note that Proposition 2.2 is formulated for a particular set of boundary conditions and specific powers for δ, nevertheless following the proof given in appendix A.3, these conditions can be extended to more general situations.

2.4 Holography

In this section we are going to briefly introduce holography, specifically, the main tools used on chapter 4. We will start summarizing certain features of anti-de Sitter spacetime (AdS), which is a solution of Einsteins equations, independently of holography. Nevertheless, as we will see after the presentation of the holographic principle, it is crucial for the denominated AdS/CFT conjecture; our framework in chapter 4.

2.4.1 Anti-de Sitter Spacetime

AdS is a maximally symmetric solution of the vacuum Einstein equations with negative cosmological constant $\Lambda < 0$,

$$R_{\mu\nu} - \frac{1}{2} R g_{\mu\nu} + \Lambda g_{\mu\nu} = 0. \tag{2.4.1}$$

A maximally symmetric spacetime has the maximum number of symmetries (linearly independent Killing vectors) that a $(d+1)$-dimensional spacetime can have: $(d+1)(d+2)/2$. For vacuum solutions there are three geometries which are associated with the sign of the cosmological constant: de Sitter ($\Lambda > 0$), Minkowski ($\Lambda = 0$) and anti-de Sitter ($\Lambda < 0$). In these cases the scalar curvature is related with the cosmological constant as

$$\Lambda = 2\frac{d-1}{d+1} R. \tag{2.4.2}$$

It shows that the previously mentioned spaces can also be classified by the sign of the curvature.

AdS, which we will write as AdS_{d+1} to denote that it has $d+1$ dimensions, can be represented as the restriction of a $(d+2)$-dimensional flat space with coordinates $(X_0, X_1, \ldots, X_d, X_{d+1}) \in \mathbb{R}^{2,d}$ and line element

$$ds^2 = -(dX_0)^2 + (dX_1)^2 + \ldots + (dX_d)^2 - (dX_{d+1})^2, \tag{2.4.3}$$

to a $d+1$-dimensional hypersurface determined by

$$-(X_0)^2 + \sum_{n=1}^{d} (X_n)^2 - X_{d+1}^2 = -l^2, \tag{2.4.4}$$

where $l > 0$ and is denominated AdS radius. Note that $\mathbb{R}^{2,d}$ is invariant under the group of transformations $O(d, 2)$ and therefore the hyperboloid defined by (2.4.4) also enjoys these symmetries.

Let us introduce different coordinate systems for AdS_{d+1} in order to discuss the causal structure. We start with *global coordinates* which cover the whole space (2.4.4):

$$\begin{aligned} X_0 &= l \sec(x) \sin(\tau), \\ X_{d+1} &= l \sec(x) \cos(\tau) \\ X_i &= l \tan(x) \Omega_i, \qquad i = 1, \ldots, d, \end{aligned} \tag{2.4.5}$$

where Ω_i are angular coordinates parameterizing $\mathbb{S}^{d-1}$. The line element (2.4.3) reduces to

$$ds^2_{AdS} = \frac{l^2}{\cos^2 x} \left(-d\tau^2 + dx^2 + \sin^2 x d\Omega^2_{d-1} \right), \tag{2.4.6}$$

where $\tau \in [0, 2\pi]$, $x \in [0, \pi/2)$, $\sum_i \Omega_i^2 = 1$. Note that at this point we have closed timelike curves $\mathbb{S}^1$. They can be avoided by extending $\mathbb{S}^1$ to $\mathbb{R}$, obtaining the denominated *universal covering space* [125]. In consequence, AdS_{d+1} covers half of the space $\mathbb{R} \times \mathbb{S}^d$. The conformal boundary is located at $x = \pi/2$ ($\cos^2 x = 0$), and we observe that the boundary is a timelike hypersurface conformal to the metric

$$ds^2 = -d\tau^2 + d\Omega^2_{d-1}. \tag{2.4.7}$$

Therefore in this global coordinates, the topology of the boundary is $\mathbb{R} \times \mathbb{S}^{d-1}$ (see [125] for further details).

Another common parametrization of AdS_{d+1} is known as the *Poincaré patch*:

$$\begin{aligned} X_0 &= \frac{1}{2z} \left(z^2 + l^2 + \vec{x}^2 - t^2 \right), \\ X_i &= \frac{x_i}{z} l, \qquad i = 1, \ldots, d-1, \\ X_d &= \frac{1}{2z} \left(z^2 - l^2 + \vec{x}^2 - t^2 \right), \\ X_{d+1} &= \frac{t}{z} l, \end{aligned} \tag{2.4.8}$$

where $t \in \mathbb{R}$, $\vec{x} = (x_1, \ldots, x_{d-1}) \in \mathbb{R}^{d-1}$, $z \in \mathbb{R}^+$ and $\vec{x}^2 = \sum_{i=1}^{d-1} x_i^2$. The line element takes the form

$$ds^2_{AdS} = \frac{l^2}{z^2} \left(-dt^2 + dz^2 + d\vec{x}^2 \right). \tag{2.4.9}$$

Note that these coordinates only parametrize half of the space due to the restriction $z \in \mathbb{R}^+$. In this case the conformal boundary ($z = 0$) has a different topology, it is conformal to Minkowski space $\mathbb{R}^{1,d-1}$,

$$ds^2 = -dt^2 + d\vec{x}^2. \tag{2.4.10}$$

Deeper details about AdS spacetime and its causal structure can be found in [125].

These two systems of coordinates have salient importance in the context of the AdS/CFT conjecture. As we will see later, the correspondence maps the dynamics in AdS_{d+1} with the behavior of a CFT on the d-dimensional boundary of this spacetime. Therefore, through this relation global coordinates provide CFTs on $\mathbb{R} \times \mathbb{S}^{d-1}$ and the Poincaré patch provides CFTs on $\mathbb{R}^{1,d-1}$.

2.4.2 Holographic Principle

The *holographic principle* is an idea introduced in the early nineties by 't Hooft [126] and Susskind [127]. It asserts that in a theory of quantum gravity the degrees of freedom of a $(d+1)$-dimensional region of spacetime are not proportional to the volume of the region (as is the case for conventional quantum field theories), but rather to the d-dimensional area of the region's boundary. If this observation holds, in the quantum regime gravity cannot be described as a local QFT because local fluctuations of the geometry are not fundamental degrees of freedom. Therefore, the holographic principle asserts that a theory of quantum gravity defined in a $(d+1)$-dimensional spacetime $\mathcal{M}$ and certain non-gravitational quantum system on a fixed d-dimensional spacetime $\mathcal{B}$ which corresponds with the boundary of the previous space, $\partial\mathcal{M} = \mathcal{B}$, are equivalent.

A precise realization of the holographic principle comes from string theory. In this case, the boundary theory consists of a QFT displaying a gauge symmetry, giving the denomination: gauge/gravity duality. The most famous example is the AdS/CFT correspondence proposed by Maldacena [16]. Note that there is no proof of the conjecture, nevertheless, a large number of non-trivial evidence exists [84]. This correspondence motivated our studies in chapter 4; therefore, we will introduce the basic ideas in the next subsection. There are many useful reviews about this topic, some of them are [83, 128, 129] and textbooks [84, 130].

2.4.3 The AdS/CFT Correspondence

As we already mentioned, the AdS/CFT correspondence asserts that geometries of a gravitational theory on an asymptotically AdS spacetime with boundary geometry $\mathcal{B}$ are associated with states of a CFT on $\mathcal{B}$. Some examples are: the vacuum state, low- and high-energy states of the CFT which are respectively equivalent to the empty spacetime, to small excitations of this space (gravitational waves) and to different geometries with the same asymptotic behavior as AdS. As we have mentioned in section 2.4.1 the boundary geometry is not fixed and depends on the coordinates. In AdS_{d+1}, for the Poincaré patch $\mathcal{B}$ is Minkowski space $\mathbb{R}^{1,d-1}$, while for global coordinates it is $\mathbb{R} \times \mathbb{S}^{d-1}$. This property can be summarized using the Fefferman-Graham theorem [131] (see also [132]), which asserts that the metric of asymptotically AdS spacetimes near the boundary can be written in

the form

$$ds^2 = \frac{l^2}{z^2}\left(dz^2 + \tilde{g}_{\mu\nu}(z,x)dx^\mu dx^\nu\right), \tag{2.4.11}$$

where the boundary is placed at $z = 0$. The near-boundary expansion of this metric satisfies

$$\tilde{g}_{\mu\nu}(z,x) = \tilde{g}_{(0)\mu\nu}(x) + \tilde{g}_{(2)\mu\nu}(x)z^2 + \ldots, \tag{2.4.12}$$

noting that in even boundary dimensions logarithmic terms must also be included. $g_{(0)\mu\nu}$ is the metric of $\mathcal{B}$, and higher terms depend on this one and in possible additional fields present in the bulk [133].

The most prominent example consists of the duality between IIB superstring theory on $AdS_5 \times S^5$ and $\mathcal{N} = 4$ Super Yang-Mills theory in $3+1$-dimensions. It relates free parameters on both sides of the correspondence as

$$\frac{\lambda}{4\pi N} = g_s, \qquad \lambda = \frac{l^4}{\alpha'^2}, \tag{2.4.13}$$

where l is the AdS radius, g_s the string coupling, α' is related to the string length as $l_s = \sqrt{\alpha'}$, g_{YM} is the Yang-Mills coupling, N is the rank of the gauge group $SU(N)$ and λ the 't Hooft coupling $\lambda = g_{YM}^2 N$. This identification is extremely useful due to the fact that it allows considering limits where one side becomes tractable. In consequence, we can extract information from the other side by using the correspondence.

As it was mentioned in the introduction, we are interested in dynamical properties of AdS ruled by Einstein's equations. Therefore, the convenient limit for our interests consists of reducing the gravity side to classical gravity. It is obtained by taking the string coupling to zero $g_s \to 0$ and by making the string length much smaller than the curvature, it is $\sqrt{\alpha'}/l \to 0$. Using (2.4.13) we observe that the limit taken on the gravity side leads to $\lambda \to \infty$, $N \to \infty$ and $g_{YM} \to 0$, obtaining a strongly coupled CFT on the other side. This limit is known as the *weak form* of the AdS/CFT conjecture and results in a weak/strong correspondence.

The precise map between these two different theories arises by matching the symmetries on both sides. This map allows establishing the denominated *holographic dictionary* of the AdS/CFT correspondence in terms of the equivalence of generating functions. Which consists of the Gubser-Klebanov-Polyakov-Witten (GKPW) relation [134, 135]

$$Z_{\text{string}} = Z_{CFT}. \tag{2.4.14}$$

The generating function of the CFT takes the form in Euclidean signature

$$Z_{CFT}\left[\phi_{(0)}\right] = e^{-W_{CFT}\left[\phi_{(0)}\right]} = \left\langle e^{\int d^d x \phi_{(0)}(x)\mathcal{O}(x)} \right\rangle_{CFT}, \tag{2.4.15}$$

where ϕ and $\mathcal{O}$ represent particular fields on the gravity and gauge sides respectively. The action was deformed with the presence of sources represented by $\phi_{(0)}$ (the leading term of the near-boundary expansion of ϕ),

$$S' = S - \int d^d x \phi_{(0)}(x)\mathcal{O}(x). \tag{2.4.16}$$

On the other hand, in the weak form of the correspondence that we are considering the gravity side is governed by the action $S_{SUGRA}[\phi]$. It consists of the Kaluza-Klein reduction of the type IIB supergravity on $\mathrm{AdS}_5 \times S^5$. The relation (2.4.14) is reduced to

$$S_{SUGRA}[\phi]\Big|_{\lim_{z\to 0}\phi(z,x)z^{\Delta-d}=\phi_{(0)}(x)} = W_{CFT}\left[\phi_{(0)}\right], \tag{2.4.17}$$

where Δ is the dimension of the operator $\mathcal{O}$ and $S_{SUGRA}[\phi]$ is evaluated on-shell, namely, the action is evaluated on field configurations ϕ, which solve the EOMs with $\phi_{(0)}$ as the leading term of the near-boundary expansion. This relation provides the necessary information to calculate the connected correlation functions for the operator $\mathcal{O}$ of the CFT through the gravity side. They can be computed by applying functional derivatives on the generating function with respect to the source, $\phi_{(0)}$,

$$\langle \mathcal{O}(x_1)\dots\mathcal{O}(x_n)\rangle_{CFT,c} = -\frac{\delta}{\delta\phi_{(0)}(x_1)}\cdots\frac{\delta}{\delta\phi_{(0)}(x_n)} S_{SUGRA}[\phi]\Big|_{\lim_{z\to 0}\phi(z,x)z^{\Delta-d}=\phi_{(0)}} \tag{2.4.18}$$

The action $S_{SUGRA}[\phi]$ evaluated on-shell, with field configurations which present asymptotic expansions with the leading power $\phi_{(0)}$, is typically divergent. It is a consequence of the integration at both limits $z \to 0$ (denominated UV) and $z \to \infty$ (denominated IR). It claims for a renormalization process which leaves the correlation functions finite. The developed procedure is known as *holographic renormalization* [136] (see [133] for a review). The idea consists of regularising the action S_{SUGRA} by restricting the integral to $z \geq \epsilon$ and isolating the divergent terms when $\epsilon \to 0$. This action is denoted by S_{reg}. Once it is done we add counterterms which remove the divergent terms. In consequence, the actual action we must consider has the form

$$S_{ren} = \lim_{\epsilon\to 0}\left(S_{reg} + S_{GH} + S_{ct}\right), \tag{2.4.19}$$

where S_{GH} is the Gibbons-Hawking term [137] and the counterterms action. Hence, the correct expression of the correlation functions (2.4.18) is

$$\langle \mathcal{O}(x_1)\dots\mathcal{O}(x_n)\rangle_{CFT,c} = -\frac{\delta}{\delta\phi_{(0)}(x_1)}\cdots\frac{\delta}{\delta\phi_{(0)}(x_n)} S_{ren}[\phi]\Big|_{\lim_{z\to 0}\phi(z,x)z^{\Delta-d}=\phi_{(0)}} \tag{2.4.20}$$

Let us introduce the example of a massive scalar field

$$S_\phi = -\frac{1}{2}\int dz dx^d \sqrt{-g}\left(\partial_\mu\phi\partial^\mu\phi + m^2\phi^2\right), \tag{2.4.21}$$

where the EOM is

$$\left(\Box_g - m^2\right)\phi = 0, \qquad \Box_g = \frac{1}{\sqrt{-g}}\partial_\mu\left(\sqrt{-g}g^{\mu\nu}\partial_\nu\right). \tag{2.4.22}$$

Considering an asymptotically AdS geometry and the near-boundary form of the metric $g_{\mu\nu}$ expressed as (2.4.11), we observe that the two independent solutions in z of the Klein-Gordon equation (it is a second order differential equation in each variable) have leading terms at $z \to 0$:

$$\phi_-(z,x) \sim \phi_-(x) z^{\Delta_-}, \qquad \phi_+(z,x) \sim \phi_+(x) z^{\Delta_+}, \tag{2.4.23}$$

where the powers $\Delta_\pm$ satisfy

$$\Delta_\pm = \frac{d}{2} \pm \sqrt{\left(\frac{d}{2}\right)^2 + m^2 l^2}. \tag{2.4.24}$$

and thereby $\Delta_+ \geq \Delta_-$. Inserting a field with leading term $\phi(z,x) \sim \phi_\alpha(x) z^\alpha$ in S_ϕ we observe that it is finite if $\alpha \geq d/2 - 1$. We say that a solution of the EOM is normalizable (non-normalizable) if it leaves the action finite (divergent). In consequence, ϕ_+ is normalizable due to $\Delta_+ \geq d/2$ by definition, while Δ_- depends on d and $m^2 l^2$. This last exponent is normalizable if the mass satisfies the inequality

$$-\left(\frac{d}{2}\right)^2 \leq m^2 l^2 \leq -\left(\frac{d}{2}\right)^2 + 1, \tag{2.4.25}$$

allowing the exchange of roles of ϕ_+ and ϕ_- in our interpretations. The upper bound comes from the previous requirement that the action remains finite, while the lower one is known as Breithenlohner-Freedman bound [138, 139]. Despite the instability of scalar fields with negative m^2 in flat space, in the case of AdS_{d+1} they are stable for

$$m^2 \geq -\left(\frac{d}{2l}\right)^2. \tag{2.4.26}$$

The holographic renormalization procedure we have described above identifies the next fields on the gravity side, with the vacuum expectation values (vev) of operators and their sources on the QFT in odd dimensions (see [133, 136] for even dimensions), for example:

- Scalar field $\phi(z,x) \leftrightarrow$ Scalar operator $\mathcal{O}$:

$$\langle \mathcal{O}(x) \rangle_s = \frac{1}{\sqrt{-g_{(0)}(x)}} \frac{\delta S_{ren}}{\delta \phi_{(0)}(x)} = l^{d-1}(2\Delta_+ - d)\phi_{\Delta_+}(x). \tag{2.4.27}$$

- Metric $g_{\mu\nu} \leftrightarrow$ Energy-momentum tensor $\mathcal{T}_{ij}$:

$$\langle \mathcal{T}_{ij}(x) \rangle = \frac{2}{\sqrt{-g_{(0)}(x)}} \frac{\delta S_{ren}}{\delta g^{ij}_{(0)}(x)} = \frac{d l^{d-1}}{16\pi G} g_{(d),ij}(x). \tag{2.4.28}$$

Here $\phi, g_{\mu\nu}$ live in the bulk while $\mathcal{O}, \mathcal{T}_{ij}$ on the boundary, with i, j denoting boundary coordinates.

These 1-point functions are not independent, they can be related through Ward identities. They are obtained by considering fluctuations of the different sources present in our system

and imposing the invariance of the action [133, 136]. For the case of a scalar field coupled to gravity the variation of the action takes the form

$$\delta S_{ren} = \int d^d x \sqrt{g_{(0)}} \left(\frac{1}{2} \langle \mathcal{T}_{ij} \rangle \, \delta g^{ij}_{(0)} + \langle \mathcal{O} \rangle \, \delta \phi_{(0)} \right) \tag{2.4.29}$$

with fluctuations

$$\delta g^{ij}_{(0)} = - \left(\partial^i \xi^j + \partial^j \xi^i \right), \qquad \delta \phi_{(0)} = \xi^i \partial_i \phi_{(0)}. \tag{2.4.30}$$

Therefore, in order to leave (2.4.29) invariant the next Ward identity must be satisfied

$$\partial^i \langle \mathcal{T}_{ij} \rangle = - \langle \mathcal{O} \rangle \, \partial_j \phi_{(0)}. \tag{2.4.31}$$

In chapter 4 we will study dynamical properties of asymptotically AdS spacetimes subject to time-dependent boundary conditions. The tools developed in the current section will be useful to interpret the results in the context of holography, mapping the phenomenology to the behavior of the CFT present on the boundary.

3

Cubic Resonant Systems

This chapter is motivated by well known nonlinear equations that appear in many physical contexts. We will address an important subset where the phenomenon of resonance drives the dynamics at long times. We will find remarkable effects, some of which strongly resemble the behavior unraveled in the FPUT problem [61] (see [62] for a modern review). Trying to cover a vast range of physical systems we will maintain a high degree of generality. For this reason, we will study the weakly nonlinear regime of *fully resonant* PDEs with cubic nonlinear terms. In particular, we will focus on the resonant condition $w_n + w_m = w_k + w_j$. Of course, more general systems can be considered based on additional resonances of the form $w_n \pm w_m = \pm w_k \pm w_j$. Nevertheless, as we already argued in sections 2.1 and 2.2, the channel $w_n + w_m = w_k + w_j$ is always present for this kind of systems with odd nonlinearities, in contrast with the other ones. After the development of our results we will present a large number of models which show that this restriction to a single resonant channels is not too restrictive.

Our starting point will be the *resonant system* derived in section 2.2,

$$i\frac{d\alpha_n}{d\tau} = \sum_{m=0}^{\infty}\sum_{k=0}^{n+m} C_{nmk(n+m-k)}\alpha_k\alpha_{n+m-k}\bar{\alpha}_m, \tag{3.0.1}$$

where α_n are complex dynamical variables (n ranges from 0 to ∞) and the *interaction coefficients*, C_{nmkl}, satisfy the symmetries

$$C_{nmkl} = C_{mnkl} = C_{nmlk} = C_{klnm}. \tag{3.0.2}$$

These symmetries are pretty common among resonant models, and therefore they do not constrain too much the systems covered by (3.0.1)-(3.0.2).

The resonant system (3.0.1) is Hamiltonian with the Hamiltonian

$$H = \sum_{\substack{n,m,k,l=0 \\ n+m=k+l}}^{\infty} C_{nmkl}\bar{\alpha}_n\bar{\alpha}_m\alpha_k\alpha_l \tag{3.0.3}$$

and the symplectic form $i\sum_n d\bar{\alpha}_n \wedge d\alpha_n$. The symmetry conditions on C_{nmkl} mentioned under (3.0.1) are straightforwardly understood from this expression for the Hamiltonian, and in particular, they ensure that the Hamiltonian is real. Besides the Hamiltonian, the system generically admits (for any values of the interaction coefficients C) the following two conserved quantities:

$$N = \sum_{n=0}^{\infty} |\alpha_n|^2, \tag{3.0.4}$$

$$J = \sum_{n=0}^{\infty} n|\alpha_n|^2, \tag{3.0.5}$$

which follow by Noether's theorem from the global and local phase rotation symmetries,

$$\alpha_n \to e^{i\varphi}\alpha_n, \qquad \alpha_n \to e^{in\theta}\alpha_n, \tag{3.0.6}$$

respectively. Additional structures may arise for specific values of C.

The resonant system has an additional salient property. After the derivation of (3.0.1) from the original system the dependence on the small nonlinearity parameter has been completely scaled out with the introduction of the slow time τ, and there are no small parameters left. In fact, (3.0.1) enjoys a scaling symmetry:

$$\alpha_n(\tau) \to \lambda\alpha_n(\lambda^2\tau), \tag{3.0.7}$$

for any λ. As long as $|\alpha_n|$ and $\lambda|\alpha_n|$ are such that the original system is suitably approximated by (3.0.1), the relevant dynamics is the same.

Note that (3.0.1) is not exactly the resonant system derived in (2.2.43) or (2.2.71); nevertheless they can be rewritten in this form through the transformation

$$\alpha_n \to \alpha_n/\sqrt{w_n}, \qquad C_{nmkj} \to \sqrt{w_n w_m w_k w_j}C_{nmkj}. \tag{3.0.8}$$

This kind of systems often arise in weakly nonlinear analysis of PDEs with cubic nonlinearity whose spectrum of frequencies of linearized perturbations is fully resonant. Examples of such equations are the Gross-Pitaevskii equation describing Bose-Einstein condensates in harmonic traps [68–74], various nonlinear problems in anti-de Sitter spacetime [34–36, 41, 75, 76, 78, 81], in particular, those studied in relation to its conjectured nonlinear instability [6, 42], and an asymptotically anti-de Sitter wormhole spacetime [140, 141]. In such situations, because of the presence of resonances, amplitudes and phases of linearized modes acquire slow drifts due to effects of nonlinearities (no matter how small the nonlinearities are). The leading part of this drift effect is accurately described by (3.0.1).

This chapter is divided as follows. In section 3.1, we impose constraints on the interaction coefficients which allow for an analytic treatment of (3.0.1). In particular, we will construct a very large class of resonant systems that admits special analytic solutions, which furthermore display periodic perfect energy returns to the initial configurations as well as families of stationary states bifurcating from single-mode solutions. Our analysis also provides an additional conserved quantity for all of these systems, and the general solution of the condition on the interaction coefficients producing a very large collection of resonant systems.

Despite the large class of systems constructed in section 3.1, we are aware that an analytic resolution of (3.0.1) is not commonly accessible. For this reason, in section 3.2 we develop a systematic analytic approach by focusing on solutions with spectra localized around single-mode solutions. This analysis is common for almost any collection of interaction coefficients and allows extracting clear information for its range of validity. In particular we explicitly show the cases of the two lowest modes.

In section 3.3, a collection of models displaying a resonant system of the form (3.0.1) is presented. We see as a group of them belonging to the class of systems developed in section 3.1, while the other ones are studied with the tools of section 3.2. As a particular example of the second group of models, we consider a spherically symmetric massless scalar field in AdS_4. This allows us to demonstrate that in the gravitational case the energy returns are not exact. Furthermore, our analysis predicts and explains specific integer numbers of direct-reverse cascade sequences that result in particularly accurate energy returns (elaborate hierarchies of more and less precise returns arise if one waits for appropriate longer multiple periods in this manner).

Finally, in section 3.4, we give a global view of the results obtained in this chapter.

3.1 Solvable Cubic Resonant Systems

In the resonant system (3.0.1), the information related to the original model from which it was derived is completely encoded in the interaction coefficients. Taking advance of this fact, we decided to study (3.0.1) in a general form, imposing certain restrictions on C_{nmkl} to obtain analytic solutions. To this end, we shall assume the symmetries (3.0.2) and $C_{0000} \neq 0$, which allows one to rescale the time variable and set

$$C_{0000} = 1, \tag{3.1.1}$$

a convention we shall adopt through this section.

In order to ease the presentation of this section, we only present the main results, leaving the proofs and technical details for appendix A.3.2.

3.1.1 Three-Dimensional Invariant Manifolds

Before introducing the main results of this section we require the following definitions, all of which only require knowledge of C_{nmkl} and of a real number $\gamma \geq 1/2$,

$$\beta \equiv C_{2020}, \qquad \gamma \equiv \left(\frac{f_0 f_2}{f_1^2}\right)^2, \qquad G \equiv \frac{1}{2\gamma - 1}, \tag{3.1.2}$$

$$f_n = \begin{cases} \dfrac{1}{\sqrt{n!}} & \text{if } \gamma = \frac{1}{2}, \\ \sqrt{\dfrac{(G)_n}{n!}} & \text{if } \gamma > \frac{1}{2}, \end{cases} \tag{3.1.3}$$

$$g_p^{(n,m)} \equiv \sum_{k=0}^{n+m} k^p \frac{f_k f_{n+m-k}}{f_n f_m} C_{nmk,n+m-k}. \tag{3.1.4}$$

The case $\gamma < 1/2$ will not be studied because, in these situations f_n is imaginary and has multiple zeros. Additionally, all the models we currently know have $\gamma \geq 1/2$. The main results of this section consists of the next proposition

Proposition 3.1.1.1: *Given C_{nmkl}, if there exists $\gamma \geq 1/2$ such that the following expressions are satisfied*

$$g_0^{(n,m)} = 1, \qquad g_2^{(n,m)} = c_2(n^2 + m^2) + c_1 nm + c_0(n+m), \quad \forall n, m = 0, 1, 2 \ldots \tag{3.1.5}$$

then, c_0, c_1, c_2 are univocally determined

$$c_0 = \frac{1 - 2\beta}{2}, \qquad c_1 = 2\gamma(1 - 2\beta), \qquad c_2 = \beta, \tag{3.1.6}$$

the resonant system (3.0.1) *admits solutions of the form*

$$\alpha_n(\tau) = f_n \left(b(\tau) + n a(\tau)\right) \left(p(\tau)\right)^n, \tag{3.1.7}$$

provided that three ordinary differential equations[1]*, are satisfied by $a(t)$, $b(t)$ and $p(t)$. For all solutions of* (3.0.1) *of the form* (3.1.7)*, $|\alpha_n|^2$ is periodic in time*[2] *and the quantity*

$$Z = \begin{cases} \displaystyle\sum_{n=0}^{\infty} \sqrt{(n+1)(n+G)}\, \bar{\alpha}_{n+1} \alpha_n & \text{if } \gamma > \frac{1}{2}, \\ \displaystyle\sum_{n=0}^{\infty} \sqrt{n+1}\, \bar{\alpha}_{n+1} \alpha_n & \text{if } \gamma = \frac{1}{2}. \end{cases} \tag{3.1.8}$$

is conserved.

[1] These equations can be found in appendix A.3.2, (A.3.56)-(A.3.58).

[2] Its exact expression can be found in the proof of this proposition, given in appendix A.3.2.

Additionally, we also obtained the following results

Proposition 3.1.1.2: (3.1.7) *contains a biparametric family of stationary solutions*[3] *of the form*

$$p = qe^{-i\omega(q,c)\tau}, \qquad b = \beta(q,c)e^{-i\lambda(q,c)\tau}, \qquad a = \kappa(q,c)e^{-i\lambda(q,c)\tau}, \tag{3.1.9}$$

for which $Z = 0$.[4]

Proposition 3.1.1.3: *for a given resonant system* (3.0.1) *satisfying* (3.1.5), *the range of motion of* $|p|^2$, *defined by* $(1-p_-^2)/(1-p_+^2)$ *where* $p_+ \equiv max(|p|)$ *and* $p_- \equiv min(|p|)$, *is uniformly bounded*[5] *for all solutions within the ansatz* (3.1.7).

This sequence of propositions reports interesting results. Let us explain them in a schematic form.

- Suppose that there is a set of interaction coefficients C_{nmkl} which satisfy the symmetries (3.0.2) and also $C_{0000} \neq 0$, such that we can rescale time and set $C_{0000} = 1$.
- We choose a particular value of $\gamma \geq 1/2$.
- We calculate f_n with (3.1.3) and (3.1.2).
- We calculate $g_0^{(n,m)}$ and $g_2^{(n,m)}$ with (3.1.4).
- If $g_0^{(n,m)}$ and $g_2^{(n,m)}$ satisfy (3.1.5) we can apply Proposition 3.1.1.1.
- Then, the ansatz (3.1.7) forms a three-dimensional manifold of solutions of the resonant system, which is reduced to three ODEs parametrized by β and γ. The energy per mode of these solutions, $|\alpha_n|^2$ is periodic and Z conserved during the evolution.
- In particular, there is a biparametric family of stationary solutions defined by (3.1.7) and $Z = 0$.
- For solutions of (3.1.7) the energy transfer to higher modes cannot be made more and more turbulent[6] without limit by tuning the initial conditions.

We want to remark that the ansatz (3.1.7) contains the first two modes initial data

$$|\alpha_0(0)|, |\alpha_1(0)| \neq 0, \qquad \alpha_{n\geq 2}(0) = 0. \tag{3.1.10}$$

[3]The denomination "stationary" comes from the fact that modes do not exchange energy, $|\alpha_n(t)|^2 = \text{cte}\ \forall n$.

[4]the explicit expressions of $\omega, \beta, \lambda, \kappa$ in terms of q, c can be found in appendix A.3.2.

[5]The bound only depends on γ and it can be found in the appendix A.3.2, (A.3.89).

[6]By "turbulent" we mean the process of excitation of α_n with high values of n starting from initial data supported by low-lying α_n. Since α_n with high n correspond to amplitudes of short wavelength modes of the linearlized system, thus excitation of α_n with high n means weakly nonlinear transfer of energy to short wave length, which is the definition of weak turbulence [7].

It is obtained in the limit $p(0) \to 0$ and $a(0) \to \infty$ while the product $a(0)p(0)$ goes to a non-vanishing finite number. In consequence, for systems belonging to the family presented above, the two-mode initial data (3.1.10) displays periodic energy transfer between modes.

These results also report an important fact. Sometimes the computation of explicit formulas C_{nmkl} in terms of n, m, k, l, is difficult, it can implicate complicated integrals or summations which make the explicit expressions unmanageable. Nevertheless, we have proved that they are not always required to obtain analytic results. On occasions, the direct calculation of $g_0^{(n,m)}$ and $g_2^{(n,m)}$ is more accessible thanks to some summation properties of the eigenfunctions of the problem. If they satisfy (3.1.5), Propositions 3.1.1.1 to 3.1.1.3 are applied and a great amount of information is immediately extracted.

We want to remark that β has little impact on the dynamics within the invariant manifold (3.1.7) (see (A.3.75) in appendix A.3.2). For solutions of the form (3.1.7), the spectrum $|\alpha_n|^2$ only depends on β through overall time scaling, while the phases of α_n may be β-sensitive. The value $\beta = 1/2$ is special, in this case any solution covered by the three-dimensional manifold is a stationary state.

3.1.2 A Stronger Condition

We have previously established that imposing the summation identities (3.1.5) provides for the existence of three-dimensional invariant manifolds of the cubic resonant system (3.0.1), within which the flow is analytically solvable. We have also seen that, within these three-dimensional invariant manifolds, the complex quantity Z, given by (3.1.8), is conserved. We shall now explore a stronger condition one can impose on the interaction coefficients of (3.0.1) which enforces this new conservation law for all solutions, irrespectively of whether they belong to the three-dimensional invariant manifolds. We note that conservation of Z has been previously known in resonant systems related to the Gross-Pitaevskii equation [68, 72, 73], but not for other systems in the large class considered here. In particular, our derivations automatically supply this extra conserved quantity for a few explicit systems in the literature for which it has been previously unknown [75, 76].

This condition is

$$\mathcal{D}_{nmkl} = 0, \tag{3.1.11}$$

where the central object $\mathcal{D}$ is defined by

$$\mathcal{D}_{nmkl} = \tag{3.1.12}$$

$$\begin{cases} (n-1+G)\, S_{(n-1)mkl} + (m-1+G)\, S_{n(m-1)kl} - (k+1)S_{nm(k+1)l} - (l+1)S_{nmk(l+1)} & \text{if } \gamma > \frac{1}{2}, \\ S_{(n-1)mkl} + S_{n(m-1)kl} - (k+1)S_{nm(k+1)l} - (l+1)S_{nmk(l+1)} & \text{if } \gamma = \frac{1}{2}. \end{cases}$$

Where G is given by (3.1.2), f_n is given by (3.1.3), and we have introduced the definition of S_{nmkl}:

$$S_{nmkl} \equiv \begin{cases} f_n f_m f_k f_l C_{nmkl} & n, m, k, l \geq 0, \\ 0 & \text{if any index is negative}, \end{cases} \tag{3.1.13}$$

From direct inspection, conditions (3.1.11)-(3.1.12) only relate the values of S_{nmkl} with the same value of $n+m-k-l$. The sectors with different values of $n+m-k-l$ completely decouple from each other. For that reason, we can choose to only look at $n+m=k+l+1$, which contains all the interaction coefficients in our equation (3.0.1), having (3.1.11)-(3.1.12) satisfied in this sector is sufficient to have all of our subsequent conclusions on the dynamics of (3.0.1) hold. Or we may as well impose (3.1.11)-(3.1.12) for all values of n, m, k, l, as we shall do in the next section, since the values of S_{nmkl} for $n+m \neq k+l+1$ do not contribute to the dynamics of (3.0.1), and may be chosen as we wish. In particular, may be chosen to satisfy (3.1.11)-(3.1.12), for example setting them to zero.

From the imposition of (3.1.11) three crucial propositions are derived:

Proposition 3.1.2.1: $\mathcal{D}_{nmkl} = 0$ *implies* (3.1.5). *Therefore, Propositions 3.1.1.1 to 3.1.1.3 apply to any resonant system satisfying this condition.*

Proposition 3.1.2.2: *if the interaction coefficients satisfy* $\mathcal{D}_{nmkl} = 0$, Z, *defined in* (3.1.8), *is a conserved quantity of the resonant system* (3.0.1).

Proposition 3.1.2.3: *if* $\mathcal{D}_{nmkl} = 0$, *all solutions of* (3.1.7) *can be reached by acting on the stationary solutions* (3.1.9) *with symmetry transformations associated with the conserved quantities* $N, J, \mathrm{Re}(Z), \mathrm{Im}(Z)$, (they can be found in (3.0.4), (3.0.5), (3.1.8) respectively).

Again, the schematic description of these results consists of:

- Suppose that there is a set of interaction coefficients C_{nmkl} which satisfy the symmetries (3.0.2) and also $C_{0000} \neq 0$, such that we can rescale time and set $C_{0000} = 1$.
- We choose a particular values of $\gamma \geq 1/2$.
- We calculate f_n with (3.1.3) and (3.1.2).
- We calculate S_{nmkl} with (3.1.13).
- If $\mathcal{D}_{nmkl} = 0$ for $n+m-k-l = 1$ the Propositions 3.1.2.1 to 3.1.2.3 apply to the resonant system subject to C_{nmkl}. Then, the results of the previous sections apply to this resonant system.
- The complex quantity Z is a conserved quantity of the resonant system.
- More direct implications will be obtained in the subsequent sections.

It is exciting to observe that despite the vast content of these propositions, they only depend on $\mathcal{D}_{nmkl} = 0$, which in the majority of cases is almost trivial to check. In section 3.1.1 the key conditions required the computation of summations $g_0^{(n,m)}$ and $g_2^{(n,m)}$, given in (3.1.4), while here we have reduced the computational cost, substituting the summation by a simple algebraic equation. As we will see in the subsequent sections, the analytic properties of $\mathcal{D}_{nmkl} = 0$ are not only restricted to the three-dimensional manifold delimited by (3.1.7). It provides an excellent manageability for analytic manipulations.

3.1.3 A Stronger Condition: General Solution

Condition $\mathcal{D}_{nmkl} = 0$ is a linear finite difference equation that one can hope to analyze explicitly. In fact, in this section we shall solve it in terms of the generating function corresponding to the interaction coefficients. This will completely characterize resonant systems satisfying $\mathcal{D}_{nmkl} = 0$. Below we present results for the two relevant cases in (3.1.12), $\gamma > 1/2$ and $\gamma = 1/2$, technical details and proofs can be found in appendix A.3.2.

We want to find solutions to $\mathcal{D}_{nmkl} = 0$, given in (3.1.11)-(3.1.12), $(\gamma > 1/2)$

$$(n-1+G)S_{(n-1)mkl}+(m-1+G)S_{n(m-1)kl}-(k+1)S_{nm(k+1)l}-(l+1)S_{nmk(l+1)} = 0 \quad (3.1.14)$$

or $(\gamma = 1/2)$

$$S_{(n-1)mkl} + S_{n(m-1)kl} - (k+1)S_{nm(k+1)l} - (l+1)S_{nmk(l+1)} = 0. \quad (3.1.15)$$

Both of them subject to symmetries $S_{nmkl} = S_{mnkl} = S_{nmlk} = S_{klnm}$. Introducing the generating functions for S_{nmkl},

$$S(y,z,v,w) = \sum_{n,m,k,l=0}^{\infty} S_{nmkl}\, y^n z^m v^k w^l, \quad (3.1.16)$$

we can collect the information of (3.1.14) or (3.1.15) in PDEs for $S(y,z,v,w)$ by $(\gamma > 1/2)$

$$\sum_{n,m,k,l=0}^{\infty} \big[y(y\partial_y + G)S_{n-1,mkl}y^{n-1}z^m v^k w^l + z(z\partial_z + G)S_{n,m-1,kl}y^n z^{m-1}v^k w^l$$
$$-\partial_v S_{nm,k+1,l}y^n z^m v^{k+1}w^l - \partial_v S_{nmk,l+1}y^n z^m v^k w^{l+1}\big] = 0, \quad (3.1.17)$$

where we must enforce $S_{nmkl} = 0$ for any negative values of the indices, which amounts to $S(y,z,v,w)$ being non-singular near the origin. Hence, we obtain the differential equation for $\gamma > 1/2$

$$y(y\partial_y + G)S + z(z\partial_z + G)S - (\partial_v + \partial_w)S = 0, \quad (3.1.18)$$

and for $\gamma = 1/2$

$$(y+z)S - (\partial_v + \partial_w)S = 0. \quad (3.1.19)$$

Then, two new propositions can be constructed.

Proposition 3.1.3.1: *the general solution of* (3.1.18), *subject to the symmetries inhered from* S_{nmkl} *and the regularity of* (3.1.16) *and its derivatives at the origin, is*

$$S(y,z,v,w) = \frac{\mathcal{F}\left(\ln\left[\frac{(1-vy)(1-wz)}{(1-vz)(1-wy)}\right]\right)}{[(1-vy)(1-vz)(1-wy)(1-wz)]^{G/2}}, \quad (3.1.20)$$

where $\mathcal{F}(x) = \mathcal{F}(-x)$ *is an arbitrary symmetric function only restricted by regularity.*

Proposition 3.1.3.2: *the general solution of* (3.1.19), *subject to the symmetries inhered from* S_{nmkl} *and the regularity of* (3.1.16) *and its derivatives at the origin, is*

$$S(y,z,v,w) = \mathcal{G}(y-z, v-w)e^{(y+z)(v+w)/2}, \tag{3.1.21}$$

where $\mathcal{G}$ *is non-singular at the origin, even in both arguments and symmetric under the permutation of the two arguments.*

With these two propositions we have obtained all the interaction coefficients that satisfy $\mathcal{D}_{nmkl} = 0$, and in consequence also the Propositions 3.1.1.1 to 3.1.1.3 and 3.1.2.1 to 3.1.2.3. An interesting question that naturally emerges now is the possibility of relating each set of interaction coefficients acquired from (3.1.20) or (3.1.21), with the original system from which the resonant equation (3.0.1) was derived. Currently, it is an open question which probably has a negative answer, because once we apply the averaging method or the multi-scales method, part of the information about the original system is neglected, leaving only the resonant channels. Nevertheless, we are engaged by the idea of decoding the information contained in the interaction coefficients. For the moment we can only go in one direction, from the full system to the resonant one and checking if $\mathcal{D}_{nmkl} = 0$ is satisfied.

Note also that the general expressions of the generating functions depend on G (γ) but they have arbitrary functions. This fact means that for each γ there are infinite resonant systems satisfying $\mathcal{D}_{nmkl} = 0$. This arbitrariness, is also transferred to β

$$\beta \equiv C_{0202} = \frac{1}{4}\partial_z^2\partial_w^2 S(y,z,v,w)\Big|_{y,z,v,w=0}, \tag{3.1.22}$$

through the value of its derivatives $\mathcal{F}'(0)$ and $\mathcal{F}''(0)$ at the origin ($\mathcal{G}^{(1,1)}(0,0)$ and $\mathcal{G}^{(2,0)}(0,0)$ if $\gamma = 1/2$). In consequence, C_{nmkl} are not completely determined by (γ, β); nevertheless, the three-dimensional manifold, given by $\alpha_n = f_n(b+na)p^n$, is completely determined by these two parameters (see (A.3.56)-(A.3.58) in appendix A.3.2). For each system with the same values of γ and β, the solutions contained in the ansatz display the same dynamics.

3.1.4 Complex Plane Representation and Stationary States

Following with our development of the family of resonant systems given by $\mathcal{D}_{nmkl} = 0$, we are going to take advantage of the results obtained in the previous section to construct a complex plane representation of (3.0.1). Nevertheless, this section only contains the information we have considered necessary for a global understanding; technical details can be found in appendix A.3.2.

The results are properly expressed in terms of the rescaled variables

$$\beta_n = \frac{\alpha_n}{f_n}, \tag{3.1.23}$$

and the following generating functions:

$$u(\tau,z) = \sum_{n=0}^{\infty} \beta_n z^n, \qquad \tilde{u}(\tau,z) = \sum_{n=0}^{\infty} \frac{\bar{\beta}_n}{z^n}, \tag{3.1.24}$$

so that

$$\beta_n(\tau) = \frac{1}{2\pi i}\oint \frac{dz}{z^{n+1}} u(\tau, z), \qquad \bar{\beta}_n = \frac{1}{2\pi i}\oint dz\, z^{n-1}\, \tilde{u}(\tau, z). \tag{3.1.25}$$

Combining the resonant system (3.0.1) with (3.1.13), (3.1.23), (3.1.25), Propositions 3.1.3.1, 3.1.3.2, multiplying with z^n and summing over n, one gets the complex plane representation of (3.0.1) for the family of systems determined by (3.1.11)-(3.1.12):

$$\frac{i}{\Gamma(G)}\partial_\tau \partial_z^{G-1}(z^{G-1}u(\tau, z)) = \frac{1}{(2\pi i)^3}\oint \frac{ds}{s}\oint \frac{dv}{v}\oint \frac{dw}{w} S(z, s, 1/v, 1/w)\tilde{u}(\tau, s)u(\tau, v)u(\tau, w), \tag{3.1.26}$$

with Γ being the usual Euler's Γ-function, z, s, v, w complex variables and ∂_z^{G-1} a fractional derivative (see appendix A.3.2).

Making use of this representation, we have obtained stationary states of the form

$$\alpha_n(\tau) = A_n e^{-i\lambda\tau} \tag{3.1.27}$$

bifurcating from single-mode ($\alpha_n = 0\ \forall n \neq k$) that solve (3.0.1), where $\lambda \in \mathbb{R}$ and A_n are complex constants. These single-mode solutions supported by mode number k are present in any resonant system of the form (3.0.1), irrespectively of the values of the interaction coefficients C_{nmkl}. The precise structure of these stationary states can be concisely written in terms of derivatives of the generating function $u(\tau, z)$ such that

$$u(\tau, z) = e^{-i\lambda\tau}u(z), \qquad \partial_z^{G-1}(z^{G-1}u(z)) = \frac{(\bar{p} - z)^N}{(1 - pz)^{N+G}}. \tag{3.1.28}$$

This structure consists of different families of stationary solutions; each of them is determined by $N = 0, 1, 2, \ldots$ and continuously parametrized by p. Indeed, if $p = 0$, $\partial_z^{G-1}(z^{G-1}u)$ is proportional to z^N, and hence u itself is proportional to z^N, i.e., the only nonvanishing α_n is α_N, a single-mode solution. We must clarify that the above formula was originated as a guess based on numerical experimentation, once the ansatz was established an analytic proof was developed through (3.1.26) (see appendix A.3.2 for more in-depth details).

We have specified $u(z)$ through the result of acting on it with $\partial_z^{G-1}z^{G-1}$. What about $u(z)$ itself? We can say that it is of the form

$$u(z) = \sum_{k=0}^{N} \frac{c_k}{(1 - pz)^{k+1}}, \tag{3.1.29}$$

though we are not aware of simple explicit expressions for c_k. In terms of modes these solutions have the form

$$\alpha_n(\tau) = f_n p(\tau)^n \sum_{k=0}^{N} n^k a_k(p(\tau)), \tag{3.1.30}$$

where a_k are completely characterized by p.

3.1.5 Additional Families of Solvable Resonant Systems

Until this point we have studied a kind of interaction coefficients which provided solutions of the form (3.1.7). The condition for the closure of the ansatz consisted of the summation identities (3.1.5). In this section we are going to explore the existence of a more general ansatz and the required identities for its closure. Specifically, we will focus on a polynomial solution of the form

$$\alpha_n(\tau) = f_n p(\tau)^n \sum_{i=0}^{N} a_i(\tau) n^i. \tag{3.1.31}$$

Our interest consists of obtaining an intuitive notion about the form of the summations $g_p^{(n,m)}$, (3.1.4), which the interaction coefficients must satisfy to provide the closure of the ansatz considering the functions a_i completely free. Of course, even if we discard (3.1.31), additional constraints for a_i can appear which validate a restricted version. Examples of these restricted versions are the stationary solutions (3.1.30) obtained in the previous section. The next proposition provides some light to this question.

Proposition 3.1.5.1: *If the summations* (3.1.4) *have the form*

$$g_l^{(n,m)} = \sum_{i=0}^{\kappa l+\delta} g_i n^i m^{\kappa l+\delta-i}, \tag{3.1.32}$$

with $\kappa, \delta \in \mathbb{N}$, $g_i \in \mathbb{R}$ *such that* $g_l^{(n,m)} = g_l^{(m,n)}$. *The ansatz* (3.1.31) *only closes in* (3.0.1), *leaving all the function* a_i *and* p *free, in the next situations*

$$g_l^{(n,m)} = \sum_{i=0}^{l} g_i n^i m^{l-i} \quad \text{and } N = 1 \tag{3.1.33}$$

$$g_l^{(n,m)} = \sum_{i=0}^{l+1} g_i n^i m^{l+1-i} \quad \text{and } N = 0 \tag{3.1.34}$$

Note that (3.1.33) coincides (after the appropriate rescaling to achieve (3.1.1)) with the identities (3.1.5) and the ansatz (3.1.7). On the other hand (3.1.34) means

$$g_0^{(n,m)} = \eta + \sigma(n+m), \tag{3.1.35}$$

and

$$\alpha_n(\tau) = f_n b(\tau) p(\tau)^n. \tag{3.1.36}$$

Although a rescaling could set η or σ to 1 in (3.1.35) leaving a single freedom, we will work with both to cover the case where one of them is zero. This situation is less interesting than (3.1.33) because solutions of (3.1.36) consists of stationary states as is provided by the next proposition.

Proposition 3.1.5.2: *if* (3.1.35) *is satisfied; then, the solutions of* (3.1.36) *are stationary states of the form*

$$\alpha_n(\tau) = A e^{i(\lambda+n\omega)\tau}, \tag{3.1.37}$$

where A *is the amplitude and the expressions for* λ, ω *can be found in the appendix A.3.2.*

3.1.6 Overview

Starting with the resonant system (3.0.1), we have studied constraints on the interaction coefficients C_{nmkl} which allowed classifying them in different families. The first classification was based on the summation identities $g_p^{(n,m)}$ given in (3.1.4). Specifically we have mainly studied the class determined by

$$g_0^{(n,m)} = 1, \qquad g_2^{(n,m)} = c_2(n^2+m^2) + c_1 nm + c_0(n+m). \tag{3.1.38}$$

They allowed the development of a collection of propositions which provide features shared by all members of the family. In particular, they guarantee that the ansatz (3.1.7),

$$\alpha_n = f_n(b+na)p^n, \tag{3.1.39}$$

is consistent and forms a three-dimensional dynamical system. Any solution in this sector displays exact periodic returns of the energy spectrum $|\alpha_n|^2$ and have a lack of turbulent behaviors in this sector. We have also found that the dynamics of this sector is completely determined by γ and β.

We have furthermore explored the stronger condition $\mathcal{D}_{nmkl} = 0$, (3.1.11)-(3.1.12), which implies (3.1.38), and provides the additional conserved quantity Z for the resonant system. The condition $\mathcal{D}_{nmkl} = 0$ is simple enough to analyze it in full generality and obtain solutions for the interaction coefficients in terms of their generating functions $S(y,z,v,w)$, given by (3.1.20) and (3.1.21). Following this analysis we have also constructed the complex plane representation of resonant systems satisfying $\mathcal{D}_{nmkl} = 0$, (3.1.26). With this representation we obtained stationary solutions bifurcating from single-mode solutions, which where suitably expressed in terms of the generating function

$$u(\tau,z) = e^{-i\lambda\tau}u(z), \qquad \partial_z^{G-1}(z^{G-1}u(z)) = \frac{(\bar{p}-z)^N}{(1-pz)^{N+G}}. \tag{3.1.40}$$

Note that $\mathcal{D}_{nmkl} = 0$ implies results which cannot be reached by the identities (3.1.38). They are the conservation of Z for the resonant system, the general expressions for C_{nmkl} and the stationary solutions (3.1.40) with $N > 1$ ($N = 0, 1$ are contained in the three-dimensional manifold). These results require specific structures for $g_p^{(n,m)}$ for any p; in consequence, imposing conditions on the lowest summations we can only reach these results restricted to the three-dimensional manifold (3.1.39).

Finally we have also explored the compatibility of a more general ansatz than (3.1.39), with extended summation identities based on higher order polynomials for α_n (3.1.31) and $g_p^{(n,m)}$ (3.1.32). This analysis only provided an additional family of systems defined by

$$g_0^{(n,m)} = \eta + \sigma(n+m), \tag{3.1.41}$$

which admit solutions of the form

$$\alpha_n(\tau) = f_n b(\tau) p(\tau)^n. \tag{3.1.42}$$

3.2 Strong Localisation Limit

As we have seen in section 3.1, a direct analytic investigation of the resonant system (3.0.1) is possible for an exclusive group of interaction coefficients. In the majority of situations, it is beyond practically imaginable limits. Nevertheless, there are special regimes in which this system is analytically tractable. Central objects of these regions are single-mode solutions. Remember that they are exact solutions in which all amplitudes are zero except for one mode ($\alpha_n = 0\ \forall n \neq k$). The vicinities of such single-mode solutions form stability islands in the majority of situations [6, 29, 30, 34, 56]. While it is common to linearize in the environment of such single-mode solutions and their generalizations [56, 142], which results in linear systems that are potentially tractable, our approach here will also gain leverage by relying on single-mode solutions, but in a way different from linearization, and much more useful for our purposes.

Instead of linearizing around single-mode solutions, we shall assume that all other modes are exponentially suppressed in proportion to their "distance" from the dominant mode. We shall see that, in the limit when this exponential suppression becomes strong, the equations dramatically simplify. We denominate this regime the *strong localization limit* (SLL). Such techniques have been applied in [58] to the analysis of stationary solutions of (3.0.1) and related resonant systems. While the equations are still nonlinear (unlike in the linearization approach mentioned above), they can be solved iteratively starting with the dominant mode. This structure is very convenient for elucidating whether the energy returns of special initial data around single modes may be exact. Namely, if the energy per mode, $E_n = |\alpha_n|^2$, after spreading through the spectrum exactly returns to its initial distribution. If the returns are exact, they are exact for all modes, while a failure of exact returns shall be seen in the approach we are adopting in a finite number of steps, since the discovery of any given non-returning mode guarantees that the returns in the whole system cannot be exact. We are particularly interested in initial data with all of the energy in the two lowest modes, namely (3.1.10). This choice is motivated on the one hand by the results of section 3.1, where this kind of initial configurations display periodic behaviors for systems belonging to the special class of (3.1.11). On the other hand by the study of the AdS instability problem, in [34] was observed that for (3.1.10), the resonant system shows a close return (within a few percent) of the energy distribution to the initial configuration after a few direct and reverse cascades of energy to shorter wavelength modes and back. In the next sections we will present the derivations for modes 0 and 1 and solve the first equations subject to the initial condition (3.1.10).

3.2.1 Solutions Dominated by Mode 0

We shall assume that the spectrum is exponentially suppressed as one moves away from the dominant mode 0:

$$\alpha_n(\tau) = \delta^n\, q_n(\tau), \tag{3.2.1}$$

with $\delta \ll 1$. Then, after using the resonant condition $n+m=k+l$, (3.0.1) becomes

$$i\dot{q}_n = \sum_{m=0}^{\infty} \sum_{k=0}^{n+m} \delta^{2m}\, C_{nmk,n+m-k} q_k q_{n+m-k} \bar{q}_m. \tag{3.2.2}$$

At leading order in δ, only the terms with $m=0$ survive:

$$i\dot{q}_n = \bar{q}_0 \sum_{k=0}^{n} C_{n0k,n-k} q_k q_{n-k}. \tag{3.2.3}$$

While this equation is still nonlinear, it offers a tremendous simplification over (3.0.1), since it can be solved recursively: once solutions for the modes up to q_n have been constructed, finding q_{n+1} amounts to solving a single linear ODE. We display this structure by writing out the equations for the first few modes:

$$\begin{aligned}
i\dot{q}_0 &= C_{0000}|q_0|^2 q_0, && (3.2.4)\\
i\dot{q}_1 &= 2C_{1010}|q_0|^2 q_1, && (3.2.5)\\
i\dot{q}_2 &= 2C_{2020}|q_0|^2 q_2 + C_{2011}\bar{q}_0 q_1^2, && (3.2.6)\\
i\dot{q}_3 &= 2C_{3030}|q_0|^2 q_3 + 2C_{3021}\bar{q}_0 q_1 q_2, && (3.2.7)\\
i\dot{q}_4 &= 2C_{4040}|q_0|^2 q_4 + 2C_{4031}\bar{q}_0 q_1 q_3 + C_{4022}\bar{q}_0 q_2^2. && (3.2.8)
\end{aligned}$$

By applying the scaling symmetry of (3.0.1), one can always set $|q_0|^2$ to 1. In particular, in order to elucidate whether energy returns of the two-mode initial data of the form (3.1.10) are exact, we solve (3.2.3) with the initial conditions $q_0(0)=1$, $q_1(0)=1$, $q_{n\geq 2}=0$. (The phases of $q_0(0)$ and $q_1(0)$ can be adjusted as necessary by the symmetry transformations (3.0.6), while the magnitude of $q_1(0)$ can be set to 1 by defining $\delta = |\alpha_1(0)|$.) The solutions for q_0 and q_1 are

$$q_0(\tau) = e^{-iC_{0000}\tau}, \qquad q_1(\tau) = e^{-2iC_{1010}\tau}. \tag{3.2.9}$$

Note that the energies in these first two leading modes are time-independent, which implies that close to mode 0 the cascade to higher energies is necessarily very weak (the situation will be more interesting for solutions dominated by mode 1). For higher q_n, one then obtains

$$i\dot{q}_n - 2C_{n0n0}q_n = \bar{q}_0 \sum_{k=1}^{n-1} C_{n0k,n-k} q_k q_{n-k}. \tag{3.2.10}$$

The structure of solutions is easily understood recursively: the right-hand side consists of terms oscillating with frequencies given by linear combinations (with integer coefficients) of C_{0000}, C_{1010}, ..., $C_{n-1,0,n-1,0}$. Hence, q_n will consist of terms that oscillate[7] with frequencies given by linear combinations (with integer coefficients) of C_{0000}, C_{1010}, ..., C_{n0n0}. It is only if *all* q_n constructed in this manner (for two-mode initial conditions) oscillate with a common period that one gets exact energy returns.

[7] As we will see in the statement of Proposition 3.2.1.1, there is a possible caveat in relation to this reasoning in the sense that, if a resonance occurs between the oscillatory terms on the right-hand side of (3.2.10) and the frequency $2C_{n0n0}$ on the left-hand side, growing (rather than purely oscillatory) terms will be produced in the solution for q_n.

For the resonant system (3.0.1), one can straightforwardly proceed with this algorithm. The result for $q_2(\tau)$, which is

$$q_2(\tau) = \frac{-2iC_{2011}}{C_{0000} - 4C_{1010} + 2C_{2020}} \sin \frac{(C_{0000} - 4C_{1010} + 2C_{2020})\tau}{2} e^{i(C_{0000}-4C_{1010}-2C_{2020})\frac{\tau}{2}}, \tag{3.2.11}$$

shows that $|q_2(\tau)|^2$ is periodic. Thus, energy returns are perfect at this order. Nevertheless, the periodicity can be broken at the next order, given by

$$q_3(\tau) = \frac{2C_{2011}C_{3021}}{\lambda_1\lambda_2(\lambda_2 - \lambda_1)} \left((\lambda_2 - \lambda_1) - \lambda_2 e^{-i\lambda_1\tau} + \lambda_1 e^{-i\lambda_2\tau}\right) e^{-i2C_{3030}\tau}, \tag{3.2.12}$$

where

$$\lambda_1 = -2C_{0000} + 6C_{1010} - 2C_{3030}, \tag{3.2.13}$$

$$\lambda_2 = -C_{0000} + 2C_{1010} + 2C_{2020} - 2C_{3030}. \tag{3.2.14}$$

At this level we cannot guarantee the periodicity of $|q_3|$ without additional information about the interaction coefficients.

Higher modes can be solved similarly. Nevertheless, the next proposition provides the structure of the solution of (3.2.10) for a large class of systems:

Proposition 3.2.1.1: *If the RHS of* (3.2.10) *does not contain solutions of the homogeneous equation (it is equivalent to* $\Omega_{nkl} - 2C_{n0n0} \neq 0 \ \forall n, l, k > 0$*); then, its solution is*

$$q_n(\tau) = \sum_{l=0}^{n-1} \sum_{k=1}^{\mathcal{N}_{nl}} A_{nkl} e^{-i\Omega_{nkl}\tau}, \tag{3.2.15}$$

where $\mathcal{N}_{nl}$*,* Ω_{nkl} *and* A_{nkl} *are integer, real and complex numbers respectively. The meaning of each component and the expressions of* Ω_{nkl} *can be found below, in* (3.2.17)-(3.2.18) *or in appendix A.3.2.*

Although this proposition does not report the full solution of (3.2.10) (A_{njk} are not determined), it provides the fundamental structure. In some situations with little information about a reduced set of interaction coefficients, C_{n0n0}, Proposition 3.2.1.1 provides crucial results. An interesting example will be seen in section 3.3.7 in the context of a scalar field in AdS_4 in presence of backreaction. A second example is the case of interaction coefficients satisfying

$$C_{n0n0} = \eta + \sigma n. \tag{3.2.16}$$

For this particular situation the computations become extremely simple. We could perform a rescaling to set either σ or η to 1, but we leave them free to also consider the case in which any of these parameters is zero. Although we have omitted the explicit expressions for Ω_{nkl} in Proposition 3.2.1.1 in order to simplify the statement, now they will be presented to avoid interruptions in the explanation:

$$\Omega_{nkl} = \sum_{j=1}^{n} a_{nj}^{(k)} \theta_j - l\theta_0, \tag{3.2.17}$$

where n denotes the mode at which the frequency belongs, $\theta_0 = C_{0000}$, $\theta_{n>0} = 2C_{n0n0}$ and $a_{nj}^{(k)}$ are the positive integer solutions for the constraints

$$\sum_{j=1}^{n} a_{nj}^{(k)}\ j = n \qquad \sum_{j=1}^{n} a_{nj}^{(k)} = l+1 \qquad 0 \leq a \leq n \qquad 0 \leq l < n, \qquad a, l \in \mathbb{Z}. \quad (3.2.18)$$

Each set of solutions $\{a_{nj}^{(k)}\}$ subject to n, l, is labelled by k, which goes from $k = 1, 2, ..., \mathcal{N}_{nl}$, being $\mathcal{N}_{nl}$ the total number of these solutions.

Then, inserting (3.2.16) we obtain

$$\Omega_{nkl} = 2\sigma \sum_{j=1}^{n} a_{nj}^{(k)} j + 2\eta \sum_{j=1}^{n} a_{nj} - l\eta. \quad (3.2.19)$$

This expression is easily solved noting that the first (second) summation corresponds with the first (second) constraint of (3.2.18). In consequence, frequencies have the simple expression

$$\Omega_{nkl} = 2\sigma n + \eta l + 2\eta. \quad (3.2.20)$$

Now we can check the condition $\Omega_{nkl} - \theta_n \neq 0\ \forall n, l, k > 0$, in this case

$$\Omega_{nkl} - \theta_n = \eta l, \quad (3.2.21)$$

thereby if $\eta \neq 0$, as $l = 0$ is excluded, we can apply Proposition 3.2.1.1 giving the solution for (3.2.3),

$$q_0(\tau) = e^{-i\eta\tau}, \qquad q_n(\tau) = \sum_{l=0}^{n-1} A_l e^{-i(2\sigma n + \eta l + 2\eta)\tau}. \quad (3.2.22)$$

From this expression, depending on the values of σ, η we can infer useful information. For example, if $\sigma, \eta \in \mathbb{Q}$ $(\eta \neq 0)$ we immediately know that any solution for (3.2.3) is periodic.

3.2.2 Solutions Dominated by Mode 1

We shall now assume a hierarchically organized spectrum dominated by mode 1:

$$\alpha_0(\tau) = \delta\, q_0(\tau), \quad \alpha_{n\geq 1}(\tau) = \delta^{n-1}\, q_n(\tau), \quad (3.2.23)$$

with $\delta \ll 1$. We then get from (3.0.1), after using the resonant condition $n + m = k + l$, the following equation for mode 0:

$$i\dot{q}_0 = \sum_{m=2}^{\infty} \sum_{k=1}^{m-1} C_{0mk,m-k} \bar{q}_m q_k q_{m-k} \delta^{2m-4} + 2 \sum_{m=1}^{\infty} C_{0m0m} \bar{q}_m q_m q_0 \delta^{2m-2} + C_{0000} \bar{q}_0 q_0 q_0 \delta^2, \quad (3.2.24)$$

and for all higher modes,

$$i\dot{q}_n = \sum_{m=1}^{\infty} \sum_{k=1}^{n+m-1} C_{nmk,n+m-k} \bar{q}_m q_{n+m-k} q_k \delta^{2m-2} + \sum_{k=1}^{n-1} C_{n0k,n-k} \bar{q}_0 q_k q_{n-k} + 2 \sum_{m=1}^{\infty} C_{0n0n} \bar{q}_0 q_0 q_n \delta^2.$$

Retaining only the leading terms, we obtain

$$i\dot{q}_0 = C_{0211}\bar{q}_2 q_1^2 + 2C_{0101}|q_1|^2 q_0, \tag{3.2.25}$$

and

$$i\dot{q}_n = \bar{q}_1 \sum_{k=1}^{n} C_{n1k,n+1-k} q_k q_{n+1-k} + \bar{q}_0 \sum_{k=1}^{n-1} C_{n0k,n-k} q_k q_{n-k}. \tag{3.2.26}$$

To appreciate the structure, we write out the first few equations explicitly:

$$\begin{aligned}
i\dot{q}_0 &= 2C_{0101}|q_1|^2 q_0 + C_{0211}\bar{q}_2 q_1^2, && (3.2.27)\\
i\dot{q}_1 &= C_{1111}|q_1|^2 q_1, && (3.2.28)\\
i\dot{q}_2 &= 2C_{2121}|q_1|^2 q_2 + C_{2011}\bar{q}_0 q_1^2, && (3.2.29)\\
i\dot{q}_3 &= 2C_{3131}|q_1|^2 q_3 + C_{3122}\bar{q}_1 q_2^2 + 2C_{3021}\bar{q}_0 q_1 q_2, && (3.2.30)\\
i\dot{q}_4 &= 2C_{4141}|q_1|^2 q_4 + 2C_{4132}\bar{q}_1 q_2 q_3 + C_{4022}\bar{q}_0 q_2^2. && (3.2.31)
\end{aligned}$$

One first solves (3.2.28), where one can set $|q_1|^2 = 1$ as before using the scaling symmetry. After that, (3.2.27) and (3.2.29) form a system of two coupled linear equations for q_0 and q_2. Once q_0, q_1 and q_2 have been thus obtained, all the higher equations are solved recursively one-by-one, in a manner completely analogous to what we have previously described for solutions dominated by mode 0.

Implementing this solution in practice for $q_0(0) = 1$, $q_1(0) = 1$ and $q_{n>1}(0) = 0$ (as before, the complex phases can be eliminated using the symmetries (3.0.6), while the magnitude of $q_0(0)$ can be fixed by redefining δ), one gets

$$\begin{aligned}
q_1(\tau) &= e^{-iC_{1111}\tau}, && (3.2.32)\\
q_0(\tau) &= \left(\cos\frac{\lambda\tau}{2} + \frac{i\beta}{\lambda}\sin\frac{\lambda\tau}{2}\right) e^{-i(2C_{0101}+\beta/2)\tau}, && (3.2.33)\\
q_2(\tau) &= \frac{-2iC_{1102}}{\lambda}\sin\frac{\lambda\tau}{2} e^{-i(2C_{2121}+\beta/2)\tau}, && (3.2.34)
\end{aligned}$$

where $\beta = 2\left(C_{1111} - C_{0101} - C_{2121}\right)$ and $\lambda = \sqrt{\beta^2 - 4C_{1102}^2}$. In what follows, we assume $\lambda \in \mathbb{R}$, which is the case for systems we are going to deal with, as well as for all the systems studied in this thesis. Note that, here, one gets nontrivial flows of energy among the first subleading modes, unlike the case dominated by mode 0. These flows of energy are always periodic with period $2\pi/\lambda$, as far as the three lowest modes are concerned. The first order at which violations of periodicity may enter is in mode q_3, which is described by the following solution:

$$q_3(\tau) = \frac{C_{1102}}{2\gamma\lambda^2(\gamma^2-\lambda^2)}\left(a + be^{i\lambda\tau} + ce^{2i\lambda\tau} + de^{i(\lambda+\gamma)\tau}\right) e^{i(-\lambda+2C_{0101}-2C_{2121}-C_{1111})\tau}, \tag{3.2.35}$$

with

$$\begin{aligned} a &= 2\gamma(\gamma-\lambda)\left(C_{1102}C_{2213}+(\beta+\lambda)C_{1203}\right), \\ b &= 4(\lambda^2-\gamma^2)\left(C_{1102}C_{2213}+\beta C_{1203}\right), \\ c &= 2\gamma(\gamma+\lambda)\left(C_{1102}C_{2213}+(\beta-\lambda)C_{1203}\right), \\ d &= -4\lambda^2\left(C_{1102}C_{2213}+(\beta-\gamma)C_{1203}\right), \\ \gamma &= -2C_{0101}+C_{1111}+2C_{2121}-C_{3131}. \end{aligned} \tag{3.2.36}$$

This process could be continued for higher modes. In this situation we have not formulated the analogous of Proposition 3.2.1.1 for the SLL around mode 0. Nevertheless, for our future interests in sections 3.3.7 and 3.3.8, the iterative resolution until $n = 3$ is enough.

3.3 Fully Resonant Models

In this section we are going to present some models studied in the literature which display a fully resonant spectrum and a resonant system of the form (3.0.1). We will apply to them some of the techniques developed in the previous sections.

3.3.1 Conformal Flow

In this section we will describe the origin and the construction of the resonant system known as *conformal flow*, originally derived in [75].

3.3.1.1 The Model

The model from which the conformal flow was obtained consists of the conformally coupled scalar field (see [143] for additional information)

$$S=\int d^4x\sqrt{-g}\left(\frac{1}{16\pi G}R-\frac{1}{2}\partial_\mu\phi\partial^\mu\phi-\frac{1}{12}R\phi^2-\frac{\lambda}{4}\phi^4\right), \tag{3.3.1}$$

in the Einstein cylinder with topology $\mathbb{R}\times\mathbb{S}^3$ and line element

$$ds^2=-dt^2+r^2\left(d\chi^2+\sin^2\chi\left(d\theta^2+\sin^2\theta d\varphi^2\right)\right), \tag{3.3.2}$$

where $(t,\chi,\theta,\varphi)\in\mathbb{R}\times[0,\pi]\times[0,\pi]\times[0,2\pi)$, r is the radius of $\mathbb{S}^3$, λ the coupling constant for the nonlinearities and R the curvature scalar. The backreaction of the metric is not considered; hence the curvature of this space remains constant $R=6/r^2$. The EOM for the scalar field takes the form

$$\left(\Box_g-\frac{1}{6}R\right)\phi-\lambda\phi^3=0, \tag{3.3.3}$$

where $\Box_g \equiv (\partial_\mu \sqrt{-g} g^{\mu\nu} \partial_\nu)/\sqrt{-g}$.

After a sequence of: rescaling $t \to t/r, \phi \to r\sqrt{\lambda}\phi$, restricting to spherically symmetric fields such that $\phi(t,\chi)$ and transforming $\phi(t,\chi) = v(t,\chi)/\sin(\chi)$, the equation (3.3.3) is expressed as

$$v_{tt} - v_{\chi\chi} + \frac{v^3}{\sin^2\chi} = 0, \tag{3.3.4}$$

with boundary conditions $v(t,0) = v(t,\pi) = 0$ required by regularity of solutions.

3.3.1.2 The Resonant System

We are going to consider the evolutions of small amplitudes of $v(t,x)$ and $v_t(t,x)$. The linear modes and spectrum restricted to the imposed boundary conditions has the form

$$e_n(x) = \sin((n+1)x), \qquad \omega_n = n+1, \qquad n = 0, 1, ... \tag{3.3.5}$$

Now, following the method of multi-scales displayed in section 2.2 we expand the solution in terms of the linearized modes,

$$v(t,x) = \epsilon \sum_{n=0}^{\infty} \sin((n+1)x) \left(\alpha_n(\epsilon^2 t) e^{i(n+1)t} + \bar{\alpha}_n(\epsilon^2 t) e^{-i(n+1)t}\right). \tag{3.3.6}$$

After finalising the application of the method a resonant system of the form (3.0.1), which has been denominated *conformal flow*, is obtained

$$i\frac{d\alpha_n}{d\tau} = \sum_{m=0}^{\infty} \sum_{k=0}^{n+m} C_{nmk(n+m-k)} \alpha_{n+m-k} \alpha_k \bar{\alpha}_m \tag{3.3.7}$$

where $\tau \equiv \epsilon^2 t$ and

$$C_{nmkl} = \frac{\min(n,m,k,l)+1}{\sqrt{(n+1)(m+1)(k+1)(l+1)}}. \tag{3.3.8}$$

The deep details of this section can be consulted in [75].

An important remark made in [75] consists of the relation between the line element (3.3.2) and the one for AdS_4:

$$d\tilde{s}^2 = \frac{1}{\cos^2\chi}\left(-dt^2 + d\chi^2 + \sin^2\chi\left(d\theta^2 + \sin^2\theta d\phi^2\right)\right), \tag{3.3.9}$$

with $\chi \in [0, \pi/2)$. The metrics are conformally equivalents $g = \cos^2\chi\, \tilde{g}$. In consequence, considering the conformally coupled massless scalar field in AdS_4, with the transformation $\tilde{\phi} = \phi \cos x$ the equation (3.3.3) is recovered. Note however that on this occasion the boundary conditions are $\phi(t, \pi/2) = 0$ and therefore the solutions of this last model form a subset of (3.3.3), obtained by $\phi(t,x) = -\phi(t, \pi - x)$. Taking into account that the metrics are static, the particular value of the curvature scalar in AdS_4 is $R = -\frac{12}{l^2}$ and the

conformal coupling in these dimensions is 1/6; hence, the EOM is equivalent to a massive scalar field with $m^2 = -2$.

In the case of AdS_4, due to the boundary is placed at $\pi/2$ the linearized spectrum of modes is restricted to $w_n = 2n + 2$, namely, (3.3.7)-(3.3.8) are truncated to odd modes α_{2m+1}. Inserting this truncation in equation (3.3.7) we observe that the result is exactly the same. In consequence, the conformal flow also describes the long-time evolution of a small scalar field with mass $m^2 = -2$ in AdS_4 (without backreaction).

We can check that this system can be studied with the formalism we have developed. The next proposition clarifies that the conformal flow belongs to the class of systems studied in section 3.1.

Proposition CF: (3.3.8) *satisfies* $\mathcal{D}_{nmkl} = 0$ *for* $n + m - k - l = 1$ *with* $G = 2$ *and* $\beta = 1/3$, *defined in* (3.1.2).

This result immediately enables the results of section 3.1 for the conformal flow. In particular, the existence of a three-dimensional invariant manifold of time-periodic solutions and stationary states, as well as the conservation of Z, (3.1.8). The three-dimensional manifold was already obtained in [75]; nevertheless, the new conserved quantity is a novel result of our formalism.

3.3.2 Gross-Pitaevskii Equation with a Harmonic Potential

The nonlinear Scrödinger equation (NLSE), also known as Gross-Pitaevskii equation (GPE), describes a mean-field dilute Bose-Einstein condensate (BEC) of identical bosons of mass m in a potential $V(\tilde{\mathbf{r}})$. As we have previously argued we are interested in potentials providing a fully resonant spectrum. In particular, we shall consider a harmonic trap of frequency ω,

$$i\hbar\partial_{\tilde{t}}\tilde{\Psi} = -\frac{\hbar^2}{2m}\tilde{\nabla}^2\tilde{\Psi} + \frac{m\omega^2}{2}\tilde{r}^2\tilde{\Psi} + \frac{4\pi\hbar^2 a}{m}|\tilde{\Psi}|^2\tilde{\Psi}, \tag{3.3.10}$$

where a is the s-wave scattering length which can be either positive (repulsive interaction) or negative (attractive interaction). Through the transformations

$$\frac{\tilde{t}}{t} = \omega^{-1}, \qquad \frac{\tilde{r}}{r} = \sqrt{\frac{\hbar}{m\omega}}, \qquad \frac{\tilde{\Psi}}{\Psi} = \sqrt{g\frac{m\omega}{4\pi\hbar|a|}}, \tag{3.3.11}$$

equation (3.3.10) can be rewritten in the dimensionless form

$$i\partial_t\Psi = -\frac{1}{2}\nabla^2\Psi + \frac{1}{2}r^2\Psi \pm g|\Psi|^2\Psi, \tag{3.3.12}$$

where the plus (minus) sign comes from $a > 0$ ($a < 0$) and we have introduced g as the coupling of the nonlinearities. We shall adopt the form (3.3.12) from now on.

Different versions of the GPE have been used in diverse contexts including, for example, optics [144, 145], plasma physics [146] and even in cosmology [147, 148]. It describes with

precision most of the physics of BEC dilute gases [149, 150]. Particularly, it contains exotic phenomenology as the appearance of quantized vortices under the presence of rotation [151–153] or, with an attractive nonlinearity, the collapse of the wave function, by diverging at some point of space in finite-time [154]. This last scenario can happen in cold atom BECs when the scattering length a controlling the effective atom-atom interaction is negative [155–157]. The phenomenon, sometimes nicknamed "Bosenova" because of the subsequent explosion, has been demonstrated in a series of experiments which have attained a notable degree of control [158–161] and modelled using GPE [162–166]. As we can observe in these examples, the GPE is of real-world significance as a model of effective dynamics of cold atomic gases, but also fascinating from a purely mathematical perspective for its phenomenological complexity. There is a vast literature about the GPE, comprising analytic results, numerics and experiments [151–154, 167–173].

In particular, in this section we will focus on the weakly nonlinear regime; namely $g \ll 1$, analysing the case of two spatial dimensions which allows an analytic treatment as we will see. This 2-dimensional setup can be effectively achieved experimentally from a 3-dimensional BEC [174].

3.3.2.1 Two-Dimensional Gross-Pitaevskii Equation

In this section we are going to consider the GPE in two spatial dimensions,

$$i\partial_t\Psi = -\frac{1}{2}\left(\partial_r^2 + \frac{1}{r}\partial_r + \frac{1}{r^2}\partial_\phi^2\right)\Psi + \frac{1}{2}r^2\Psi + g|\Psi|^2\Psi, \tag{3.3.13}$$

for small values of the coupling $0 < g \ll 1$ (the sign of the coupling in fact does not affect the weakly nonlinear dynamics, for this reason we only consider the positive sign in (3.3.13)).

The linearized problem ($g = 0$) corresponding to (3.3.13) is an ordinary two-dimensional isotropic harmonic oscillator with eigenvalues $\omega_n = n + 1$ and normalized eigenfunctions (see, e.g., [175]) given by

$$\Psi_{nm} = \sqrt{\frac{1}{\pi}\frac{((n-|m|)/2)!}{((n+|m|)/2)!}}\, r^{|m|} L_{\frac{n-|m|}{2}}^{|m|}(r^2)\, e^{-r^2/2} e^{im\phi}. \tag{3.3.14}$$

Here, the energy level index n is a nonnegative integer and the angular momentum index $m \in \{-n, -n+2, \ldots, n-2, n\}$. The generalized Laguerre polynomials $L_n^\alpha(x)$ can be defined through the generating function

$$G_\alpha(t,x) = \sum_{n=0}^{\infty} t^n L_n^\alpha(x) = \frac{e^{-\frac{tx}{1-t}}}{(1-t)^{\alpha+1}}. \tag{3.3.15}$$

They are orthogonal with the weight $x^\alpha e^{-x}$ on the interval $0 \le x < \infty$.

Expanding the exact solution Ψ in terms of the linearized modes

$$\Psi(t,r,\phi) = \sum_{nm} \alpha_{nm}(t)\, e^{-i\omega_n t}\Psi_{mn}(r,\phi), \tag{3.3.16}$$

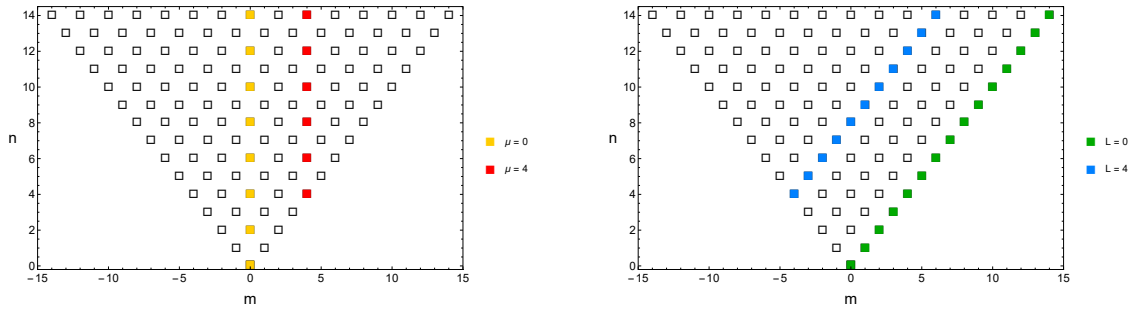

Figure 3.1: Truncations of the tower of modes of the two-dimensional Gross-Pitaevskii equation to fixed angular momentum (left) and Landau levels (right).

and using the methods of multi-scales or averaging, given in sections 2.2.2 and 2.2.3 respectively, it allows constructing the resonant system (3.0.1) which captures the dynamics at scales of $1/g$,

$$i\,\frac{d\alpha_{nm}}{d\tau} = \sum_{\substack{n+n_1=n_2+n_3\\ m+m_1=m_2+m_3}} C^{mm_1m_2m_3}_{nn_1n_2n_3}\,\bar{\alpha}_{n_1m_1}\alpha_{n_2m_2}\alpha_{n_3m_3}, \tag{3.3.17}$$

where $\tau = gt$ and the interaction coefficients take the form

$$C^{mm_1m_2m_3}_{nn_1n_2n_3} = \int \Psi_{nm}\Psi_{n_1m_1}\Psi_{n_2m_2}\Psi_{n_3m_3}\,r\,dr\,d\phi. \tag{3.3.18}$$

A mathematical analysis of the validity of time-averaging specifically adapted to NLSE can be found in [176]. General properties of the resonant system (3.3.17) have been analyzed in [68]. In particular, it was shown in [68] that (3.3.17) enjoys many conservation laws, some of which have no counterparts for the original equation (3.3.13), and hence they are only approximately conserved by (3.3.13), though the precision of their conservation becomes arbitrarily good for small coupling. We shall see below the restrictions imposed by these general conservation laws on the specific truncations of (3.3.17) we are interested in.

We note that because the n- and m-conservation conditions present in the sum in (3.3.17), the equation can be consistently truncated to any set of modes satisfying $An + Bm = C$ with arbitrary numbers A, B, C. If only modes satisfying this relation are nonzero in the initial state, no other modes will get excited in the course of evolution. We are specifically concerned with two types of such truncations. First, we can retain only modes of some fixed angular momentum $m = \mu$, which without loss of generality we shall assume to be nonnegative. Second, we can retain modes with $n - m = 2L$, where L is referred as the "Landau level" number. (The lowest Landau level has previously received a good amount of attention, including treatments along our present lines in [70, 72, 73].) The two types of truncations are depicted in Fig. 3.1.

3.3.2.1.1 Fixed Angular Momentum

First, we are going to consider the resonant system (3.3.17) truncated to modes of angular momentum μ. Introducing the notation

$$\alpha_n \equiv \alpha_{\mu+2n,\mu}, \qquad C_{njkl} \equiv C^{\mu\mu\mu\mu}_{njkl}, \tag{3.3.19}$$

the equation (3.3.17) is written as

$$i\,\frac{d\alpha_n}{d\tau} = \sum_{j=0}^{\infty}\sum_{k=0}^{n+j} C_{njkl}\bar{\alpha}_j\alpha_k\alpha_l. \tag{3.3.20}$$

We want to express the resonant systems in terms of the formalism given in section 3.1, with this goal in mind the transformations

$$\tau \to \tau/C_{0000}, \qquad C_{njkl} \to C_{njkl}/C_{0000} \tag{3.3.21}$$

are required to achieve (3.1.1). After these transformations, the interaction coefficients take the form

$$C_{njkl} = 2\frac{\Gamma(\mu+1)\Gamma\left(\frac{1}{2}\right)}{\Gamma\left(\frac{1}{2}+\mu\right)}\mathcal{N}_n\mathcal{N}_j\mathcal{N}_k\mathcal{N}_l\int_0^\infty d\rho\; e^{-2\rho}\rho^{2\mu}L_n^{(\mu)}(\rho)L_j^{(\mu)}(\rho)L_k^{(\mu)}(\rho)L_l^{(\mu)}(\rho) \tag{3.3.22}$$

where $\mathcal{N}_n = \sqrt{\Gamma(n+1)/\Gamma(n+\mu+1)}$. Note that the interaction coefficients are written in their integral form, they can in principle be evaluated by substituting explicit expressions for the Laguerre polynomials given by

$$L_n^\mu(\rho) = \sum_{k=0}^{n}(-1)^k\frac{(n+\mu)!}{k!\,(n-k)!(k+\mu)!}\rho^k \tag{3.3.23}$$

and evaluating the remaining integrals of the form $\int d\rho\,\rho^A e^{-2\rho}$. The resulting expression is, however, a quadruple sum with summation ranges depending on n, j, k and l. We have not been able to bring this sum to a manageable form that could be employed in explicit derivations. Nevertheless, with the next proposition it is not necessary for our purpose.

Proposition rGP: (3.3.22) *satisfies* $\mathcal{D}_{nmkl} = 0$ *for* $n+m-k-l=1$ *with* $G=\mu+1$ *and* $\beta = 3/8$, *defined in* (3.1.2).

In light of this proposition, the formalism of section 3.1 and all of their consequences are immediately applied. Particularly, we obtain that (3.3.20)-(3.3.22) have a three-dimensional invariant manifold defined by (3.1.7), formed by time-periodic solutions or stationary states of the form (3.1.28), and also the conservation of Z, (3.1.8), for the resonant system. The conservation of N, J, Z was previously obtained in [68] for the full system (3.3.13) and independently of our formalism.

We want to remark that all the formulas we have presented for this resonant system hold for any real positive values of μ; even if only integer values arise starting from the two-dimensional Gross-Pitaevskii equation. In consequence, Proposition rGP also apply to the interaction coefficients (3.3.22) for $\mu > 0$. They form a continuous family of resonant systems satisfying $\mathcal{D}_{nmkl} = 0$.

3.3.2.1.2 Landau Levels

Now, we will modify the truncation to study the Landau levels ($n - m = 2L$), it is in principle completely straightforward. However, the explicit form of linear wavefunctions (3.3.14) is rather inconvenient for this purpose, since both positive and negative values of m are present within each excited Landau level (see Fig. 3.1) and hence the absolute values of m present in (3.3.14) make dependences on index numbers rather awkward. To remedy this unwelcome feature, we shall start by rewriting (3.3.14) in a slightly different form using identities satisfied by the Laguerre polynomials.

From (3.3.23), remembering that factorials of negative numbers are infinite, one gets

$$L_n^a(\rho) = (-1)^a \frac{(n+a)!}{n!} \rho^{-a} L_{a+n}^{-a}(\rho) \tag{3.3.24}$$

for any integer a. (Note that L_{a+n}^{-a} does not contain any powers of ρ below ρ^a.) Using this formula, we obtain

$$\sqrt{\frac{((n-|m|)/2)!}{((n+|m|)/2)!}} \rho^{|m|/2} L_{\frac{n-|m|}{2}}^{|m|}(\rho) = (-1)^{\frac{1}{2}(m-|m|)} \sqrt{\frac{((n-m)/2)!}{((n+m)/2)!}} \rho^{m/2} L_{\frac{n-m}{2}}^{m}(\rho). \tag{3.3.25}$$

We then define

$$\alpha_n \equiv (-1)^{\frac{|n-L|-(n-L)}{2}} \alpha_{n+L,n-L}, \tag{3.3.26}$$

with n running from 0 to ∞. The sign factor inserted compensates for the sign factor in (3.3.25), simplifies the subsequent expressions, and brings our sign conventions in accord with [68] for the remainder of our treatment. Truncating (3.3.17) to the above set of modes results in

$$i \frac{d\alpha_n}{d\tau} = \sum_{j=0}^{\infty} \sum_{k=0}^{n+j} C_{njk,n+m-k} \bar{\alpha}_j \alpha_k \alpha_{n+j-k}, \tag{3.3.27}$$

with (after applying transformations (3.3.21))

$$C_{njkl} = \frac{2^{2L+1} L!^4}{(2L)! \sqrt{n!j!k!l!}} \int_0^{\infty} d\rho \, e^{-2\rho} \rho^{n+j-2L} L_L^{n-L}(\rho) L_L^{j-L}(\rho) L_L^{k-L}(\rho) L_L^{l-L}(\rho). \tag{3.3.28}$$

On this occasion C can also be computed explicitly using (3.3.23), but such expressions contain multiple sums and are of little practical use. There is a particular case, corresponding to the denominated lowest Landau level ($L = 0$), where there is a manageable form for C,

$$C_{nmkl}^{(L=0)} = \frac{(n+m)!}{2^{n+m} \sqrt{n!m!k!l!}}. \tag{3.3.29}$$

Nevertheless, there is a new proposition which allows avoiding the necessity of these computations.

Proposition xLL: (3.3.28) *satisfies* $\mathcal{D}_{nmkl} = 0$ *for* $n + m - k - l = 1$ *with* $\gamma = 1/2$ *and* $\beta = (3L-1)/4(2L-1)$, *defined in* (3.1.2).

This proposition is analogous to the previous one; it enables the results of section 3.1 for (3.3.27)-(3.3.28). In particular the existence of time-periodic solutions and stationary states for the ansatz (3.1.7) and the conservation of Z given by (3.1.8). The existence of the three-dimensional invariant manifold for this truncation to the Landau levels was firstly obtained in [72] for the Lowest Landau level ($L = 0$) and the extension to higher L was implemented in [73]. The conservation of Z is a result of [68] for the full equation (3.3.13).

3.3.2.1.3 Discussion

We have considered truncations of the Gross-Pitaevskii resonant system (3.3.17) to sets of modes at fixed angular momentum and fixed Landau level (Fig. 3.1), and demonstrated that such truncations belong to the class of systems displayed in section 3.1. In consequence, all the formalism applies to this situation and special analytic solutions are immediately obtained. Now, we are going to take advantage of the opportunity of having on our hands a system which can be studied in a laboratory. It is especially instructive to examine the position space form of our solutions.

First, for fixed angular momentum truncations within the ansatz (3.1.7), using (3.1.3) with $G = \mu + 1$ one finds (omitting an irrelevant overall phase factor)

$$\Psi(r,\phi,t) = \sum_n \alpha_n e^{-i(\mu+2n)t}\Psi_{\mu+2n,\mu}(r,\phi) = r^\mu e^{i\mu(\phi-t)}e^{-r^2/2}\sum_n (b+an)\, p^n e^{-2int} L_n^\mu(r^2). \tag{3.3.30}$$

Using (3.3.15), one obtains

$$\begin{aligned}\Psi &= r^\mu e^{i\mu(\phi-t)}e^{-r^2/2}\left(b+\frac{a}{p}\xi\partial_\xi\right)G_\mu(\xi,r^2)\Big|_{\xi=s} \\ &= \frac{r^\mu e^{i\mu(\phi-t)}e^{-\frac{r^2}{2}\frac{1+s}{1-s}}}{(1-s)^{\mu+1}}\left(b(\tilde{g}t)+\frac{(\mu+1)s}{1-s}a(\tilde{g}t)-\frac{r^2 s}{(1-s)^2}a(\tilde{g}t)\right),\end{aligned} \tag{3.3.31}$$

where $s(t) = p(\tilde{g}t)e^{-2it}$, and a, b, p are functions of the slow time $\tilde{g}t$, as explicitly shown. (We have absorbed the μ-dependent time rescaling factor mentioned under (3.3.21) into the modified coupling $\tilde{g}$). This represents rapidly oscillating rings of wavefunction density with the superposed slow periodic parameter modulations.

For nonzero angular momentum ($\mu > 0$ in our conventions), the wavefunction vanishes at $r = 0$ because of the usual angular momentum barrier. More interestingly, there is at most one more value of the radial coordinate where the wavefunction has a node; such a node appears if the expression in parentheses in (3.3.31) has a zero for positive r^2. Otherwise, there is not quite a node but just a dip in density. Snapshots of the condensate density of representative solutions can be seen on Fig. 3.2. In the literature, such objects have been referred to as 'ring dark solitons,' see e.g. [177]. They have been mostly studied, however, in the presence of strong nonlinearity, where the solitons are supported by nonlinear effects

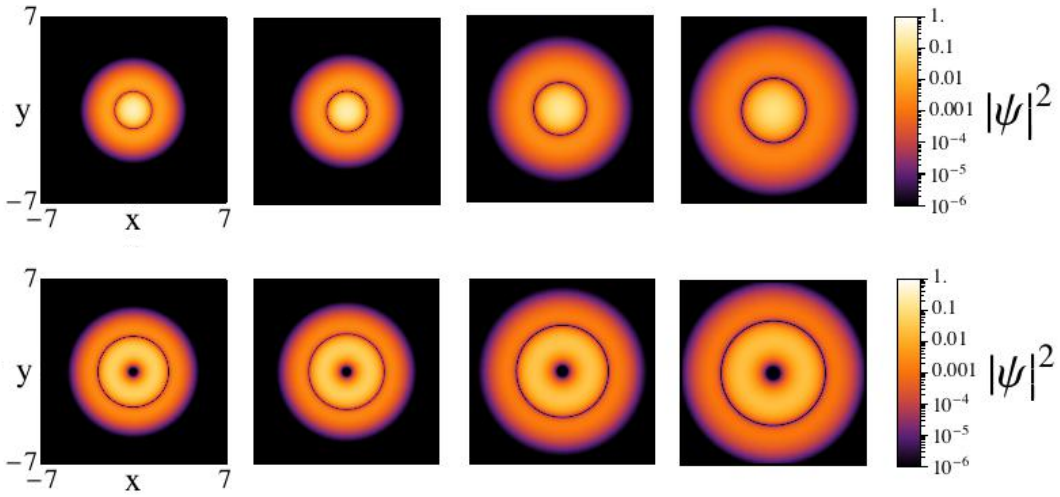

Figure 3.2: Snapshots of the condensate density $|\psi(t,x,y)|^2$ for resonant solutions in the fixed angular momentum sector with $\mu = 0$ (upper row) and $\mu = 4$ (lower row). For both, the initial data are pa = 0.5, b = 0.5, p = 0, and the coupling is $g = 0.01$. The limits of the axes and their labels are identical to the first plot of each row. Time points are, from left to right, $t = 201,\ 3832.1,\ 7663.9,\ 11501.4$ for the upper row and $t = 219.9,\ 22003,\ 43999.4,\ 66001.7$ for the lower one.

and the harmonic trap is merely a perturbation. In contrast, in our weakly nonlinear regime, the 'solitons' are mainly supported by the harmonic trap, with the nonlinearities giving rise to slow modulation of the parameters; see e.g. [178,179] for discussions of other dark solitons near the linear regime.

Stability of dark rings with static ring profiles (i.e., time-independent $|\Psi|^2$) has been extensively studied in the literature on Bose-Einstein condensates [180–182]. There are interesting instabilities trigerring pattern formation. While our solutions given by (3.3.31) also feature dark rings, the ring radius rapidly oscillates with the trap frequency, and there is no immediate mathematical relation to the dark rings with static profiles. Stability of our oscillating rings would be an interesting, question to investigate. In [178], the question of stability is treated for related oscillating dark solitons for the one-dimensional Gross-Pitaevskii equation in a harmonic trap. In [179], analogous oscillating dark shells in three dimensions are studied by predominantly numerical methods, with evidence for their stability at sufficiently small coupling.

Turning to the case of Landau levels, first we must introduce the useful generating function

$$G_L(s,\rho) = \sum_{n=0}^{\infty} \frac{s^n}{n!} L_L^{n-L}(\rho) = \frac{e^s (s-\rho)^L}{L!}. \tag{3.3.32}$$

Its derivation can be found in appendix A.3.2 at (A.3.180). Now we are ready to combine (3.1.3) with $\gamma = 1/2$, (3.1.7), (3.3.14), (3.3.16), (3.3.25)-(3.3.26) and (3.3.32) to find (omitting an irrelevant overall phase factor)

$$\Psi(t,r,\phi) = \sqrt{\frac{L!}{\pi}} \frac{e^{-r^2/2}}{z^L} \left(b + a\xi\partial_\xi\right) G_L(\xi, r^2)\big|_{\xi=pz}, \tag{3.3.33}$$

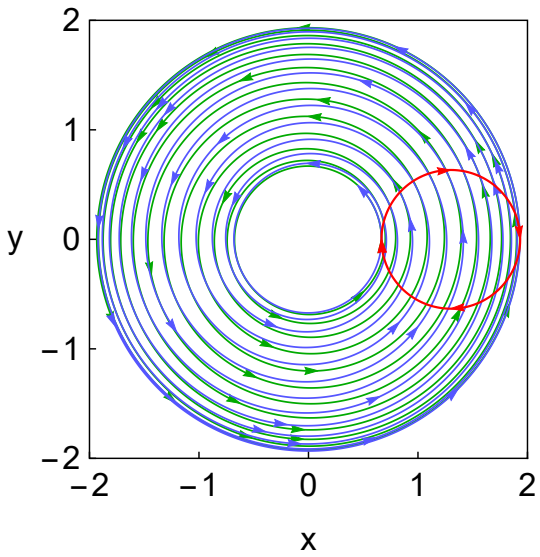

Figure 3.3: Trajectory of the vortex in the lab frame for the initial data $a = 0.32$, $b = -0.22$, $p = 1$ and coupling constant g $= 1$, chosen for illustrative purposes. The radius of the orbit is slowly modulated with the frequency ω. The in- and out-spiralling phases are plotted in blue and green, respectively. The red circle depicts the orbit in the rotating frame.

where $z \equiv re^{i(\phi - t)}$. Direct evaluation yields

$$\Psi = \frac{e^{-r^2/2} e^{p(\tilde{g}t)z}}{\sqrt{L!\pi}} \left(p(\tilde{g}t) - \bar{z}\right)^{L-1} \left[(b(\tilde{g}t) + a(\tilde{g}t)p(\tilde{g}t)z)(p(\tilde{g}t) - \bar{z}) + a(\tilde{g}t)p(\tilde{g}t)L\right], \tag{3.3.34}$$

where we have explicitly displayed the dependence of $a(\tilde{g}t)$, $b(\tilde{g}t)$, $p(\tilde{g}t)$ on the slow time $\tilde{g}t$. (Again, transformation (3.3.21) has been absorbed by introducing $\tilde{g}$ instead of g.)

This expression describes periodically modulated (due to slow time dependence of a, b, p) precession around the origin of an array consisting of a combination of vortices-antivortices. The lowest Landau level, $L = 0$, is the simplest situation with a vortex given by the only zero of (3.3.34) located at $z = -b/ap$. The slow-motion of this object can be obtained by combining the EOMs (A.3.56)-(A.3.58) with the conserved quantities (A.3.60)-(A.3.63) given in appendix A.3.2, (see [72] for a detailed derivation),

$$z_v(\tilde{g}t) = \frac{Z}{N} + ce^{i\Omega\tilde{g}t}, \tag{3.3.35}$$

where z_v denotes the position of the vortex, N, Z are the conserved quantities (3.0.4) (3.1.8), c a constant determined with the initial conditions and Ω the frequency given in (A.3.72). This equation corresponds to a circular motion centred at Z/N. Hence, the complete behavior of the vortex consists of fast rotations around the origin at scales $\mathcal{O}(1)$, combined with the slow-drift at $\mathcal{O}(1/\tilde{g})$ which periodically enlarges and shrinks the radius of the circular orbits ($\tilde{g} = 0$), deriving in a continuous succession of in- and out-spirals. This explanation is summarized in Fig. 3.3 and in the first row of Fig. 3.4.

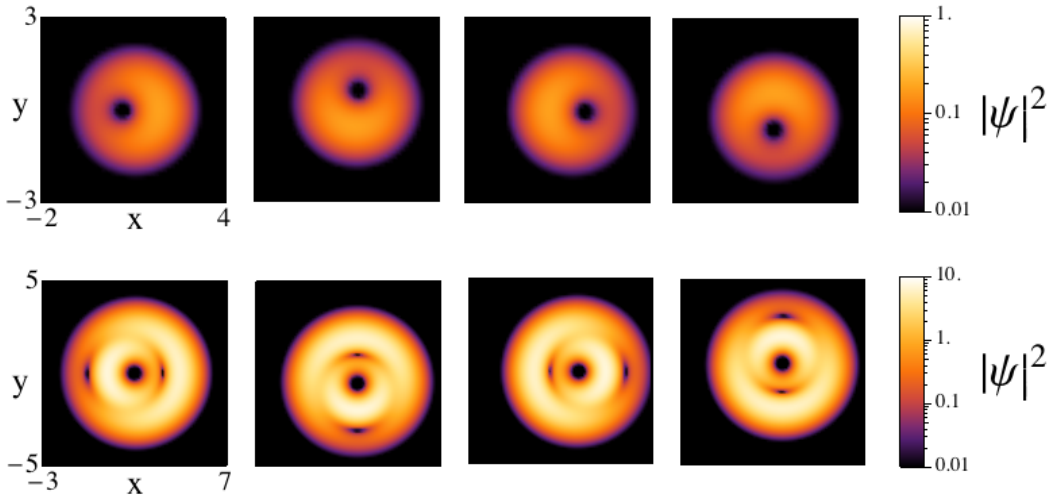

Figure 3.4: Snapshots of the condensate density $|\psi(\tau, x, y)|^2$ for resonant solutions in the Landau levels $L = 0$ (upper row) and $L = 4$ (lower row). The representation is in the maximally rotating frame and the visible movements represent slow modulations described by our resonant solutions. In the laboratory frame, the whole picture rapidly rotates around the origin. The initial data are $a = 0.32,\ b = -0.22,\ p = 1$ for the upper row and $a = 1,\ b = -0.5,\ p = 2$ for the lower one, while the time points are, from left to right, $\tau = 0,\ 20,\ 40,\ 60$ and $\tau = 0,\ 0.54,\ 1.08,\ 1.62$ respectively. The limits of the axes and their labels are identical to the first plot of the sequence.

For subsequent levels, $L > 0$, the distribution of zeros consists of a degree $L-1$ antivortex at $z = \bar{p}$ and a vortex-antivortex pair whose location is given by the two zeros of the between square brackets of (3.3.34),

$$\left(z + \frac{b}{ap}\right)(\bar{z} - p) = L. \tag{3.3.36}$$

Snapshots of the corresponding wavefunction density are given in Fig. 3.4. The three defects we mentioned (two antivortices and a vortex) in fact always lie on the same straight line. This can be seen by taking the imaginary part of (3.3.36),

$$\mathrm{Im}\left[z\left(p + \frac{\bar{b}}{\bar{a}\bar{p}}\right) + \frac{b}{a}\right] = 0, \tag{3.3.37}$$

which defines a straight line to which all roots of (3.3.36) belong. Since $z = \bar{p}$ evidently satisfies the above equation, it lies on the same straight line.

Finally we want to remark that small arrays of vortices have been studied in the literature on Bose-Einstein condensates with variational methods [183–185], and have even been created experimentally [186]. In our context, special configurations in this class can be accessed by rigorous asymptotic methods, and we provided analytic solutions for the vortex dynamics.

3.3.3 Maximally Rotating Scalar Field on the d-Sphere

In this section we are going to consider the resonant system, subject to a particular truncation, of a scalar field on the Einstein cylinder originally derived and studied in [76].

3.3.3.1 The Model

The model consists of a complex scalar field on the Einstein cylinder of topology $\mathbb{R}\times\mathbb{S}^d$ and line element

$$ds^2=-dt^2+d\theta_1^2+\sum_{n=2}^{d}\left(\prod_{i=1}^{n-1}\sin^2\theta_i\right)d\theta_n^2, \tag{3.3.38}$$

where the angles of the d-sphere are denoted by $\theta_1,...\theta_d$. θ_d plays a special role in the expressions, and it will be rewritten as $\varphi\equiv\theta_d$. The particular EOM is

$$-\partial_{tt}\phi+\Delta_{\mathbb{S}^d}\phi-\frac{(d-1)^2}{4}\phi=|\phi|^2\phi, \tag{3.3.39}$$

where $\Delta_{\mathbb{S}^d}$ denotes the d-sphere Laplacian, which respects the recursive relation

$$\Delta_{\mathbb{S}^d}=\frac{1}{\sin^{d-1}\theta_{d-1}}\partial_{\theta_{d-1}}\left(\sin^{d-1}\theta_{d-1}\partial_{\theta_{d-1}}\right)+\frac{1}{\sin^2\theta_{d-1}}\Delta_{\mathbb{S}^{d-1}}. \tag{3.3.40}$$

The mass term corresponds with the conformal mass; nevertheless, it is a consequence of our deepest motivation. We suitably selected the mass to provide a fully resonant linearized spectrum and the conformal mass was the only possibility.

3.3.3.2 The Resonant System

Now, we are going to consider the regime where the fields $\phi,\dot{\phi}$ have small amplitudes. In this limit the linear equation dominates the dynamics. Their modes consist of the hyperspherical harmonics on $\mathbb{S}^d$ expressed through the recursive relation

$$Y_{nl\mu}(\theta_1,...,\theta_{d-1},\varphi)=N_{nl}\sin^l\theta_1 C_{n-l}^{\left(l+\frac{d}{2}-1\right)}\left(\cos\theta_1\right)Y_{l\mu}\left(\theta_2,...,\theta_{d-1},\varphi\right), \tag{3.3.41}$$

where N_{nl} is the suitable normalization constant, $C_n^{(\lambda)}(x)$ are the Gegenbauer polynomials and μ represents the other indices of lower-dimensional harmonics. They satisfy

$$\Delta_{\mathbb{S}^d}Y_{nl\mu}=-n(n+d-1)Y_{nl\mu}, \tag{3.3.42}$$

and thereby the linearized spectrum of (3.3.39) is $w_n=n+(d-1)/2$.

As consequence of the fully resonant spectrum, in this limit we can derive the resonant system to catch the non-trivial dynamics at long times. On this occasion, we shall use the method of multi-scales displayed in section 2.2. First, we must expand the solution in modes as

$$\phi=\epsilon\sum_{nl\mu}\left(\alpha_{nl\mu}(\epsilon^2t)e^{iw_nt}+\beta_{nl\mu}(\epsilon^2t)e^{-iw_nt}\right)Y_{nl\mu}, \tag{3.3.43}$$

following the subsequent steps we obtain a resonant system which couples α and β,

$$\frac{d\alpha_{n_1 l_1 \mu_1}}{d\tau} = \sum_{\substack{n_2 l_2 \mu_2 \\ n_1+n_4=n_3+n_4}} \sum_{n_3 l_3 \mu_3} \sum_{n_4 l_4 \mu_4} C_{n_1 l_1 \mu_1 \ldots n_4 l_4 \mu_4} \bar{\alpha}_{n_2 l_2 k_2} \alpha_{n_3 l_3 \mu_3} \alpha_{n_4 l_4 \mu_4}$$

$$+ 2 \sum_{\substack{n_2 l_2 \mu_2 \\ n_1+n_4=n_3+n_4}} \sum_{n_3 l_3 \mu_3} \sum_{n_4 l_4 \mu_4} C_{n_1 l_1 \mu_1 \ldots n_4 l_4 \mu_4} \bar{\beta}_{n_2 l_2 k_2} \beta_{n_3 l_3 \mu_3} \alpha_{n_4 l_4 \mu_4} \tag{3.3.44}$$

and

$$\frac{d\beta_{n_1 l_1 \mu_1}}{d\tau} = \sum_{\substack{n_2 l_2 \mu_2 \\ n_1+n_4=n_3+n_4}} \sum_{n_3 l_3 \mu_3} \sum_{n_4 l_4 \mu_4} C_{n_1 l_1 \mu_1 \ldots n_4 l_4 \mu_4} \bar{\beta}_{n_2 l_2 k_2} \beta_{n_3 l_3 \mu_3} \beta_{n_4 l_4 \mu_4}$$

$$+ 2 \sum_{\substack{n_2 l_2 \mu_2 \\ n_1+n_4=n_3+n_4}} \sum_{n_3 l_3 \mu_3} \sum_{n_4 l_4 \mu_4} C_{n_1 l_1 \mu_1 \ldots n_4 l_4 \mu_4} \bar{\alpha}_{n_2 l_2 k_2} \alpha_{n_3 l_3 \mu_3} \beta_{n_4 l_4 \mu_4}. \tag{3.3.45}$$

This system of equations has a large number of couplings which make it complicated for an analytic treatment. In order to simplify the problem, we will restrict the resonant system to special sectors. The first choice consists of setting $\beta = 0$, which is consistent with the equations. In this case, the remaining dynamical variable is $\alpha_{nl\mu}$ which is still too complicated, requiring a new truncation. Note that $l = \mu = 0$ in $d = 3$ corresponds with the conformal flow introduced in section 3.3.1; nevertheless, we will focus on the maximally rotating sector, namely $l = \mu = n$. This sector corresponds with modes of maximum angular momentum for each w_n. For this restriction there is only a single index, hence, we define

$$\alpha_n \equiv \frac{\alpha_{nnn}}{\sqrt{n + \frac{d-1}{2}}}. \tag{3.3.46}$$

The maximally rotating modes have the form

$$e_n = Y_{nnn} = \sqrt{\frac{\Gamma\left(n + \frac{d+1}{2}\right)}{\Gamma(n+1)}} \prod_{j=1}^{d-1} \sin^n \theta_j e^{-in\varphi}, \tag{3.3.47}$$

and the resonant system for this truncation becomes

$$i\frac{d\alpha_n}{d\tau} = \sum_{m=0}^{\infty} \sum_{k=0}^{n+m} C_{nmk(n+m-k)} \bar{\alpha}_m \alpha_k \alpha_{n+m-k} \tag{3.3.48}$$

with

$$C_{nmkl} = \frac{\kappa}{\sqrt{\left(n + \frac{d-1}{2}\right)\left(m + \frac{d-1}{2}\right)\left(k + \frac{d-1}{2}\right)\left(l + \frac{d-1}{2}\right)}} \int d\Omega_d \bar{e}_n \bar{e}_m e_k e_l$$

$$= \frac{\Gamma\left(\frac{d+1}{2}\right)}{\Gamma\left(\frac{d-1}{2}\right)^2}\sqrt{\frac{\Gamma\left(n+\frac{d-1}{2}\right)}{\Gamma(n+1)}\frac{\Gamma\left(m+\frac{d-1}{2}\right)}{\Gamma(m+1)}\frac{\Gamma\left(k+\frac{d-1}{2}\right)}{\Gamma(k+1)}\frac{\Gamma\left(l+\frac{d-1}{2}\right)}{\Gamma(l+1)}\frac{\Gamma(n+m+1)}{\Gamma\left(n+m+\frac{d+1}{2}\right)}}, \tag{3.3.49}$$

where $d\Omega_d = d\varphi\prod_{j=1}^{d-1}\sin^{d-j}\theta_j d\theta_j$ and κ is a numerical constant coming from a time-rescaling to satisfy (3.1.1).

In this situation there is a special dimension, $d = 3$. Only for this case we can formulate the following proposition.

Proposition mrSd: *for* $d = 3$, (3.3.49) *satisfies* $\mathcal{D}_{nmkl} = 0$ *for* $n + m - k - l = 1$ *with* $G = 1$ *and* $\beta = 1/3$, *defined in* (3.1.2).

Then, for the topology $\mathbb{R}\times\mathbb{S}^3$ the resonant system has analytic solutions as a three-dimensional invariant manifold composed by time-periodic solutions and stationary solutions bifurcating from each single-mode, and the additional conserved quantity Z for any solution of the equations. The invariant manifold was a result obtained in [76] while the existence of Z is a novel result of our formalism displayed in section 3.1.

3.3.4 Maximally Rotating Scalar Field in AdS$_{d+1}$

In this section we are going to consider the resonant system subject to a particular truncation of a scalar field in AdS$_{d+1}$ originally derived and studied in [76].

3.3.4.1 The Model

The model consists of a massive complex scalar field with a cubic nonlinear terms in AdS$_{d+1}$ (without backreaction). The line element is

$$ds^2 = \frac{1}{\cos^2 x}\left(-dt^2 + dx^2 + \sin^2 x d\Omega_{d-1}^2\right), \tag{3.3.50}$$

where $d\Omega_{d-1}^2$ is the line element of $\mathbb{S}^{d-1}$. The EOM becomes

$$\left(-\partial_{tt} + \frac{1}{\tan^{d-1} x}\partial_x \tan^{d-1} x\partial_x + \frac{1}{\sin^2 x}\Delta_{\mathbb{S}^{d-1}} - \frac{m^2}{\cos^2 x}\right)\phi - \frac{|\phi|^2\phi}{\cos^2 x} = 0, \tag{3.3.51}$$

where $\Delta_{\mathbb{S}^{d-1}}$ is the Laplacian of $\mathbb{S}^{d-1}$ given in (3.3.40) and the boundary conditions $\phi(t,\pi/2,\Omega) = 0$.

3.3.4.2 The Resonant System

Supposing small amplitudes for the fields $\phi, \dot{\phi}$ to achieve the weakly nonlinear limit, the reduced equation takes the form

$$\left(-\partial_{tt} + \frac{1}{\tan^{d-1} x}\partial_x \tan^{d-1} x\partial_x + \frac{1}{\sin^2 x}\Delta_{\mathbb{S}^{d-1}} - \frac{m^2}{\cos^2 x}\right)\phi(t,x,\Omega) = 0, \tag{3.3.52}$$

where its modes satisfy

$$e_{nlk} = N_{nlk} \cos^{\delta} x \sin^{l} x P_n^{\left(\delta-\frac{d}{2}, l+\frac{d}{2}-1\right)}(-\cos 2x) Y_{lk}(\Omega) \tag{3.3.53}$$

and the spectrum

$$w_{nlk} = 2n + l + \delta \tag{3.3.54}$$

where N_{nlk} is the appropriate normalization constant, $P_n^{a,b}(x)$ the Jacobi polynomials and $\delta = d/2 + \sqrt{(d/2)^2 + m^2}$. Observe the important property that the spectrum is fully resonant for any mass and dimensions. Then, considering small amplitudes we can apply the methods to capture the dynamics at times $1/\epsilon^2$ described in section 2.2. For example, following the method of multi-scales, first of all the solution must be expanded in modes as

$$\phi(t, x, \Omega) = \epsilon \sum_{nlk} \left(\alpha_{nlk}(\epsilon^2 t) e^{i w_{nlk} t} + \beta_{nlk}(\epsilon^2 t) e^{-i w_{nkl} t}\right) e_{nlk}(x, \Omega). \tag{3.3.55}$$

On this occasion, we will also restrict our study to $\beta = 0$ and the maximally rotating subsector. This truncation consists of modes with the maximum value of l and k for each w_{nlk}, namely, $n = 0$. As the dynamics has been restricted to a single mode-number we define our new variables as

$$\alpha_n \equiv \frac{\alpha_{0,n,n}}{\sqrt{n+\delta}}, \tag{3.3.56}$$

In this truncation the linear modes become

$$e_n(x, \theta_1, ...\theta_{d-2}, \varphi) = \sqrt{\frac{\Gamma(n+\delta+1)}{\Gamma(n+1)}} \cos^{\delta} x \sin^{n} x \prod_{j=1}^{d-2} \sin^{n} \theta_j e^{-in\Delta\phi}, \tag{3.3.57}$$

where $\theta_1, ..., \theta_{d-2}, \varphi$ represent the angles of $\mathbb{S}^{d-1}$. The resonant system takes the usual form

$$i\frac{d\alpha_n}{d\tau} = \sum_{m=0}^{\infty} \sum_{k=0}^{n+m} C_{nmk(n+m-k)} \bar{\alpha}_m \alpha_k \alpha_{n+m-k} \tag{3.3.58}$$

with

$$\begin{aligned} C_{nmkl} &= \frac{\kappa}{\sqrt{(n+\delta)(m+\delta)(k+\delta)(l+\delta)}} \int_0^{\pi/2} dx \, \frac{\tan^{d-1} x}{\cos^2 x} \int d\Omega_{d-1} e_n e_m e_k e_l \\ &= \frac{\Gamma(2\delta)}{\Gamma(\delta)^2} \sqrt{\frac{\Gamma(n+\delta)}{\Gamma(n+1)} \frac{\Gamma(m+\delta)}{\Gamma(m+1)} \frac{\Gamma(k+\delta)}{\Gamma(k+1)} \frac{\Gamma(l+\delta)}{\Gamma(l+1)}} \frac{\Gamma(n+m+1)}{\Gamma(n+m+2\delta)}, \end{aligned} \tag{3.3.59}$$

where κ is a numerical constant coming from a time rescaling to satisfy (3.1.1).

We want to remark that for $\delta = 1$ (3.3.58)-(3.3.59) contains the case of the maximally rotating scalar on $\mathbb{S}^3$ discussed in section 3.3.3. In that situation, a scalar field on $\mathbb{S}^d$, provided a family of interaction coefficients parametrized by the dimension of the hyper-sphere; nevertheless, only in the case $d = 3$ the identity $\mathcal{D}_{nmkl} = 0$ was satisfied. On this occasion the next proposition shows a different scenario.

Proposition mrAdS: (3.3.59) *satisfies* $\mathcal{D}_{nmkl} = 0$ *for* $n+m-k-l=1$ *with* $G=\delta$ *and* $\beta = \frac{1}{2}\frac{\delta+1}{2\delta+1}$, *defined in* (3.1.2).

This result is very interesting, we have obtained a continuous family of resonant systems belonging to the formalism we have derived in section 3.1. Although there are two free parameters, the mass and the dimension, they are combined in a special manner to leave a single freedom, δ. This system and the existence of the three-dimensional invariant manifold were obtained in [76], while the existence of the conserved quantity Z and the stationary solutions (3.1.28) as novel results of our formalism displayed in section 3.1 ([77]).

3.3.5 A Nonrelativistic Limit for AdS Perturbations

In this section we will present the resonant system and some of its properties obtained from the nonrelativistic limit ($c \to \infty$) of a scalar field in AdS. These results were derived in [78].

3.3.5.1 The Model

The initial model consists of a complex massive scalar field minimally coupled to gravity in (d+1)-dimensions:

$$S = S_{EH} + S_\phi = \frac{c^4}{16\pi G}\int d^{d+1}x\sqrt{-g}\,(R-2\Lambda) - \int d^{d+1}x\sqrt{-g}\left(\frac{\hbar^2}{m}\partial_\mu\phi\partial^\mu\bar{\phi} + mc^2|\phi|^2\right), \tag{3.3.60}$$

The EOMs take the form

$$\frac{1}{\sqrt{-g}}\partial_\mu\sqrt{-g}\partial^\mu\phi - \frac{m^2c^2}{\hbar^2}\phi = 0, \tag{3.3.61}$$

$$G_{\mu\nu} + \Lambda g_{\mu\nu} = \frac{8\pi G}{c^4}T_{\mu\nu} \tag{3.3.62}$$

where $G_{\mu\nu}$ is the Einstein's tensor and $T_{\mu\nu}$ the energy-momentum tensor given by

$$T_{\mu\nu} = -\frac{2}{\sqrt{-g}}\frac{\delta S_\phi}{\delta g^{\mu\nu}}. \tag{3.3.63}$$

In [78] the authors considered AdS_{d+1} spacetime, which has the particular value for the cosmological constant: $\Lambda = -d(d-1)/2l^2$ (see section 2.4.1). The nonrelativistic limit requires an expansion in powers of $1/c$ for which the leading orders of the scalar solution and the line element were taken as

$$\phi(t,x) = e^{-i\frac{mc^2}{\hbar}t}\psi(t,x), \tag{3.3.64}$$

$$ds^2 = -c\left(1+\frac{2A(t,x)}{c^2}\right)dt^2 + \left(1+\frac{2B(t,x)}{c^2}\right)\sum_{n=1}^{d}(dx^n)^2, \tag{3.3.65}$$

where $x \in \mathbb{R}^d$. This limit requires also that $l \to \infty$ when $c \to \infty$ leaving the ratio $c/l \to \omega$ finite. This condition can be rewritten as

$$\lim_{c\to\infty} \Lambda c^2 = -\frac{d(d-1)}{2}\omega^2. \tag{3.3.66}$$

Introducing (3.3.64)-(3.3.66) in (3.3.61)-(3.3.62), after several manipulations which can be consulted in [78], the resulting equations are

$$i\partial_t\psi = -\frac{\hbar^2}{2}\Delta\psi + \frac{1}{2}m\omega^2|x|^2\psi + V\psi, \tag{3.3.67}$$

$$\Delta V = 8\pi G\frac{d-2}{d-1}|\psi|^2, \tag{3.3.68}$$

where Δ is the d-Lapacian. With it, we have obtained that the nonrelativistic limit of a complex massive scalar field in AdS_{d+1} is governed by the Schrödinger-Newton equation with the harmonic potential. This equation was denominated Schrödinger-Newton-Hook (SNH) by the authors of [78].

Finally, equations (3.3.67)-(3.3.68) can be gathered in a single one by using the method of Green's function. Additionally, we will restrict the solutions to be spherically symmetric (denoting the radial coordinate as r). Performing the appropriate rescaling in t, r and ψ, the final equation is expressed in the dimensionless form

$$i\partial_t\psi(t,r) = -\frac{1}{2}\left(\partial_{rr} + \frac{d-1}{r}\partial_r - w^2r^2\right)\psi(t,r) - \left(\int_0^\infty ds\, s^{d-1}\frac{|\psi(t,s)|^2}{\max[r^{d-2}, s^{d-2}]}\right)\psi(t,r). \tag{3.3.69}$$

3.3.5.2 The Resonant Model

Now we are going to consider the weakly nonlinear regime of equation (3.3.69). Its linear modes and spectrum are represented by (see [175])

$$e_n(r) = \left(\frac{2n!}{\Gamma\left(n+\frac{d}{2}\right)}\right)^{1/2} L_n^{\left(\frac{d}{2}-1\right)}(r^2)e^{-\frac{r^2}{2}}, \tag{3.3.70}$$

and

$$w_n = 2n + \frac{d}{2}, \tag{3.3.71}$$

where $L_n^{(a)}(x)$ are the Laguerre polynomials. The spectrum is fully resonant and therefore we can follow the procedures displayed in section 2.2 to derive the resonant system. For example, considering the method of multi-scales we must write the solutions in terms of linear modes as

$$\psi(t,r) = \epsilon\sum_{n=0}^{\infty}\alpha_n(\epsilon^2 t)e^{-iw_nt}e_n(r). \tag{3.3.72}$$

Following the subsequent steps of the method, the resonant system takes the form

$$i\frac{d\alpha_n}{d\tau} = \sum_{m=0}^{\infty}\sum_{k=0}^{n+m} C_{nmk(n+m-k)}\bar{\alpha}_m\alpha_k\alpha_{n+m-k}, \tag{3.3.73}$$

with interaction coefficients composed as

$$C_{nmkl} = \frac{1}{2}\left(\tilde{C}_{nmkl} + \tilde{C}_{nmlk}\right) \tag{3.3.74}$$

where

$$\tilde{C}_{nmkl} = 2\int_0^\infty r\ dr \int_0^\infty \min(r^{d-2}, s^{d-2})e_n(r)e_m(s)e_k(s)e_l(r)\ s\ ds. \tag{3.3.75}$$

This family of resonant systems is parametrized by the dimension, d. Nevertheless, in [78] it was proved that $d = 4$ is special from our point of view. The result is summarized in the next proposition.

Proposition nrAdS: (3.3.74) *satisfies* $\mathcal{D}_{nmkl} = 0$ *for* $n + m - k - l = 1$ *with* $G = 2$ *and* $\beta = \frac{3}{8}$, *defined in* (3.1.2).

In consequence, the resonant system derived for a nonrelativistic free spherically symmetric scalar field in AdS_5, (3.3.73)-(3.3.75), enjoys the results obtained in section 3.1. Namely, it has analytic solutions as time-periodic solutions given by (3.1.7) and stationary solutions of the form (3.1.28) and the conserved quantity Z.

3.3.6 The Cubic Szegö Equation

3.3.6.1 The Model and the Resonant System

The resonant system (3.0.1) is strongly coupled; any triad $m, k, l \in \mathbb{N}$, satisfying $n = k + l - m$ contributes to $\dot{\alpha}_n$. This fact makes the resonant system highly complicated for an analytic analysis. Only special structures of the interaction coefficients allow this task for particular subsectors of α_n. With the goal of obtaining a better understanding of this kind of equations, a simple toy model consists of setting the interaction coefficients to one, namely $C_{nmkl} = 1$. The resulting resonant system becomes

$$i\frac{d\alpha_n}{d\tau} = \sum_{m=0}^{\infty}\sum_{k=0}^{n+m} \bar{\alpha}_m\alpha_k\alpha_{n+m-k}. \tag{3.3.76}$$

This system was introduced and studied in [64], where it was derived as the resonant system of the *cubic Szegö equation*. Following this line, [65–67] performed a deeper study of its properties. We must highlight its most relevant features as: it is Lax-integrable (in consequence it has infinite conserved quantities), the existence of finite dimensional invariant manifolds, and that it presents analytic solutions displaying weak turbulence.

It is remarkable that a simple toy model holds all these features. See [75] for a brief and excellent introduction.

The cubic Segö equation was introduced in [64] as the differential equation

$$i\partial_t u = \Pi\left(|u|^2 u\right), \tag{3.3.77}$$

where $u(t,z)$ is the complex function

$$u(t,z) = \sum_{n=0}^{\infty} \alpha_n(t) z^n, \qquad \sum_{n=0}^{\infty} |\alpha_n|^2 < \infty, \tag{3.3.78}$$

defined on the unit circle in the complex plane:

$$\mathbb{S}^1 = \{z \in \mathbb{C}, |z| = 1\}, \tag{3.3.79}$$

and Π is an operator (denominated Szegö operator) which removes negative powers, namely,

$$\Pi\left(\sum_{n\in\mathbb{Z}} \alpha_n z^n\right) = \sum_{n=0}^{\infty} \alpha_n z^n. \tag{3.3.80}$$

3.3.6.2 Analytic Solutions

As we have already mentioned, (3.3.76)-(3.3.77) admit several analytic solutions. For example combinations of the form

$$u(t,z) = \sum_{n=0}^{N} \frac{b_n(t)}{1 - p_n(t) z}, \qquad |p_n| < 1, \qquad N \geq 2. \tag{3.3.81}$$

Nevertheless, the most interesting solution from our point of view has the form

$$u(t,z) = \frac{b(t) + a(t) z}{1 - p(t) z}, \qquad |p| < 1, \tag{3.3.82}$$

which in terms of modes it is

$$\alpha_0 = b, \qquad \alpha_{n\geq 1} = (a + bp) p^{n-1}. \tag{3.3.83}$$

Solutions of this ansatz are time-periodic, but the most salient feature consists of the fact that the single-mode

$$|\alpha_1(0)| \neq 0, \qquad |\alpha_{n\neq 1}(0)| = 0. \tag{3.3.84}$$

is unstable, and the ansatz (3.3.83) captures this instability. For initial data of the form

$$\alpha_0(0) = 2\epsilon, \qquad \alpha_1(0) = 1, \qquad |\alpha_{n\geq 2}(0)| = 0, \tag{3.3.85}$$

the function $p(t)$ takes the form

$$\frac{-i}{\sqrt{1+\epsilon^2}}\sin\omega t e^{-2i\epsilon t^2}, \quad \omega = 2\epsilon\sqrt{1+\epsilon^2}. \tag{3.3.86}$$

We can observe that despite the energy transfer is periodic (a and b are also periodic), high modes become arbitrarily excited as $\epsilon \to 0$ because $|p(T)| \approx 1 - \epsilon/2$, where $\sin(\omega T) = 1$.

Despite this brief exhibition of analytic properties, we must remark that this system does not satisfy (3.1.11) and therefore the formalism given in section 3.1 cannot be applied. This fact can be easily checked by direct computations of $\mathcal{D}_{nmkl}$ for $n+m = k+l+1$. Another option is to compute identities (3.1.4), we observe that for $f_n = 1$ (that is $G = 1$)

$$g_0^{(n+m)} = n+m+1, \qquad g_2^{(n+m)} = (n+m)\left(\frac{(n+m)^2}{3} + \frac{(n+m)}{2} + \frac{1}{6}\right), \tag{3.3.87}$$

which they do not match with (3.1.5). Nevertheless, $g_0^{(n,m)}$ belongs to the class

$$g_0^{(n,m)} = \eta + \sigma(n+m), \tag{3.3.88}$$

displayed in section 3.1.5. In consequence, we immediately obtain a family of stationary solutions given by Proposition 3.1.5.2. In terms of the generating function $u(t,z)$ this family of solutions has the form

$$u(t,x) = \frac{b(t)}{1-p(t)z}, \tag{3.3.89}$$

which is already contained in (3.3.82) for $a = 0$.

3.3.6.3 The Strong Localization Limit

Despite that for this resonant system we have a large class of analytic solutions it is particularly interesting to observe as its manageability is also transferred to the SLL. Special interest arouses the instability of mode 1.

Equation (3.3.76) is written in the form such that the results displayed in section 3.2 are directly applicable. First, we will focus on the SLL around mode 0. In this case $C_{n0k(n-k)} = 1$ and the reduced resonant system becomes

$$\begin{aligned} &i\dot{q}_0 - q_0 = 0,\\ &i\dot{q}_1 - 2q_1 = 0,\\ &i\dot{q}_n - 2q_n = \bar{q}_0 \sum_{k=1}^{n-1} q_k q_{n-k}, \qquad n > 1, \end{aligned} \tag{3.3.90}$$

where we have set $|q_0| = 1$ as was explained in section 3.2. We could solve this system of equations iteratively starting with $n = 0$, but instead of it, we will use Proposition

3.2.1.1 and the results below it. Note that $C_{n0n0} = 1$ is a particular case of (3.2.16) with $\eta = 1, \sigma = 0$. Hence, we obtain the frequencies Ω_{nkl} from (3.2.20),

$$\Omega_{nkl} = l + 2. \tag{3.3.91}$$

It clearly satisfies $\Omega_{nkl} - 2C_{0n0n} > 0$ for any $n, l > 0$, in consequence Proposition 3.2.1.1 can be applied to obtain the structure of the solution for the SLL around mode 0,

$$q_0(t) = e^{-it}, \qquad q_n(t) = \sum_{l=0}^{n-1} A_l e^{-i(l+2)t}. \tag{3.3.92}$$

Note that any solution is at least 2π-periodic.

After inspecting the SLL around mode 0 it is modes 1's turn. It will be interesting to observe the manifestation of the instability displayed by this mode. First we are going to exhibit the equations (3.2.27)-(3.2.31), which after imposing $C_{n1n1} = C_{2011} = 1$ and $|q_1| = 1$ take the form

$$\begin{aligned}
i\dot{q}_0 - 2q_0 &= \bar{q}_2 q_1^2, && (3.3.93)\\
i\dot{q}_1 - q_1 &= 0, && (3.3.94)\\
i\dot{q}_2 - 2q_2 &= \bar{q}_0 q_1^2, && (3.3.95)\\
i\dot{q}_3 - 2q_3 &= \bar{q}_1 q_2^2 + 2\bar{q}_0 q_1 q_2, && (3.3.96)\\
i\dot{q}_4 - 2q_4 &= 2\bar{q}_1 q_2 q_3 + \bar{q}_0 q_2^2. && (3.3.97)
\end{aligned}$$

Solving the first three equations we already see the consequence of the instability,

$$q_1(t) = e^{-it}, \qquad q_0(t) = Ae^{-it} + Bte^{-it}, \qquad q_2(t) = -\left(\bar{A} + i\bar{B}\right) e^{-it} - \bar{B}te^{-it}. \tag{3.3.98}$$

Expressions for q_0, q_2 have a continuously growing term which invalidates the perturbative expansion at times $1/\delta$; namely, secular terms are present. The instability is manifested in the SLL as a collection of secular terms for any mode different from q_1. It prevents catching the periodic behavior of certain configurations as is the case of (3.3.85).

3.3.7 Massless Scalar Field in Global AdS

In this section we will a free spherically symmetric massless scalar field in AdS minimally coupled to gravity and its weakly nonlinear dynamics. In particular, we are going to reexamine the issue of energy returns in global AdS_4. Further details to the ones provided here can be found in [6, 35, 36, 42]. Although this model can be included as a particular case of the massive scalar field considered in the next section, this situation was more extensively studied than the massive case, and therefore we treat them independently.

3.3.7.1 The Model

The model consists of Einstein's gravity with a negative cosmological constant

$$\Lambda = -\frac{d(d-1)}{2} \tag{3.3.99}$$

in d spatial dimensions, with a minimally coupled free massless scalar field. It is governed by the action

$$S = \frac{1}{16\pi G}\int d^{d+1}x\sqrt{-g}\,(R-2\Lambda) - \frac{1}{2}\int d^{d+1}x\sqrt{-g}\,(\partial_\mu\phi\partial^\mu\phi)\,. \tag{3.3.100}$$

The EOMs are

$$R_{\mu\nu} - \frac{1}{2}g_{\mu\nu}R + \Lambda g_{\mu\nu} - 8\pi G\left(\partial_\mu\phi\partial_\nu\phi - \frac{1}{2}g_{\mu\nu}(\partial\phi)^2\right) = 0 \tag{3.3.101}$$

and

$$\frac{1}{\sqrt{-g}}\partial_\mu\left(\sqrt{-g}g^{\mu\nu}\partial_\nu\phi\right) = 0. \tag{3.3.102}$$

One can consistently truncate to spherically symmetric configurations, corresponding to the metric ansatz

$$ds^2 = \frac{1}{\cos^2 x}\left(-fe^{-2\delta}dt^2 + \frac{dx^2}{f} + \sin^2 x\, d\Omega_{d-1}^2\right), \tag{3.3.103}$$

where $f(x,t)$, $\delta(x,t)$ and $\phi(x,t)$ only depend on the time coordinate t and the radial coordinate x, which is defined on the interval $[0,\pi/2)$. We shall set $8\pi G = d-1$.

Following [6], we introduce

$$\Phi \equiv \phi', \qquad \Pi \equiv f^{-1}e^{\delta}\dot{\phi} \tag{3.3.104}$$

(where $\dot{} \equiv \partial_t$, $' \equiv \partial_x$), and also the following two predefined functions

$$\mu(x) \equiv (\tan x)^{d-1} \qquad \text{and} \qquad \nu(x) \equiv \frac{(d-1)}{\mu'(x)} = \frac{\sin x\cos x}{(\tan x)^{d-1}}. \tag{3.3.105}$$

The EOMs are then written as

$$\dot{\Phi} = \left(fe^{-\delta}\Pi\right)', \qquad \dot{\Pi} = \frac{1}{\mu}\left(\mu fe^{-\delta}\Phi\right)', \tag{3.3.106a}$$

$$f' = \frac{\nu'}{\nu}(f-1) - \mu\nu\left(\Phi^2+\Pi^2\right)f, \qquad \delta' = -\mu\nu\left(\Phi^2+\Pi^2\right), \tag{3.3.106b}$$

$$\dot{f} = -2\mu\nu f^2 e^{-\delta}\Phi\Pi. \tag{3.3.106c}$$

Static solutions of these equations are the AdS-Schwarzschild black holes $f(x,t) = 1 - M\nu(x)$, $\delta(x,t) = 0$ and $\phi(x,t) = 0$, while unperturbed AdS_{d+1} corresponds to $f = 1$, $\delta = \phi = 0$.

Note that because of the spherical symmetry imposed by our ansatz (3.3.103), the metric has no propagating degrees of freedom. At each given time slice, the constraint equations (3.3.106b) can be integrated to express the metric components in terms of the matter distribution given by $\phi(x,t)$ at the same moment of time. Specifically the integral forms of f and δ are

$$f(t,x) \quad = 1 - e^{\delta(t,x)}\nu(x)\int_0^x dy\ \mu(y)e^{-\delta(t,y)}\left(\Phi(t,y)^2+\Pi(t,y)^2\right) \tag{3.3.107}$$

$$\delta(t,x) \quad = \begin{cases} -\int_0^x dy\ \mu(y)\nu(y)\left(\Phi(t,y)^2+\Pi(t,y)^2\right) & \text{if } \delta(t,0)=0 \\ \int_x^{\pi/2} dy\ \mu(y)\nu(y)\left(\Phi(t,y)^2+\Pi(t,y)^2\right) & \text{if } \delta(t,\pi/2)=0 \end{cases} \tag{3.3.108}$$

3.3.7.2 The Resonant System

The structure of the EOMs allows the perturbative expansion around the AdS-background

$$\phi(t,x)=\sum_{n=0}^{\infty}\epsilon^{2n+1}\phi_{2n+1}(t,x),\qquad f(t,x)=1-\sum_{n=1}^{\infty}\epsilon^{2n}f_{2n}(t,x),\qquad \delta(t,x)=\sum_{n=1}^{\infty}\epsilon^{2n}\delta_{2n}(t,x). \tag{3.3.109}$$

This procedure leads to an infinite system of equations of the form

$$\Box_{\rm AdS}\,\phi_{2n+1}=S_{2n+1}[\phi_l], \tag{3.3.110}$$

where $l<2n+1$, $\Box_{\rm AdS}$ is the Laplacian in (a non-dynamical) AdS_{d+1} and $S_{2n+1}[\phi_l]$ symbolically denotes all the nonlinear terms with a factor ϵ^{2n+1} (which are local in time but nonlocal in space), arising from integrating out f and δ. The leading term in $S_{2n+1}[\phi_l]$ is cubic; explicit expressions can be found in [6, 36]. Only this cubic part is significant for our present discussion, since that is what affects the specific weakly nonlinear regime we focus on, see [36]. One might find it strange that we talk about gravitational dynamics in AdS, while under the assumption of spherical symmetry the metric is non-dynamical and one ends up with a nonlinear wave equation for a scalar field in a fixed AdS background. Nonetheless, there are closely related constructions, which are purely gravitational, without any matter, and utilize a 'squashed' generalization of our ansatz, see [43]. Such extensions effectively result in nonlinear wave equations very similar to the one we have for the scalar field, but now satisfied by the metric components in the absence of any matter.

The problem of weakly nonlinear gravitational dynamics of the AdS-scalar field system under the assumption of spherical symmetry is thus reduced to a complicated nonlinear wave equation in a fixed AdS background. This highlights the relation between gravitational stability of AdS and simpler nonlinear wave equations in AdS that have been considered in the literature as toy models, for example, the $\lambda\phi^4$ theory in nondynamical AdS, see [39, 75, 76]. Our aim shall be to develop an effective treatment of this dynamics for small fields ϕ of order ε on long time scales of order $1/\varepsilon^2$. This is the regime in which interesting phenomenology, including black hole formation ('turbulent instability'), has been observed in numerical experiments starting with [6].

Before proceeding with weakly nonlinear analysis, one must thoroughly understand the linearized problem, i.e. the equation

$$\Box_{\rm AdS}\,\phi_1=0, \tag{3.3.111}$$

which under the assumption of spherical symmetry takes the form

$$\ddot{\phi}_1-\mathcal{L}\phi_1=0\qquad\text{with}\qquad \mathcal{L}\equiv\frac{1}{\mu(x)}\partial_x\left(\mu(x)\partial_x\right). \tag{3.3.112}$$

Imposing Dirichlet boundary conditions $\phi(t,\pi/2)=0$ we observe that the spectrum is fully resonant; the eigenvalues for the operator $\mathcal{L}$ are ω_n^2, with

$$\omega_n=d+2n,\quad n=0,1,..., \tag{3.3.113}$$

and the eigenfunctions have the form

$$e_n(x) = k_n \cos^d x \, P_n^{\left(\frac{d}{2}-1,\frac{d}{2}\right)}(\cos 2x) \qquad \text{with} \qquad k_n = \frac{2\sqrt{n!(n+d-1)!}}{\Gamma\left(n+\frac{d}{2}\right)}. \tag{3.3.114}$$

Here, $P_n^{(a,b)}(x)$ are Jacobi polynomials of degree n.

The particular application of the methods of multi-scales and averaging was introduced in [34] and developed analytically in [35,36]. Following the method of averaging described in section 2.2.3, one starts by expanding solutions of (3.3.110) in terms of linearized eigenmodes (3.3.114) as

$$\begin{aligned}\phi(x,t) &= \varepsilon \sum_{n=0}^{\infty} \left(\alpha_n(t) e^{-i\omega_n t} + \bar{\alpha}_n(t) e^{i\omega_n t}\right) e_n(x), \\ \dot{\phi}(x,t) &= -i\varepsilon \sum_{n=0}^{\infty} \omega_n \left(\alpha_n(t) e^{-i\omega_n t} - \bar{\alpha}_n(t) e^{i\omega_n t}\right) e_n(x),\end{aligned} \tag{3.3.115}$$

and equivalently rewriting (3.3.110) as a system of equations for α_n; namely, the *periodic standard form*. Thereby the method of averaging may be applied to simplify this equation in a way that does not affect its accuracy on timescales of order $1/\varepsilon^2$. The result is a resonant system of the form

$$i\omega_n \frac{d\alpha_n}{d\tau} = \sum_{m=0}^{\infty} \sum_{k=0}^{n+m} C_{nmk(n+m-k)}\, \bar{\alpha}_m \alpha_k \alpha_{n+m-k}, \tag{3.3.116}$$

where the *slow time* $\tau \equiv \varepsilon^2 t$ has been introduced. For this gravitational system we are considering here, the explicit expressions for C are very complicated and can be found in [36]. In Appendix A.4, we extend them to the case of a massive scalar field, which will be discussed in section 3.3.8 (in consequence the current situation is included by setting $m^2 = 0$).

Equation (3.3.116) can be transformed in (3.0.1) by the transformation

$$\alpha_n \to \frac{\alpha_n}{\sqrt{\omega_n}}, \qquad C_{nmkl} \to \sqrt{\omega_n \omega_m \omega_k \omega_l} C_{nmkl}. \tag{3.3.117}$$

Nevertheless, the literature in relation to this model extensively uses (3.3.116); for this reason we will also follow this form to allow an easier inclusion of our results.

Note that equation (3.3.116) only connects the resonant channel $\omega_n + \omega_m = \omega_k + \omega_l$ ($n + m = k + l$) despite the spectrum (3.3.113) allows resonances $\omega_n = \omega_k \pm \omega_l \pm \omega_m$. In consequence, the resonant system should have the form (2.2.70) with additional channels interacting through the coefficients U_{nmkl} and Q_{nmkl}, but such terms can be shown to vanish specifically in AdS due to special selection rules [35–38].

Correspondingly, there is an emergent $U(1)$ symmetry rotating the phases of α_n by a common shift, which is manifest in (3.3.116) but absent in (3.3.110). In immediate relation

to the extra $U(1)$ symmetry resulting from selection rules, there is an extra conservation law [36, 39, 40] for the associated 'particle number'

$$N = \sum \omega_n |\alpha_n|^2 \tag{3.3.118}$$

in addition to the total 'linearized energy'

$$E = \sum \omega_n^2 |\alpha_n|^2, \tag{3.3.119}$$

generically conserved by resonant systems. Note that (3.3.118) is the same quantity as (3.0.4), the last expression is obtained after applying the transformation (3.3.117). While (3.3.119) is a linear combination between (3.0.4) and (3.0.5) after applying (3.3.117) (E is more common than J in the literature). Therefore, the transformations associated with these conserved quantities are also (3.0.6).

In the next sections, we are going to examine solutions for (3.3.116) starting with two-mode initial data

$$|\alpha_0(0)|, |\alpha_1(0)| \neq 0, \qquad \alpha_{n\geq 2}(0) = 0. \tag{3.3.120}$$

In particular, the energy distribution between the modes may be quantified by

$$E_n(t) = \omega_n^2 |\alpha_n(t)|^2, \tag{3.3.121}$$

and we may scan the evolution of two-mode initial data for return moments when the deviation from the initial energy distribution is small.

Due to the scaling symmetry of (3.0.7) we can transform any initial data (3.1.10) to satisfy

$$E_0(0) + E_1(0) = 1. \tag{3.3.122}$$

Thereafter, it is sufficient to study the quantity

$$\Delta(t) = 1 - E_0(t) - E_1(t). \tag{3.3.123}$$

If $\Delta(t)$ is 0, joint conservation of (3.3.118) and (3.3.119) guarantees that $E_0(t) = E_0(0)$ and $E_1(t) = E_1(0)$, i.e., we have found a perfect return, while $0 < \Delta(t) \ll 1$ signifies an accurate but imperfect return. As we have see through this section, for resonant systems which satisfy $\mathcal{D}_{nmkl} = 0$, as well as, for the cubic Szegö equation, $|\alpha_n|$ is periodic for the two-mode initial data (3.3.120). In consequence, $\Delta(t)$ periodically drops to 0, signalling exact returns. In this case, we shall look closely into similar return phenomena for the gravitational resonant system (3.3.116), which is only possible numerically.

3.3.7.3 Numerical Analysis

Before describing the results of our own numerical experiments, we briefly summarize what has been done in this area before to introduce the motivation of this section. Already in [34], one of the themes was the observation of accurate but imperfect returns of

energy to the initial configuration for two-mode initial data in the resonant system for gravitational AdS_4 perturbations (3.3.116) (there referred to as the Two-Time-Framework approximation). These numerical studies were performed at the resolution available at that time, which amounted to truncating the resonant system to the lowest 30 or 47 modes, and returns with a precision of a few percent were observed. The evolution was seen to proceed in a sequence of direct and reverse energy cascades, and the third reverse cascade led to a more accurate return to the initial energy distribution than the first two. Subsequently, a few developments occurred, including the derivation of analytic expressions for the interaction coefficients of the AdS resonant systems in terms of the AdS mode functions in [35,36] and an algorithm to convert these expressions into explicit (but very complicated) functions of the mode numbers in [56]. While this has allowed simulations of the resonant dynamics with much higher precision, the question of energy returns has not been properly readdressed in the literature following these developments.

We reiterate our reasons to revisit the question of energy returns in AdS_4. Our current perspective is quite different from the predominant views at the time [34] was written. Indeed, in the years that have passed, a number of examples have emerged, where resonant systems closely related to the one studied in [34] display *exact*, rather than approximate, energy returns. These include the models summarized in sections from 3.3.1 to 3.3.5 which cover different setups as nonlinear probe fields in AdS [75, 76] as well as nonlinear Schrödinger equations in harmonic potentials that arise from AdS systems in a nonrelativistic limit [72–74, 78]. This puts the results of [34] in a different light and calls for their re-examination. Note that the limited precision of [34] (mode number cut-off at a few dozens modes) makes it impossible to distinguish exact and approximate returns. In particular, in application to the systems of 3.3.1 to 3.3.5, where we have *analytically* showed that returns are exact, such simulations would have indicated approximate returns (the imperfection in this case being a pure artifact of truncating the infinite-dimensional system).

To elucidate the issue of energy returns in global AdS_4, we have performed simulations with up to 500 modes studying the dependence of the return accuracy on the mode number cut-off as well as on the arithmetic precision. For some initial energy distributions between the two lowest modes, the returns we observe are strikingly accurate. Fig. 3.5a provides an illustration in this regard: we study the evolution of two-mode initial data which are fairly generic (not particularly close to one-mode initial data) over a sequence of nine direct-reverse cascades. After each three cascades, we have a return to the initial configuration that is visually indistinguishable from exact, and furthermore the whole pattern periodically repeats after each three oscillations in a way that is visually indistinguishable from exact periodicity. All of this happens in (our high-precision numerical truncation of) the infinite-dimensional nonlinear resonant system (3.3.116) that has no small parameters! Note that the plot given in Fig. 3.5a is visually extremely similar to an analogous plot (see Fig. 3.5b) in the LLL resonant system (section 3.3.2, $L = 0$), where we have analytically proved in section 3.3.2 that the energy returns are exact. Fig. 3.6 provides four illustrations where we can observe the behavior of the energy flow for different initial energy distributions between the first two modes: Fig. 3.6a is particularly close

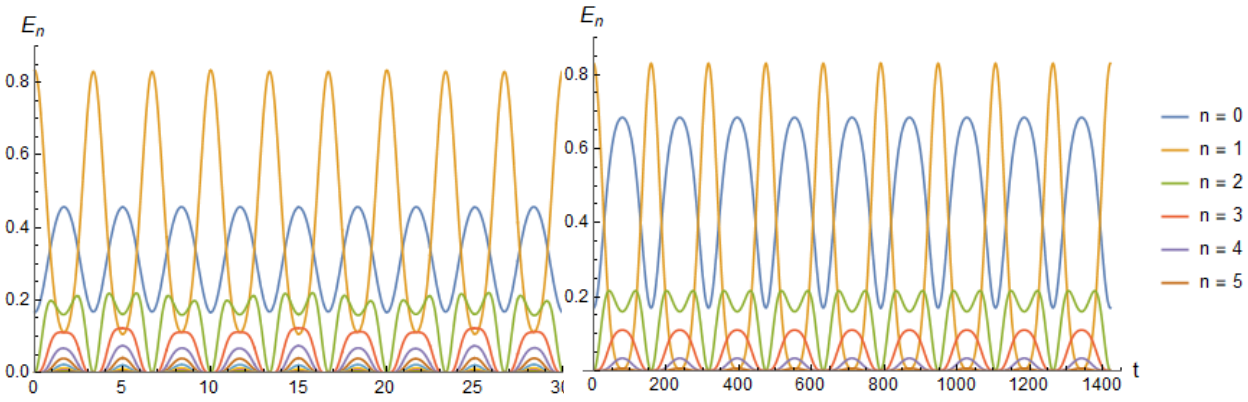

(a) AdS_4 (b) LLL

Figure 3.5: Nearly periodic dynamics of the spectrum for the gravitational AdS_4 resonant system vs. exactly periodic dynamics for the Landau level $L = 0$ displayed in section 3.3.2.1.2, denominated *Lowest Landau level* (LLL). The tiny deviations from exact periodicity in (a) are not visually discernible. The initial condition is (3.1.10, 3.3.122) with $E_0 = 0.17$ for both plots.

to the second mode and the evolution appears periodic after each direct-reverse cascade, while in Fig. 3.6b and Fig. 3.6c the apparent periodicity only emerges after three direct-reverse cascades. Finally Fig. 3.6d describes initial data for which the evolution visibly deviates from perfect periodicity, although it is remarkable that the deviations are still pretty small.

And yet, spectacular as some of these returns are, they are not exact. This by itself is not conclusive, since returns in numerical simulations of truncated systems would not have been exact even if returns in the infinite-dimensional dynamical system were exact. We thus have to quantify the dependence of the accuracy of returns on the initial data, as well as on the mode number cut-off, arithmetic precision and other numerical imperfections. To set the stage, we present in Fig. 3.7 plots showing the dependence of two essential quantities on the initial energy of mode 0 for two-mode initial data. The first quantity (fig 3.7a) is the minimal value of Δ defined by (3.3.123) over the first three direct-reverse cascades, which quantifies the energy return precision (evidently, in computing the minimum we exclude the initial part of the first direct cascade where Δ is small simply because the system has not had enough time yet to deviate from the initial conditions). We see that the worst returns are around $E_0 \approx 0.6$ at a level slightly better than 10%, while for most other initial data away from that value the returns have precision better than 1%. The second quantity we plot (in fig 3.7b) measures the strength of the turbulent cascade starting with the given two-mode initial data. The energy spectrum of configurations that undergo regular evolution is suppressed exponentially for large mode numbers, $E_n(t) \sim n^{\gamma(t)} \exp(-\rho(t)n)$ with $\rho(t) > 0$, and turbulent singularity formation, in particular, would correspond to $\rho(t)$ hitting zero at a certain time [41, 50, 187]. We quantify the strength of a turbulent cascade by determining how small $\rho(t)$ becomes during the time interval of interest. Therefore, we first fit the logarithm of the spectrum $\log E_n(t)$

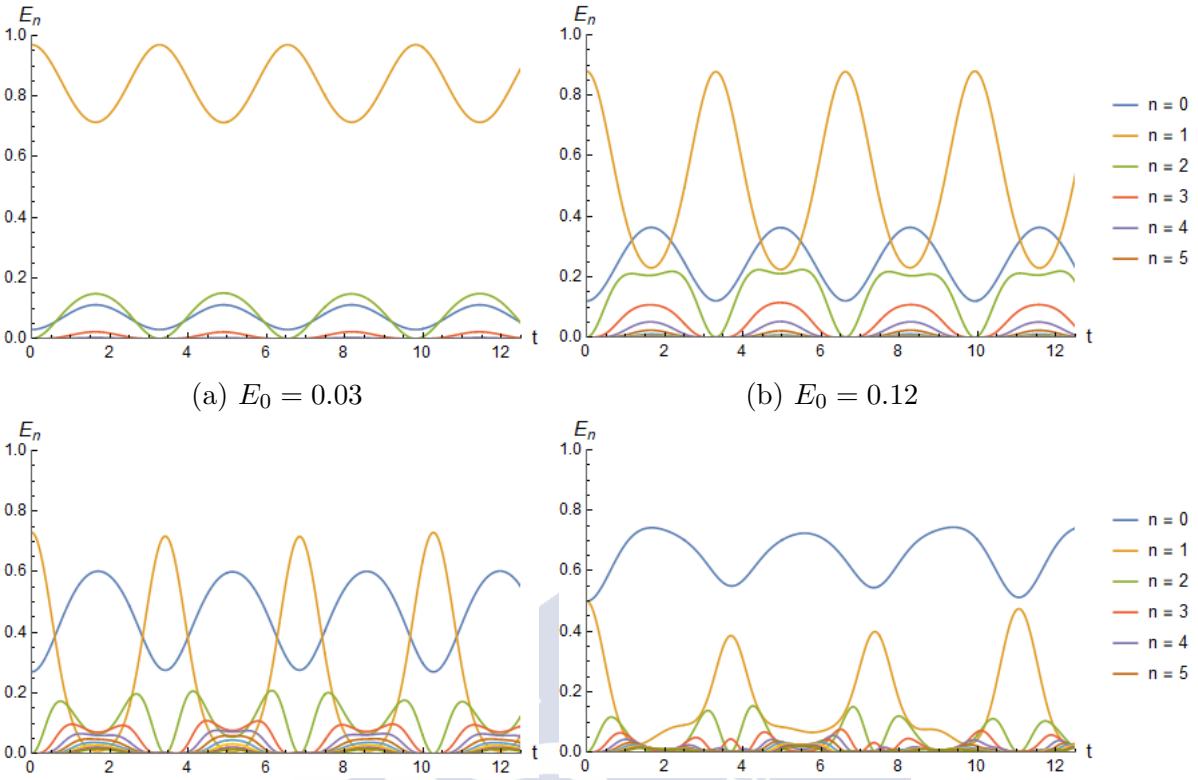

(a) $E_0 = 0.03$ (b) $E_0 = 0.12$

(c) $E_0 = 0.27$ (d) $E_0 = 0.5$

Figure 3.6: This sequence of time evolutions of four two-mode initial data (3.1.10, 3.3.122) shows that (a) the energy transfer between modes appears to evolve in a periodic way when the initial condition is close to mode 1 (a), that for larger E_0 the evolution is apparently periodic only after three oscillations (b,c), and that for equal-energy initial conditions, the returns are visibly not exact, but still more accurate after three oscillations (d).

to $-\rho(t)n + \gamma(t)\log n$ and then plot the minimal value of ρ attained over the first three oscillations. We see that the energy return imperfections are especially strong in the region where the turbulent cascade is strong as well. A strong turbulent cascade means, in particular, a stronger sensitivity to the mode number cut-off (as one would need to appreciably excite modes above the cut-off to keep the evolution exact, but those modes are excluded from simulations). This makes the problem of interpreting the deviations from exact returns rather subtle. Since we are entering the realm of precision questions, we must categorize and quantify the uncertainties incurred by our numerics. There are of course generic small errors arising from numerical integration of the equations of motion, but we feel that the following three aspects are particularly important, since they are specific to the sequences of direct and reverse cascades of energy we study:

1) *Mode number truncation:* Restricting to a finite number of modes is expected to have little effect if the energy mostly remains locked within a set of low-lying modes. In our case, an energy cascade develops, transferring the energy to higher modes. While the cascade is self-limiting (unlike in the fully turbulent case of [41], where $\rho(t)$ develops a zero), it can

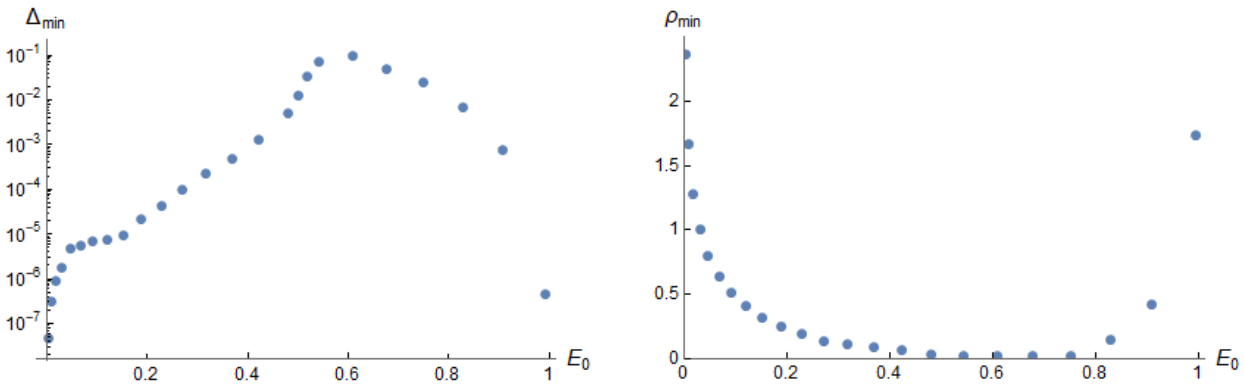

(a) (b)

Figure 3.7: Energy return precision (a) and the minimal spectral suppression exponent (b) plotted against the initial energy of mode 0 for two-mode initial data (3.1.10, 3.3.122). Small values of the curve in (b) correspond to strong turbulent cascades of energy.

be quite strong, as evident from Fig. 3.7b. What we observe in numerical experiments is that, as the cascade hits the mode number cut-off and then starts receding, a comb-like pattern of spikes in the spectrum forms. This pattern undergoes an evolution of its own and remains visible in future direct-reverse cascade oscillations. As we can observe in Fig. 3.8a, these comb patterns are pure numerical artifacts, and do not reflect the true dynamics of the infinite-dimensional model, since the parts of the spectrum overrun by the comb artifacts disagree between simulations with different mode number cut-offs. Such artifacts are generically visible for numerical simulation of resonant systems, including those for which exact analytic solutions starting with two-mode initial data are known (and do not display such comb-like features). While the total energy in the comb-like artifacts is very small at the moment of their formation, it is difficult to predict how they affect future direct-reverse cascade sequences, since the system is nonlinear and prone to chaotic divergence of trajectories.

2) *Arithmetic precision:* There is a very peculiar way in which direct-reverse cascade sequences amplify numerical errors, including the most basic rounding errors caused by the finiteness of arithmetic precision. Indeed, assume that in the exact solution a particular mode number k oscillates between energies E_k^{max} and E_k^{min}. In our scenario of near-perfect returns $E_k^{min} \ll E_k^{max}$, while for perfect returns $E_k^{min} = 0$. Since we are integrating the equations numerically and with finite precision, E_k^{max} contains a relative error given by at least the arithmetic precision, for example 10^{-15}. As the cascade recedes and the energy drops, the *absolute error* in E_k cannot decrease. Therefore, when one arrives at the bottom of the reverse cascade, the energy is E_k^{min}, but the absolute error is still $10^{-15}E_k^{max}$ (in particular, values of E_k^{min} below $10^{-15}E_k^{max}$ can never be reached, even if the exact solution corresponds to $E_k^{min} = 0$). The relative error is now $10^{-15}E_k^{max}/E_k^{min}$, much greater than the rounding errors themselves. This relative error will be transported upstream in the next direct cascade and will result in a large absolute error $10^{-15}(E_k^{max})^2/E_k^{min}$ at the peak of the cascade. Thus we can see that repeated transport of absolute errors downstream and

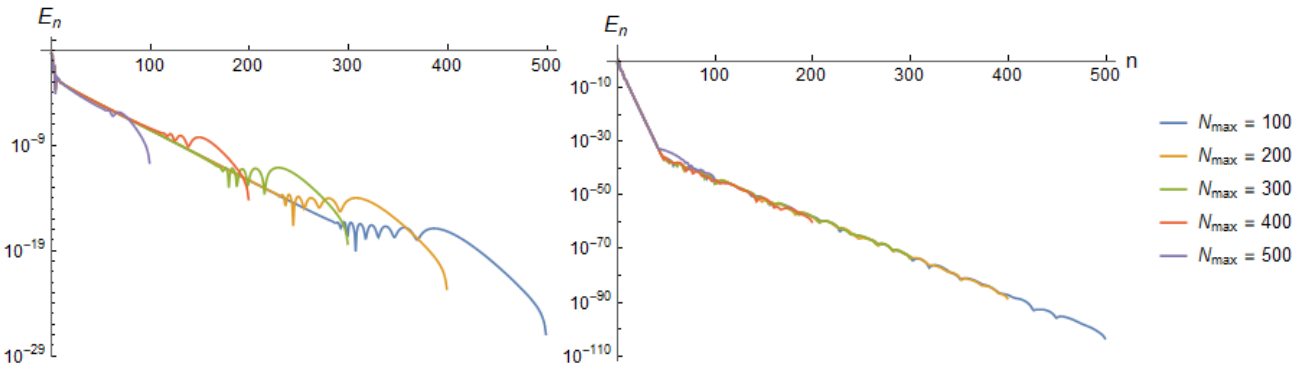

(a) $E_0 = 0.5,\ t = 3.75$ (b) $E_0 = 0.17,\ t = 3.5$

Figure 3.8: Energy spectrum of the two-mode initial data (3.1.10, 3.3.122) at the bottom of the first reverse cascade for different mode number cut-off. In (a) the direct cascade is strong, in which case the most relevant effects are produced by the cut-off. In (b) the direct cascade is weak, and 'shelf' artifacts (discussed in the main text and originating from the finite arithmetic precision) dominate the imperfections of the spectrum.

relative errors upstream in direct-reverse cascade sequences leads to strong amplification of numerical imprecision (and would of course compromise exact returns even if they were present in the underlying dynamical system). In practice, we can see the formation of flat 'shelf' artifacts in the high mode number part of our spectrum as the first cascade recedes, as in Fig. 3.8b (these artifacts precisely reflect the inability of the spectum to go below $10^{-15}E_k^{max}$ in numerical simulations). Such artifacts continue to evolve in future spectrum oscillations. As the near-perfect returns we observe occur after three direct-reverse cascade cycles, assessing the ultimate impact of these imperfections on the return precision is subtle.

3) *Interaction coefficients:* Small errors in the interaction coefficients C can produce important errors in the evolution governed by (3.3.116). This is particularly important when high modes are involved, as computing the interaction coefficients typically requires numerical integrations of oscillatory functions with frequencies that grow with the mode numbers. These integrals have to be evaluated for each resonant quartet of modes satisfying $n+m = j+k$, and the number of such quartets grows like $O(N_{max}^3)$, where N_{max} is the mode number cut-off. In addition, in order to obtain accurate values of the coefficients C when N_{max} is large, one needs to evaluate their expressions on a very dense grid and with increased arithmetic precision, which further increases the burden. To avoid these problems we computed the fully analytic expression for C in AdS_4 described in [56], which enables us to evaluate C safely for high modes. See appendix A.4 for the details of this computation. The remaining burden is then the computational cost of the simulations, which makes it hard to go beyond $N_{max} = 500$.

We remark that improving on either 1) or 2) beyond the level of our current simulations would be very demanding in terms of computational costs. While a break-through in our numerical precision does not appear viable at this moment, we have performed some basic

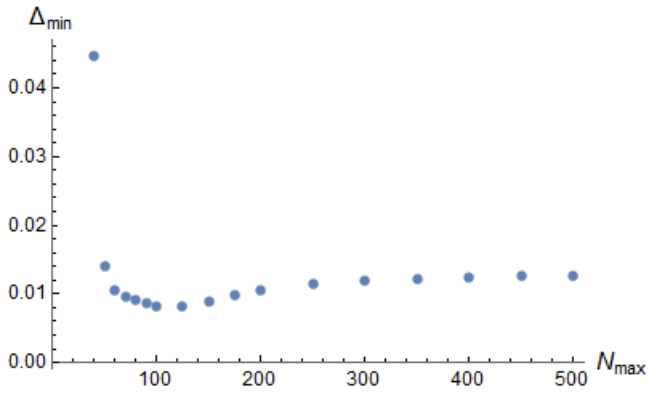

Figure 3.9: Energy return precision for two-mode initial data $E_0 = 0.5$ as a function of the mode number cut-off.

comparison of the return precision computed at different values of numerical approximation parameters (as well as a study of artifacts that we have briefly summarized in the passages above). In Fig. 3.9, we show the dependence of return precision on the number of modes included in our simulations. As one can see, the return precision substantially increases as the cut-off is raised from values around 50 (typical of the simulations of [34]), but after 200 stabilizes at a small nonzero value. At a naive level, this can be seen as an indication that the returns are not exact in the underlying dynamical system (3.3.116). One has to keep in mind that other factors hindering perfect returns (finite arithmetic precision, possible chaotic enhancement of artifacts over the course of three direct-reverse cascade oscillations) have not been taken (and are very difficult to take) into account.

We conclude that our numerical analysis indicates strikingly accurate, but likely imperfect energy returns for two-mode initial data, though it is not possible as of now to control all possible sources of imperfection. There is, however, one particular aspect that can be further elucidated. Our motivation to take a closer look at energy returns in global AdS_4 has largely come from the similarity of the observed dynamics to the known related analytically tractable cases which satisfy $\mathcal{D}_{nmkl} = 0$, where the returns are exact. This similarity extends in a few other ways, in particular the ultraviolet parts of the spectra remain approximately exponential for all times (only the slope of their logarithmic plot changes). However, for the systems with $\mathcal{D}_{nmkl} = 0$, energy returns for *any* two-mode initial data (3.1.10) are exact. This type of dynamics can be excluded for the resonant system (3.3.116) by inspecting solutions close to mode 0 or mode 1, which are analytically tractable. This will show that the resonant dynamics of AdS_4 cannot be strictly in the same class as those of the similar resonant systems with $\mathcal{D}_{nmkl} = 0$, which do exhibit perfect energy returns.

3.3.7.4 Analytical Analysis

Our problem, to discern between exact energy returns and accurate but inexact returns is strongly affected by the numerical noise and cuttoff effects as we have seen in the

previous section. Clearly claims for an analytic treatment, unfortunately, direct analytic investigations of the particular resonant system (3.3.116) are beyond practical imaginable limits; nevertheless, there are special regimes in which this system is analytically tractable. Here we will apply the method described in section 3.2 which perfectly fits the necessities of our problem.

The numerical study performed in the previous section scanned several initial data consisting in the first two-modes (3.1.10), going from the neighborhood of the first single-mode $n = 0$ until the environment of the second mode $n = 1$, covering the intermediate configurations. They provided inconclusive results close to single-mode (see Fig. 3.7). With the SLL we will focus on the neighborhoods of these single-modes. This structure is very convenient for our purposes, since we are trying to understand whether the energy returns may be exact. If the returns are exact, they are exact for all modes, while a failure of exact returns shall be seen in the approach we are adopting in a finite number of steps, since the discovery of any given non-returning mode guarantees that the returns in the whole system cannot be exact.

3.3.7.4.1 Solutions dominated by mode 0

Note that to directly apply the results of section 3.2.1 we must perform the transformation (3.3.117) and impose the ansatz (3.2.1). Namely, we must assume that the spectrum is exponentially suppressed as one moves away from the dominant mode 0:

$$\alpha_n = \delta^n \frac{q_n(t)}{\sqrt{\omega_n}}, \tag{3.3.124}$$

with $\delta \ll 1$. After transforming $C^{\text{new}}_{nmkl} = C^{\text{old}}_{nmkl}/\sqrt{\omega_n\omega_m\omega_k\omega_l}$ and neglecting powers of δ greater than zero, (3.3.116) takes the form (3.2.3).

Now, using the results displayed in 3.2.1, we can evaluate if the first four modes have common periods. From (3.2.9) we directly obtained that $|q_0| = |q_1| = 1$, while (3.2.11) reports that $|q_2|$ is periodic, in our particular case the period is $T_2 = \frac{10}{123}\pi^2$. It is at the level of $|q_3|$, (3.2.12), when the periodicity can be broken; on this occasion (3.2.13)-(3.2.14) have the values $\lambda_1 = \frac{3057}{70\pi}$, $\lambda_2 = \frac{267}{14\pi}$ meaning that at $|q_3(t)|^2$ the energy flow has a periodicity of $T_3 = \frac{140\pi^2}{3}$, so that T_3 is exactly 574 times greater than T_2. Inspecting the next step of our iterative solution, we conclude that $|q_4|^2$ is also periodic with $T_4 = 420\pi^2$.

We could continue this iterative process mode by mode. Nevertheless, we found an important property in relation to the interaction coefficients, which despite being highly complicated, provides key information. It consists of the fact that, in AdS_4 the interaction coefficients of satisfy

$$C_{nnnn} = \frac{a_n}{\pi}, \qquad C_{nmnm} = \frac{a_{nm}}{\pi}, \qquad C_{nmkl} = \frac{a_{nmkl}}{\pi\sqrt{b_{nmkl}}}, \tag{3.3.125}$$

where $a_n, a_{nm}, a_{nmkl}, b_{nmkl} \in \mathbb{Q}$. In particular,

$$2\pi C_{0000} = 45, \tag{3.3.126}$$

$$2\pi C_{0n0n} = \frac{108 + 90n - 33n^2 - 58n^3 - 21n^4 - 2n^5}{n(n+1)(n+2)(n+3)} + 6n(2n+3)\left(\sum_{k=1}^{n} \frac{1}{k(2k-1)} + \frac{2}{2n+1}\right).$$

Hence, in light of these rational relations, combined with the structure provided by Proposition 3.2.1.1, where the frequencies are linear combinations of C_{0000} and C_{0n0n}, we obtain that any finite set of modes have a common period. We observe that the common period of $q_0, q_1, \ldots q_n$ grows rather rapidly with n (for instance, we get estimates of order 10^{22} for $n = 25$). As a direct consequence of these results, $|q_n|^2$, which are what is important for our topic of energy returns, also have common periods of the same form, typically somewhat shorter than the common periods of q_n. There is a different form

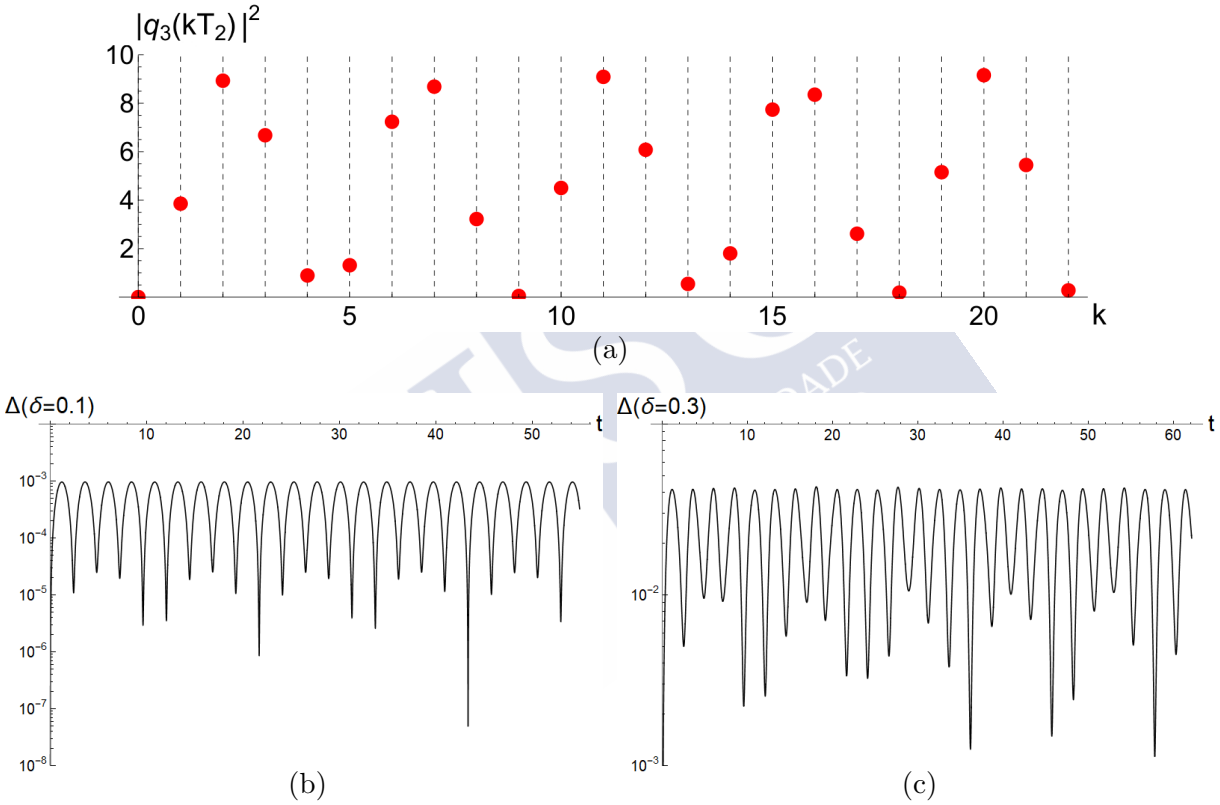

Figure 3.10: Analytics vs. numerics for two-mode initial data dominated by mode 0:
(a) analytic prediction for return accuracy based on (3.2.12) and showing accurate returns after 4, 5, 13 and 14 oscillations, and extremely accurate returns after 9 and 18 oscillations;
(b) Δ defined by (3.3.123) for the numerical solution of the full resonant system (3.3.116) with two-mode initial data corresponding to $\delta = 0.1$ perfectly reproducing the analytic pattern;
(c) the same for $\delta = 0.3$, already quite far from the single-mode initial data limit, but still accurately reproducing returns after 4 and 5 oscillations.

of accurate-but-imperfect returns, which is less spectacular than what we have described above in the limit $\delta \to 0$, but more relevant for not-so-long times and not-so-small δ. As we demonstrated above, there are long multiple periods after which large sets of $q_{n\geq 2}$ simultaneously vanish, providing for very accurate energy returns in the lowest two modes.

The basic 'crude' return period is set by T_2, the period of q_2. At $t = kT_2$ with an integer k, $q_2 = 0$ and hence one gets approximate returns. If at this moment, the value of q_3 defined by (3.2.12) is numerically small, even if it is not zero, one gets an improved return precision. In Fig. 3.10, we have performed comparisons of this analytic picture with numerical simulations of the resonant system (3.3.116). First, we have plotted $|q_3(kT_2)|^2$ and identified the specific small numbers of periods k after which one expects improved return precision. We have then run numerical simulations of (3.3.116) with initial data $\alpha_0(0) = 1/\sqrt{3(3+5\delta^2)}$, $\alpha_1(0) = \delta/\sqrt{5(3+5\delta^2)}$, which are a rescaled version of (3.2.1) corresponding to the normalization (3.3.122). At $\delta = 0.1$, which corresponds to 1.6% of the total energy initially in mode 1, the pattern of returns exactly matches our analytic predictions. At $\delta = 0.3$, which corresponds to 13% of the total energy initially in mode 1, already very far from the strict $\delta \to 0$ limit, the latter part of the return history is upset, but the first two accurate returns (after 4 and 5 oscillations) still match our analytic picture. Our treatment is thus robust, and retains predictive power even outside the region of very small δ.

To summarize, the expansion of equation (3.3.116) in powers of δ around mode 0 enabled us to verify that the energy transfer between the modes is not exactly periodic for initial conditions close to mode 0. Nevertheless, there are rational relations between the AdS_4 interaction coefficients such that arbitrarily precise returns to the initial energy distribution starting from two-mode initial data[8] sufficiently close to mode 0 occur if one waits long enough. Many other return patterns of varying accuracy are seen even for moderate initial ratios of energies of modes 0 and 1 in the initial state. This is very much in the spirit of the original FPU paradox. Corrections at subleading orders in δ may be effectively considered starting with (3.2.2), and are likely to display many further patterns thanks to the ubiquitous presence of rational numbers in the problem, but we shall not explore this systematically.

3.3.7.4.2 Solutions dominated by mode 1

We shall now assume a hierarchically organized spectrum dominated by mode 1. To apply the results of section 3.2.2 we must impose the ansatz

$$\alpha_0 = \delta\,\frac{q_0(t)}{\sqrt{\omega_0}}, \quad \alpha_{n\geq 1} = \delta^{n-1}\,\frac{q_n(t)}{\sqrt{\omega_n}}, \tag{3.3.127}$$

with $\delta \ll 1$, redefine $C^{\text{new}}_{nmkl} = C^{\text{old}}_{nmkl}/\sqrt{\omega_n\omega_m\omega_k\omega_l}$ and retain only the leading terms. This procedure restricts the resonant system (3.3.116) to the SLL (3.2.25)-(3.2.26).

Now, we can directly make use of the results in 3.2.2. From (3.2.32)-(3.2.34) the modes q_0, q_1, q_2 are periodic while (3.2.35) shows that the first deviation from perfect returns can happen at q_3. The explicit computation of (3.2.36) yields $\lambda/\gamma = 7\sqrt{3665}/149 \approx 2.84$.

[8] Note that we have not essentially used the assumption $q_{n\geq 2} = 0$ in our reasoning, and hence the picture of arbitrarily precise returns over long periods should apply to more general initial data hierarchically suppressed away from mode 0 as in (3.2.1).

Note that irrational numbers emerge here already in the periods of low-lying modes, unlike the case of initial data dominated by mode 0 we have considered previously.

Suppose for a moment that one had $\lambda/\gamma = 3$. Then $E_3 \sim |q_3|^2$ computed from (3.2.35) would have been proportional to

$$\left|a + be^{i\lambda t} + ce^{2i\lambda t} + de^{4i\lambda t/3}\right|^2, \tag{3.3.128}$$

which oscillates with period of $6\pi/\lambda$, which is thrice the period of $|q_0|^2$, $|q_1|^2$, $|q_2|^2$. One would thus have found exact returns after three direct-reverse cascades as far as the first four modes are concerned.

Now, for the actual resonant system we study, λ/γ is of course not exactly 3. This shows that the third energy return cannot be exact, at least for initial data close to mode 1, no matter how close we get to exact returns in our numerical simulations. At the same time, the fact that 2.84... is close to 3 explains why we are seeing very accurate returns after three direct-reverse cascades (and also why the returns after the first two direct-reverse cascades are less exact), as in Figs. 3.5a and 3.6d.

One can extend the above argument into a more quantitative analysis by plotting $|q_3(kT_2)|^2$ at integer k with q_3 given by (3.2.35) and $T_2 = 2\pi/\lambda$, as we did before for solutions dominated by mode 0. Since $q_2(kT_2) = 0$ by construction, having a small q_3 at the same moment signifies a return of enhanced precision. We have displayed the results of this analysis in Fig. 3.11. As in the previous section, at $\delta = 0.1$, our predictions are perfect, and at $\delta = 0.3$, already quite far from the single-mode data limit, we still accurately predict the first two returns.

Note that, in general, our analysis gives a nice perspective on why direct-reverse cascade oscillations are ubiquitously seen in numerical simulations of various resonant systems. For solutions dominated by mode 1, for example, the first three modes perform an infinite sequence of direct-reverse cascades, while the higher modes hold only a small amount of energy and provide cosmetic modifications to the cascades. (Furthermore, even these higher modes oscillate with frequencies comparable to the lowest modes.)

3.3.8 Massive Scalar Field in Global AdS

In this section we will sketch the model based on a free spherically symmetric massive scalar field in global AdS_4 and its weakly nonlinear regime.

3.3.8.1 The Model

The action of the model is

$$S = \frac{1}{16\pi G}\int d^{d+1}x\sqrt{-g}\,(R - 2\Lambda) - \frac{1}{2}\int d^{d+1}x\sqrt{-g}\left(\partial_\mu\phi\partial^\mu\phi + m^2\phi^2\right), \tag{3.3.129}$$

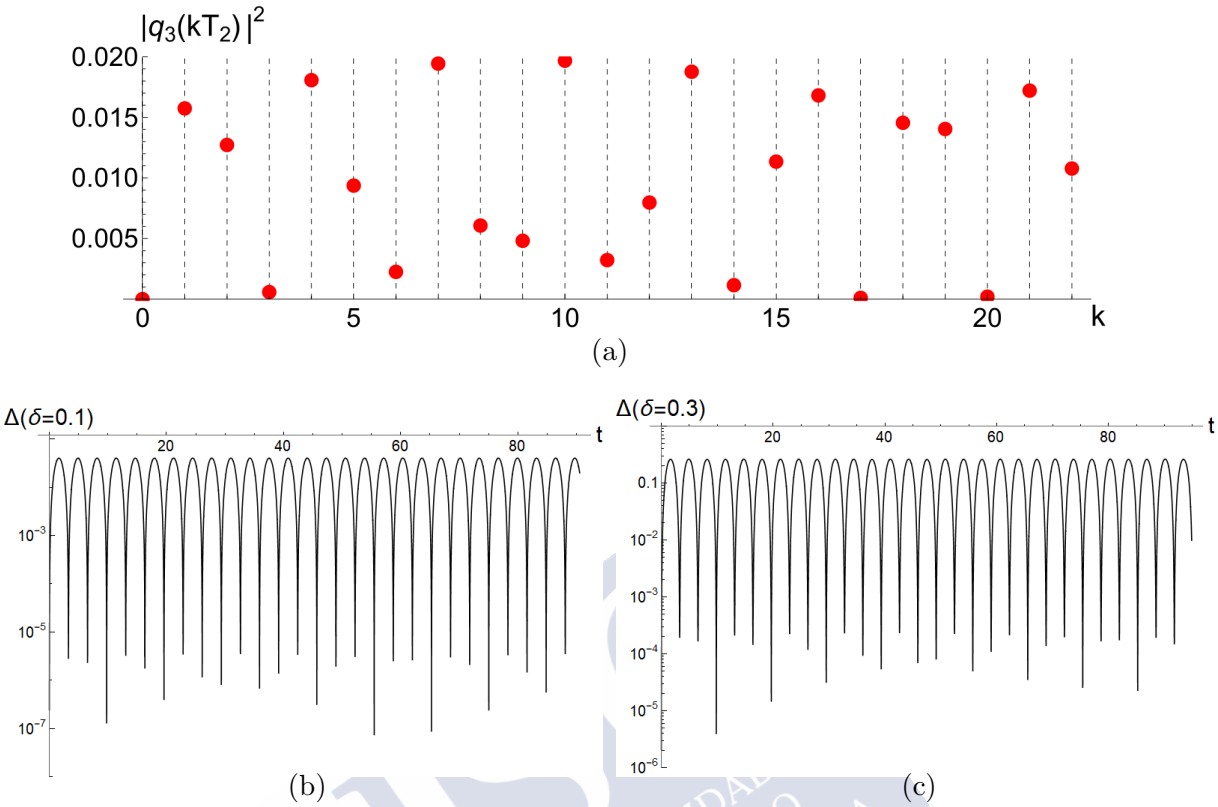

Figure 3.11: Analytics vs. numerics for two-mode initial data dominated by mode 1:
(a) analytic prediction for return accuracy based on (3.2.35) and showing accurate returns after 3, 6 and 14 oscillations, and extremely accurate late-time returns after 17 and 20 oscillations;
(b) Δ defined by (3.3.123) for the numerical solution of the full resonant system (3.3.116) with two-mode initial data corresponding to $\delta = 0.1$ perfectly reproducing the analytic pattern;
(c) the same for $\delta = 0.3$, already quite far from the single-mode initial data limit, but still accurately reproducing returns after 3 and 6 oscillations.

where $\Lambda = -d(d-1)/2$. The ansatz for the line element is the same as for the massless case, (3.3.103). Using the definitions (3.3.104)-(3.3.105) the EOMs become (we have set $8\pi G = d-1$)

$$\dot{\Phi} = \left(f e^{-\delta}\Pi\right)', \tag{3.3.130a}$$

$$\dot{\Pi} = \frac{1}{\mu}\left(\mu f e^{-\delta}\Phi\right)' - m^2 \frac{\phi}{\cos x^2} e^{-\delta}, \tag{3.3.130b}$$

$$\delta' = -\mu\nu\left(\Pi^2 + \Phi^2\right), \tag{3.3.130c}$$

$$f' = \frac{\nu'}{\nu}(f-1) - \mu\nu\left(\Pi^2 + \Phi^2\right) f - m^2 \tan x \phi^2, \tag{3.3.130d}$$

$$\dot{f} = -2\mu\nu f^2 e^{-\delta}\Phi\Pi. \tag{3.3.130e}$$

The metric functions can be written in the integral form

$$f(t,x) = 1 - e^{\delta(t,x)}\nu(x)\int_0^x dy\ \mu(y)e^{-\delta(t,y)}\left(\Phi(t,y)^2 + \Pi(t,y)^2 + m^2\frac{\phi(t,y)^2}{\cos y^2}\right), \quad (3.3.131)$$

$$\delta(t,x) = \begin{cases} -\int_0^x dy\ \mu(y)\nu(y)\left(\Phi(t,y)^2 + \Pi(t,y)^2\right) & \text{if } \delta(t,0) = 0 \\ \int_x^{\pi/2} dy\ \mu(y)\nu(y)\left(\Phi(t,y)^2 + \Pi(t,y)^2\right) & \text{if } \delta(t,\pi/2) = 0 \end{cases} \quad (3.3.132)$$

which show that the system of equations is fully determined by Φ and Π at each given time slice.

3.3.8.2 The Resonant System

On this occasion the EOMs also allow a (naive) perturbative expansion in powers of ϵ

$$\phi(t,x) = \sum_{n=0}^{\infty}\epsilon^{2n+1}\phi_{2n+1}(t,x), \qquad A(t,x) = 1 + \sum_{n=1}^{\infty}\epsilon^{2n}A_{2n}(t,x), \qquad \delta(t,x) = \sum_{n=1}^{\infty}\epsilon^{2n}\delta_{2n}(t,x), \quad (3.3.133)$$

to generate an infinite-system of equations of the form

$$\left(\Box_{AdS} - m^2\right)\phi_{2n+1} = S_{2n+1}\left[\phi_l\right], \quad (3.3.134)$$

where $l < 2n+1$, $\Box_{AdS}$ is the Laplacian in (a non-dynamical) AdS_{d+1} and $S_{2n+1}[\phi_l]$ symbolically denotes all the nonlinear terms with ϵ^{2n+1}. The linear equation on this occasion is written as

$$\ddot{\phi}_1 - \mathcal{L}\phi_1 = 0, \qquad \mathcal{L} \equiv \frac{1}{\mu(x)}\partial_x\left(\mu(x)\partial_x\right) - \frac{m^2}{\cos^2 x} \quad (3.3.135)$$

The spectrum of the operator $\mathcal{L}$ takes the form

$$\omega_n = 2n + \Delta, \qquad n = 0, 1, ..., \quad (3.3.136)$$

and the eigenfunctions

$$e_n(x) = k_n \cos x^{\Delta} P_n^{\left(\frac{d}{2}-1,\ \Delta-\frac{d}{2}\right)}(\cos 2x) \qquad k_n = 2\sqrt{\frac{(n+\Delta/2)\Gamma(n+1)\Gamma(n+\Delta)}{\Gamma(n+d/2)\Gamma(n+\Delta-d/2+1)}}, \quad (3.3.137)$$

where $\Delta = \frac{d}{2} + \sqrt{\left(\frac{d}{2}\right)^2 + m^2}$ and $P_n^{(a,b)}(x)$ are the Jacobi polynomials.

From (3.3.136) we observe that the spectrum is fully resonant independently of the mass of the scalar. To take into account the relevant effects at times $1/\epsilon^2$, we derive the resonant system through the method of averaging. First, it requires that the system of equations is written in the *periodic standard form*. For this purpose, the fields are expanded for small amplitudes ($\epsilon \ll 1$) as

$$\phi(x,t) = \varepsilon\sum_{n=0}^{\infty}\left(\alpha_n(t)e^{-i\omega_n t} + \bar{\alpha}_n(t)e^{i\omega_n t}\right)e_n(x), \quad (3.3.138)$$

$$\dot{\phi}(x,t) = -i\varepsilon \sum_{n=0}^{\infty} \omega_n \left(\alpha_n(t) e^{-i\omega_n t} - \bar{\alpha}_n(t) e^{i\omega_n t}\right) e_n(x).$$

Following the procedure displayed in section 2.2.3 we reach to the resonant system for the massive scalar field in terms of the *slow time* $\tau \equiv \epsilon^2 t$,

$$i\omega_n \frac{d\alpha_n}{d\tau} = \sum_{m=0}^{\infty} \sum_{k=0}^{n+m} C_{nmk(n+m-k)} \bar{\alpha}_m \alpha_k \alpha_{n+m-k}. \tag{3.3.139}$$

Note that in addition to the resonant channel (2.2.66) displayed in (3.3.139), which is present for any value of Δ, the two additional ones, (2.2.67)-(2.2.68), emerge for integer values of this parameter. Thereby, in these special circumstances (3.3.139) should have terms involving interaction coefficients U_{nmkl} and Q_{nmkl} as in (2.2.70). Nevertheless, in the situations we have considered, $d = 3$, $\Delta = 2, 3$, they do not contribute. For $d = 3$, $\Delta = 3$ ($m^2 = 0$) they vanish as we have explained in the previous section, while for $d = 3$, $\Delta = 2$ ($m^2 = -2$) our numerical computations strongly suggest that they also vanish (at least for modes lower than 500). Analytic computations of particular coefficients report the same results. The particular expressions for the interaction coefficients can be found in appendix A.4.

Our main goal to introduce the massive term of the scalar consists of obtaining a continuous freedom in the interaction coefficients. As can be seen in Appendix A.4 they depend on m^2 through Δ. In consequence, we examine whether performing a fine tune of the mass allows for access to more accurate returns. In this situation, after writing (3.3.139) as (3.0.1) through the transformations given in (3.3.117), we directly computed the SLL around mode 1 to obtain clear answers without typical numerical contamination present in simulations. We did not find a suitable strategy to compute analytically the interaction coefficients for general mass, and therefore our inspection is limited to low modes for which the interaction coefficients were computed one by one. As is reflected in section 3.2.2, for the SLL around mode 1, q_0, q_1, q_2 are perfectly periodic and it is q_3 which can break this . Computing (3.2.36) we observe a dependence on m^2; as can be seen in Fig. 3.12, it allows adjusting the parameters in (3.2.35) to make q_3 periodic. Unfortunately, we did not find exact time-periodic dynamics for the full resonant system (3.3.139).behavior

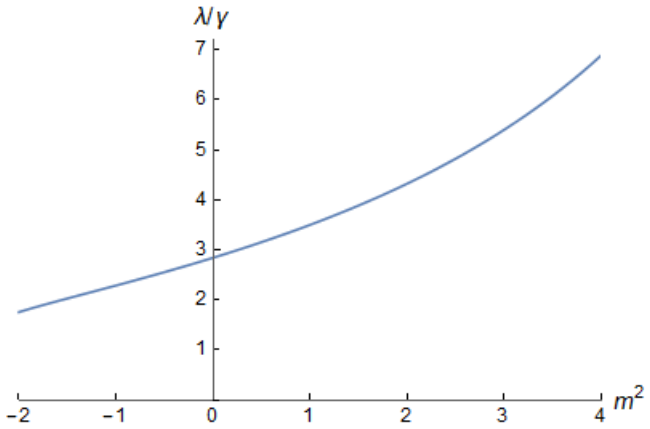

Figure 3.12: Dependence of λ/γ on the mass of the scalar field. Adjusting m^2, $|q_3|^2$ can be made exactly periodic. For example, on can choose m^2 such that $\lambda/\gamma = 3$, as briefly considered in section 3.2.2.

3.4 Summary

In this section we have studied the weakly nonlinear regime of cubic systems displaying a fully resonant spectrum. Specifically the ones for which the resonant system (3.0.1) can be derived after the application of the perturbation methods presented in section 2.2. Nevertheless, as the information about the original model is contained in the interaction coefficients C_{nmkl}, we have adopted a different point of view. Instead of studying the properties of a resonant system derived from a particular model, we have considered the resonant system (3.0.1) as our starting point without taking into account its origin.

After that, certain conditions have been imposed for the interaction coefficients which allow gathering them in different classes. This classification was based on the summation identities $g_p^{(n,m)}$, (3.1.4). It is a suitable choice for multiple reasons:

- Under an appropriate ansatz, equation (3.0.1) does not directly deal with C_{nmkl} but with $g_p^{(n,m)}$.
- They avoid the dependence of explicit expressions for C_{nmkl} which could be more difficult to obtain than $g_p^{(n,m)}$.
- They are strong enough conditions to allow an analytic treatment.
- They are weak enough conditions to cover a large number of systems.

In particular, we have focused our effort on the class delimited by the polynomial structure for $g_0^{(n,m)}, g_2^{(n,m)}$ given in (3.1.5). Under these conditions a collection of propositions was derived. They reported salient results as the consistency of the linear ansatz (3.1.7), which forms a three-dimensional dynamical subsystem, and properties for any of its solutions as the periodicity of the energy per mode, a bound for the energy transferred to higher

modes (meaning a lack of turbulent behaviors) and the additional conserved quantity Z, (3.1.8), for solutions covered by the ansatz.

Motivated by the conservation of Z in the three-dimensional system formed by (3.1.7), we have explored the stronger condition $\mathcal{D}_{nmkl} = 0$, (3.1.11), which in particular sets Z as a conserved quantity for the resonant system (3.0.1). In this situation new propositions have been obtained, showing that the current class of systems defined by (3.1.11) is contained inside the previous class delimited by the summation identities (3.1.5). Nevertheless, it is not clear yet if both conditions are equivalent or $\mathcal{D}_{nmkl} = 0$ is stronger than (3.1.5). In any of these possible scenarios the results obtained for (3.1.5) are also applied to our new class.

We want to remark the extreme simplicity of condition $\mathcal{D}_{nmkl} = 0$ and the enormous consequences it has. With the summation identities (3.1.5) we avoided the necessity of computing the explicit expression of C_{nmkl} paying the price of performing certain summations. Nevertheless, $\mathcal{D}_{nmkl}$ does not even require any summation. If we have C_{nmkl} explicitly expression as a function of the mode numbers: n, m, k, l, it is almost straightforward checking if they belong to the family of systems displayed here, while with the integral form of the interaction coefficients we require some identities of the linear modes. This simplicity of $\mathcal{D}_{nmkl} = 0$ allowed analysing it in full generality and obtain the explicit expression of the generating function for the interaction coefficients, (3.1.20) and (3.1.21).

Given the suitability of polynomial structures for both, summation identities (3.1.4) and the ansatz for α_n, we have also considered more general conditions based on higher order polynomials, (3.1.31) and (3.1.32). This analysis only provided two families of interaction coefficients consistent with the resonant system (3.0.1) and the freedom of all the parameters in the ansatz. One of them was the class already mentioned, defined by (3.1.5) with a linear ansatz (3.1.7), while the second one consisted of identities (3.1.35) and ansatz (3.1.36). For this last family, we found that they display stationary states for any solution of (3.1.36). Nevertheless, we did not perform a deeper study of this class.

Despite the large classes of systems considered until this point, which display sectors allowing an exact analytic resolution, we are aware that it is not the common picture. For this reason, we have sought certain limits, valid for almost all the interaction coefficients, where information can also be extracted analytically. Specifically, we considered perturbations around single-mode solutions, but instead of truncating the perturbative expansion to a specific order, for example, linear perturbations of the single-mode, an exponentially decaying spectrum centred at the single-mode has being considered (SLL). On this occasion the truncation has been done at higher order corrections of this spectrum. Hence, a reduced form of (3.0.1) is obtained which can be solved iteratively.

Here we have developed the leading order of the SLL for modes 0 and 1. In both situations equations for modes q_0, q_1, q_2, q_3 have been solved subject to initial conditions consisting of two-mode initial data (3.1.10), although general conditions could be used. In the case of the SLL of mode 0 these solutions reflect that the energy per mode, which is proportional to $|q_n|^2$ remains constant for $n = 0, 1$ while for $n = 2$ it is periodic as long as the expansion is free of secular terms at this level. The condition that our perturbative expansion is free

of secular terms is not too strong; indeed, it is the most common situation. Therefore, we can claim that at leading order in the SLL, the majority of systems display exact energy returns for modes from 0 to 2. It is at the next level, $n = 3$, where additional conditions for the interaction coefficients must be introduced to guarantee the periodicity of energy flows. If we had continued with the resolution of higher modes, more restrictions would have been needed to preserve the periodicity of the energy. Finally, for this system we have obtained the general structure of the solution for the leading order equations (as long as the interaction coefficients guarantee the lack of secular terms). With this structure we extracted useful information, for example, the periodicity of each mode is guaranteed if $C_{n0n0} \in \mathbb{Q}$. Note however that it does not mean the existence of a common period, for which a stronger condition is required.

Turning to the case of the leading order of the SLL close to mode 1, the results are slightly different from the previous situation. On this occasion only the energy of $n = 1$ is constant, while $|q_0|$ and $|q_2|$ are coupled and display a periodic behavior (if secular terms are not present). Again, additional conditions to preserve the periodicity must be introduced at level $n = 3$. In contrast with the SLL around mode 0, for this case we have not derived the general structure for the leading order solutions, remaining at the level $n = 3$ was enough for the particular systems we have considered.

Until this point, we have worked in a general framework constrained by certain restrictions which allowed developing analytic results. After that, a large number of interesting resonant systems were presented; for which some of the developed techniques were applied. Many of them belong to the class defined by $\mathcal{D}_{nmkl} = 0$, reflecting that it is not a too restrictive condition. Despite these systems have been already presented before, we want to summarize how they fit in our general framework and the multidisciplinary class we have developed.

- **Conformal Flow (CF)**

  Introduced in section 3.3.1. In terms of our formalism the CF is described as $(\beta, \gamma) = \left(\frac{1}{3},\ \frac{3}{4}\right)$ and

  $$S_{nmkl} = \min(n, m, k, l) + 1. \tag{3.4.1}$$

  This system was introduced in [75] and also studied in [142, 188]. In particular, the three-dimensional manifold of periodic solutions and the families of stationary solutions were obtained in these studied. Nevertheless, the conservation of Z is a novel result of our formalism.

- **Maximally rotating scalar field on $\mathbb{S}^3$ ($\mathbf{mr}\mathbb{S}^3$)**

  Introduced in section 3.3.3. In [76], it was found that it admits a three-dimensional invariant manifold, but the extra conserved bilinear Z was not identified at that time. This system corresponds to $(\beta, \gamma) = \left(\frac{1}{3},\ 1\right)$ and

  $$S_{nmkl} = \frac{1}{1 + n + m}. \tag{3.4.2}$$

  The three-dimensional manifold was already obtained in [76]; while the conservation of Z and the families of stationary solutions are a novel result of our formalism.

- **Maximally rotating scalar fields in $\mathbf{AdS}_{d+1}$ ($\mathbf{mr}AdS_{d+1}$)**

  Introduced in section 3.3.4. The maximally rotating truncation results in a one-parameter family of resonant systems admitting three-dimensional invariant manifolds [76]. In our formalism, they correspond to (β, γ) given by

$$\beta(\delta) = \frac{1}{2}\frac{\delta+1}{2\delta+1}, \qquad \gamma(\delta) = \frac{1}{2}\frac{\delta+1}{\delta}, \tag{3.4.3}$$

  and

$$S_{nmkl} = \frac{\Gamma(2\delta)}{\Gamma(\delta)^2}\frac{\Gamma(n+\delta)\Gamma(k+\delta)\Gamma(m+\delta)\Gamma(l+\delta)}{\Gamma(n+1)\Gamma(k+1)\Gamma(m+1)\Gamma(l+1)}\frac{\Gamma(n+m+1)}{\Gamma(n+m+2\delta)}. \tag{3.4.4}$$

  The three-dimensional manifold was already obtained in [76]; while the conservation of Z and the families of stationary solutions are a novel result of our formalism.

- **Rotating sectors of the two-dimensional Gross-Pitaevskii equation ($\mathbf{rGP}_{2+1}$)**

  Introduced in section 3.3.2. It also has a one-parameter family of resonant systems, [73], with

$$\beta(\mu) = \frac{3}{8}, \qquad \gamma(\mu) = \frac{1}{2}\frac{\mu+2}{\mu+1}. \tag{3.4.5}$$

  (Only integer values of μ emerge from truncations of the Gross-Pitaevskii equation, but all relevant properties are preserved for general values of μ). The interaction coefficients are given by

$$S_{nmkl} = 2\frac{\Gamma(\mu+1)\Gamma\left(\frac{1}{2}\right)}{\Gamma\left(\mu+\frac{1}{2}\right)}\int_0^\infty d\rho\, e^{-2\rho}\rho^{2\mu}L_n^\mu(\rho)L_m^\mu(\rho)L_k^\mu(\rho)L_l^\mu(\rho), \tag{3.4.6}$$

  where L_n^μ are the associated Laguerre polynomials.

  The conserved quantity Z was already obtained in [68]; while the three-dimensional manifold and the stationary states are novel results of this formalism.

- **Lowest Landau Level (LLL) equation**

  Introduced in section 3.3.2. In [72], explicit analytic solutions of the form (3.1.7) were found for this system. In our present language, this system corresponds to $(\beta, \gamma) = \left(\frac{1}{4},\ \frac{1}{2}\right)$ and

$$S_{nmkl} = \frac{(n+m)!}{2^{n+m}n!m!k!l!}. \tag{3.4.7}$$

  The conserved quantity Z was already obtained in [68]; while the three-dimensional manifold and the stationary states are novel results of this formalism.

- **Excited Landau levels of the two-dimensional Gross-Pitaevskii equation** (xLL_{2+1})

Introduced in section 3.3.2. They are parametrized by an integer $L \geq 1$ (while the case $L = 0$ is simply the lowest Landau level mentioned above), and correspond to

$$\beta(L) = \frac{1}{2} - \frac{L-1}{4(2L-1)}, \qquad \gamma(L) = \frac{1}{2}, \tag{3.4.8}$$

[73]. The interaction coefficients are again given in terms of the Laguerre polynomials:

$$S_{nmkl} = \frac{2^{2L+1}(L!)^4}{(2L)!n!m!k!l!} \int_0^\infty d\rho\, e^{-2\rho}\rho^{n+m-2L} L_L^{n-L}(\rho) L_L^{m-L}(\rho) L_L^{k-L}(\rho) L_L^{l-L}(\rho). \tag{3.4.9}$$

The conserved quantity Z was already obtained in [68]; while the three-dimensional manifold and the stationary states are novel results of this formalism.

- **Nonrelativistic Limit of $\mathbf{AdS}_5$ ($\mathbf{nrlAdS}_5$)**

  Introduced in section 3.3.5. It is interesting to observe that this formalism also captures particular limits of dynamical spacetime backgrounds. On this occasion corresponds to $(\beta, \gamma) = \left(\frac{3}{8}, \frac{3}{4}\right)$, [78]. The interaction coefficients are rewritten in terms of the Laguerre polynomials as

$$S_{nmkl} = \frac{1}{2}\left(\tilde{S}_{nmkl} + \tilde{S}_{nmlk}\right), \tag{3.4.10}$$

  where

$$\tilde{S}_{nmkl} = \int_0^\infty d\rho \int_0^\infty d\sigma\, \min(\rho,\sigma) e^{-(\rho+\sigma)} L_n^{(1)}(\rho) L_m^{(1)}(\sigma) L_k^{(1)}(\sigma) L_l^{(1)}(\rho) \tag{3.4.11}$$

  The authors of [78] used our formalism to study this system.

An important feature extracted in section 3.1.1 from the study of three-dimensional invariant manifolds of the form (3.1.7) is that their dynamics is fully determined by β and γ. This allows us to compactly summarize the previous literature in Fig. 3.13.

We want to remark that β has little impact on the dynamics within the invariant manifold (3.1.7) (see appendix A.3.2). For solutions of the form (3.1.7), the spectrum $|\alpha_n|^2$ only depends on β through overall time scaling, while the phases of α_n may be β-sensitive. The value $\beta = 1/2$ is special, as in this case the spectrum does not evolve in time at all. This case is represented by the first excited Landau level ($L = 1$) of the two-dimensional Gross-Pitaevskii equation.

In addition to resonant systems belonging to the class delimited by $\mathcal{D}_{nmkl} = 0$, we have also considered a representative of the class given in (3.1.35). It is the Cubic Szëgo system introduced in section 3.3.6. It was explained there that this system displays excellent analytical properties; unfortunately, they are not shared by other representatives of the family (3.1.35). We have also observed as the SLL around mode 0 can be easily solved

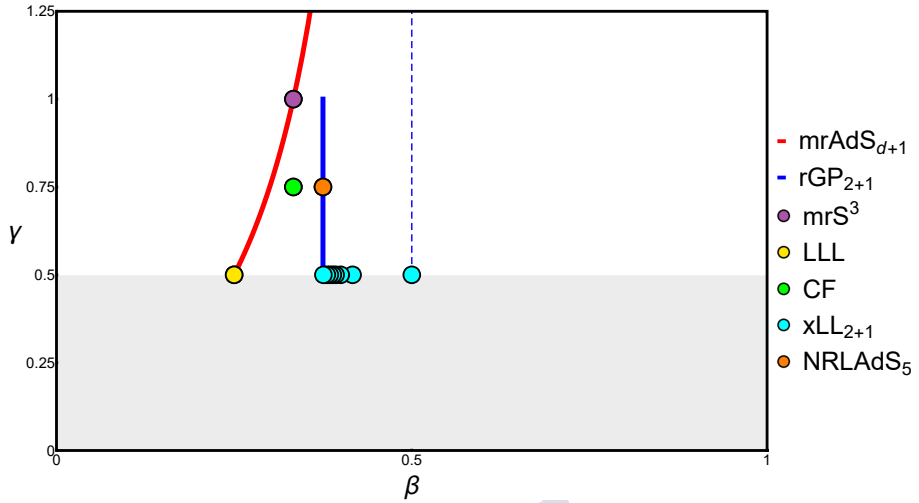

Figure 3.13: Currently known systems with three-dimensional invariant manifolds of the form (3.1.7) arising from the weakly nonlinear analysis of equations of mathematical physics, parametrized by (β, γ). The vertical dashed line represents the special value $\beta = 1/2$ for which the spectrum $|\alpha_n|^2$ does not evolve. We have not explored the shaded region $\gamma < 1/2$, since f_n of (3.1.7) is assumed real in our construction, and this assumption does not work in the shaded region.

at leading order and as any solution is at least 2π-periodic. Finally, it was also shown that the SLL for mode 1 reflected the instability of this mode with the presence of secular terms.

After introducing systems which allow exact analytic solutions, we have also considered the weakly nonlinear regime of a free spherically symmetric scalar field in AdS minimally coupled to gravity. In particular, the issue of energy returns to the initial configuration for two-mode initial data in the resonant approximation has been addressed. Having performed numerical simulations with much higher precision than what has been previously seen in the literature, we have observed returns of striking accuracies, exemplified by Fig. 3.5. The numerics also provided indications, however, that the small imperfections we see cannot be purely due to numerical artifacts. To elucidate the situation, we have performed an analytic study of solutions dominated by one of the two lowest modes (the SLL) and proved that the accurate returns we have observed numerically are inexact in this limit dominated by one of the two modes. This should be contrasted with the scenario observed by the systems satisfying $\mathcal{D}_{nmkl} = 0$, where perfect returns occur for all two-mode initial data of the form (3.1.10).

As usual in FPU-like situations, it is natural to expect that the near-perfect returns arise due to proximity to another dynamical system for which the returns are exact. Following this line, the mass of the scalar has been introduced to achieve a free parameter in the interaction coefficients. It allows for fine-tuning C_{nmkl} in order to improve the quality of returns. We have explored this scenario in the context of our analytic treatment of solutions dominated by mode 1 in section 3.2.2. We have seen that by adjusting the mass of the scalar field, it is possible to make the return of mode 3 exact (Fig. 3.12). This

evidently qualitatively improves the precision of returns for initial data near mode 1, as the discrepancy is now in the strongly suppressed modes starting from mode 4, but the scenario still falls short of providing exact returns. We also note that the nonrelativistic version of the AdS dynamics (which technically corresponds to the limit of infinite scalar field mass), introduced in section 3.3.5, displays perfect returns in AdS_5, rather than in AdS_4 (returns in AdS_5 at finite masses, on the other hand, are not close to being perfect).

We comment explicitly on what we have achieved in comparison to [34], where the topic of FPU-like behaviors in weakly nonlinear AdS_4 dynamics was first brought up. In [34], the focus was on reporting, among other things, the return after three direct-reverse cascades for two-mode initial data with equal energies that can be seen in our Fig. 3.6d. Since the simulations were performed with a rather limited precision, the results were in principle consistent with perfect returns upset exclusively by numerical artifacts, especially in light of the subsequent discovery of closely related systems for which the returns are exact. We have now ruled out this possibility. At the same time, we have observed imperfect returns of precision much higher than what is suggested by the material of [34] and repeating over many oscillation cycles, as seen in Fig. 3.5. More importantly, our analytic investigations have generated a neat picture of returning behaviors for initial data sufficiently close to mode 0 or mode 1, and allowed for the identification of specific multiple oscillation periods after which enhanced returns occur. This picture remains valid even for initial data with moderate energy ratios of the two lowest modes. The rational relations between the AdS_4 interaction coefficients we have displayed allude to hierarchies of returns, with specific longer waiting times resulting in returns of better and better accuracy. One in fact sees returns of striking accuracy at late times in Fig. 3.10c, outside the domain where our concrete analytic approximation is valid. This suggests that there are further structures to be explored. Elaborate patterns of returns of varying precision over long times are known from the original FPU problem.

4

Time-Dependent Boundary Conditions

In the previous chapter we have studied the weakly nonlinear regime of systems on bounded domains subject to time-independent boundary conditions. Specifically, the conditions provided a fully resonant spectrum which allowed the derivation of the resonant system. In contrast, in this chapter we are going to explore time-dependent boundary conditions. They introduce non-normalizable modes (defined in section 2.1) in the spectrum of linear modes. We will see that in the context of the models considered here, the presence of these modes is interpreted as an exchange of energy through the boundary. Therefore, from a physical point of view, time-dependent conditions provide an excellent framework in the study of out-of-equilibrium dynamics. Some of these conditions belong to the class denominated quenches. It consists of altering the parameters of the system in time[1] when it is in a particular state, to study the response of the system. Many important results have been found in this way, and we refer the reader to the relevant literature [189–199].

Following a similar line with the previous chapter, our interest is focused on systems or regimes where the dynamics is mainly governed by linear modes while nonlinearities have relevant effects at longer timescales. For this reason, we require boundary conditions which provide a balance between the injected and extracted energy through the short-timescale and do not depend on the long-timescale. This condition will be relaxed later with the introduction of quenches. Therefore, the simplest candidates to initiate our exploration of the long-time dynamics are time-periodic boundary conditions. They will allow us to

[1]The typical definition of quench involves a quick alteration of the parameters of the system; nevertheless, in our situation we will also consider long-time variations.

use the machinery developed in section 2.3 in order to find time-periodic solutions (TPSs) and study their stability. In particular, our situation will be restricted to asymptotically AdS systems. It allows interpreting our results in terms of the AdS/CFT correspondence. The holographic dictionary relates the non-normalizable modes present on the gravity side with sources on the CFT side. Thereby, the time-dependent boundary conditions are translated to time-dependent sources for the CFT. In consequence, on the QFT side we have a (holographic) periodically driven system[2].

Additionally to our personal motivations, periodically driven systems have notably received attention during the last years under the name of *Floquet systems*. Probably the most exciting idea for a physicist consists of having a few buttons which provide absolute control over a physical system. Of course it is an idealisation, nevertheless the idea of Floquet engineering pursue this philosophy [86]. A small periodic external perturbation will not allow an absolute control; but at least, it provides a certain degree of manageability. For example, a harmonic drive composed of two parameters: the amplitude and the frequency of oscillations, can report relevant results if they are suitably chosen. Beyond the control of the system, they also allow new phenomenology such as: synchronisation [92], modification of the band structure (e.g. *Topological insulators* [93]) or counter-intuitive effects such as the stabilisation of unstable equilibrium points of the phase-space [94–96] or time crystals [97, 98]. The most illustrative example in this context is the Kapitza's pendulum [94, 95]; namely, a rigid pendulum where its rotation origin is shaken harmonically in the vertical direcction. Fig. 4.1 shows the stabilization of the unstable equilibrium point (the inverted position). There we observe as a small periodic source can modify the nature of points in the phase-space.

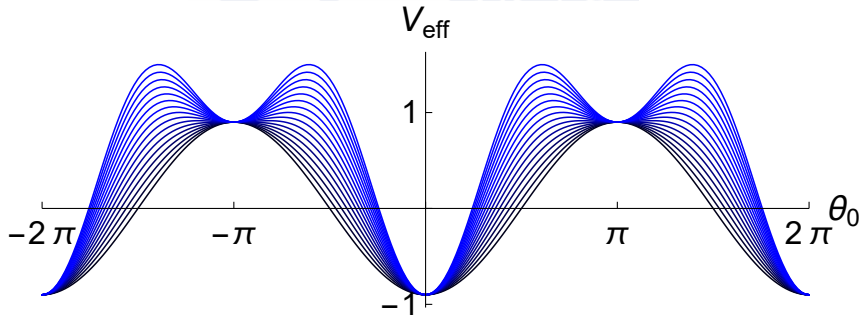

Figure 4.1: Effective potential of the Kapitza pendulum of length l under the action of gravity g and vibrations of amplitude A and frequency ω. θ_0 corresponds with the averaged angle in a period $2\pi/\omega$ between the pendulum and the negative direction of the vertical axis. Each line corresponds to a value of $A\omega$. From black ($A\omega < \sqrt{2gl}$) to blue ($A\omega > \sqrt{2gl}$), the change in the stability of the inverted position happens at $A\omega = \sqrt{2gl}$.

The study of holographic Floquet systems has been already initiated in [101–108]. These references were motivated by the study of systems driven out of equilibrium. The majority of them tried to observe how it affects the crucial features of certain models. [101–103]

[2]In our setups the drive consists of the boundary conditions

deal with holographic superconductors, therein the phase diagrams were constructed and the dependence of the superconducting transition temperature with the parameters of the drive was studied. [104] tries to elucidate if the properties of a holographic Weyl semimetal are preserved or destroyed under the action of a rotating electric field. Using a similar setup, [106] studies as the phase diagram strongly depends on the amplitude and frequency of the electric field; the system behaves as an insulator or a conductor for certain combinations of these parameters. On the other hand the models of [105, 107] are less sophisticated than the previous ones; they consist of a scalar field in an asymptotically AdS geometry. Nevertheless, they take advantage of this fact to consider more complicated nonlinear effects. In [101–104, 106, 108] the backreaction of the metrics was not considered, restricting the study to probe limits. In contrast, in [105] the first contribution to the backreaction was computed, while in [107] the full effects were taken into account. A constant in all these studies is the fact that the states are thermal from the beginning due to the presence of a horizon; in consequence, the system has a temperature.

Our situation is crucially different, we are interested in the evolution of initial conditions on horizonless geometries. If a horizon is present, then part of the absorbed energy will fall behind it, and never reach back to the boundary. Unavoidably, the mass would then grow monotonically and the black hole horizon end up reaching the boundary, i.e. the dual geometry reaches an infinite temperature state. Instead of it, we will focus our effort on the long-time evolution of relatively small initial data. The initial data that lead Bizon and Rostworowski conjecture [6] that global AdS was unstable, can be realized as the energy injection after a sudden quench of arbitrary small amplitude. This is why, one of the relevant questions now is whether a similar patter can be observed at long-times for certain values of the parameters that label the periodic boundary conditions. There are also more interesting properties to be studied. For example: whether TPSs exist, whether they are stable, what the final states of possible instabilities are, whether the systems display synchronization properties with the drive,...

We are interested in generic properties of, and robust predictions for, time-dependent holographic models. It therefore makes sense to study simplified versions, also known as bottom-up models, containing the minimal set of ingredients. In global AdS, due to spherical symmetry, we will need to add a massless scalar. We will also inspect the AdS soliton geometry in the Poincaré patch. There the gravity sector is already evolving non-triviallly. Our study for both models follows the same main steps. We will start with the introduction of the model and the boundary conditions used. First, TPSs will be constructed through the methods developed in section 2.3. After that, the linear stability of these objects will be inspected making use of the Floquet theory displayed in section 2.3.2.1 and the numerical method of 2.3.2.2. This analysis will allow the delimitation of regions of stability and a controlled inspection of the instabilities triggered by exponentially growing linear modes. Finally, the boundary conditions will be modified to admit quenches which provide a dynamical construction of TPSs.

4.1 Driven Scalar Field in Global AdS

In this section we will study a free spherically symmetric massless scalar field in global AdS_4 subject to time-periodic boundary conditions. The simplicity of this model makes it the perfect candidate to initiate our study. It provides a low number of ingredients which allow for a proper isolation of their effects.

4.1.1 The Model

The model has been already introduced in section 3.3.7; nevertheless, in that case the scalar field was subject to Dirichlet boundary conditions $\phi(t, \pi/2) = 0$. We shall present the setup again to highlight different points, which became relevant after our immersion in the context of driven systems.

The action governing our model has the form

$$S = \frac{1}{16\pi G}\int d^4x\sqrt{-g}\,(R - 2\Lambda) - \frac{1}{2}\int d^4x\sqrt{-g}\,(\partial_\mu\phi\partial^\mu\phi)\,, \tag{4.1.1}$$

with $\Lambda = -3/l^2$. We will set $8\pi G = 2$ and $l = 1$. The isotropic ansatz for the metric of AdS_4 has the form

$$ds^2 = \frac{1}{\cos^2 x}\left(-fe^{-2\delta}dt^2 + f^{-1}dx^2 + \sin^2 x\, d\Omega_2^2\right), \tag{4.1.2}$$

where $x \in [0, \pi/2)$ is the radial coordinate. The effective system of equations is conveniently expressed in terms of the following variables (where $\dot{} \equiv \partial_t$, $' \equiv \partial_x$)

$$\Phi \equiv \phi', \qquad \Pi \equiv f^{-1}e^{\delta}\dot{\phi}. \tag{4.1.3}$$

With these definitions and making use of two predefined functions

$$\mu(x) \equiv (\tan x)^2 \qquad \text{and} \qquad \nu(x) \equiv \frac{2}{\mu'(x)} = \frac{\sin x\cos x}{(\tan x)^2}, \tag{4.1.4}$$

the EOMs are then written as

$$\dot{\Phi} = \left(fe^{-\delta}\Pi\right)', \qquad \dot{\Pi} = \frac{1}{\mu}\left(\mu fe^{-\delta}\Phi\right)', \tag{4.1.5a}$$

$$f' = \frac{\nu'}{\nu}(f-1) + \delta' f, \qquad \delta' = -\mu\nu\left(\Phi^2 + \Pi^2\right), \tag{4.1.5b}$$

$$\dot{f} = -2\mu\nu f^2 e^{-\delta}\Phi\Pi. \tag{4.1.5c}$$

This system of equations admits asymptotic expansions in powers of x at the origin and boundary which guarantee the regularity of solutions. They must satisfy at the origin

$$\phi(t,x) \;=\; \tilde{\phi}_0(t) + \tilde{\phi}_2(t)x^2 + \mathcal{O}(x^4), \tag{4.1.6}$$

$$\delta(t,x) = \tilde{\delta}_0(t) + \tilde{\delta}_2(t)x^2 + \mathcal{O}(x^4), \tag{4.1.7}$$
$$f(t,x) = 1 + \tilde{f}_2(t)x^2 + \mathcal{O}(x^4), \tag{4.1.8}$$

and at the boundary

$$\phi(t,x) = \phi_b(t) + \phi_2(t)\xi^2 + \phi_3(t)\xi^3 + \mathcal{O}(\xi^4), \tag{4.1.9}$$
$$\delta(t,x) = \delta_o(t) + \delta_2(t)\xi^2 + \mathcal{O}(\xi^4), \tag{4.1.10}$$
$$f(t,x) = 1 + f_2(t)\xi^2 + f_3(t)\xi^3 + \mathcal{O}(\xi^4), \tag{4.1.11}$$

with $\xi = (\pi/2 - x)$. The near-boundary expansion contains four degrees of freedom: $\phi_0(t), \phi_3(t), f_3(t)$ and $\delta_0(t)$. The last one is a constant of integration that must be fixed by hand, we will use $\delta(t,\pi/2) = \delta_0(t) = 0$, this choice identifies t at the boundary into the local proper time, thereby being referred to as the boundary gauge. The other three are not independent. The near boundary expansion of the equations of motion forces them to be related as follows $\dot{f}_3(t) = 6\dot{\phi}_0(t)\phi_3(t)$, coming from equation (4.1.5c). As a matter of fact, this equation turns out to be a consequence of the (time component of the) Ward Identity associated with diffeomorphism invariance of the theory. These quantities have an interpretation in terms of the AdS/CFT dictionary: $\phi_0(t)$ is dual to the source of the QFT, while $\phi_3(t)$ is proportional to the vev $\langle \mathcal{O}_\phi \rangle$. Following the holographic renormalization prescription described in section 2.4, we can extract the value of the energy density $m \equiv \langle T_{tt} \rangle = -1/2 f_3$ (where T_{ab} is the energy-momentum tensor of the dual QFT). Therefore the injection and extraction of energy in the system must obey the relation

$$\dot{m} = -3\dot{\phi}_0(t)\phi_3(t). \tag{4.1.12}$$

While $\phi_0(t)$ corresponds with the boundary conditions, over which we have control, the determination of $\phi_3(t)$ requires the resolution of the system of equations at each time-step. Therefore we do not have absolute control over the energy transferred through the boundary, only after evolving initial conditions we can track its . Despite this fact, we observe that a special kind of solutions could exist which have a perfect balance between the energy injected into and extrabehaviorcted from the system. They require synchronization between the dynamics in the bulk and the boundary, in a way such that (4.1.12) becomes periodic with a vanishing averaging in a period.

Now, we must make an appropriate decision about the kind of periodic boundary conditions we want for our system. It can be implemented in multiple manners, the simplest and most natural choice is a single harmonic of the form

$$\phi(t,\pi/2) = \rho\cos(\omega t). \tag{4.1.13}$$

Going to the weakly nonlinear limit ($\|\phi\|, \|\dot{\phi}\| \ll 1$) we can see that it is a suitable choice. In this regime these boundary conditions (4.1.13) are satisfied by a single non-normalizable mode of the system, the one with eigenvalue ω^2. Any other periodic drive consists of a combination of at least two non-normalizable modes; it would provide a dependence in more parameters, blurring the isolation of independent effects of each of them. The question now is whether these linearized solutions can be extended at higher amplitude of the drive, into full finite amplitude solutions of the non-linear system.

4.1.2 Time-Periodic Solutions

In this section we are going to construct TPSs through the methods of section 2.3. In this situation, the roles of u and v in section 2.3 are now played by ϕ and Π respectively. Nevertheless, this case is simplified by the fact that the EOMs admit a perturbative expansion restricted to odd powers of the perturbative parameter[3] (3.3.109), leaving the ansatz (2.3.24) for TPSs as

$$\phi(t,x)=\sum_{n=0}^{\infty}\cos((2n+1)\omega t)\hat{\phi}_n(x),\qquad \Pi(t,x)=\sum_{n=0}^{\infty}\sin((2n+1)\omega t)\hat{\Pi}_n(x), \tag{4.1.15}$$

with boundary conditions

$$\phi(t,\pi/2)=\rho\cos(\omega t),\qquad \Pi(t,\pi/2)=-\rho\omega\sin(\omega t). \tag{4.1.16}$$

Now rewriting the system of equations (4.1.5a)-(4.1.5b) in the appropriate form (see appendix A.5) we are ready to directly apply the numerical method of section 2.3.1.2 for the construction of TPSs.

After this brief explanation about the structure of the problem, we are ready to present the main results. In Fig. 4.2 we observe as TPSs form a surface in the three-dimensional space spanned by the frequency ω and the amplitudes of the scalar field at the boundary, ρ, and origin, $\rho_0=\phi(0,0)$. This surface cuts at $\omega=0$ on a line of configurations where the scalar takes a constant radial profile, in particular $\rho_0=\rho$. At the intersection of this surface with the plane $\rho=0$ we find the lines of TPSs with homogeneous boundary conditions originally constructed in [28]. These curves start from the bottom plane $\rho_0=0$ at the values $\Omega_n=2n+3$, given by the spectrum of normal frequencies of the massless scalar in AdS_4. As the value of ρ_0 is increased, the nonlinear dressing of the linearized solution shifts the value of the frequency and gives rise to the wiggly curves depicted in Fig. 4.2. The different sectors indicated with $I, II, III, \ldots$ correspond to TPSs whose profile $\phi(0,x)$ have $0,\ 1,\ 2,\ldots$ nodes respectively, Fig. 4.3.

Note that the existence of TPSs is a nontrivial result. In our setup the metric is not static, these solutions require a perfect synchronization between the fluctuations of the metric functions f, δ, the scalar field in the bulk and the boundary conditions. Additionally, given the external driving force, the natural expectation would be that the system get increasingly excited. Nevertheless, TPSs preserve an exact balance between the energy injected into and extracted from the system through a period. This fact can be observed by introducing the profile (4.1.15) and the boundary conditions (4.1.16) in the Ward identity (4.1.12), after averaging over a period $T=2\pi/\omega$ the variation of the energy density vanishes.

[3] It can be seen from the perturbative resolution performed in section 2.3.1.1. In this situation nonlinear terms (2.3.16) satisfy

$$S_{2n}(x,\tau)=0,\qquad S_{2n+1}(x,\tau)=\sum_{k=0}^{n}S_{2n+1,2k+1}(x)\cos((2k+1)\tau). \tag{4.1.14}$$

In consequence, only odd Fourier modes are present.

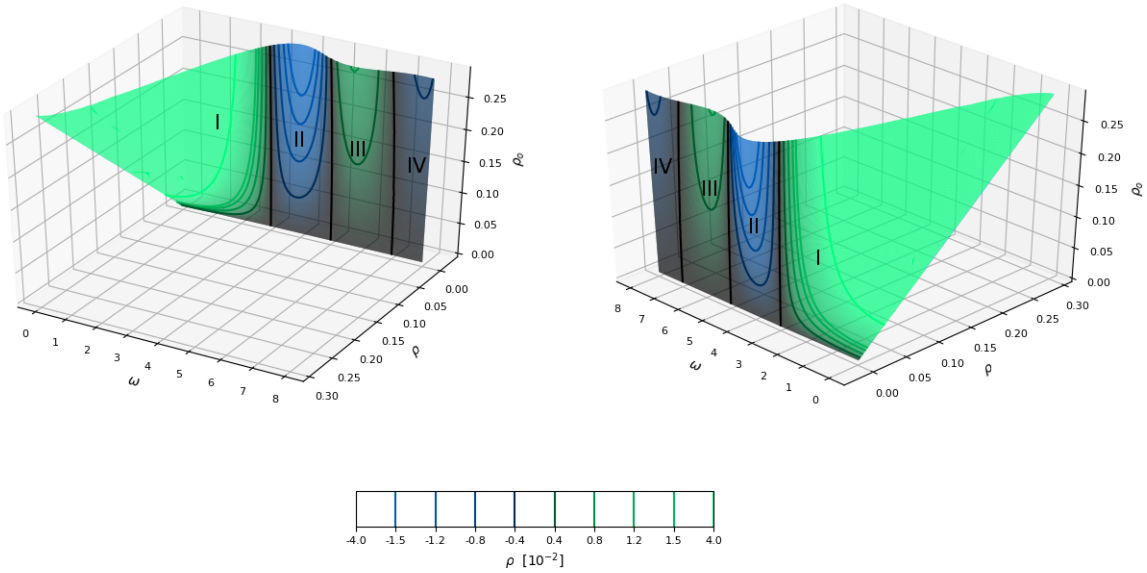

Figure 4.2: Surface of TPSs subject to the harmonic drive (4.1.15).

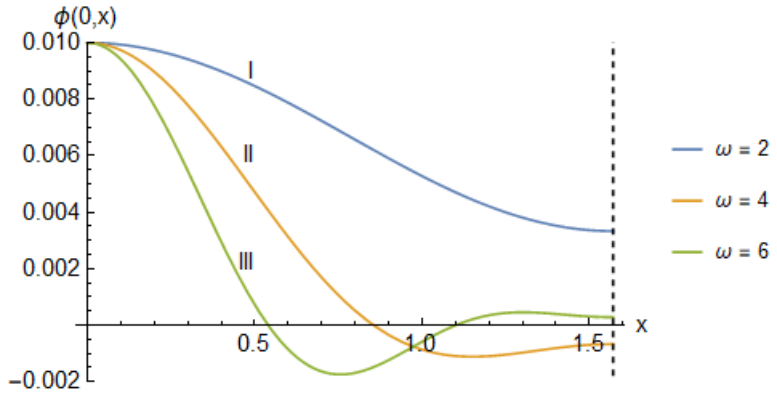

Figure 4.3: : Profiles $\phi(0,t)$ of TPSs in regions I, II and III in Fig. 4.2 having the same value of the scalar field at the origin, $\rho_0 = 0.01$ and different frequency ω. The black dashed line represents the boundary at $x = \pi/2$. As the number of nodes increases, the energy density tends to concentrate deeper in the bulk. The relative sign ρ and ρ_0 correlates with the even or odd number of nodes.

4.1.3 Linear Stability

Once TPSs are constructed we are going to study their linear stability through the method developed in section 2.3.2.2. In this situation the ansatz (2.3.57) for linear fluctuations $\tilde{\phi}$ and $\tilde{\Pi}$, of TPSs (Floquet modes) is divided in two, odd and even Fourier modes. This is a consequence of the structure of TPSs (4.1.15); odd and even modes decouple once they are inserted in the equations of linear perturbations presented in appendix A.5. For this reason the ansatz (2.3.57) becomes (odd multiples of the frequency)

$$\begin{aligned}\tilde{\phi}(t,x) &= e^{i\lambda t}\left(\sum_{n=0}^{\infty}\tilde{\phi}_n^{(1)}(x)\cos((2n+1)\omega t)+\sum_{n=0}^{\infty}\tilde{\phi}_n^{(2)}(x)\sin((2n+1)\omega t)\right),\\ \tilde{\Pi}(t,x) &= e^{i\lambda t}\left(\sum_{n=0}^{\infty}\tilde{\Pi}_n^{(1)}(x)\sin((2n+1)\omega t)+\sum_{n=0}^{\infty}\tilde{\Pi}_n^{(2)}(x)\cos((2n+1)\omega t)\right),\end{aligned} \tag{4.1.17}$$

and (even multiples multiples of the frequency)

$$\begin{aligned}\tilde{\phi}(t,x) &= e^{i\lambda t}\left(\sum_{n=0}^{\infty}\tilde{\phi}_n^{(1)}(x)\cos(2n\omega t)+\sum_{n=1}^{\infty}\tilde{\phi}_n^{(2)}(x)\sin(2n\omega t)\right),\\ \tilde{\Pi}(t,x) &= e^{i\lambda t}\left(\sum_{n=1}^{\infty}\tilde{\Pi}_n^{(1)}(x)\sin(2n\omega t)+\sum_{n=0}^{\infty}\tilde{\Pi}_n^{(2)}(x)\cos(2n\omega t)\right).\end{aligned} \tag{4.1.18}$$

We are interested in fluctuations of TPSs which preserve the drive, in consequence the boundary conditions are imposed to satisfy:

$$\tilde{\phi}_n^{(1)}(\pi/2)=\tilde{\phi}_n^{(2)}(\pi/2)=\tilde{\Pi}_n^{(1)}(\pi/2)=\tilde{\Pi}_n^{(2)}(\pi/2)=0. \tag{4.1.19}$$

Note that any other choice means a no longer harmonic drive. It would have a long-time dependence (if $\lambda\neq 0$) incurring in the breaking of the periodicity of our conditions. From a physical point of view, this election is also natural. Having a source under control is relatively easy taking into account that a TPS requires the generation of a state in the bulk which is perfectly synchronized with the source. Physically we understand that imperfections in the source are negligible in comparison to the deviation from a TPS incurred during the generation process.

Both, TPSs and their linear modes were numerically constructed using the strategies displayed in sections 2.3.1.2 and 2.3.2.2 respectively. Nevertheless for homogeneous boundary conditions, $\rho=0$ in (4.1.16), TPSs have been also obtained perturbatively following section 2.3.1.1 (see [112] for more in-depth details). We note that they satisfy the necessary conditions to apply Proposition 2.1. In consequence, these TPSs have a Floquet mode connecting two arbitrarily close TPSs with $\rho=0$, which contains a secular terms and therefore it is not properly described by ansatz (4.1.17) and (4.1.18)[4]. This fact prevents us to talk about the linear stability of these TPSs; nevertheless, this particular mode does

[4]Our numerical code works with (4.1.17) and (4.1.18) and this mode is incorrectly perceived as a zero-mode ($\lambda=0$).

not trigger an instability (see the discussion below Proposition 2.1). In consequence, we will omit this mode when we talk about the linear stability of TPSs with $\rho = 0$.

For inhomogeneous boundary conditions ($\rho \neq 0$) we have not performed the analytic resolution of the perturbative expansion of TPSs; however, we can qualitatively guarantee that conditions for the application of Proposition 2.2 are satisfied. Hence, it reports an important result; considering families of TPSs with the same value of ρ, solutions where the frequency ω is a local extrema have a zero-mode ($\lambda = 0$). As we said, in this case it is a qualitative result, but provides strong evidence about possible locations of transitions of stability.

In Fig. 4.4 have gathered all the information obtained until this point in a plot (ω, ρ_0). It shows the level curves $\rho_0(\omega, \rho)$ of constant ρ and the regions of linear stability (shaded) and instability (white). The black lines emerging from Ω_0 and Ω_1 correspond to TPSs with homogeneous boundary conditions originally constructed in [28, 112]. These lines are linearly stable until the value ρ_0 we have studied. There is evidence that they become unstable above some value of ρ_0 [112]; unfortunately, it remained out of our practical reach. From Fig. 4.4 we can also observe that they form a transition between white wedges placed on their lefts and the shaded regions on their rights. We have also found that the other boundary of these wedges consists of the points of curves $\rho_0(\omega, \rho)$ with constant ρ where the frequency ω has a maximum (as a qualitative application of Proposition 2.2 predicted). Fig. 4.5 illustrates this scenario. Here, a particular line formed by TPSs with constant ρ is shown as well as its five lowest Floquet exponents. These plots also illustrate as the lowest exponent becomes imaginary after the maximum of ω, confirming the linear instability of these solutions. The white wedge placed in the middle of region II has a different nature. As is shown in Fig. 4.6, the Floquet exponents: λ_0 and λ_1 are real until they merge close to $\omega = 3.95$. For linear modes between the two mergers (green line), their exponents generate a small imaginary part in addition to the real one, producing an exponentially growing perturbation. In consequence, this fact triggers an instability. We will dedicate the next section to the exploration of the instabilities we have determined here.

4.1.4 End States of Instabilities

It is interesting to explore the possibilities offered by linearly unstable TPSs (white wedges in Fig. 4.4). When there is an instability triggered by a single exponentially growing linear mode $(\tilde{\phi}_0, \tilde{\Pi}_0)$, a way to extract clear information from the instability consists of isolating its contribution by making its effects greater than perturbations coming from the numerical noise ($\sim 10^{-7}$ in our standard simulations). The protocol consists of preparing the initial data of our time-evolution code as the TPS (ϕ_p, Π_p) only perturbed by the unstable mode $(\tilde{\phi}_0, \tilde{\Pi}_0)$ at $t = 0$:

$$\phi(0, x) = \phi_p(0, x) + \epsilon\tilde{\phi}_0(0, x), \qquad \Pi(0, x) = \Pi_p(0, x) + \epsilon\tilde{\Pi}_0(0, x), \tag{4.1.20}$$

where ϵ is a parameter used to regulate the amplitude of the perturbation ($\epsilon > 10^{-6}$ ensures no relevant contamination from numerical noise). We have observed different

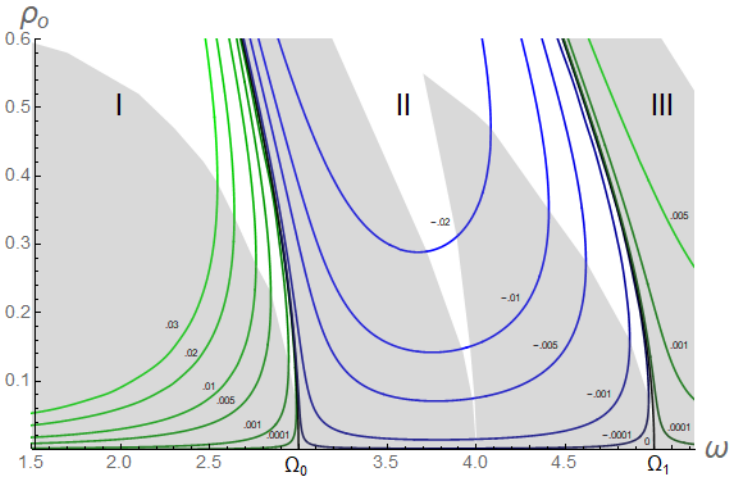

Figure 4.4: Level curves of the TPS surface plotted in Fig 4.2. Each curve corresponds to curves $\rho_0(\omega, \rho)$ of constant ρ (small numbers near each curve). Shaded (white) regions represent linearly stable (unstable) TPSs. Regions I, II, III reflect the nodes of the solutions, $0, 1, 2$ respectively.

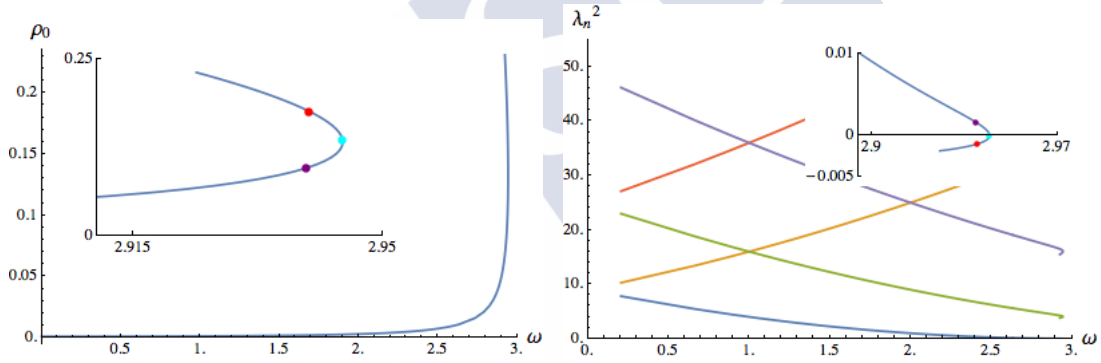

Figure 4.5: Left: Line of TPSs with $\rho = 0.001$. In the inset, purple, cyan and red dots mark solutions below, on and above the turning point. Right: Floquet exponents $\lambda_0^2, \ldots, \lambda_4^2$ for the TPSs shown in the left plot. Solutions above the turning point become linearly unstable ($\mathrm{Im}(\lambda_0) \neq 0$). In the inset, we zoom in this behavior. The color coding is the same as for the left inset.

phenomenology depending on the unstable TPS and the sign of ϵ (taking $\tilde{\phi}_0(0,0) > 0$). For TPSs far enough from the shaded regions, if $\epsilon > 0$ the instability leads the system to a black hole formation, while for the opposite sign the solution develops a long-time envelope (much larger than the period of the perturbed TPS, $T = 2\pi/\omega$) with the average mass $\langle m \rangle_T$ beating downward from the constant behavior for TPSs, see Fig. 4.7 for an example of these situations. By contrast, close to shaded regions we have observed the existence of unstable TPSs which do not develop a horizon for both signs of the perturbation. Instead of it, the system has long-time pulsations of $\langle m \rangle_T$ beating upward (downward) for positive (negative) ϵ, see Fig. 4.8. Finally, TPSs belonging to the white wedge placed in

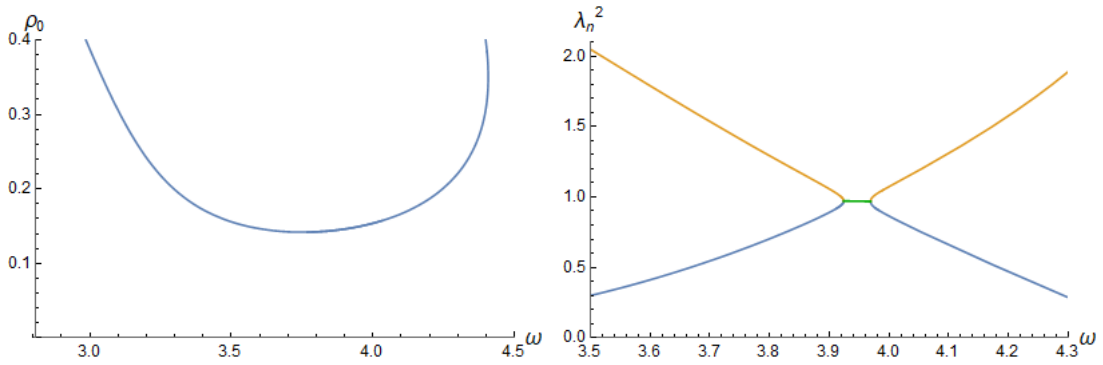

Figure 4.6: Left: Line of TPSs with $\rho = -0.01$. Right: Floquet exponents λ_0^2 (blue) and λ_1^2 (yellow) for TPSs shown in the left plot. They are real except in the region between mergers (green line) where a small imaginary part is developed in addition to the real one. In consequence, TPSs with linear modes belonging to the green line are linearly unstable.

the middle of region II (see Fig. 4.4) have a remarkable different behavior in comparison with the ones displayed in Fig. 4.7 and Fig. 4.8. We have already seen that the linear instability of this region is triggered by a different mechanism; the merger of two linear modes (see Fig. 4.6). It is in contrast with the simple transition of a Floquet exponent from a real to a purely complex number of the other zones (see Fig,4.5). In this case, it can be appreciated in Fig. 4.9, that the instability leads the system to a disordered phase where a large number of frequencies are strongly excited. Nevertheless, despite this strong presence of high harmonics, the solution remains regular and a black hole is not formed. This last situation does not exclude a gravitational collapse beyond the time we have studied or for other TPSs in this region.

From a holographic point of view, the collapse to a black hole is interpreted as the thermalization of a quantum pure state (consisting of a Floquet condensate) to form a mixed state with temperature. This thermal phase was studied in [107] in the Poincaré patch. Therein, the authors considered the dynamics of a periodically driven scalar under the presence of a horizon provided by the Schwarzschild-AdS$_4$ geometry. Nevertheless, the pulsating phases are more intriguing, some of them develop pulsations which seem to be almost periodic due to the repetition of a similar sequence at almost regular times. In the examples of Fig. 4.8 the time between consecutive peaks of pulsations is $T_+ = 398 \pm 1$ for positive ϵ and $T_- = 405 \pm 1$ for the opposite sign. They provide certain evidence of the possible existence of a solution with a long-time periodicity where, at the limit of an infinite period converges to an unstable TPS.

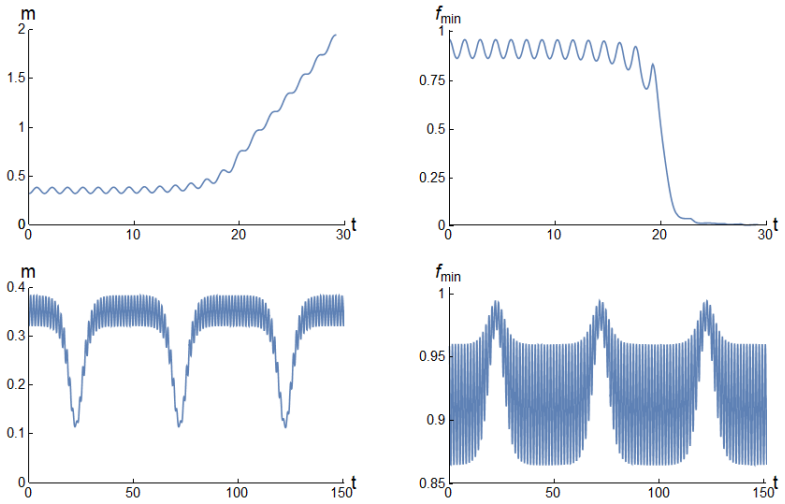

Figure 4.7: Numerical evolutions of the initial data (4.1.20) for the TPS: $\rho = 0.09, \omega \approx 2.1478$ and $\rho_0 = 0.7$. The upper plots correspond to $\epsilon = 10^{-4}$ and the lower ones to $\epsilon = -10^{-4}$. Plots on the left show the evolution of the energy density, while the ones on the right show the minimum value of the metric function $f(t,x)$ at each time ($f_{min} \equiv \min_x [f(t,x)]$). We observe as a positive perturbation leads to a black hole formation (f_{min} goes to zero) and a negative perturbation leads the system to a pulsating phase.

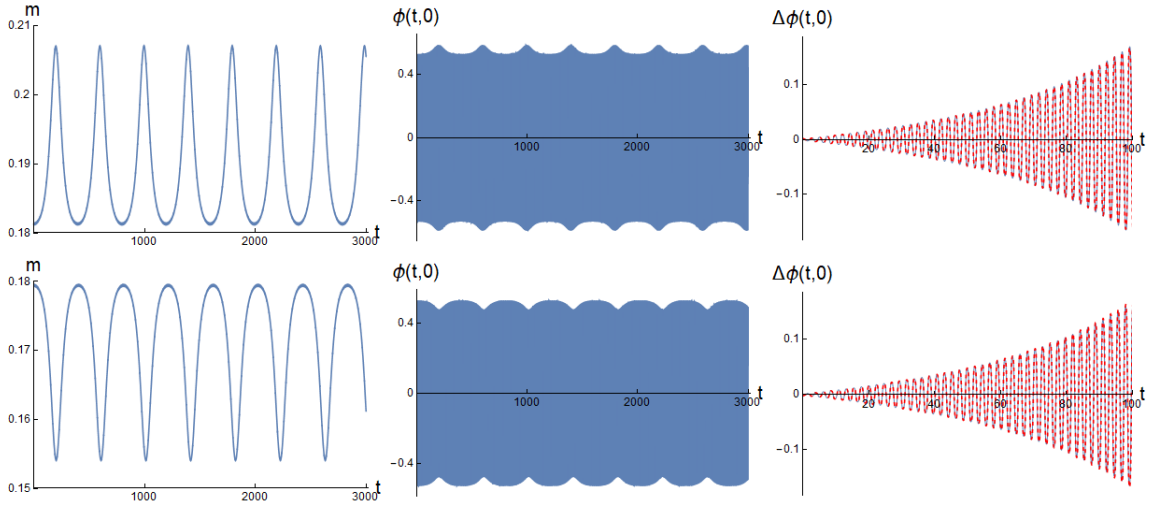

Figure 4.8: Numerical evolutions of the initial data (4.1.20) for the TPS: $\rho = 10^{-4}, \omega \approx 2.74$ and $\rho_0 = 0.53$. The upper plots correspond to $\epsilon = 10^{-3}$ and the lower ones to $\epsilon = -10^{-3}$. The plots on the left show the evolution of the energy density, the ones on the middle the evolution of $\phi(t,0)$ and, finally, the ones on the right the difference $\Delta\phi(t,0) = \phi(t,0) - \phi_p(t,0)$ is plotted in blue and $\epsilon\tilde{\phi}(t,0)$ in a dashed red line. Blue areas are formed by oscillations of frequency ω; they are densely concentrated in these figures because the range of these plots are much greater than the period of these oscillations.

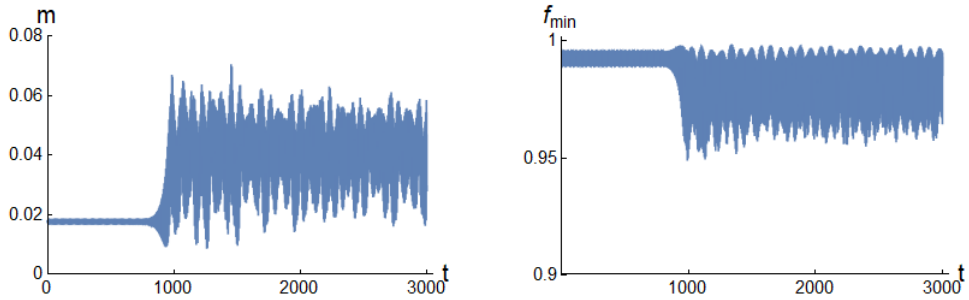

Figure 4.9: Numerical evolution of the initial data (4.1.20) for the TPS: $\rho = -0.01, \omega \approx 3.941$ and $\rho_0 = 0.1487$. This solution belongs to the green line presented in Fig. 4.6; in consequence, it is linearly unstable. In this case both signs of the perturbation ϵ ($|\epsilon| = 10^{-6}$) display the same disordered behavior. Although the dynamics is deviated from a TPS to this disordered phase, a black hole is not formed and the functions remain regular. Note the difference with unstable TPSs presented in Fig. 4.7 and Fig. 4.8. They belong to the white wedge in region I while the current situation is placed in the unstable region emerging from $\omega = 4$.

4.1.5 Dynamical Construction of Stable TPSs

In this section we study the response of TPSs and AdS under the variation of the parameters of the harmonic boundary conditions (4.1.16), amplitude and frequency, in time. The protocol of quenches we will use is introduced and explained in appendix A.2. Specifically, the structure of quenches in amplitude $\rho(t)$ and frequency $\omega(t)$, the duration of the quench denoted by β and the instantaneous frequency $\nu(t)$[5], have been presented there. Fig. 4.10 shows the evolution of the main functions $\rho(t)$ and $\omega(t)$ we are going to use in this section. Currently we will focus on the regimes of slow ($\beta \gg 2\pi/\max_t[\nu(t)]$) variations, as well as, in the synchronization properties of the system. Particularly, we will refer to quenches of long duration $\beta \gg 2\pi/\max_t[\nu(t)]$ as *adiabatic quenches*. In the previous section we solved the problem of constructing initial data corresponding to TPSs. Now we will show that they can also be obtained through a dynamical process and that this allows the exploration of certain regions of the phase-space.

We have observed that if the initial state is a TPS (or AdS) with boundary parameters (ρ_i, ω_i) and the pair of functions $(\rho(t), \nu(t))$, connecting the initial (ρ_i, ω_i) and final (ρ_f, ω_f) values, exists such that for any arbitrary time t_a, there is a stable TPS subject to the harmonic drive $\phi(t, \pi/2) = \rho(t_a)\cos(\nu(t_a)t)$; then, the state after the quench converges to the TPS parametrized by (ρ_f, ω_f) as β becomes larger. It can be seen in Fig. 4.11 that this result was achieved numerically, therefore, we have a limited resolution and the behavior for $\beta \to \infty$ cannot be reached. If β is large enough such that the difference between the

[5]The proper definition of frequency for a function of the form $\cos(\omega(t)t)$is

$$\nu(t) \equiv \frac{d}{dt}\left(\omega(t)t\right).$$

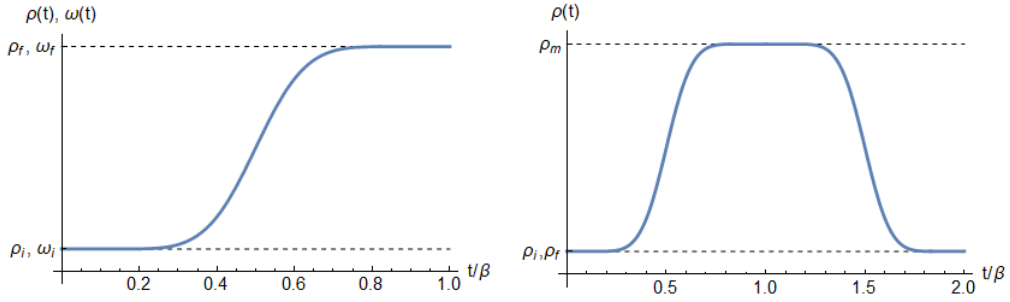

Figure 4.10: Left: functions $\rho(t)$ and $\omega(t)$ during the quench form (ρ_i, ω_i) to (ρ_f, ω_f). Right: function $\rho(t)$ during a quench, of duration 2β, in amplitude $(\omega(t) = \text{cte})$ with the same initial and final values $\rho_f = \rho_i$ and an intermediate value ρ_m.

final state and the target TPS is lower than the numerical noise ($\sim 10^{-7}$), performing quenches with duration beyond this value reports the same results. This fact can be observed in Fig. 4.11, where the difference between quenches with $\beta = 1500, 2000, 3000$ and the target TPS saturates at the level of numerical noise.

The measurement of the difference between a particular state of the system and the target TPS is done through the function defined in (A.2.9), in this situation for ϕ and f it takes the forms

$$\Delta\phi(t) = \left(\int_0^{\frac{\pi}{2}} dx \left(\phi(t,x) - \phi_{\rm p}(t,x)\right)^2 \right)^{\frac{1}{2}}, \tag{4.1.21}$$

$$\Delta f(t) = \left(\int_0^{\frac{\pi}{2}} dx \left(f(t,x) - f_{\rm p}(t,x)\right)^2 \right)^{\frac{1}{2}}, \tag{4.1.22}$$

where ϕ_p and f_p are associated with TPSs.

Once we have observed that stable TPSs can be obtained through adiabatic quenches, we are going to used this mechanism to construct TPSs with homogeneous boundary conditions ($\rho = 0$) from empty AdS. Namely, we move the system along a path in Fig. 4.4 connecting a point with $\rho_0 = \rho = 0$, placed on the left shaded area of region II, with a point $\rho_0 \neq 0$, $\rho = 0$ placed on the black line emerging from Ω_0. In consequence our quench has $\rho_i = \rho_f = 0$, and for this purpose we will use the quench (A.2.8) displayed in appendix A.2. The function $\omega(t)$ is displayed in the left plot of Fig. 4.10, while the function $\rho(t)$ is shown in the right plot of this figure. The particular example we present here consists of the quench with duration $2\beta = 2500$ connecting empty AdS, $(\rho_i, \omega_i) = (0, 3.1)$, with a TPSs with homogeneous boundary conditions, $(\rho_f, \omega_f) = (0, 2.9)$. Fig. 4.12 shows the evolutions of m and $\langle\mathcal{O}\rangle$ through the process. Fig. 4.13 shows as the quench approaches the state of the system to the target TPS. We understand these deviations from the required TPS due to the fact that β is not large enough.

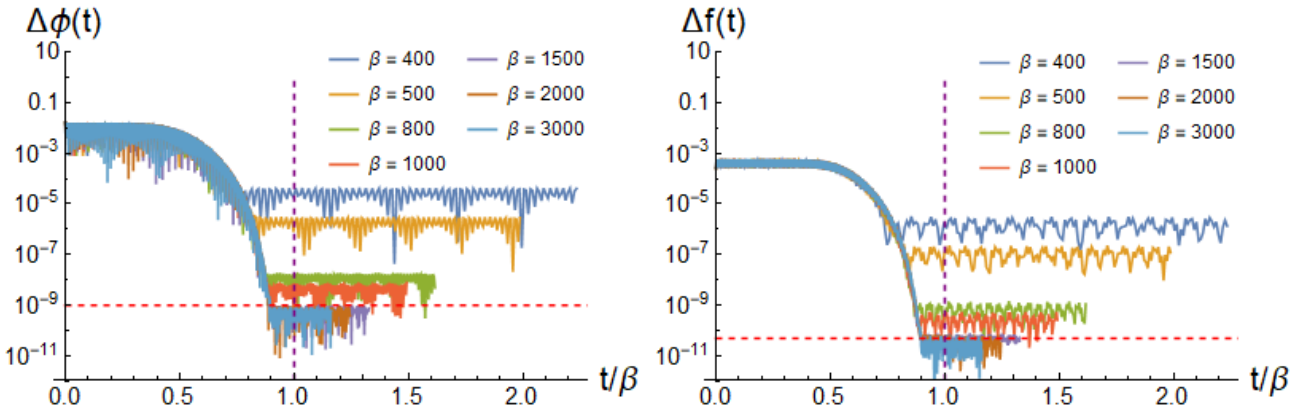

Figure 4.11: These plots show, through the functions (4.1.21)-(4.1.22), how the approach of the system to the TPS (ρ_f, ω_f) is improved with the duration of the process, β. The dashed purple line denotes the end of the quench, while the red one is placed at the level of the numerical noise of ϕ, f. We observe the saturation of this approach for $\beta = 1500, 2000, 3000$. This particular example consists of the quench (A.2.5) connecting empty AdS $(\rho_i, \omega_i) = (0, 2.9)$ with $(\rho_f, \omega_f) = (10^{-3}, 2.9)$ for different values of β.

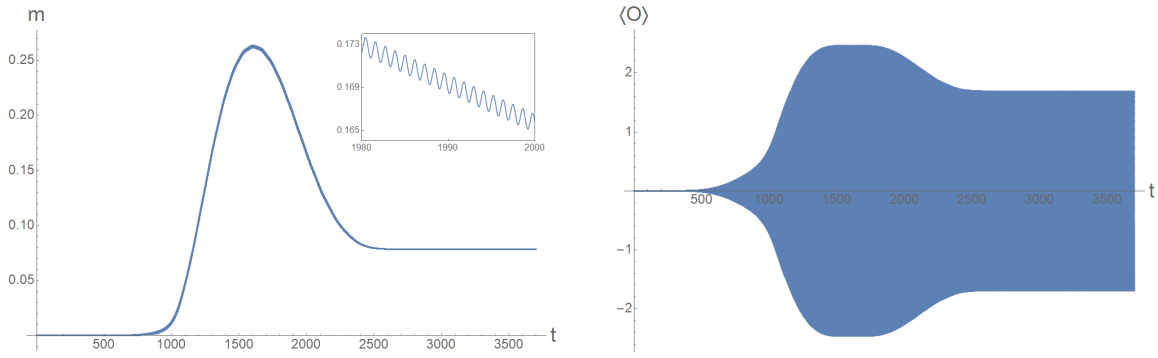

Figure 4.12: Time evolution of m and $\langle \mathcal{O} \rangle$ along the quench (A.2.8) from $(\rho_i, \omega_i) = (0, 3.1)$ to $(\rho_f, \omega_f) = (0, 2.9)$ and $\rho_m = 10^{-3}$. The blue region corresponds to a highly dense number of fast oscillations compared with the duration of the process. In the first plot this region is not appreciated, but as the inset shows it is also present.

4.1.6 Dynamical Construction of Unstable TPSs

In the previous section, the behavior of the system under a slow modification of the parameters of the harmonic drive has been analyzed. In the limit of infinite slow quench ($\beta \to \infty$), the system responds to the drive change "adiabatically". This means, reproducing the succession of TPSs that instantaneously match the drive data (frequency ω and amplitude ρ).

In this section we will examine the opposite limit. In particular, if the duration of the

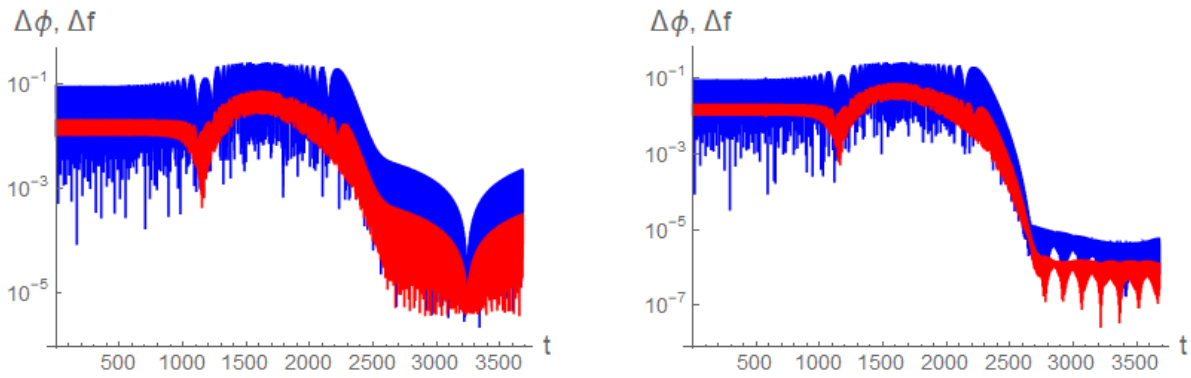

Figure 4.13: Time evolution of $\Delta\phi$ (blue) and Δf (red). Through ϕ and f we measure the "distance" between the final configurations after the quench with two TPSs: one with $\omega = 2.9$ (left), and another one with $\omega = 2.89992$ (right). The agreement is better in the second case.

process is similar to the period of oscillations ($\beta \sim 2\pi/\omega$) the results are not relevant, the system does not keep up with the variation of the drive. If this state is highly excited, it is natural to expect the formation of a black hole. Nevertheless, we have found a salient effect at intermediate durations, ($\beta > 2\pi/\omega$). For certain frequencies, there is a critical value β_c which separates two radically different regimes.

- For $\beta > \beta_c$ the system remains regular after the quench, although it is not able to reach synchronization with the drive. We observe in Fig. 4.14 that for β close enough to β_c the quench leads to a pulsating phase similar to the lower row of Fig. 4.8. We also appreciate as decreasing $(\beta - \beta_c)$ (guaranteeing that it remains positive) the plateau between pulsations increases. Namely, the system spends a progressively longer time in this intermediate state.

- For $\beta < \beta_c$, the quench results in an energy injection process strong enough to trigger gravitational collapse. After a transitory regime m increases without bound, while the value f_{min} drops to zero, signalling the initial formation of an apparent horizon. The duration of this transitory regime grows with smaller $|\beta - \beta_c|$. After f_{min} approaches zero, the harmonic drive keeps injecting energy continuously into the system, which increases its mass monotonically. Representative examples of the behavior just described can be found in Fig. 4.14.

Note the remarkable similarity between these processes after the finalization of their respective quenches and the evolution of the unstable TPS subject to boundary conditions $(\rho, \omega) = (0.09, 2.4178)$ displayed in Fig. 4.7. This TPS seems to be an unstable attractor for which the quantity $(\beta - \beta_c)$ is related to the amplitude of the unstable linear mode, ϵ in the case of (4.1.20). This observation allows us to identify this transition as a type I critical phenomenon in gravitational collapse [22]. In this context, the novelty of this transition stems from the fact that it is not triggered by varying smoothly a one-parameter

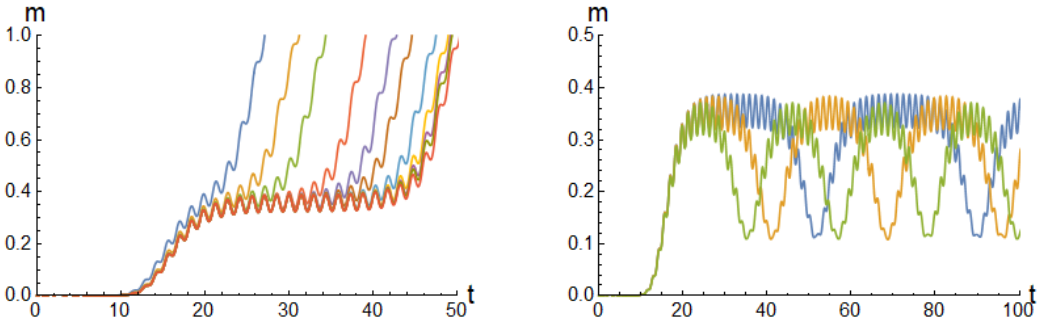

Figure 4.14: Both plots show the quench in amplitude from empty AdS $(\rho_i, \omega_i) = (0, 2.1478)$ to $(\rho_f, \omega_f) = (0.09, 2.1478)$. The plot on the left contains quenches with duration $\beta < \beta_c$ and the plot on the right quenches with $\beta > \beta_c$. In this case $\beta_c \approx 26.41343$. The duration of quenches in the left plot is from left to right: $\beta = 25,\ 26,\ 26.3,\ 26.4,\ 26.41,\ 26.412,\ 26.413,\ 26.4132,\ 26.41325,\ 26.41327,\ 26.4133$. On the right one again from left to right: $\beta = 26.5,\ 26.42,\ 26.4135$.

family of initial data [15, 200]; instead, it appears upon varying a one-parameter family of time-dependent boundary conditions for the scalar field.

To clarify this point, we will analyse the exponential deviation from the plateau as a function of $|\beta - \beta_c|$. For this purpose the analysis is simplified if we remove fast oscillations, leaving only the exponential time-dependence. Then, observing from Fig. 4.14 that the exponential deviation from the plateau does not have relevant oscillatory factors (these oscillations would grow exponentially) we will work with the averaged mass per period,

$$\langle m \rangle_T (t) \equiv \frac{1}{T} \int_{t-T/2}^{t+T/2} dt' m(t'). \tag{4.1.23}$$

Now, making the assumption that after the quench the system is close to an unstable TPSs we suppose that during the plateau this quantity can be expanded at first order,

$$\langle m \rangle_T (t) = \langle m_0 \rangle_T + \alpha(\beta - \beta_c)^\gamma e^{\lambda(t-t^*)} + ..., \tag{4.1.24}$$

where $\alpha, \gamma, \lambda \in \mathbb{R}$, m_0 corresponds to $\beta = \beta_c$ (if our supposition is true it must be the mass of the TPS) and t^* is a time where the mass takes a value where the linear approximation (4.1.24) properly works. Therefore, if we select a specific value of $\langle m \rangle_T (t)$ denoted by $\bar{m}^*$, common for all our quenches, and we measure the difference $\Delta t = t - t^*$ needed to reach it, i.e. $\bar{m}^* \equiv \langle m \rangle_T (\Delta t + t^*)$, we obtain the the following relation

$$\Delta t \sim -\frac{\gamma}{\lambda} \log |\beta - \beta_c| + a. \tag{4.1.25}$$

Note that γ and λ cannot be determined from this analysis; this process only perceives γ/λ. Despite this fact we still have some information to restrict γ; the behavior of the system depends on the sign of $(\beta - \beta_c)$, it means that γ must be an odd power. The most

natural value is $\gamma = 1$, although some symmetries of the problem could set to zero the coefficient of the linear term. For a proper determination of these quantities, we must calculate the Floquet exponent λ using the ansatz (4.1.17)-(4.1.18).

In Fig. 4.15 we observe that the relation (4.1.25) holds for quenches from empty AdS $(0, 2.1478)$ to $(0.09, 2.1478)$. From this analysis we obtain

$$\beta_c = 26.41343, \qquad \text{and} \qquad \lambda/\gamma = 0.4268. \tag{4.1.26}$$

While from the study of the linear stability of the unstable TPS subject to $(\rho, \omega) = (0.09, 2.4178)$, we obtained that the Floquet exponent of the unstable mode is $\lambda_0 = 0.4255$. λ/γ and λ_0 have a good agreement, therefore $\gamma = 1$. This agreement with the Floquet exponent provides strong evidence that the unstable attractor placed at $\beta = \beta_c$ is this TPS. Therefore, we have obtained a process to dynamically construct certain unstable TPSs. Unfortunately, we did not find this phenomenon for TPSs close to the region of linear stability.

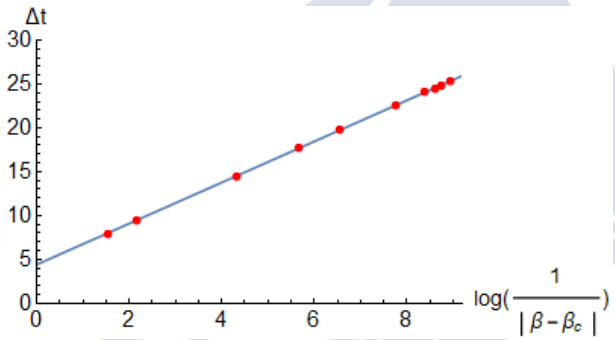

Figure 4.15: Scaling of the exponential deviation from the plateau displayed between $20 < t < 40$ in Fig. 4.14. Red points correspond with quenches contained in Fig. 4.14 while the solid line was obtained with a linear fit of these data.

4.1.7 Summary

In this section a free spherically symmetric massless scalar field in global AdS_4 was studied under the action of time-periodic boundary conditions of the form

$$\phi(t, \pi/2) = \rho \cos(\omega t). \tag{4.1.27}$$

We started by constructing TPSs subject to these conditions. For this purpose we used the methods displayed in section 2.3. These solutions formed a 2-dimensional surface in a 3-dimensional space consisting of the frequency ω, the amplitude ρ and the value of the scalar field at the origin $\rho_0 = \phi(0, 0)$, Fig. 4.2.

Once the central objects of our study were determined, we addressed the issue of their stability. The method developed in section 2.3.2.2 allowed studying the linear stability.

Specifically, it determined the first linear modes and their Floquet exponents. The information gathered until this point was suitably summarized in Fig. 4.4. In this figure the different regions of linearly stable and unstable TPSs were presented. All the linearly unstable TPSs reached by our codes were characterized by having a single exponentially growing modes, while the other modes remained bounded. Therefore, in order to extract clear information from the exploration of their instabilities, we prepared initial data consisting of the TPS with a small addition or subtraction of the unstable mode (4.1.20). We found that the system evolves to different states depending on the TPS and the sign of the perturbation. For example, we found gravitational collapse (Fig. 4.7), the development of a long-time envelope which pulsates increasing or decreasing the energy density in the system (Fig. 4.8) and a disordered phase (Fig. 4.9).

After that, we explored the synchronization properties of the system through a protocol of quenches of duration β. It was found that if the parameters of the boundary conditions (ρ, ω) slowly evolve in time $(2\pi/\max_t [\nu(t)] \ll \beta)$, the system modifies its state to match the TPS associated with instantaneous values $(\rho(t), \nu(t))$, Fig. 4.11. Namely, we have obtained a protocol to dynamically construct stable TPSs from empty AdS_4.

Once this synchronization property was understood, we initiated the exploration of faster variation of the boundary parameters $(2\pi/\max_t [\nu(t)] < \beta)$. In this case, we fixed the frequency and only the amplitude evolved from zero to ρ_f. Following this protocol an unexpected result was obtained, a critical value of the duration of the quench, β_c, exists such that if the quantity $|\beta_c - \beta|$ is small enough, the state of the system after the quench is the unstable TPS associated with (ρ_f, ω) and perturbed with its exponentially growing linear mode with an amplitude proportional to $(\beta_c - \beta)$. Namely, these unstable TPSs are attractors of this process, Fig. 4.14, and the have obtained a protocol to construct them.

4.2 Driven Gravitational Waves in the AdS Soliton

The important question that motivates this section is elucidating whether the physics uncovered in the previous section is specific to the particularities of a spherically symmetric scalar field in AdS_4 or, on the other hand, displays some degree of universality. To this end, we will consider another geometry, the AdS soliton, which enjoys different properties. For example, in contrast with global AdS_4, where the the topology of the boundary is $\mathbb{R} \times \mathbb{S}^2$, the spectrum is fully resonant and there is no mass gap between this space and the smallest possible black hole; in the current setup the topology of the boundary is $\mathbb{R} \times \mathbb{T}^2$, the spectrum is not resonant and there is a mass gap with the smallest black hole.

4.2.1 The Model

In this section we consider the 4-dimensional AdS soliton geometry under purely gravitational fluctuations with harmonic boundary conditions. The current setup admits

nontrivial dynamics for the vacuum Einstein equations with the metric ansatz,

$$ds^2 = \frac{l^2}{z^2}\left(-f(t,z)e^{-2\delta(t,z)}dt^2 + \frac{dz^2}{\left(1-\frac{z^3}{z_0^3}\right)f(t,z)} + \left(1-\frac{z^3}{z_0^3}\right)e^{b(t,z)}dx^2 + e^{-b(t,z)}dy^2\right), \tag{4.2.1}$$

where the AdS soliton corresponds to $b(t,z) = \delta(t,0) = 0, f(t,z) = 1$. The AdS radius is represented by l (which will be set to 1), the range of z goes from the boundary placed at $z = 0$ to the tip of the cigar $z = z_0$ (which will be set to 1), where the proper length along the x-direction vanishes and spacetime ends. For regularity at the tip it is required that the x coordinate is compact with periodicity $l_x = 4\pi z_0/3$. It would be nice to have similar arguments at work for the other coordinate y, enforcing on it a periodicity l_y by singularity avoidance at deeper bulk scale $z_1 \geq z_0$. Unfortunately, no such solution is known[6]. In our setup, the coordinate y can be compactified for free, as long as its period l_y is longer than l_x. Thus, we will envisage the geometry (4.2.1) as being dual to a strongly coupled CFT placed on a rectangular region with sides $l_y > l_x$ and periodic/antiperiodic boundary conditions for bosonic/fermionic fields. It is on this setup that our investigations aim at unveiling detectable effects of the gravitational drive parametrized by the strain field $b(t,z)$. A nonzero $b(t,z)$ introduces an anisotropy in the boundary geometry; for small amplitudes, it acts like the h_+ strain of a gravitational wave propagating along the direction perpendicular to the dual quantum system.

In terms of the following variables (where $\dot{} \equiv \partial_t$, $' \equiv \partial_z$)

$$B(t,z) = b'(t,z), \qquad P(t,z) = \frac{e^{\delta}}{f}\dot{b}, \tag{4.2.2}$$

the equations of motion can be written in the form

$$\dot{B} = \left(fe^{-\delta}P\right)', \tag{4.2.3}$$

$$\dot{P} = \frac{z^2}{2}\left(\left(-3+2\frac{(1-z^3)}{z^2}B\right)fe^{-\delta}\right)', \tag{4.2.4}$$

$$f' = \frac{12}{z(4-z^3)}(1-f) + \delta' f, \tag{4.2.5}$$

$$\delta' = \frac{z}{4-z^3}\left(-3z^2B + (1-z^3)B^2 + P^2\right). \tag{4.2.6}$$

There is yet one additional equation given by the momentum constraint

$$\dot{f} = \frac{z}{z^3-4}\left((3z^2+2(z^3-1)B)P\right)f^2e^{-\delta}, \tag{4.2.7}$$

which is not independent from (4.2.3)-(4.2.6). This equation will be used to test the time evolution of the system performed by our code (see appendix A.6).

[6]See however [201] for a discussion on a singular geometry that has some of the desired ingredients. The first order phase transition upon exchange of periodicities have been discussed in several places, see for example [202] [203] [204].

Regular solutions must satisfy the asymptotic expansions at the tip (z=1)

$$\begin{aligned} f(t,z) &= e^{-\tilde{b}_0(t)} + \tilde{f}_2(t)(1-z) + \mathcal{O}((1-z)^2), \\ b(t,z) &= \tilde{b}_0(t) + \tilde{b}_2(t)(1-z) + \mathcal{O}((1-z)^2), \\ \delta(t,z) &= \tilde{\delta}_0(t) + \tilde{\delta}_2(t)(1-z) + \mathcal{O}((1-z)^2), \end{aligned} \tag{4.2.8}$$

and close to the boundary (z=0)

$$\delta(t,z) = \frac{1}{8}\dot{b}_0(t)^2 z^2 + \mathcal{O}(z^4), \tag{4.2.9}$$

$$f(t,z) = 1 - \frac{1}{4}\dot{b}_0(t)^2 z^2 + f_3(t) z^3 + \mathcal{O}(z^4), \tag{4.2.10}$$

$$b(t,z) = b_0(t) - \frac{1}{2}\ddot{b}_0(t) z^2 + b_3(t) z^3 + \mathcal{O}(z^4). \tag{4.2.11}$$

On this occasion the freedom in δ_0 has been already fixed to $\delta(t,0) = 0$, to ease the construction of TPSs. The condition $f(t,1) = e^{-b(t,1)}$ has been imposed in order to avoid a conical singularity at the tip. The remaining freedoms: $b_0(t), b_3(t), f_3(t)$ are linked by equation (4.2.7) as

$$\dot{f}_3(t) = \frac{3}{4}\dot{b}_0(t)\left(2b_3(t) - 1\right). \tag{4.2.12}$$

Following the holographic renormalization given in section 2.4, the energy-momentum tensor of the CFT, $\mathcal{T}_{ab}$, can be computed. Hence, the energy density takes the form $m \equiv \langle \mathcal{T}_{tt} \rangle = -\frac{1}{4}\left(1 + 2f_3(t)\right)$. Combining this expression with (4.2.12) we obtain

$$\dot{m} = \frac{3}{8}\dot{b}_0(t)\left(1 - 2b_3(t)\right). \tag{4.2.13}$$

The energy transferred through the boundary does not only depend on the boundary conditions, $b_0(t)$. It requires the resolution of the system of equations at each time to obtain $b_3(t)$ and then $\dot{m}(t)$. It means that we do not know a priori the exchange of energy between the system through the boundary. Nevertheless, analysing the RHS of (4.2.13), we observe that the reasoning followed for the scalar field in AdS_4 can be applied in this situation. If the dynamics in the bulk is synchronized with the source such that $\dot{m}$ is periodic with a zero averaging per period, it guarantees the exact balance between the energy injected into and extracted from the system. In light of the rich phenomenology displayed by a harmonic drive in section 4.1, the simplicity of these conditions and the fact that our techniques have an almost direct application in this context, we also consider a harmonic drive of the form

$$b_0(t) = \rho \cos(\omega t). \tag{4.2.14}$$

In the weakly nonlinear regime ($|b| \ll 1$) these conditions are satisfied with a single non-normalizable mode, the one with eigenvalue ω^2. Any other time-periodic boundary conditions require the presence of at least two non-normalizable modes, providing a larger number of parameters which blur the simplicity of our setup.

Finally, before introducing our results, we must clarify that from an analytical point of view the system of equations (4.2.3)-(4.2.7) is properly expressed in terms of the z

coordinate; nevertheless, the numerical modelling requires a better resolution at the tip ($z = z_0$). In consequence, from a numerical point of view we must perform a coordinate transformation to properly describe the environment of this point. We will also use this transformation to reorder the asymptotic expansion (4.2.8) around the tip to obtain functions with a defined parity; an important feature in our construction of TPSs. We have found that the transformation used in [205] is suitable for our purposes, it is

$$z = z_0(1 - r^2). \tag{4.2.15}$$

Note that in this case, an equispaced grid in r concentrates points close to the tip in z. The second requirement is also fulfilled, expressed in terms of r, functions $b(t, r), f(t, r), \delta(t, r)$ are symmetric at the tip. We must also clarify that in this new coordinate the tip and the boundary are exchanged, the tip is placed at $r = 0$ and the boundary at $r = 1$ ($z_0 = 1$). Results presented in the following sections have been obtained making use of r, and they will be expressed in this coordinate. The EOMs (4.2.4)-(4.2.7) in terms of r can be found in appendix A.5.2.

4.2.2 Time-Periodic Solutions

In this section we are going to construct TPSs of the EOMs (4.2.3)-(4.2.7) (expressed in r, see appendix A.5.2) subject to the time-dependent boundary conditions (4.2.14).

For this purpose, the change from z to r is crucial at this point; functions $b(t, r), f(t, r), \delta(t, r)$ are symmetric at the tip, allowing us to make use of the methods developed in section 2.3. In this situation the roles of u, v in that section are now played by b, P respectively. In contrast with the case studied in section 4.1, where the Fourier spectrum of TPSs consisted of odd modes, these TPSs will have the whole set of modes. The current static background around which TPSs are constructed is the AdS soliton: $b = \delta = 0,\ f = 1$. This geometry, subject to the metric ansatz (4.2.1) admits a perturbative expansion of the form

$$b(t, r) = \sum_{n=1}^{\infty} \epsilon^n b_n(t, r), \qquad f(t, r) = 1 + \sum_{n=1}^{\infty} \epsilon^n f_n(t, r), \qquad \delta(t, r) = \sum_{n=1}^{\infty} \epsilon^n \delta_n(t, r), \tag{4.2.16}$$

where all the positive integer powers are present. We must remark that through this thesis, the current model is the only one which does not enjoy a fully resonant spectrum. At first order in ϵ and imposing homogeneous boundary conditions $\rho = 0$, nontrivial solutions for $b_1(t, z)$ only exist for a discrete set of frequencies Ω_n, yielding the normal mode spectrum $\Omega_n \approx 2.149,\ 4.790,\ 7.116,\ 9.389, \ldots$ In this case, the linear equation was solved numerically and our results show an excellent agreement with [205]. For finite amplitudes, these solutions can be uplifted to form the TPSs with homogeneous boundary conditions.

In this case, as consequence of the structure of the asymptotic expansion (4.2.16)[7], the

[7]The presence of all the positive integer powers in (4.2.16) reports non-vanishing nonlinear terms $S_{n>1} \neq 0$ in (2.3.16).

ansatz for TPSs is exactly (2.3.24),

$$b(t,r) = \sum_{n=0}^{\infty} \cos(n\omega t)\hat{b}_n(r), \qquad P(t,r) = \sum_{n=1}^{\infty} \sin(n\omega t)\hat{P}_n(r), \tag{4.2.17}$$

with boundary conditions[8]

$$b(t,1) = \rho\cos(\omega t), \qquad P(t,1) = -\rho\omega\sin(\omega t). \tag{4.2.18}$$

After explaining the structure of the problem we are going to present the main results. We observe that TPSs form a surface in a 3-dimensional space defined by the amplitude of the drive ρ, its frequency ω and the value at the tip $\rho_t = b(0,0)$. However, as we already saw in the case of a scalar field in AdS_4, the relevant information is more suitably summarized in the plot (ω, ρ_t), Fig. 4.16. This figure shows the level curves $\rho_t(\omega,\rho)$ of constant ρ, the regions of linear stability (shaded) and instability (white) which we will study in the following sections, as well as wedges where TPSs were not found (yellow). On the right hand side of Fig. 4.16, similarly to the case of a scalar field, the black line signals TPSs with homogeneous boundary conditions, it emerges from a linearized normal mode frequency, Ω_0, and tilts toward lower values of ω. Solutions for moderate values of ρ_t (> 0.25) are very difficult to obtain. While solutions below $\rho_t < 0.25$ can be obtained reliably with the pseudospectral construction of section 2.3.1.2. Due to this limitation, we used an additional method to scan the regions where our numerical resolution of (4.2.17) fails. It consists of the dynamical construction of TPSs through slow quenches. This result was already introduced in section 4.1.5 for a scalar field in global AdS_4, and it will be justified for our current situation in section 4.2.5. On this occasion, we have focused our effort on region I; namely, TPSs without nodes and frequency $0 < \omega \leq \Omega_0$. On the left side of this region, $\omega \to 0$, TPSs converge to a nontrivial static profile with $\rho_t = 2\rho$, while on the right side they are delimited by TPSs with $\rho = 0$.

Finally, Fig. 4.16 shows an interesting phenomenon based on resonances, the yellow areas. For specific frequencies ω, the ansatz for TPS, (4.2.17), resonates with higher normal modes, and this resonance triggers a new kind of behavior. In the limit of weak nonlinearities ($\rho_t, \rho \ll 1$), an argument for the existence of these resonances is as follows. Recall that, from the perturbative analysis, all multiples of the frequency ω are present (4.2.17). If this sequence hits some normal mode frequency, i.e, if $m\omega = \Omega_n$, then the forcing term will contain a solution with $\rho = 0$ for the linear equation, leading, as usual, to the appearance of secular terms that drive the system far away from the original TPS. It can reflect that for certain frequencies the perturbative expansion leading to the ansatz (4.2.17) is not valid at larger scales. This argument shows a serious problem, the set of frequencies of linear modes $\{\Omega_n\}$ is infinite and then the number of resonances $\omega = \Omega_n/m$. It means that the shaded area of Fig. 4.16 has infinite lines crossing it. Nevertheless, we have observed that their width quickly decreases with n and m.

We expect that this phenomenon also happens in the case of the scalar field studied in the previous section. There the spectrum of modes with homogeneous boundary conditions is

[8]Remember that we have set $\delta(t, z = 0) = 0$, which expressed in terms of r becomes $\delta(t, r = 1) = 0$.

$\Omega_n = 2n+3$, while the structure of TPSs only contains odd multiples of the frequency ω. Therefore, in this case the resonances should be present around frequencies of the form $\omega = \Omega_n/(2m+1)$ with $n, m = 0, 1, 2, \ldots$ Following the results obtained in the current section, we also expect that the width is associated with the the values of n and m, thereby $\omega = 1$ should be the widest resonance.

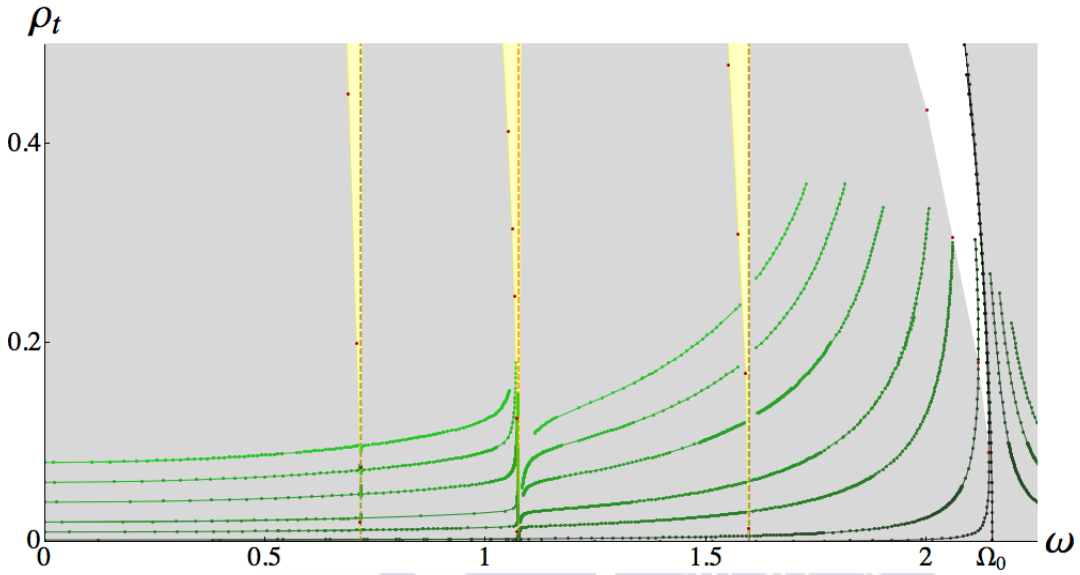

Figure 4.16: Solid lines are level curves $\rho_t(\omega, \rho)$ of constant ρ. Points in the shaded region correspond to linearly stable TPSs. Solutions in the white region are linearly unstable; once perturbed, they evolve either to pulsating geometries or black holes. Red points signal the data constructed through quasistatic quenches needed to determine the thresholds of shaded areas. Emerging from Ω_0, we see the first line of nonlinear gravitational normal modes (solid black), which corresponds to TPSs with $\rho = 0$. Dashed lines indicate resonances between the frequency of a Fourier mode of the TPS, $m\omega$, and a normal mode, Ω_n, (from left to right $\omega = \Omega_0/3, \Omega_1/3$ in brown, and $\Omega_0/2$ in orange). Around these resonances (yellow regions), no TPSs were found. More resonances are expected at $m\omega = \Omega_n$ for $n, m \in \mathbb{N}$, nevertheless they are so narrow that are difficult to determine.

4.2.3 Linear Stability

In this section we are going to address the issue of the linear stability of TPSs. Following section 2.3.2.2, te ansatz for linear fluctuations $\tilde{b}$, $\tilde{P}$, of TPSs (2.3.57) has the form

$$\tilde{b}(t,r) = e^{i\lambda t}\left(\sum_{n=0}^{\infty}\tilde{b}_n^{(1)}(r)\cos(n\omega t) + \sum_{n=1}^{\infty}\tilde{b}_n^{(2)}(r)\sin(n\omega t)\right),$$
$$\tilde{P}(t,r) = e^{i\lambda t}\left(\sum_{n=1}^{\infty}\tilde{P}_n^{(1)}(r)\sin(n\omega t) + \sum_{n=0}^{\infty}\tilde{P}_n^{(2)}(r)\cos(n\omega t)\right). \qquad (4.2.19)$$

We are interested in fluctuations of TPSs which preserve the source, thereby the boundary conditions must satisfy: $\tilde{b}_n^{(1)}(1) = \tilde{b}_n^{(2)}(1) = \tilde{P}_n^{(1)}(1) = \tilde{P}_n^{(2)}(1) = 0$. Any other choice modifies the harmonic conditions. It would have a long-time dependence incurring in the breaking of the periodicity of our conditions.

Both, TPSs and their linear modes are numerically constructed using the strategy displayed in sections 2.3.1.2 and 2.3.2.2 respectively. Additionally, TPSs subject to homogeneous boundary conditions ($\rho = 0$) have been also constructed following the perturbative procedure explained in section 2.3.1.1. We note that they satisfy the necessary conditions to apply Proposition 2.1. In consequence, these TPSs have a Floquet mode connecting two arbitrarily close TPSs with $\rho = 0$, which contains a secular term and therefore it is not properly described by ansatz (4.2.19)[9]. This fact prevents us to talk about the linear stability of these TPSs; nevertheless, this particular mode does not trigger an instability (see the discussion below Proposition 2.1). In consequence, we will omit this mode when we discuss about the linear stability of TPSs with $\rho = 0$.

In the case of inhomogeneous boundary conditions, $\rho \neq 0$, we have not performed the resolution of the perturbative expansion; however, we can qualitatively guarantee that conditions for the application of Proposition 2.2 are also satisfied. Hence, it reports strong evidence about the existence of a zero-mode ($\lambda = 0$) at any local extrema of ω for a continuous family of TPSs with the same value of ρ.

The regions of linear stability (shaded) and instability (white) were represented in Fig. 4.16. We observe that on the right side of this figure the black line (TPSs with $\rho = 0$), corresponds to the right boundary of an instability region. The solutions on the line are themselves linearly stable, and their energy density increases monotonically as we move upward. It is expected that this linear stability is lost when the energy density reaches an extremum, a point that would correspond to a Chandrasekar-like limit. Unfortunately, this region has remained unreachable to our codes. The other boundary of the white region, where the transition from linearly stable to unstable TPSs happens, corresponds with the local maximums of ω along the level curves $\rho_t(\omega, \rho)$ of constant ρ. Fig. 4.17 illustrates this fact by tracking the lowest values of λ_n for the curve of constant $\rho = 0.001$. This result confirms the evidence obtained with a qualitative application of Proposition 2.2.

4.2.4 End States of Instabilities

Once we have constructed TPSs and studied their linear stability, we have the required machinery to explore the end points of the present instabilities. The exploration of the linearly unstable TPSs (the white wedge in Fig. 4.16), which only have a single exponentially growing linear mode, was done through numerical evolutions of unstable TPSs (b_p, P_p). The simplest form to extract clear information consisted of perturbing these solutions with their unstable mode $(\tilde{b}_0, \tilde{P}_0)$ with an amplitude greater than the numerical

[9] Our numerical code works with (4.2.19), and this mode is incorrectly perceived as a zero-mode ($\lambda = 0$).

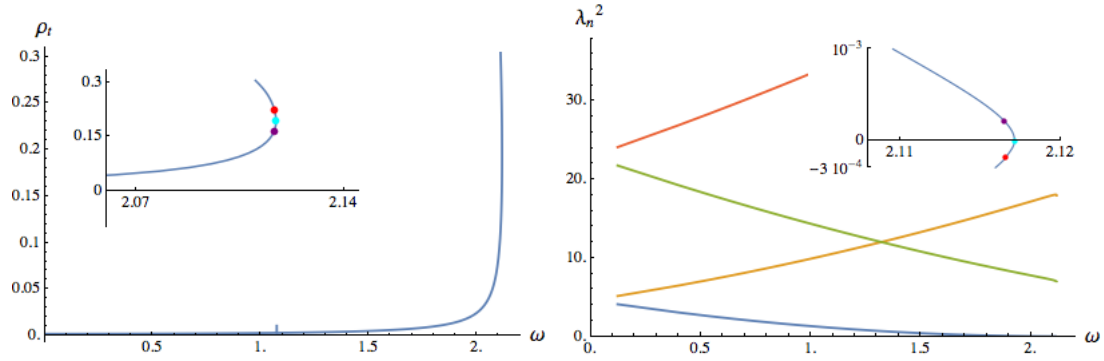

Figure 4.17: Left: Line of TPSs with $\rho = 0.001$. In the inset, purple, cyan and red dots mark solutions below, on and above the turning point. Right: Floquet exponents $\lambda_0^2, \ldots, \lambda_3^2$ for the TPSs shown in the left plot. Solutions above the turning point become linearly unstable ($\mathrm{Im}(\lambda_0) \neq 0$). In the inset, we zoom in this behavior. The color coding is the same as for the left inset.

noise ($\sim 10^{-6}$ in standard simulations). For this purpose we prepared initial data of the form:

$$b(0,r) = b_p(0,r) + \epsilon \tilde{b}_0(0,r), \qquad P(0,r) = P_p(0,r) + \epsilon \tilde{P}_0(0,r), \tag{4.2.20}$$

where ϵ is a parameter introduced to control the degree of perturbation induced in the TPS. For initial data (4.2.20) with the same amplitude $|\epsilon|$ but opposite sign, the instability leads the system to different states. Our numerical construction of TPSs through the resolution of (4.2.17) only accessed to a small region of the white wedge placed close to the thresholds of stability. In consequence, the unstable TPSs we had at hand only displayed long-time pulsations in different direction depending on the sign of ϵ. Fig. 4.18 shows an example of this behavior. We observe as the system access to a state where the energy pulsates upward ($\epsilon > 0$) or downward ($\epsilon < 0$). The sequence of peaks is also pretty regular, the time between them is $T_+ = 2130 \pm 2$ for positive ϵ and $T_- = 2136 \pm 2$ for the opposite sign. Note that although in this setup there are no black holes for $m < 0$, this kind of pulsating behavior is not expected due to the fact that the system does not have impediments in absorbing energy to surpass this threshold and collapse. Although we did not reach to unstable TPSs for which the positive perturbation $\epsilon > 0$ leads the system to gravitational collapse, this behavior is expected for high amplitudes ρ_t and ρ. In section 4.2.6 we will observe this phenomenon through the realization of quenches with a duration close to the critical value β_c.

4.2.5 Dynamical Construction of Stable TPSs

In this section we study the response of TPSs and the AdS soliton under the variation in time of the parameters of the harmonic drive (4.2.18), amplitude and frequency. The protocol of quenches we will use is introduced and explained in section A.2. Especially,

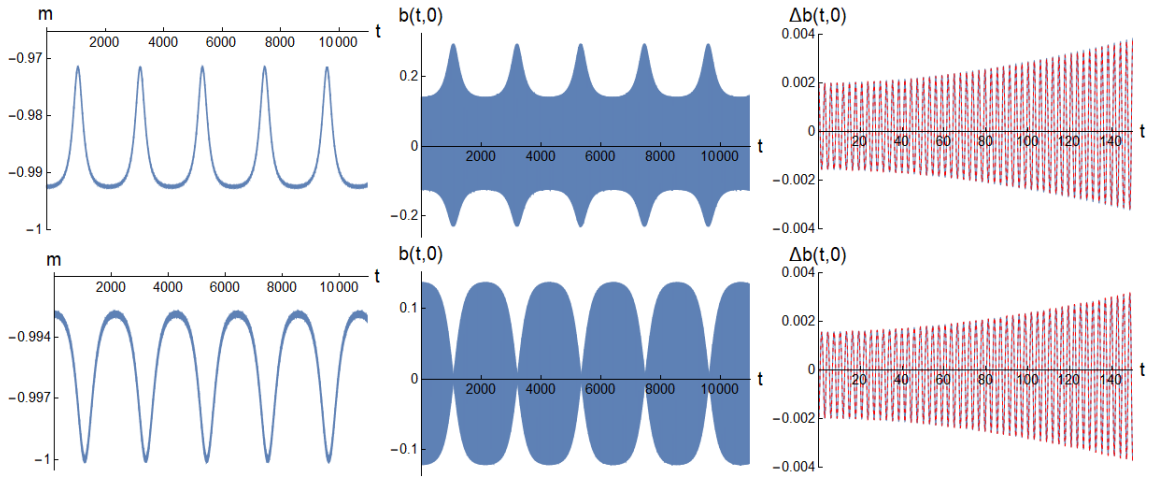

Figure 4.18: Numerical simulations of the initial data (4.2.20) for the TPS: $\rho = 10^{-4}$, $\rho_t = 0.14$ and $\omega = 2.137$. The upper plots correspond to $\epsilon = 10^{-3}$ and the lower ones to $\epsilon = -10^{-3}$. The plots on the left show the evolution of the energy density, the middle ones the evolution of $b(t,0)$ and, finally, the ones on the right the difference $\Delta b(t,0) = b(t,0) - b_p(t,0)$ is plotted in blue and $\epsilon\tilde{b}_0(t,0)$ in a dashed red line.

the structure of quenches in amplitude $\rho(t)$ and frequency $\omega(t)$, the duration of the quench denoted by β and the instantaneous frequency $\nu(t)$ have been presented there. We are interested in the regimes of slow ($\beta \gg 2\pi/\max_t[\nu(t)]$)[10] variations as well as the synchronization properties of the system. In the previous section we solved the problem of constructing initial data corresponding to TPSs. Now we will show that they can also be achieved through a dynamical process and that this allows the exploration of certain regions of the phase-space. The quenches presented in this section correspond to the function $\rho(t)$ displayed in the left plot of Fig. 4.10 and $\omega(t) = \text{cte}$ (see (A.2.5) in appendix A.2).

We have observed that if the initial state is a TPS (or the AdS soliton) with boundary parameters (ρ_i, ω_i) and the pair of functions $(\rho(t), \nu(t))$, connecting the initial (ρ_i, ω_i) and final (ρ_f, ω_f) values, exists such that for any arbitrary time t_a, there is a stable TPS subject to the harmonic drive $b(t,1) = \rho(t_a)\cos(\nu(t_a)t)$, then the final state converges to the TPS parametrized by (ρ_f, ω_f) as β becomes larger. As can be seen in Fig. 4.19 that this result was achieved numerically; therefore, we have a limited resolution and the behavior for $\beta \to \infty$ cannot be reached. If β is large enough such that the difference between the final state and the target TPS is lower than the numerical noise ($\sim 10^{-6}$), performing quenches with a duration beyond this value will report the same results. This fact can be observed in Fig. 4.19, where the difference between quenches with $\beta = 1300, 1500$ and the target TPS saturates at the level of numerical noise. Note that for "large enough" β we refer to quenches with a duration much longer than the periodicity of any intermediate TPS, $2\pi/\max_t[\nu(t)]$.

[10] On some occasions we will refer to these processes as *adiabatic quenches*.

The measurement of the difference between a state and the target TPS is done through the function defined in (A.2.9), in this situation for b and f it takes the forms

$$\Delta b(t) = \left(\int_0^1 dr \left(b(t,r) - b_{\rm p}(t,r)\right)^2\right)^{\frac{1}{2}}, \tag{4.2.21}$$

$$\Delta f(t) = \left(\int_0^1 dr \left(f(t,r) - f_{\rm p}(t,r)\right)^2\right)^{\frac{1}{2}}, \tag{4.2.22}$$

where b_p and f_p are associated with the TPS.

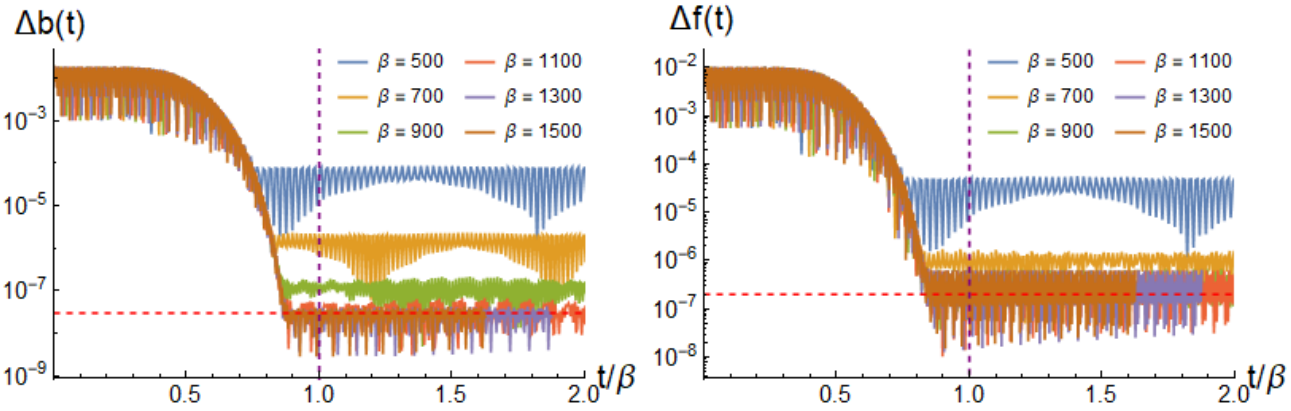

Figure 4.19: These plots show, through the functions (4.1.21)-(4.1.22), how the state after a quench accurately approaches the TPS (ρ_f, ω_f) with the duration of the process, β. The dashed purple line denotes the end of the quench, while the red one is placed at the level of the numerical noise of ϕ, f. We observe the saturation at this point. This particular example consists in the quench (A.2.5) connecting AdS $(\rho_i, \omega_i) = (0, 2.078)$ to $(\rho_f, \omega_f) = (10^{-3}, 2.078)$ for different values of β.

We will use the result that stable TPSs can be dynamically constructed to compensate for the difficulties of our code to construct TPSs with $\rho_t > 0.25$. Hence, through adiabatic quenches we can extend our study. This fact allows us to explore the environment of stable TPSs beyond the linear regime. For this purpose, we will consider a periodic drive of frequency ω, for which we will try to determine what is the maximum amplitude ρ that the system can support without undergoing gravitational collapse.

This search will be performed through adiabatic quenches in amplitude presented in (A.2.5). It starts from the static AdS soliton and slowly amplifies the amplitude ρ until a final value ρ_f leaving fixed the boundary frequency ω. In our numerical searches, β will be taken much larger than the period of the drive, e.g., $\beta = \mathcal{O}(10^3/\omega)$. In light of Fig. 4.19 the system should move along TPSs subject to instantaneous values $(\rho(t), \nu(t))$. Nevertheless, after reaching some amplitude, this adiabatic response might stop holding, and our task will be to map out when this occurs. For this purpose we will fix ω to a given value and take ρ_f large enough to ensure that the system undergoes gravitational collapse

at a given $\rho_{col} < \rho_f$. The reader can find an example of one such adiabatic quench in Fig. 4.20 and 4.21.

In Fig. 4.22 we explore the threshold for collapse. The blue area contains the TPSs that are accessible from the AdS soliton by the build-up protocol we have described. The blue line signals the loss of adiabaticity through a strong mixing with higher harmonics of the drive. This leads to a non-periodic and even chaotic response. Remarkably, the system does not undergo gravitational collapse and resists an increasingly intense drive until the red curve is crossed. The resonance wedges in this plot are in precise correspondence with the ones shown in yellow in Fig. 4.16.

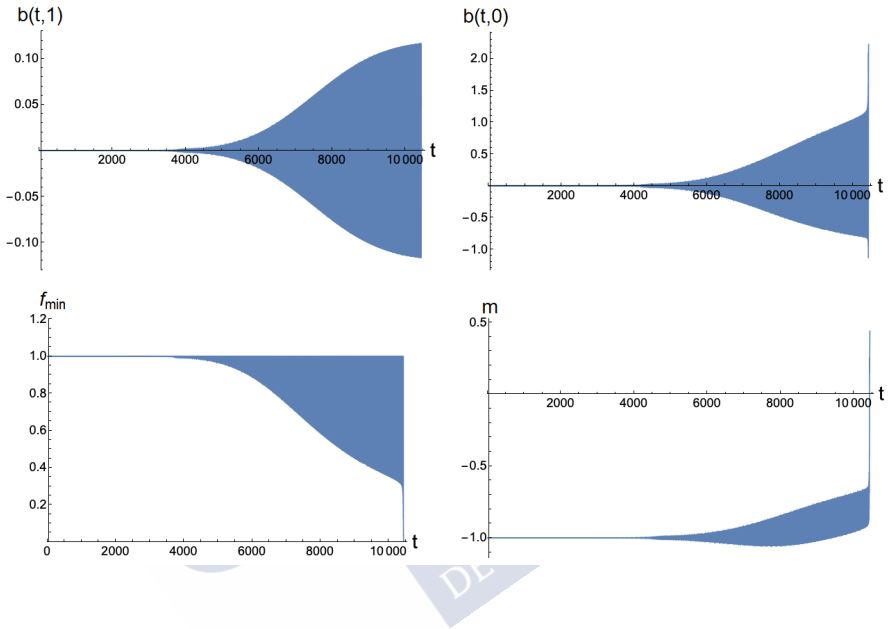

Figure 4.20: Numerical simulation of a adiabatic quench with $\omega = 1.6$ and time span $\beta = 1.5 \times 10^4$. In the upper two plots $b(t,1) = b_0(t)$ at the boundary and $b(t,0)$ at the tip are shown. The oscillations of frequency ω are so dense that they cannot be appreciated, only a blue area is observed. All magnitudes evolve adiabatically following a series of TPSs until a sharp threshold at $b_0(t_{col}) = 0.117$ is reached. There the instability sets in, as reflected in the sharp gain of net energy density m, and the formation of an apparent horizon, signalled by the function $\min_r f(t,r)$ approaching zero. The momentum constraint is satisfied to a part in 10^{-4} throughout the whole process.

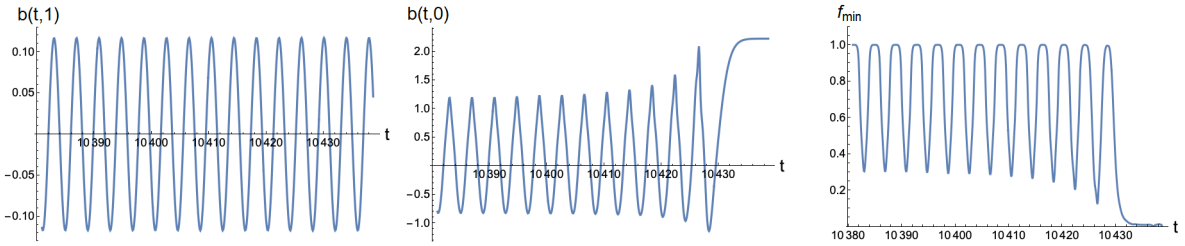

Figure 4.21: The same scenario depicted in Fig. 4.20, where the final part of the evolution is shown. The extreme slowness of the amplitude increase contrasts with the abruptness of the sudden collapse that occurs in a few oscillations. The anharmonicity of the oscillation, as well as the lack of symmetry $b \to -b$, can be seen in the plot of $b(t, 0)$ at the tip.

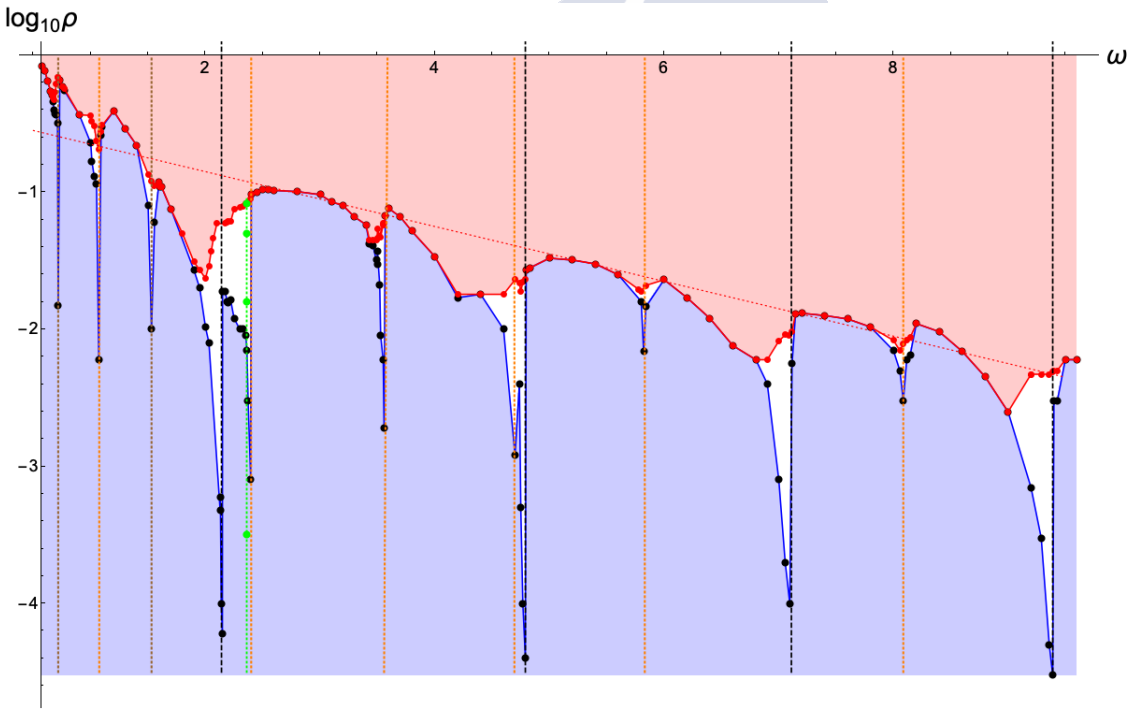

Figure 4.22: In blue, regions where TPSs are reached adiabatically from the AdS-soliton (at the bottom) by means of a slow build-up of the drive amplitude (vertical path). Traversing the blue curve the solution stops being a TPS. Points in the white region correspond either to multiperiodic or chaotic solutions. The vertical dashed lines indicate the frequencies of the linearized normal modes. Their halves, $\Omega_n/2$, are signalled by dotted vertical orange segments. In brown, $\Omega_0/3$ and $\Omega_1/3$ (see Fig. 4.16). In green, the build-up protocol shown in Fig. 4.23 with the snapshots in Fig. 4.25. The red dotted diagonal is a fit to the highest values and decreases as $\rho \sim 10^{-\omega/5}$.

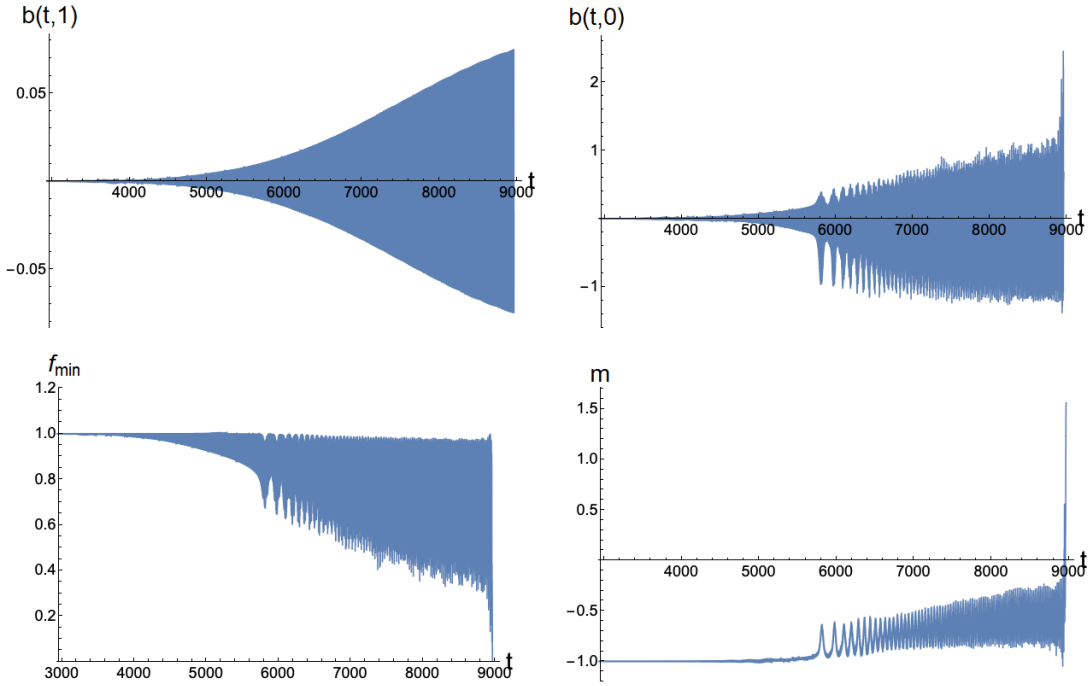

Figure 4.23: Numerical simulation of a adiabatic quench with $\omega = 2.375$ and a time span $\beta = 1.5 \times 10^4$ (see green dotted line in Fig. 4.22). All magnitudes evolve smoothly until an abrupt change is observed at $t \approx 5800$ with $b_0 \approx 0.013$. This transition signals the coupling to higher nonlinear modes. The momentum constraint is always satisfied within one part in 10^{-4}.

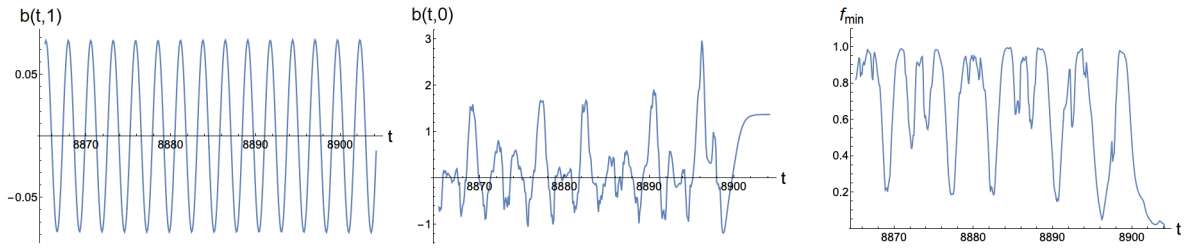

Figure 4.24: The same scenario depicted in Fig. 4.21, now for the protocol at $\omega = 2.375$ of Fig. 4.23. The evolution for $t > 8000$ becomes chaotic, as shown by the time evolution of the $b(t, z_0)$ at the tip.

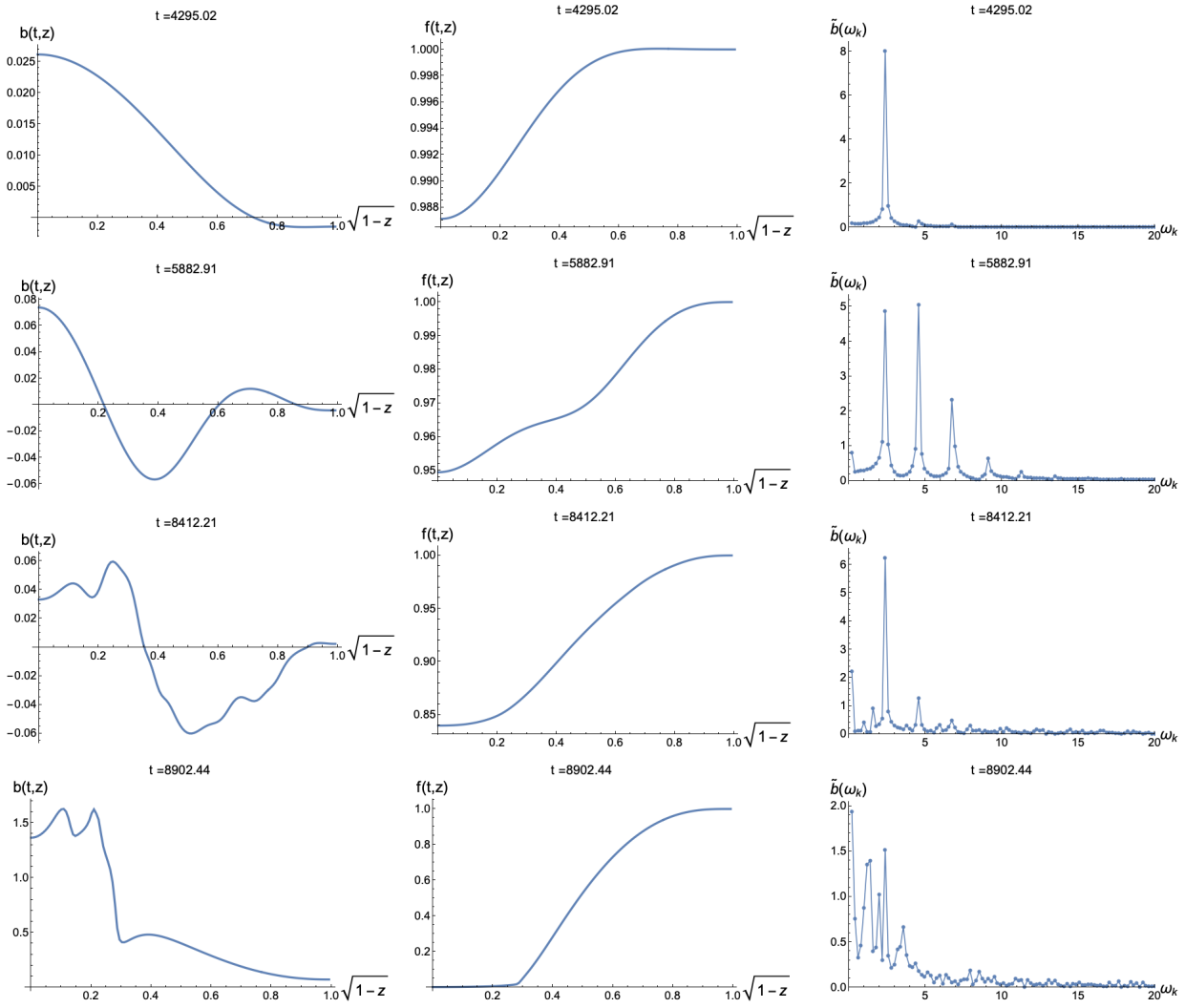

Figure 4.25: Four snapshots of the build-up protocol of Fig. 4.23 corresponding to $\omega = 2.375$ (see green dots in Fig. 4.22). The Fourier transform of $b(t, 0)$ at the tip, over a time span of $\Delta t = 400$, is shown on the right. The resonant coupling to the higher normal modes is apparent at $t = 8412$. For higher drive amplitudes a cascade towards higher frequencies is behind a wiggly, yet regular, profile for $b(t, r)$. Finally, the apparent horizon starts forming near $r = 0.3$ as seen in the last plot of $f(t, r)$.

In Fig. 4.23 we can see the evolution of several magnitudes as the amplitude ramps up from zero with $\omega = 2.375$ and crosses the blue line. When $\rho(t)$ reaches 0.013, the geometry shows a strong modulation, as illustrated by the behavior of b at the tip, $b(t, 0)$, and the minimum of the emblackening factor, $\min_r [f(t, r)]$. This is a clear signal of interference among two or more frequencies. In Fig. 4.24 we plot the time evolution of two interior points, the $b(t, 0)$ and $\min_r[f(t, r)]$, in the last time lapse before the collapse. As compared with the TPS case in Fig. 4.21, we see the interior evolution becoming chaotic. This, however, has been sustained without horizon formation since $t \sim 8000$ at least, [11] corresponding to a sizable window in the amplitude of the drive.

In order to make this statement more precise, we show four snapshots of the fields b and f in Fig. 4.25; to the right, we represent the Fourier transform of a sequence containing 400 seconds of the driving. In the first row, at $t = 4295$, i.e. for low amplitude, the TPS Fourier content is solely given by the drive frequency. At $t = 5882$ a clear resonant enhancement of the higher normal modes is observed. Indeed, normal modes $\Omega_2 = 4.790 \sim 2\omega$ and $\Omega_3 = 7.11 \sim 3\omega$ are natural higher harmonics of the drive frequency.[12] In the third row, at $t = 8412$, the dynamics looks again dominated by the (now more intense) driving. However it starts populating all frequencies, the shape becomes irregular, and the motion chaotic, as seen in Fig. 4.24. Finally, at $t = 8902$, an apparent horizon starts forming. Past this point, and since the external drive remains active, the system is expected to keep absorbing energy while the apparent horizon grows without bound. Following [107], a set of different regimes will take over as for the inexorable temperature growth of the quantum system.

4.2.6 Dynamical Construction of Unstable TPSs

In the previous section, we have focused on the dynamical construction of TPSs through quenches with a duration $\beta \gg 2\pi/\omega$, for which the amplitude of the drive increases very slowly toward its final value. This was motivated by the observation that, for such adiabatic quenches, the system responds adiabatically, passing through a succession of TPSs with the correct instantaneous boundary conditions $(\rho(t), \nu(t))$. Conversely, if we depart from this limit, the response of the system stops being adiabatic, and other time-dependent geometries are excited.

In section 4.1, the same situation was explored for a massless scalar field in global AdS_4. It was found that, for frequencies ω sufficiently close to the linear instability line, a remarkable phenomenon took place. Specifically, there existed a critical build-up time span, β_c, at which the system underwent a sharp transition between two radically different late-time regimes:

- For $\beta > \beta_c$, a horizonless solution with long-time pulsations decreasing the energy density was reached.

[11] By t we will hereafter implicitly imply the pure number t/z_0

[12] This situation bears a strong resemblance with the multioscillator solution in [206]. Here this solution lives *on top* of a sourced TPS, which triggers it resonantly at a concrete frequency and amplitude window.

- For $\beta < \beta_c$, gravitational collapse took place.

The most surprising aspect of this transition is that as $|\beta - \beta_c| \to 0$ (and at times $t > \beta$), the system spent a progressively longer time around an intermediate attractor, which turned out to be nothing but the linearly unstable TPS associated with the final driving. This observation allowed us to identify this transition as a type I critical phenomenon in gravitational collapse [22].

The purpose of this section is to demonstrate that this phenomenon is also present for the current setup. We will discuss two transitions in detail: one between two different kinds of pulsating phases, another between a pulsating phase and a collapsing geometry.[13] The averaged mass per period,

$$\langle m \rangle_T (t) \equiv \frac{1}{T} \int_{t-\frac{T}{2}}^{t+\frac{T}{2}} dt' m(t'), \tag{4.2.23}$$

will be a central quantity in our analysis.

For the first case, we consider a family of quenches that interpolate between the AdS-soliton vacuum at $t = 0$ and a drive amplitude $\rho_f = 0.001$ at $t = \beta$ at fixed frequency $\omega = 2.11$. The path followed by $\rho(t)$ is showed in the left plot of Fig. 4.10 (see (A.2.5) in appendix A.2 for further details). As Fig. 4.26 (right) shows, for $\beta > \beta_c$ the system flows to a pulsating phase whose trademark property is having an averaged energy density per period $\langle m \rangle_T$ that, as $\beta \to \beta_c^+$, develops extended plateaux separated by fast downward beats. On the other hand, as illustrated in Fig. 4.26 (left), for $\beta \to \beta_c^-$ the pulsating phase is characterized by a $\langle m \rangle_T$ that has the same plateau value, but starts beating upward.[14]

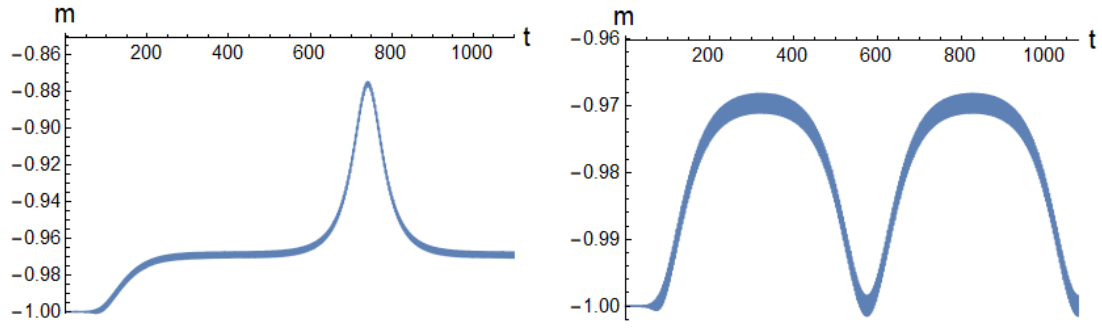

Figure 4.26: Left: For $\beta = 142.4 < \beta_c$, we obtain a pulsating phase that beats upward. Right: for $\beta = 142.7 > \beta_c$, we obtain a pulsating phase that beats downward.

[13] The simulations to be discussed next have been performed on a grid with $\Delta r = 2^{11} + 1$ points.

[14] It turns out that, as $\beta \to \beta_c^-$, the system goes from a pulsating phase that beat alternative upward and downward to pulsations that only beat upward. Fig. 4.26 shows an example only of the latter situation.

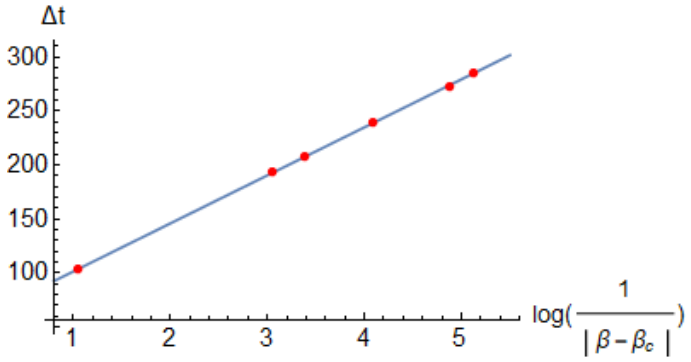

Figure 4.27: Scaling of the exponential deviation from the plateau displayed between $250 < t < 500$ in Fig. 4.28. Red points correspond to data obtained from quenches for $\beta < \beta_c$ while the solid line was obtained with a linear fit of these data.

If the transition between the two kinds of pulsating phases we have found is to be interpreted as a type I critical phenomenon, the following relation must hold

$$\Delta t = -\frac{\gamma}{\lambda} \log |\beta - \beta_c| + a, \tag{4.2.24}$$

where Δt is the permanence time around the unstable TPS, λ is the norm of the purely imaginary eigenfrequency of this TPS, and $a \in \mathbb{R}$. The permanence time Δt is best thought of as the length of the plateau; however, note that a shift in Δt can be compensated by a change in a, leaving the values of β_c and λ invariant. This implies that, strictly speaking, there is no preferred definition of Δt: any two choices related by a shift are equivalent at the level of extracting β_c and λ. Taking advantage of this freedom, for simplicity we define Δt as follows.[15] First, for build-up processes that end in a pulsating phase that starts beating upward, we define Δt as the smallest time at which $\langle m \rangle_T$ equals a particular predefined value m_0 above the plateau. In this example, we have chosen $m_0 = -0.95$. On the other hand, for build-up processes that end in a pulsating phase that beats downward, we define Δt as the time at which $\langle m \rangle_T$ reaches its first minimum after the build-up phase.

In Fig. 4.27 we observe that the relationship (4.2.24) is satisfied, we get that[16]

$$\beta_c = 142.4117, \qquad \lambda/\gamma = 0.0225. \tag{4.2.25}$$

The determination of λ and γ requires the determination of one of these parameters by a different method. Unfortunately, in this case our spectral code to obtain TPSs, their linear modes and their Floquet exponents λ_n, did not reach the unstable TPS associated with $(\rho, \omega) = (10^{-3}, 2.11)$. Nevertheless, the natural expectation is that $\gamma = 1$ and then, the Floquet exponent of the exponentially growing linear mode is presumably: $\lambda_0 = 0.0225$.

[15] We have checked that other possible definitions lead to compatible results.

[16] A word of caution is in order. While it can be argued that the value of λ obtained by this procedure is resolution-independent, this is not the case for β_c. A precise determination of β_c requires us to take the double scaling limit $\beta - \beta_c \to 0$, $N_r \to \infty$, where N_r is the number of discretization points.

For our second example, we set the boundary frequency to $\omega = 2$ and the final amplitude to $\rho_f = 0.0114$. In this case, the system transitions from a collapsing geometry to a pulsating phase as β crosses β_c from below. Relevant examples of such solutions are plotted in Fig. 4.28. Again, for $\beta \to \beta_c^{\pm}$, the length of the initial plateau gets progressively longer (see Fig. 4.29). Repeating the fitting procedure described before, we get that

$$\beta_c = 294.9735, \qquad \lambda/\gamma = 0.04535. \tag{4.2.26}$$

These values were obtained from $\beta > \beta_c$ and $\beta < \beta_c$, showing the robustness of the process. Again, the values of λ and γ cannot be obtained because our spectral code did not reach such TPS.

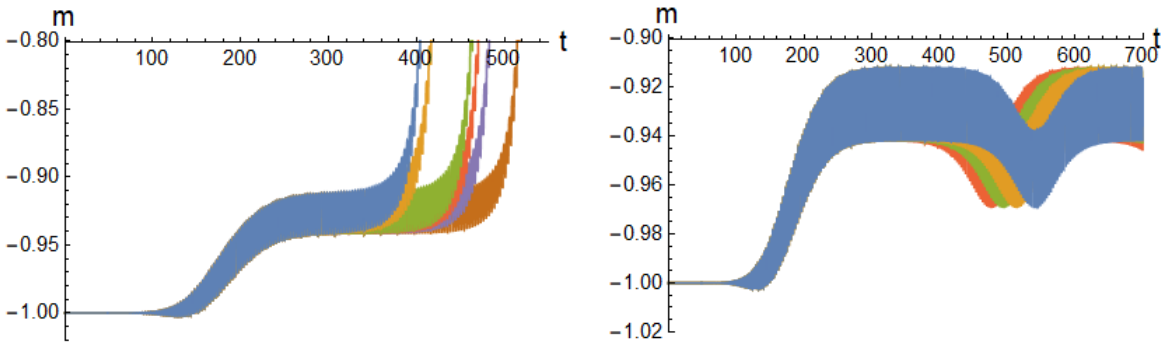

Figure 4.28: Both plots show the quench in amplitude from the AdS soliton $(\rho_i, \omega_i) = (0, 2)$ to $(\rho_f, \omega_f) = (0.0114, 2)$. The plot on the left contains quenches with duration $\beta < \beta_c$ and the plot on the right quenches with $\beta > \beta_c$. In this case $\beta_c \approx 294.9735$. The duration of quenches in the left plot are from left to right: $\beta = 294.5,\ 294.7,\ 294.94,\ 294.95,\ 294.96,\ 294.9705$. On the right one again from left to right: $\beta = 294.9755,\ 294.9805,\ 294.9905,\ 295.0105$.

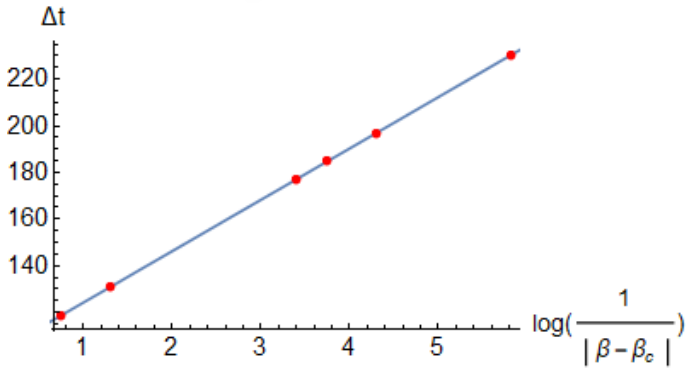

Figure 4.29: Scaling of the exponential deviation from the plateau displayed between $250 < t < 350$ in Fig. 4.28. Red points correspond to data obtained from quenches for $\beta < \beta_c$ while the solid line was obtained with a linear fit of these data.

4.2.7 Summary

In this section we have studied pure gravitational fluctuations of the AdS soliton geometry under the action of the harmonic boundary conditions

$$b(t,1) = \rho\cos(\omega t). \tag{4.2.27}$$

We have followed a line of reasoning similar to that of section 4.1. First, making use of the techniques displayed in section 2.3, we constructed TPSs. These solutions formed a surface in a 3-dimensional space consisting of the frequency ω, amplitude ρ and the value $\rho_t = b(0, r = 0)$. After that, we targeted the issue of the linear stability of these TPSs. For this purpose we used the method developed in section 2.3.2.2. Specifically, it determined the first linear modes and their Floquet exponent. The information gathered until this point was suitably summarized in Fig. 4.16. In this figure the different regions of linearly stable and unstable TPSs were presented, as well as, regions where the spectrum of TPSs resonates with linear modes of the AdS soliton with $\rho = 0$. The linearly unstable TPSs reached by our codes were characterized by having a single exponentially growing mode, while the other modes remained bounded. Therefore in order to explore these instabilities, we constructed initial data consisting of the TPS with a small addition or subtraction of the unstable mode (4.2.20). In this situation, our codes almost did not reach TPSs with $\rho_t > 0.25$. It restricted our study to relatively weak drives; therefore, we only found instabilities developing pulsations which increased (decreased) the energy density for the addition (subtraction) of the unstable linear mode (Fig. 4.18). Nevertheless, using fast quenches we obtained strong evidence that for higher amplitudes of the drive, this instability leads the system to a gravitational collapse.

Once TPSs were constructed and their liner stability determined we studied the synchronization properties of the system under slow variation in the boundary parameters (ρ, ω). For a long duration of the process $(2\pi/\max_t[\nu(t)] \ll \beta)$ we found that the system modifies its state to the TPS associated with instantaneous values $(\rho(t), \nu(t))$, Fig. 4.19. Specifically, we have obtained a protocol to dynamically construct stable TPSs from the AdS soliton. We made use of this result to compensate for the limitations of our codes for the construction of TPSs. Therefore the region beyond $\rho_t > 0.25$ was mainly explored through adiabatic quenches. Additionally, this result was also used to explore the environment of TPSs. Specifically we tested the response of the system when we perform an adiabatic quench in amplitude $\rho(t)$, leaving the frequency ω fixed, which after some time its instantaneous values $(\rho(t), \omega)$ do not have a TPS associated. Following this protocol we constructed Fig. 4.22, a map (ω, ρ) delimiting regions with a different dynamics. There we found TPSs, gravitational collapse Fig. 4.21 and a disordered phase Fig. 4.24. This last state was found around frequencies ω for which the spectrum of TPSs resonates with linear modes with homogeneous boundary conditions, showing agreement with yellow areas in Fig. 4.16.

Finally we explored a faster variation of the boundary parameters $(2\pi/\max_t[\nu(t)] < \beta)$ in order to clarify if unstable TPSs behave as attractors for $|\beta_c - \beta| \to 0$. In this case we fixed the frequency and only the amplitude evolved from zero to ρ_f. This phenomenon

was confirmed with two examples: $\rho = 0.001$, $\omega = 2.11$ and $\rho = 0.0114$, $\omega = 2$. A critical value of the duration of the quench, β_c, existed such that if the quantity $(\beta_c - \beta)$ is small enough the state of the system after the quench is an unstable TPS associated with (ρ_f, ω) and perturbed by its exponentially growing linear mode with an amplitude proportional to $(\beta_c - \beta)$. In consequence, we also obtained a protocol to dynamically construct unstable TPSs.

5

Summary and Outlook

5.1 Summary

This thesis studies the long-time dynamics of 1+1-dimensional resonant systems. Specifically, we have focused our effort on the weakly nonlinear regime, where resonances become relevant. In this limit the dynamics is mainly governed by the linearized equation, and the nonlinearities have minor contributions. This picture is preserved by the majority of systems; nevertheless, resonances provide a slow and efficient exchange of energy between modes. In consequence, the behavior of the system can be drastically modified by waiting long enough. In this last situation, standard perturbation techniques are not able to properly capture slow modifications coming from the exchange of energy through the resonant channels. Improved perturbative methods exist, that allow to go beyond this limitation. The main methods are: multi-scale and averaging. In particular, they allow the derivation of an effective system of equations which governs the long-time evolution of the system.

In chapter 3 we have considered systems with a resonant spectrum and cubic nonlinearities, which when not zero, are the dominant ones in the weakly nonlinear limit and higher terms can be neglected. Particularly, we restricted our study to systems for which the long-time dynamics is governed by the resonant equation of the form

$$i\frac{d\alpha_n}{d\tau} = \sum_{m=0}^{\infty}\sum_{k=0}^{n+m} C_{nmk(n+m-k)}\alpha_k\alpha_{n+m-k}\bar{\alpha}_m. \tag{5.1.1}$$

In this equation, τ is a long-time scale, related to the original time, through $\tau = \epsilon\, t$, where ϵ sets the scale of the nonlinear deformation. The quantities $|\alpha_n|^2$ denote the energy carried

by each mode and the interaction coefficients C_{nmkl} contain all the information about the original system. The structure of this system consists of infinite equations with infinite triads of modes contributing to each of these equations. Despite the complication of this system, we have found a set of constraints among the interaction coefficients, such that for each solution we can find an analytic subsector of solutions for (5.1.1).

One of these sets of constraints was deeply studied in section 3.1.1. In this case the resonant system admitted analytic solutions belonging to the three-dimensional manifold

$$\alpha_n(\tau) = f_n(b(\tau) + na(\tau))p(\tau)^n, \tag{5.1.2}$$

depending upon three independent functions. We also found that for these solutions the energy per mode displays periodic exact returns to the initial configuration (Proposition 3.1.1.1) and the absence of turbulent behaviors in this sector (Proposition 3.1.1.3). For another family of interaction coefficients, the accessible analytic solutions consisted of stationary states, $|\alpha_n|^2 = \text{cte}$, (Proposition 3.1.5.2).

We have furthermore explored the stronger condition $\mathcal{D}_{nmkl} = 0$, on the interaction coefficients. This condition was simple enough to analyze it in full generality and obtain solutions for the interaction coefficients in terms of their generating functions, given in Propositions 3.1.3.1 and 3.1.3.2. These expressions allowed the development of the complex plane representation of the resonant system, as well as the development of salient results. At the end of the day, we know that any resonant system of the form (5.1.1) satisfying $\mathcal{D}_{nmkl} = 0$ enjoys the following properties

- The ansatz $\alpha_n = f_n(b + na)p^n$ forms a three-dimensional manifold of solutions for the resonant system.
- For these solutions $|\alpha_n|^2$ are periodic, displaying exactly periodic energy returns.
- We cannot fine-tune the initial values of b, a, p, in order to arbitrarily transfer energy to higher modes (as is the case of Cubic Szegö).
- The resonant system has an additional conserved quantity.
- There is a uniparametric family of stationary solutions ($|\alpha_n(\tau)|^2 = \text{cte}$) bifurcating from each single-mode solution.
- The interaction coefficients have a generating function described by the general solution of $\mathcal{D}_{nmkl} = 0$ given in Propositions 3.1.3.1 or 3.1.3.2.

After the construction of families of interaction coefficients admitting analytic solutions, we have developed a specific limit for the (almost) general set of C_{nmkl}, where the resonant system (5.1.1) is significantly simplified. It consisted of assuming a spectrum dominated by a single-mode and an exponential suppression of the other modes in proportion to their "distance" from the dominant mode. This limit was denominated *strong localization limit* (SLL). At leading order this analysis allowed an iterative resolution of the relevant

subsector of (5.1.1). Specifically, we have developed the cases where the dominant mode is one of the two lowest modes.

In the second part of chapter 3, we presented a large number of models displaying a resonant system of the form (5.1.1). In particular we have seen that an important group of them belong to the class defined by $\mathcal{D}_{nmkl} = 0$, showing that this condition is not empty of physical systems. Even more, it contains certain models of a scalar field in different geometries or even Bose-Einstein condensates in a harmonic trap. For this last group of models, the results coming from the condition $\mathcal{D}_{nmkl} = 0$ led to the determination of slowly evolving vortices.

In addition to the systems satisfying $\mathcal{D}_{nmkl} = 0$, we have also introduced other resonant models. In this case we must highlight the case of a free spherically symmetric massless scalar field in AdS_4. The long-time dynamics of this model is also effectively governed by a resonant system of the form (5.1.1). In particular, we have revisited the issue of energy returns to the initial configuration for two-mode initial data

$$|\alpha_0(0)|, |\alpha_1(0)| \neq 0, \qquad \alpha_{n\geq 2}(0) = 0. \tag{5.1.3}$$

Having performed numerical simulations with much higher precision than what has been previously seen in the literature, we have observed returns of striking accuracies. The numerics also provided indications, however, that the small imperfections we see cannot be purely due to numerical artifacts. To elucidate the situation, we have performed an analytic study through the SLL of solutions dominated by one of the two lowest modes and proved that the accurate returns we have observed numerically are inexact in this limit dominated by one of the two modes. In contrast with the scenario observed for the models satisfying $\mathcal{D}_{nmkl} = 0$. Nevertheless, our analytic investigations of the SLL have generated a neat picture of returning behaviors for initial data sufficiently close to mode 0 or mode 1, and allowed for the identification of specific multiple oscillation periods after which enhanced returns occur. A relevant improvement in this direction was obtained with the discovery of rational relations between the interaction coefficients in global AdS_4. In combination with Proposition 3.2.1.1, it results in hierarchies of returns, with specific longer waiting times resulting in returns of better and better accuracy.

Trying to reach a deeper understanding of the slight imperfect returns, we have explored the vicinity of the original model in the context of our analytic treatment of solutions dominated by mode 1. We have observed that the mass of the scalar is a free parameter in the interaction coefficients; therefore adjusting it, it is possible to slightly improve the precision of returns for initial data near mode 1. Nevertheless, the scenario still falls short of providing exact returns. We also note that the nonrelativistic version of the AdS_5 dynamics, presented in section 3.3.5, (which technically corresponds to the limit of infinite scalar field mass) satisfies $\mathcal{D}_{nmkl} = 0$. In consequence, it displays perfect returns in AdS_5, rather than in AdS_4 (returns in AdS_5 at finite masses, on the other hand, are not close to being perfect).

In chapter 4, we have addressed the issue of time-periodic boundary conditions. We started by considering the same massless scalar in global AdS_4; but in this case subject

to harmonic boundary conditions of the form

$$\phi(t, \pi/2) = \rho \cos \omega t. \tag{5.1.4}$$

We started by constructing time-periodic solutions (TPSs) as extensions of the linear modes of the problem to the nonlinear regime. These solutions were a nontrivial result in the sense that they require perfect synchronization between the scalar field, the fluctuations of the metric and the boundary conditions, in a setup where the system can arbitrarily absorb energy. Once these objects were determined for an extensive range of values of ρ and ω, we addressed the issue of their linear stability. Making use of Floquet theory the phase-diagram of TPSs was constructed and regions of linear stability delimited. These results showed an excellent agreement with numerical simulations.

Crossing the line of linear stability, the natural question to ask is what is the end point of the unstable dynamics. The inspection of these instabilities was done through controlled perturbations of linearly unstable TPSs. Our findings show that generically three types of behavior can appear. Two of them can be reached from the same unstable TPS after perturbing with the leading unstable mode. The selection of one or the other only just depends upon the sign with which the fluctuation is added. In one of this states the geometry remains regular and the evolution resembles that of a TPS that develops a sequence of sharply peaked modulations at times longer than the period of the TPS. In the other, the geometry develops an apparent horizon and the scalar field vanishes outside it. This end state is a Schwarzschild AdS black hole. For unstable TPSs close enough to the region of stability, instead of a gravitational collapse we observe a pulsating phase similar to the previous one, but the peaks appear in the opposite direction. These behaviors have been observed for TPSs belonging to the same regions. The third possible end state is associated with a different region of unstable TPSs. In this case, the evolution is independent of the sign of the perturbation. After some time, modes with high frequency are excited and the evolution in the bulk becomes disordered. Any similarity with the original TPS is completely lost.

Once we acquired control over the harmonic boundary conditions (5.1.4), we explored the synchronization properties of the systems. For this purpose a long-time dependence was introduced in the drive. In particular, we studied the response of a TPS when the amplitude ρ and/or the frequency ω of the boundary conditions are slowly modified until reaching certain values. This study showed that if this long-time evolution is slow enough and for each intermediate values of the parameters there is a stable TPSs associated, then the final state is the TPSs parametrized by the final values of the amplitude and frequency. Therefore, this mechanism allows the dynamical construction of stable TPSs starting from the static metric of AdS_4. Remarkably, we have been able to use this method to build TPSs with homogeneous boundary conditions ($\rho = 0$) starting from pure AdS. The protocol involves not only a modulation in amplitude but also in frequency.

After that, we have inspected the response of TPSs when the evolutions of ρ and ω, from the initial to the final values, have a short and an intermediate duration β (in relation with the period of the TPS). The first situation did not report interesting phenomenology, in contrast with the second one, where we found unstable attractors consisting of unstable

TPSs. In this case, a critical value of β exists, for which $|\beta - \beta_c| \ll 1$ acts as the amplitude of the perturbation of these solutions, displaying the different phases if $(\beta - \beta_c)$ is positive or negative. In consequence, we have also obtained a dynamical protocol to construct certain unstable TPSs; nevertheless, not all of them were reached through this process.

In the second part of chapter 4, in order to elucidate if the phenomenology we have obtained until this point is related to particularities of global AdS, which enjoys certain uncommon properties as a fully resonant spectrum, we have investigated the driven version of the AdS_4 soliton. The time-dependent boundary conditions for the metric mimic the homogeneous strain caused by the passage of a gravitational wave in the direction perpendicular to the holographic directions. The absence of spherical symmetry allows the metric in the bulk to enjoy a nontrivial dynamics. Moreover the spectrum of linearized normal modes is not resonant in this case. We wanted to know what impact these modifications with respect to the previous case would entail on the effective long-time solutions.

Despite these differences we have found strong similarities with the scalar field in global AdS_4. In this case we also constructed TPSs and the phase-diagram, delimiting the regions of linear stability. The inspection of the end states of these instabilities also led to pulsating phases or gravitational collapse. The dynamical constructions of stable and unstable TPSs through quenches were also present. Nevertheless, taking advantage of our understanding of the case of the scalar field, we have broadened the study. In particular, we noticed the presence of regions where the structure of TPSs resonate with the linear modes (with $\rho = 0$) of the problem. In these cases TPSs were not found, and the adiabatic quenches targeting these solutions evolved to a disordered phase. This mechanism of resonances is also expected to be present in the case of the scalar field in AdS_4.

The similarities between the results obtained for both models report confidence that this phenomenology is also present in other setups. Additional models should be considered to clarify which of these properties are common for holographic periodically driven systems.

5.2 Outlook

As in any research, the results obtained in this thesis also open a number of questions which are left for the future.

- **The resonant system:**

  1. Is it possible to decode the information contained in the interaction coefficients? In a sense the effective system involves the averaging of the dynamics of a given physical model, thereby erasing some detailed structure. Is there a way to find at least one representative?
  2. What is the physical interpretation of the constraint $\mathcal{D}_{mnkl} = 0$?. How is this

relation manifested in the original system? What degrees of freedom are left unfixed by this constraint?

3. Are there other families of effective models with analytic properties similar to or more general than the $\mathcal{D}_{nmkl} = 0$ class?
4. What properties associated with $\mathcal{D}_{nmkl} = 0$ are also present for higher order resonant systems?

- **Instability of AdS:**

1. How generic is the scenario of energy returns that we have unveiled? Does it go through intact to other dimensions and/or masses of the scalar?
2. In view of the AdS/CFT correspondence, is there a way to relate energy returns with cyclic phenomena predicted for a CFT? Some of these phenomena include quantum revivals [207] as well as exact oscillations [208]. It would be very interesting to delineate this class of systems more precisely, and build explicit connections to the sort of dynamics we have described in this thesis.

- **Holographic Floquet systems:**

1. In order to clarify whether the features of our systems are "universal", going beyond the simplest matter content is a must. In particular adding Maxwell fields would make this study relevant in the context of phenomenological models used in AdS/CMT (Condensed Matter Theory). While we do not expect the gross picture to be different, the fine details may be interesting, as now there are more final states available, like for example hairy black holes. Also the possibility to rotate or drive the Maxwell field brings this study closer to real experiments performed in laboratories.
2. The observed synchronization of the bulk dynamics with a slow change of the drive, points towards a sort of adiabatic theorem being at work. A deep theoretical understanding of this (numerically) experimental fact would be very illuminating.
3. Turning the periodic drive from functional data into a real dynamical field from the boundary perspective is a fascinating challenge. In some contexts this has been termed semi-holography, but very few results have been reported so far [209].

6

Resumen

La dinámica de un sistema puede cambiar drásticamente por el mero hecho de que este se encuentre en un dominio acotado. Esto se debe a que en un dominio infinito, si las interacciones son suficientemente pequeñas, cualquier pequeña perturbación puede dispersarse sin producir efectos relevantes. En el caso de un dominio acotado esta imagen cambia completamente. La misma perturbación se dispersa sin producir un efecto significativo, sin embargo, al encontrarse sobre un dominio de tamaño finito, esta vuelve a concentrarse para interaccionar una segunda vez. Este mecanismo se repite continuamente, y a pesar de que en cada ocasión los efectos de la perturbación son mínimos, tras un gran número de repeticiones estos efectos terminan por ser considerables. De esta forma la dinámica principal del sistema puede llegar a cambiar drásticamente, llegando en algunos casos a producir una divergencia en tiempo finito. Si reducimos la cantidad de energía dentro de nuestro sistema, los efectos no lineales, que son los responsables de la deformación del sistema, pueden reducirse también. En la mayoría de situaciones, si la cantidad de energía es suficientemente baja, el mecanismo que hemos descrito anteriormente pierde eficiencia y el sistema no se ve significativamente deformado. Sin embargo, existen ciertos sistemas que presentan resonancias, las cuales proporcionan canales de interacción que no se ven anulados por la reducción de la energía en el sistema. Estos permiten un intercambio eficiente de energía entre los modos fundamentales del sistema y con ellos su deformación a largos tiempos. En estos casos la reducción de energía retrasa, pero no previene, la inevitable deformación de la dinámica dentro de nuestro dominio.

Esta imagen es común en muchas situaciones físicas, y por tanto podríamos motivar nuestro interés de diversas formas. Sin embargo, nuestra motivación particular viene del estudio de la estabilidad del espacio-tiempo de Minkowski y de anti-de Sitter. El primero es infinito y cualquier señal dispersada lo suficientemente rápido no vuelve a

concentrarse. De esta forma se garantiza que para cantidades de energía suficientemente bajas no se produce un colapso del contenido del espacio para formar un agujero negro. Sin embargo, este argumento no se puede aplicar en presencia de grandes cantidades de energía, donde se ha demostrado que la formación de un agujero negro es posible. En cambio, en el segundo caso, a pesar de ser también infinito, las señales dispersadas tardan un tiempo finito en alcanzar el infinito espacial y volver a concentrarse. Por tanto, de forma efectiva podemos entender este espacio-tiempo como un sistema encerrado en un dominio acotado. De este modo, favorecido por las resonancias de este sistema, aunque reduzcamos la cantidad de energía dentro del espacio-tiempo de anti-de Sitter, el colapso a un agujero negro puede terminar por suceder para tiempos suficientemente largos. En la última década se ha dedicado mucho esfuerzo por parte de la comunidad (principalmente motivado por la correspondencia AdS/CFT) para entender la dinámica en anti-de Sitter. En particular, se ha intentado comprender si la formación de un agujero negro sucede incluso para cantidades arbitrariamente pequeñas de energía. A pesar de las grandes evidencias que se han conseguido durante la última década (principalmente numéricas), esto es por el momento una pregunta abierta. Cierto es que hemos conseguido grandes avances en esta dirección, y con ello se han desarrollado interesantes formas de atacar este tipo de problemas, pero la respuesta rigurosa e inequívoca permanece por el momento fuera de nuestro alcance.

Esta gran diferencia en la dinámica de los espacio-tiempo de Minkowski y de anti-de Sitter, que es presumiblemente debida a la presencia de una frontera y resonancias en el segundo de los casos, nos ha motivado a intentar entender mejor el papel que juegan estos dos ingredientes.

Esta tesis estudia la dinámica a largos tiempos de ecuaciones en derivadas parciales resonantes. Concretamente nos hemos centrado en el límite de no linealidades débiles de estos sistemas. Este límite nos proporciona condiciones excelentes en las que trabajar. La dinámica es principalmente gobernada por la ecuación linealizada del sistema, la cual en la mayoría de los casos se puede resolver de forma analítica, mientras que los efectos de las no linealidades pueden ser considerados como simples perturbaciones de la dinámica principal. Esto proporciona el punto de partida de nuestro estudio. Debido a las resonancias que presentan nuestros sistema, hemos aplicado una serie de métodos perturbativos que permiten el desarrollo de un sistema de ecuaciones que describen con precisión los efectos no lineales a largos tiempos. Este conjunto de ecuaciones se conoce como *sistema resonante*, y será uno de los objetos centrales en nuestro estudio. Específicamente, el capítulo 3 está dedicado a ecuaciones en derivadas parciales resonantes con términos no lineales cúbicos que muestran un sistema resonante de la forma

$$i\frac{d\alpha_n}{d\tau} = \sum_{m=0}^{\infty}\sum_{k=0}^{n+m} C_{nmk(n+m-k)}\alpha_k\alpha_{n+m-k}\bar{\alpha}_m. \tag{6.0.1}$$

Donde τ representa el tiempo, α_n son números complejos con $n = 0, 1, 2, \ldots$ hasta infinito y los C_{nmkl} se denominan coeficientes de interacción. Las cantidades $|\alpha_n|^2$ representan la energía contenida en cada modo del sistema; por tanto, esta ecuación gobierna la transferencia de energía de unos modos a otros. Este tipo de sistemas de ecuaciones presentan la

propiedad de que toda la información del modelo original, a partir del cual fue derivado, está contenida en los coeficientes de interacción C_{nmkl}. Esta propiedad es extremadamente tentadora; estudiando los coeficientes de interacción de la forma más general posible, podemos adquirir resultados con aplicación en un amplio abanico de ramas de la física y las matemáticas. Por tanto, nuestro propósito consiste en imponer restricciones sobre los coeficientes de interacción de la forma más débil posible para mantener la generalidad, pero suficientemente fuertes como para que podamos extraer información del sistema resonante (6.0.1) de forma analítica. Esto a priori no es una tarea sencilla; el sistema resonante está constituido por infinitas ecuaciones, una para cada variable, que a su vez presentan infinitos acoplamientos entre modos. Veremos que el tratamiento analítico de (6.0.1) requiere que los coeficientes de interacción satisfagan ciertas propiedades.

Siguiendo esta estrategia hemos conseguido caracterizar dos grandes familias de sistemas resonantes que admiten ciertas soluciones analíticas. La primera de las familias presenta soluciones analíticas de la forma

$$\alpha_n(\tau) = f_n(b(\tau) + na(\tau))p(\tau)^n, \tag{6.0.2}$$

donde a, b, p son tres funciones complejas del tiempo y f_n es una función real del número del modo, n. De esta forma reducimos el problema a tres ecuaciones diferenciales ordinarias para a, b, p. Las soluciones de este sistema reducido presentan la propiedad particular de que la energía transferida entre modos se comporta de forma periódica, volviendo a la distribución inicial de energía tras cada período; es decir, las funciones $|\alpha_n|^2$ son periódicas. En cambio, la segunda familia presenta soluciones de la forma

$$\alpha_n(\tau) = f_n b(\tau)p(\tau)^n, \tag{6.0.3}$$

las cuales no presentan intercambio de energía entre modos, ya que $|\alpha_n|^2$ son funciones constantes del tiempo (denominadas soluciones estacionarias).

Tras delimitar estas dos familias nos hemos centrado en la primera, ya que presenta propiedades más interesantes. Manteniéndonos dentro de la misma familia, pero imponiendo una restricción más fuerte sobre los coeficientes de interacción, a mayores de los resultados ya conocidos hemos conseguido nuevos resultados analíticos dentro de esta subfamilia. Por ejemplo, una nueva cantidad conservada por la dinámica del sistema resonante, familias de soluciones estacionarias emergiendo desde soluciones consistentes en un único modo, y por último una forma de construir todos los coeficientes de interacción que pertenecen a esta subfamilia.

Una vez obtenidos estos resultados, y comprendiendo que, a pesar de ser familias grandes de sistemas resonantes, estos no constituyen la norma general; hemos decidido desarrollar cierto límite en el que extraer información de (6.0.1) de forma analítica, para casi cualquier conjunto de coeficientes de interacción C_{nmkl}. Este límite lo hemos denominado límite de fuerte localización (SLL por sus siglas en ingles). Consiste en suponer un espectro dominado por un único modo, donde los otros modos están suprimidos de forma exponencial en función de la "distancia" al modo dominante. Esta suposición simplifica (6.0.1) de forma que permite una resolución iterativa empezando por el modo dominante.

Concretamente, en esta tesis hemos desarrollado los casos de los dos modos más bajos, para su posterior aplicación en los modelos particulares que vamos a estudiar.

Tras desarrollar estos resultados, manteniendo un alto grado de generalidad, introduciremos un gran número de modelos particulares provenientes de sistemas físicos y matemáticos, los cuales presentan sistemas resonantes de la forma (6.0.1) que serán estudiados por medio de las técnicas que hemos obtenido. La mayoría de estos modelos consisten en campos escalares sobre diferentes geometrías, como d-esferas o anti-de Sitter en diferentes dimensiones. También consideraremos sistemas que se pueden estudiar en un laboratorio, como condensados de Bose-Einstein en presencia del potencial armónico. Incluso mostraremos un caso puramente matemático como el obtenido por medio de fijar todos los coeficientes de interacción a uno, $C_{nmkl} = 1$. Mostraremos que gran parte de estos modelos pertenecen a las familias de sistemas resonantes que hemos construido, y por tanto disfrutan de todas las propiedades que hemos obtenido para ellas. En el caso de modelos que no pertenecen a ninguna de las familias obtenidas, estos serán estudiados por medio del SLL, ya que tiene una validez mucho mayor.

Un caso concreto y de especial relevancia que consideraremos es un escalar esféricamente simétrico sin masa en AdS_4. Centrándonos en condiciones iniciales con la energía únicamente distribuida entre los dos modos más bajos,

$$|\alpha_0(0)| \neq 0, \quad |\alpha_1(0)| \neq 0, \qquad |\alpha_{n\geq 2}(0)| = 0, \tag{6.0.4}$$

mostraremos que si la energía está concentrada cerca de uno de estos dos modos, este sistema presenta retornos de energía a la configuración inicial casi perfectos. Por otro lado, también veremos que estos retornos se pueden hacer cada vez más precisos cuanto más concentremos la energía entorno al modo más bajo y esperemos un tiempo suficientemente largo. Nuestro estudio por medio del SLL, confirma de forma analítica las evidencias numéricas que se habían presentado previamente en otros trabajos. Hemos aportado un nivel de rigurosidad que nos permite relacionar este fenómeno con la paradoja Fermi-Pasta-Ulam-Tsingou [61]. Los retornos de energía casi perfectos nos han llevado a explorar sistemas cercanos a este, en busca de retornos exactamente periódicos. En concreto hemos introducido la masa del escalar, que es un parámetro continuo y nos permite explorar el entorno del sistema del campo escalar sin masa.

Tras este estudio vamos a relajar las condiciones que imponemos a nuestros sistemas de ecuaciones en derivadas parciales, permitiendo que las condiciones de contorno dependan del tiempo. Sin embargo, continuando con la línea de investigación de esta tesis vamos a imponer condiciones de contorno periódicas en el tiempo. De esta forma evitamos que la dinámica a largos tiempos se vea afectada por las peculiaridades de las condiciones de contorno en estas mismas escalas de tiempo, dejando estos efectos para la dinámica dentro del dominio. Este tipo de condiciones nos llevan de forma natural a construir soluciones periódicas en el tiempo. Estas son el sustituto de las soluciones estáticas cuando las condiciones de contorno dependen del tiempo de forma periódica. La obtención de estas soluciones nos permitirán introducirnos en el régimen no lineal y estudiarlo a través de su entorno. Para esta tarea hemos desarrollado un método basándonos en la teoría de Floquet para construir los modos lineales de estas soluciones. Estos modos nos

proporcionan información muy útil acerca de la estabilidad de las soluciones periódicas. Permitiéndonos aislar cada uno de los modos lineales para realizar estudios de forma completamente controlada.

Para esta línea de estudio nos hemos apoyado en la conjetura AdS/CFT (anti-de Sitter/teoría de campos conforme). Esta correspondencia relaciona la dinámica dentro de espacio-tiempos de $d+1$ dimensiones con las mismas propiedades asintóticas que anti-de Sitter, con la dinámica de una teoría de campos conforme fuertemente acoplada en una geometría de d dimensiones que se corresponde con la frontera del espacio-tiempo mencionado. Esto nos permite relacionar los resultados obtenidos con los de este tipo de teorías cuánticas de campos y por tanto extender la validez de nuestro estudio. En particular, la correspondencia AdS/CFT proporciona el denominado *diccionario holográfico*, el cual interpreta el contenido en cada lado de la dualidad con el contenido en el otro. Concretamente relaciona los valores de los campos en la frontera de espacio en el lado de gravedad con las fuentes presentes en la teoría cuántica de campos. Es decir, las condiciones de contorno que imponemos a nuestro espacio-tiempo son las propias fuentes de la teoría conforme. Por tanto, al ser estas periódicas nos encontramos ante un sistema (holográfico) periódicamente dirigido.

Este tipo de sistemas son también conocidos como sistemas de Floquet. Han ganado gran atención en las últimas décadas debido a su realización en el laboratorio y a las interesantes propiedades que presentan. Algunos ejemplos son: sincronización con la fuente, modificación de la estructura de bandas, estabilización de puntos inestables o cristales de tiempo. Estos sistemas presentan un cierto grado de sincronización con la fuente que los excita, adaptando su estado en función de esta. En cuanto a la modificación en la estructura de bandas, ciertos materiales se comportan como conductores o aislantes dependiendo de la fuente que los excita. Estos materiales son los denominados aislantes topológicos. Por otro lado, ciertos sistemas presentan la modificación de la estabilidad de puntos de equilibrio para ciertos valores de la fuente. Hace unos años se planteó que al igual que existen cristales espaciales (los cuales presentan una ruptura de la simetría continua de traslación espacial por una simetría discreta), existen también los cristales temporales, que salvando ciertas sutilezas, presentan una simetría discreta de traslación temporal. Bajo nuestro punto de vista, el ejemplo más ilustrativo de sistemas de Floquet es el péndulo de Kapitza. Este consiste en un péndulo rígido ordinario sometido a vibraciones de baja amplitud y alta frecuencia. Para frecuencias suficientemente altas la posición invertida del péndulo se vuelve estable.

El estudio de sistemas de Floquet holográficos ha sido iniciado recientemente en la literatura a través de [101–108]. Hasta donde sabemos, [101] constituye el primer trabajo en el que se ha tratado un sistema holográfico periódicamente dirigido. Estos artículos han sido motivados por el estudio de sistemas fuera del equilibrio. La mayoría de ellos tratan de averiguar si la presencia de fuentes periódicas afecta a propiedades fundamentales de ciertos sistemas. Por ejemplo, en [101–103] han trabajado con superconductores holográficos. Estos artículos se centraron en la construcción del diagrama de fases y la dependencia de la temperatura de transición superconductora con la amplitud y periodicidad de la fuente que excita el sistema. Por otro lado, en [104] los autores se centraron en comprobar si

las propiedades de un semimetal de Weyl se preservan o si son destruidas al excitar el sistema con un campo eléctrico rotante. Utilizando un modelo similar [106] estudian cómo el diagrama de fases depende de la amplitud y frecuencia de rotación del campo eléctrico; el sistema puede comportarse como un aislante o un conductor en función de los valores de estos parámetros. Por otro lado, [105, 107] trabajan con modelos más simples que los anteriores. Estos consisten en un campo escalar sobre una geometría asintóticamente anti-de Sitter. Sin embargo, aprovechan la simpleza de sus modelos para estudiar efectos más complejos. En [101–104, 106, 108] no se consideró la respuesta de la métrica a la presencia de energía en la geometría; mientras que en [105] se calculó la primera corrección de la respuesta de la métrica, y en [107] se consideró la respuesta completa. Una característica que se ha mantenido presente en todos estos trabajos ha sido que los estados son térmicos desde el inicio, debido a la existencia de un horizonte y en consecuencia presentan una temperatura.

Nuestra situación, como hemos mencionado anteriormente, ha sido motivada inicialmente por el estudio de propiedades dinámicas del espacio-tiempo anti-de Sitter sujeto a condiciones de contorno que permiten el intercambio de energía a través de la frontera. Teniendo en cuenta que el espacio de anti-de Sitter tiende a llevar las condiciones iniciales a un colapso gravitacional, hemos planteado condiciones de frontera que no favorezcan una acumulación arbitraria de energía dentro del espacio. Para ello, estas deben mantener un compromiso entre la energía inyectada y extraída en el sistema. De este modo una fuente periódica es la candidata perfecta ya que esperamos que inyecte y extraiga la misma cantidad de energía. Aunque otros tipos de condiciones también presentan una fenomenología muy interesante [82].

Esta motivación nos diferencia radicalmente de los otros estudios acerca de sistemas holográficos periódicamente dirigidos [101–104, 106, 108]. Vamos a considerar la respuesta completa de la métrica y la geometría inicial no presentará un horizonte. En consecuencia, no hay temperatura y los estados iniciales son puros. Por tanto, nuestro planteamiento permite seguir la evolución de estados puros y observar si esta propiedad se mantiene, o si por el contrario el sistema termaliza por medio de la formación de un agujero negro.

La estrategia que vamos a utilizar consiste en un planteamiento "de abajo a arriba". Vamos a estudiar la fenomenología que presentan nuestros modelos y comprobar si esta puede ser interpretada de forma cualitativa como la asociada a un sistema de Floquet. Es decir, trataremos de elucidar si el modelo holográfico que planteamos captura y aisla características fundamentales de los sistemas de Floquet. Como la holografía no está suficientemente desarrollada todavía para describir sistemas físicos realistas, no debemos centrarnos en un único modelo holográfico. En vez de esto, tenemos que considerar un gran número de estos modelos. De este modo comprobaremos si las características que estamos observando son compartidas por muchos modelos, obteniendo cierta confianza de que entre estos, se encuentren modelos realistas. Estas son las denominadas propiedades "universales". Concretamente en esta tesis vamos a considerar dos de estos modelos.

Empezaremos por un campo escalar sin masa y esféricamente simétrico (denotado por ϕ) en AdS_4 descrito en coordenadas globales. A través de la correspondencia AdS/CFT

nuestros resultados serán interpretados como una teoría cuántica de campos conforme fuertemente acoplada sobre una esfera. Mientras que el segundo modelo consiste en fluctuaciones puramente gravitatorias (denotadas por b) de una geometría conocida como el AdS solitón. Trabajaremos con esta geometría en cuatro dimensiones, la cual describe una teoría conforme sobre un toro. Concretamente, las condiciones de ϕ y b sobre la frontera del espacio serán muy simples, de forma que podamos comprender de forma adecuada la influencia de cada parámetro. Por este motivo impondremos condiciones periódicas consistentes en un único armónico, el cual es parametrizado únicamente por su amplitud y frecuencia.

Debido a nuestro interés en comparar los resultados provenientes de los dos modelos, vamos a seguir exactamete la misma estrategia para ambos. Nos centraremos en el estudio de soluciones periódicas en el tiempo perfectamente sincronizadas con las condiciones de contorno y en la exploración de su entorno. Para ello, como hemos mencionado anteriormente, hemos desarrollado una serie de métodos que nos permiten construir estas soluciones y sus modos normales. Esto nos ha otorgado un elevado grado de manejo sobre nuestro estudio, permitiéndonos aislar los diferentes estados finales de ciertas inestabilidades presentes. Tras esto, hemos explorado un método para construir las mismas soluciones periódicas de forma dinámica al permitir la evolución en el tiempo de la amplitud y de la frecuencia de la fuente periódica. Ha sido muy interesante observar que si esta variación es muy lenta el estado final es una solución periódica estable, mientras que si la variación de los parámetros se hace a una velocidad determinada el estado final es una solución periódica inestable.

Finalmente, daremos una visión global de esta tesis, tanto de los resultados particulares que hemos obtenido como de su relevancia en el contexto al que pertenecen; destacando las respuestas que hemos dado a ciertas preguntas así como a las nuevas preguntas que se nos platean. Así mismo, también discutiremos las líneas futuras de investigación que se pueden tomar para extender este trabajo. Por ejemplo, en el caso de los sistemas resonantes sería muy interesante construir nuevas familias de coeficientes de interacción que admitan soluciones analíticas. En el caso de los sistemas de Floquet un proyecto muy interesante consistiría en construir uno de estos sistemas utilizando un modelo semiholográfico.

USC
UNIVERSIDADE
DE SANTIAGO
DE COMPOSTELA

A

Appendix

A.1 Discretization of the System of Equations

In this appendix we are going to show the procedure to discretize the EOMs, to numerically obtain TPSs and their linear stability following the method displayed in section 2.3. For this task we use a spectral method; namely, the system of equations will be solved on a suitable collection of points known as *collocation points*. Specifically, these points will be denoted by $\{\tau_k\}$ for time and $\{x_i\}$ for space.

A.1.1 Interpolations

The first step in the process consists of interpolating the functions of our problem from their values at each collocation point. This procedure can be done in different manners. An approach consists of the expansion of functions on an orthogonal basis $\{g_n(x)\}$, such that:

$$f(x) = \sum_{n=0}^{\infty} a_n g_n(x), \tag{A.1.1}$$

where the coefficient a_n is the projection of $f(x)$ on $g_n(x)$ with weight $\mu(x)$:

$$a_n = \langle f(x), g_n(x) \rangle = \int_{x_0}^{x_f} dx\ \mu(x) f(x) g_n(x), \tag{A.1.2}$$

and x_f, x_0 are the limits of the domain. Then, the k-differentiation of this function is represented by

$$f^{(k)}(x) = \sum_{n=0}^{\infty} a_n g_n^{(k)}(x), \tag{A.1.3}$$

and their values on the *collocation points* $\{x_i\}$ require the direct evaluation

$$f^{(k)}(x_i) = \sum_{n=0}^{\infty} a_n g_n^{(k)}(x_i). \tag{A.1.4}$$

The obtainment of TPSs consists of the determination of the coefficients $\{a_n\}$. Therefore, a second order differential equation requires the calculation of the set $\{g_n(x_i), g_n^{(1)}(x_i), g_n^{(2)}(x_i)\}$. The series (A.1.1) must be truncated to match the degrees of freedoms $\{a_n\}$ with the number of constraints given by $\{x_i\}$,

$$f_n(x) = \sum_{n=0}^{N} a_n g_n(x). \tag{A.1.5}$$

This formulation has the disadvantage that the integrals (A.1.2) must be computed, for low n it is not a problem, however for high n they require an important computational cost and are affected by significant errors.

A second formulation of the problem, which directly avoids any integration, consists of approaching the function $f(x)$ in a set of $N+1$ points $\{x_i\}$ using the *Lagrange form*

$$p(x) = \sum_{n=0}^{N} f_n \ell_n(x), \qquad \ell_n(x) = \frac{\prod_{k=0, k\neq n}^{N} (x - x_k)}{\prod_{k=0}^{N} (x_n - x_k)}. \tag{A.1.6}$$

Here $f_n \equiv f(x_n)$ and $\ell_n(x)$ denotes *Lagrange polynomials* which have the property

$$\ell_n(x_i) = \begin{cases} 1 & \text{if } i = n \\ 0 & \text{if } i \neq n \end{cases}, \qquad n, i = 0, 1, ..., N. \tag{A.1.7}$$

Therefore the *Lagrange form* is exact at collocation points: $p(x_i) = f(x_i)$. Despite this relevant property, the formulation has certain inconveniences, typically it is numerically unstable and has an excessive computational cost. Nevertheless, there is a reformulated approach which avoids these problems. It is known as the *barycentric interpolations* and approximates the function $f(x)$ using the following polynomial,

$$p(x) = \frac{1}{\sum_{n=0}^{N} \frac{\lambda_n}{(x - x_n)}} \sum_{n=0}^{N} \frac{\lambda_n}{(x - x_n)} f_n, \qquad \lambda_n = \frac{1}{\prod_{k=0, k\neq n}^{N} (x_n - x_k)}. \tag{A.1.8}$$

This formula cannot be numerically applied to $x = x_i$ because it leads to an indetermination ∞/∞. To avoid this problem we directly set $p(x_i) = f_i$. Specifically we have presented the denominated *second form of the barycentric interpolation*. This formulation is particularly suitable for Chebyshev collocation points, it has been proved that it is numerically stable for points $x \in [-1, 1]$ [210]. Additionally, the weights for Chebyshev points of the second kind

$$x_n = \cos\left(n\frac{\pi}{N}\right), \qquad n = 0, 1, ..., N, \tag{A.1.9}$$

can be exactly computed in a closed form, [210, 211],

$$\lambda_0 = \frac{c}{2}, \qquad \lambda_N = (-1)^N \frac{c}{2}, \qquad \lambda_n = (-1)^n c, \text{ with } n \neq 0, N. \tag{A.1.10}$$

Note that any common factor independent of n does not contribute to the barycentric formula (A.1.8) and thereby we can set $c = 1$. If an interval of the form $x \in [a, b]$ is considered, only $c \to c(a, b)$ is modified in λ_n, then the expression (A.1.10) with $c = 1$ remains valid.

Finally, this formalism provides differential operators which acting on the set of points $\{f_n\}$ allow approaching $f^{(k)}(x)$ with the barycentric formula

$$p_k(x) = \frac{1}{\sum\limits_{n=0}^{N} \frac{\lambda_n}{(x-x_n)}} \sum_{n=0}^{N} \frac{\lambda_n}{(x - x_n)} f_n^k, \qquad f_n^k = \sum_{i=0}^{N} D_{n,i}^{(k)} f_i. \tag{A.1.11}$$

They satisfy the recurrence relation

$$D_{n,i}^{(k)} = \begin{cases} -\sum\limits_{j=0, j\neq n} D_{nj}^{(k)} & \text{if } n = i \\ \frac{k}{x_n - x_i}\left(\frac{\lambda_i}{\lambda_n} D_{nn}^{(k-1)} - D_{ni}^{(k-1)}\right) & \text{if } n \neq i \end{cases} \tag{A.1.12}$$

where $n, i = 0, 1, ..., N$ and $D_{ni}^{(0)} = \mathbb{I}_{n,i}$ is the identity matrix.

At this point we must clarify how to properly solve discrete differential equations. Suppose the problem

$$b(x) = \frac{da(x)}{dx}, \qquad a(x_p) = \beta. \tag{A.1.13}$$

Its discrete version is written as

$$b_n = \sum_{i=0}^{N} D_{n,i} a_i, \tag{A.1.14}$$

and

$$\begin{cases} \frac{1}{\sum\limits_{n=0}^{N} \frac{\lambda_n}{(x_p - x_n)}} \sum\limits_{n=0}^{N} \frac{\lambda_n}{(x_p - x_n)} a_n = \beta & \text{if } x_p \neq x_n, \ \forall n \\ a_\alpha = \beta & \text{if } x_p = x_\alpha \end{cases} \tag{A.1.15}$$

with $n = 0, 1, ..., N$. The direct resolution of the linear system is not appropriate, we have $N + 2$ equations and $N + 1$ freedoms. The procedure consists of removing an equation, ensuring that $a(x_p) = \beta$ remains in the system because it is a strong condition.

A.1.2 Discretization of the System of Equations

Our problem depends on two variables, t and x, we have to decide the interpolation for each of them. The natural basis for periodic solutions are the Fourier modes, therefore we will expand functions of time on this basis using (A.1.1). On the other hand, for the spatial coordinate we do not have enough information to select a preferential basis, in these situations the answer is clear: we must use Chebyshev polynomials [210]. These functions have an excellent convergence, interpolations (A.1.1) or (A.1.8) exponentially converge to the original function. As we will explain below, the barycentric form is suitable for a problem with the symmetries displayed by our functions. In consequence, the interpolation for the spatial variable will be done using the Chebyshev points and (A.1.8). Hence, the relevant functions of our problem $u(t,x)$ and $v(t,x)$ are written at each couple of collocation points (τ_k, x_i) as

$$u(\tau_k, x_i) = \sum_{n=0}^{K-1} \cos(n\tau_k) u_{ni}, \qquad v(\tau_k, x_i) = \sum_{n=0}^{K-1} \sin(n\tau_k) v_{ni} \tag{A.1.16}$$

Now we are going to explain why the barycentric formulation is a suitable choice for the interpolation in x. We will follow the idea displayed in [112] because it provides good results. The key point consists of taking advantage of the symmetries of the problem, all our functions are symmetric or antisymmetric (expressed in suitable coordinates). Then, we can use the double-covering which allows performing computations on $N+1$ points with the robustness of $2N+2$. Under the symmetries of our problems the spatial domain is reduced to $x \in [0, x_f]$. Nevertheless, instead of translating the interval $[-1,1]$, where the Chebyshev points are defined, we shall adopt a different approach in order to minimize the Runge effects and to avoid numerical complications coming from an excessive density of points around the origin. Taking into account that all our function are symmetric or antisymmetric at the origin, the domain can be extended as $\tilde{x} \in [-x_f, x_f]$ with each function respecting its symmetries. Then, the Chebyshev collocation points will be rescaled from $[-1,1]$ to $[-x_f, x_f]$ as

$$\tilde{x}_n = x_f \cos\left(n \frac{\pi}{2N+1}\right), \qquad n = 0, 1, ..., 2N+1. \tag{A.1.17}$$

Note that the total number of points is even in order to avoid the origin. However, we only need the values of functions on the positive subset of point $\{x_n\} = [0, x_f] \cap \{\tilde{x}_n\}$, namely

$$x_n = x_f \cos\left(n \frac{\pi}{2N+1}\right), \qquad n = 0, 1, ..., N. \tag{A.1.18}$$

The set $\{\tilde{x}_n\}$ will be denominated *full grid* while $\{x_n\}$ *physical grid*.

Now consider a function $f(x)$ on the extended domain, which we will denote by $\tilde{f}(\tilde{x})$, it is interpolated with (A.1.8) as

$$\tilde{p}(\tilde{x}) = \frac{1}{\sum_{n=0}^{2N+1} \frac{\tilde{\lambda}_n}{(\tilde{x}-\tilde{x}_n)}} \sum_{n=0}^{2N+1} \frac{\tilde{\lambda}_n}{(\tilde{x}-\tilde{x}_n)} \tilde{f}_n, \tag{A.1.19}$$

where $\tilde{f}_n = \tilde{f}(\tilde{x}_n)$ and $\tilde{\lambda}_n$ are the weights for $\{\tilde{x}_n\}$ defined in (A.1.10). Note also that our functions satisfy $f(-x) = (-1)^\alpha f(x)$, with $\alpha = 0, 1$ for even and odd functions respectively, the coefficients on the physical grid are $f_n = f_n = (-1)^\alpha \tilde{f}_{2N+1-n}$, with $n = 0, 1, ..., N$. Thereby, including that $x_n = \tilde{x}_n = -\tilde{x}_{2N+1-n}$ and $\lambda_n = \tilde{\lambda}_n = -\tilde{\lambda}_{2N+1-n}$, the values at the origin have the reduced form for even functions

$$\tilde{p}(0) = \frac{1}{\sum_{n=0}^{N} \frac{\lambda_n}{x_n}} \sum_{n=0}^{N} \frac{\lambda_n}{x_n} f_n, \tag{A.1.20}$$

while for odd functions it is simply $\tilde{p}(0) = 0$.

These symmetric properties also help us to define new differential operators which reduce the matrix multiplication from $\mathcal{O}(8(N+1)^3)$ operations to $\mathcal{O}((N+1)^3)$. Considering the parts of the k-differential operator (A.1.12) acting on $\{x_n\}$ (denoted with $+$) or acting on points $[-x_f, 0] \cap \{\tilde{x}_n\}$ (denoted with $-$) it is divided as

$$D^{(k)} = \begin{pmatrix} D^{(k)}_{++} & D^{(k)}_{+-} \\ D^{(k)}_{-+} & D^{(k)}_{--} \end{pmatrix}. \tag{A.1.21}$$

Hence, for functions $\tilde{f}(-\tilde{x}) = (-1)^\alpha \tilde{f}(\tilde{x})$, these operators are reduced to simply acting on $\{f_n\}$ instead of the full set $\{\tilde{f}_n\}$,

$$f^{(k)}_n = \sum_{i=0}^{N} \left(D^{(k)}_{++} + (-1)^\alpha D^{(k)}_{+-} \right)_{n,i} f_i \tag{A.1.22}$$

Then, the operators acting on even ($\alpha = 0$) and odd ($\alpha = 1$) functions are defined as

$$D^{(k,\pm)}_{ij} = D^{(k)}_{ij} \pm D_{i,N+1+j}, \qquad i, j = 0, 1, ..., N. \tag{A.1.23}$$

Now we are ready to write the system of equations in the discrete form, where the unknowns are the values of functions at collocation points. We write the EOMs (2.3.25)-(2.3.28) here again, to avoid an interruption of the explanation:

$$\dot{u}(t,x) = F(t,x) v(t,x), \tag{A.1.24}$$

$$\dot{v}(t,x) = \frac{1}{\mu(x)} \left[F(t,x) \left(c_{v,1}(x) + c_{v,2}(x) u'(t,x) \right) \right]', \tag{A.1.25}$$

$$F'(t,x) = c_F(x) \left(e^{-\delta(t,x)} - F(t,x) \right), \tag{A.1.26}$$

$$\delta'(t,x) = c_{\delta,1}(x) u'(t,x) + c_{\delta,2}(x) (u'(t,x))^2 + c_{\delta,3}(x) v(t,x)^2. \tag{A.1.27}$$

The functions $u(t,x)$ and $v(t,x)$ (remember the definition $\tau = \omega t$) are written at each couple of collocation points (τ_k, x_i) as

$$u(\tau_k, x_i) = \sum_{n=0}^{K-1} \cos(n\tau_k) u_{ni}, \qquad v(\tau_k, x_i) = \sum_{n=0}^{K-1} \sin(n\tau_k) v_{ni}, \tag{A.1.28}$$

where $\{u_{ni}, v_{ni}\}$ must be determined. First, we must calculate δ in terms of these variables through (A.1.27) and setting $\delta(t, x_f) = 0$. Once δ is fully determined we obtain F by using (A.1.26) and fixing its value at the boundary with $F(t, x_f) = 1$ or at the origin with $F(t, 0) = F_0(t)$ ($F_0(t)$ is determined with the asymptotic expansion of F at the origin). Finally the equations (A.1.24) and (2.3.26) can be completely expressed in terms of $\{u_{ni}, v_{ni}\}$. Of course this process was done numerically starting with a suitable seed as was explained in section 2.3. Here we have described the resolution of TPSs, the process is analogous for their Floquet modes.

A.2 Quenches

In this section we discuss our particular implementation of quenches used in chapter 4. The idea consists of selecting a parametric family of solutions of the EOMs; starting with one of these solutions we modify the parameters in time to observe the response of the system. In the context of this thesis, this family will be formed by TPSs suitably parametrized by $u(0, 0)$ and the frequency ω of the harmonic boundary conditions,

$$u(t, x_f) = \rho \cos(\omega t), \tag{A.2.1}$$

where $u(t, x)$ represents a scalar field (section 4.1) or the appropriate metric function (section 4.2) and x_f denotes the boundary. Nevertheless, it is better to implement quenches in the boundary conditions through ρ and ω. We must clarify that there can be more than one TPS for the couple (ρ, ω). To avoid this problem, we can divide the space of TPSs into continuous regions where the parametrization is well posed.

The stages of our quench consists of: for times $-\infty < t < t^*$ the system is in a TPS associated with (ρ_i, ω_i), at $t = t^*$ we allow ρ and ω to evolve in time until (ρ_f, ω_f) at $t = (t^* + \beta)$, and finally, they remain in these values for $(t^* + \beta) < t < \infty$ (where t^* denotes the time at which the quench is turned on and β its duration). In terms of functions of time, the process has the form,

$$\rho(t) = \begin{cases} \rho_i & -\infty < t < t^* \\ \rho_Q(t) & t^* \leq t < (t^* + \beta) \\ \rho_f & (t^* + \beta) \leq t < \infty \end{cases} \tag{A.2.2}$$

and

$$\omega(t) = \begin{cases} \omega_i & -\infty < t < t^* \\ \omega_Q(t) & t^* \leq t < (t^* + \beta) \\ \omega_f & (t^* + \beta) \leq t < \infty \end{cases} \tag{A.2.3}$$

In principle the functions $\rho(t)$ and $\omega(t)$ are only restricted by a few conditions:

- Continuity in time: the boundary conditions and their derivatives must be continuous functions of time.

- Continuity in space: The boundary conditions and their derivatives must guarantee that the functions of our problem are continuous at the boundary.

To avoid these obstacles, we will use no-analytic functions for $\rho_Q(t)$ and $\omega_Q(t)$. They have the useful property that at a specific time, t^*, these functions and all of their derivatives are zero. It allows performing a direct modification in the future evolution of the source. We will extensively work with the non-analytic functions:

$$q_{\pm}(t, t^*, \beta) = \frac{1}{2}\left(1 \pm \tanh\left(\frac{\beta}{t - t^*} + \frac{\beta}{t - (t^* + \beta)}\right)\right). \tag{A.2.4}$$

Using (A.2.4) we define our collection of quenches which have the form:

- Quench in amplitude

$$\rho(t) = \begin{cases} \rho_i & -\infty < t < 0 \\ (\rho_f - \rho_i)q_-(t, 0, \beta) + \rho_i & 0 \le t < \beta \\ \rho_f & \beta \le t < \infty \end{cases} \qquad w(t) = w_i \tag{A.2.5}$$

- Quench in frequency

$$\rho(t) = \rho_i \qquad w(t) = \begin{cases} \rho_i & -\infty < t < 0 \\ (\omega_f - \omega_i)q_-(t, 0, \beta) + \omega_i & 0 \le t < \beta \\ \omega_f & \beta \le t < \infty \end{cases} \tag{A.2.6}$$

- Quench in amplitude and frequency

$$\begin{aligned} \rho(t) &= \begin{cases} \rho_i & -\infty < t < 0 \\ (\rho_f - \rho_i)q_-(t, 0, \beta) + \rho_i & 0 \le t < \beta \\ \rho_f & \beta \le t < \infty \end{cases} \\ w(t) &= \begin{cases} \omega_i & -\infty < t < 0 \\ (\omega_f - \omega_i)q_-(t, 0, \beta) + \omega_i & 0 \le t < \beta \\ \omega_f & \beta \le t < \infty \end{cases} \end{aligned} \tag{A.2.7}$$

- Quench in amplitude and frequency with $\rho_f = \rho_i$ and an intermediate ρ_m

$$\begin{aligned} \rho(t) &= \begin{cases} \rho_i & -\infty < t < 0 \\ (\rho_m - \rho_i)q_-(t, 0, \beta) + \rho_i & 0 \le t < \beta \\ (\rho_i - \rho_m)q_+(t, \beta, \beta) + \rho_m & 0 \le \beta \le 2\beta \\ \rho_i & 2\beta \le t < \infty \end{cases} \\ w(t) &= \begin{cases} \omega_i & -\infty < t < 0 \\ (\omega_f - \omega_i)q_-(t, 0, 2\beta) + \omega_i & 0 \le t < 2\beta \\ \omega_f & 2\beta \le t < \infty \end{cases} \end{aligned} \tag{A.2.8}$$

On some occasions, we will be interested in a quantitative measurement of the difference between the state of the system after a quench and a specific TPS. For this purpose we define the function

$$\Delta g(t) \equiv \left(\int_0^{x_f} dx \theta(x) \left(g(t,x) - g_p(t,x) \right)^2 \right)^{\frac{1}{2}}, \tag{A.2.9}$$

where $g(t,x)$ denotes any function of the problem, $g_p(t,x)$ the same function associated with the TPS and $\theta(x) = 1$ or $\theta(x) = \mu(x)$ (the weight for the inner product of normalizable linear modes (2.1.6)). Note that for $\theta(x) = \mu(x)$ the integral (A.2.9) typically diverges; nevertheless if problematic powers at the boundary of $g(t,x)$ are cancelled in $(g(t,x) - g_p(t,x))$ the integration is safe. For example, $g(t,x) = u(t,x)$, in this case the harmful powers only depend on the boundary conditions. If $g(t,x)$ and $g_p(t,x)$ have the same conditions the integral is finite even using $\theta(x) = \mu(x)$.

Finally, if we want to follow the intermediate states of the quench, $\rho(t)$ represents the instantaneous amplitude, but $\omega(t)$ is not the instantaneous frequency, it is actually defined as

$$\nu(t) \equiv \frac{d}{dt}\omega(t)t. \tag{A.2.10}$$

Thereby we will refer to the pair $(\rho(t), \nu(t))$ as the instantaneous parameters of the source.

A.3 Proofs and Technical Details

A.3.1 Propositions Time-Periodic Solutions

The following propositions require the analytic structure for TPSs:

$$u_p(t,x,\epsilon) = \sum_{n=0}^{\infty} \cos(n\omega t) \sum_{k=0}^{\infty} u_{n,k}(x)\epsilon^k = \sum_{n=0}^{\infty} \cos(n\omega t) u_n(x,\epsilon), \tag{A.3.1}$$

$$v_p(t,x,\epsilon) = \sum_{n=1}^{\infty} \sin(n\omega t) \sum_{k=0}^{\infty} v_{n,k}(x)\epsilon^k = \sum_{n=1}^{\infty} \sin(n\omega t) v_n(x,\epsilon), \tag{A.3.2}$$

$$\omega(\epsilon) = \sum_{k=0}^{\infty} \epsilon^k \omega^{(k)}. \tag{A.3.3}$$

Proposition 2.1: *Suppose a family of TPSs given by* (A.3.1)-(A.3.3). *Then two solutions:* $\epsilon, \epsilon' = \epsilon(1+\delta)$, *arbitrarily close* ($\delta << 1$), *satisfy at first order in* δ

$$u_p(t,x,\epsilon') - u_p(t,x,\epsilon) = \left(\tilde{u}(t,x,\epsilon) + t\hat{u}(t,x,\epsilon)\right)\delta + \mathcal{O}(\delta^2) \tag{A.3.4}$$

$$v_p(t,x,\epsilon') - v_p(t,x,\epsilon) = \left(\tilde{v}(t,x,\epsilon) + t\hat{v}(t,x,\epsilon)\right)\delta + \mathcal{O}(\delta^2) \tag{A.3.5}$$

where $\tilde{u}, \tilde{v}$ *satisfy* (2.3.57) *with* $\lambda = 0$, *and* $\hat{u}, \hat{v}$ *are bounded periodic functions.*

Poof:

Suppose a family of TPSs satisfying (A.3.1)-(A.3.3). Now we take two solutions arbitrarily close, ϵ and $\epsilon' = \epsilon(1+\delta)$ with $|\delta| \ll 1$. Rewriting the frequency as $\omega(\epsilon') = \omega(\epsilon) + \Omega(\epsilon, \delta)$ where $\Omega(\epsilon, \delta) \equiv \omega(\epsilon') - \omega(\epsilon)$ and using trigonometric identities we obtain

$$u_p(t, x, \epsilon') = \sum_{n=0}^{\infty} u_n(x, \epsilon') \left[\cos(n\omega(\epsilon)t)\cos(n\Omega(\epsilon, \delta)t) - \sin(n\omega(\epsilon)t)\sin(n\Omega(\epsilon, \delta)t)\right], \tag{A.3.6}$$

$$v_p(t, x, \epsilon') = \sum_{n=1}^{\infty} v_n(x, \epsilon') \left[\sin(n\omega(\epsilon)t)\cos(n\Omega(\epsilon, \delta)t) + \cos(n\omega(\epsilon)t)\sin(n\Omega(\epsilon, \delta)t)\right], \tag{A.3.7}$$

Using $\Omega(\epsilon, \delta) = \delta\Omega_1(\epsilon) + \mathcal{O}(\delta^2)$, the resulting expression at first order in δ is

$$\begin{aligned} &u_p(t, x, \epsilon') - u_p(t, x, \epsilon) = \\ &\delta \sum_{n=0}^{\infty} \cos(n\omega t) \sum_{k=0}^{\infty} u_{n,k}(x) k\epsilon^k - \delta t\Omega_1(\epsilon) \sum_{n=0}^{\infty} n u_n(x, \epsilon) \sin(n\omega(\epsilon)t) + \mathcal{O}(\delta^2), \end{aligned} \tag{A.3.8}$$

$$\begin{aligned} &v_p(t, x, \epsilon') - v_p(t, x, \epsilon) = \\ &\delta \sum_{n=0}^{\infty} \sin(n\omega t) \sum_{k=0}^{\infty} v_{n,k}(x) k\epsilon^k + \delta t\Omega_1(\epsilon) \sum_{n=0}^{\infty} n v_n(x, \epsilon) \cos(n\omega(\epsilon)t) + \mathcal{O}(\delta^2). \end{aligned} \tag{A.3.9}$$

Now we can see as the first term has the form of (2.3.57) with $\lambda = 0$. The ansatz (2.3.57) for the linear modes can be written in terms of trigonometric functions by combining both solutions $\pm\lambda$ such that

$$\tilde{u}(t, x) = \cos(\lambda t) \sum_{n=0}^{\infty} u_n^{(1)}(x) \cos(n\omega t) + \sin(\lambda t) \sum_{n=1}^{\infty} u_n^{(2)}(x) \sin(n\omega t), \tag{A.3.10}$$

$$\tilde{v}(t, x) = \cos(\lambda t) \sum_{n=1}^{\infty} v_n^{(1)}(x) \sin(n\omega t) + \sin(\lambda t) \sum_{n=0}^{\infty} v_n^{(2)}(x) \cos(n\omega t). \tag{A.3.11}$$

Setting $\lambda = 0$, $\omega = \omega(\epsilon)$, $u_n^{(1)} = \sum k u_{n,k}(x)\epsilon^k$ and $v_n^{(1)} = \sum k v_{n,k}(x)\epsilon^k$ we can write

$$u_p(t, x, \epsilon') - u_p(t, x, \epsilon) = \delta\tilde{u}(t, x) - \delta t\hat{u}(t, x) + \mathcal{O}(\delta^2), \tag{A.3.12}$$

$$v_p(t, x, \epsilon') - v_p(t, x, \epsilon) = \delta\tilde{v}(t, x) + \delta t\hat{v}(t, x) + \mathcal{O}(\delta^2), \tag{A.3.13}$$

where $\hat{u}, \hat{v}$ correspond with the second terms in (A.3.8) and (A.3.9) respectively.

Proposition 2.2: *Suppose two families of TPSs:* $(u_{p,1}, v_{p,1}, \omega_1)$, $(u_{p,2}, v_{p,2}, \omega_2)$ *satisfying* (A.3.1)-(A.3.3) *with boundary conditions*

$$u_{p,1,2}(t, x_f, \epsilon) = \epsilon\rho_{1,2}\cos(\omega_{1,2}(\epsilon)t), \tag{A.3.14}$$

$$v_{p,1,2}(t, x_f, \epsilon) = -\epsilon\omega_{1,2}(\epsilon)\rho_{1,2}\cos(\omega_{1,2}(\epsilon)t), \tag{A.3.15}$$

which are arbitrarily close $\rho_2 = \rho_1(1+\delta)$*, with* $|\delta| \ll 1$*. Also consider that there exists* ρ_1, ϵ *such that*

$$\omega_2\left(\frac{\epsilon}{1+\delta}\right) = \omega_1(\epsilon) + \delta^2\tilde{\omega}(\epsilon) + \mathcal{O}(\delta^3), \tag{A.3.16}$$

$$u_{p,2}\left(t, x, \frac{\epsilon}{1+\delta}\right) = u_{p,1}\left(t, x, \epsilon\right) + \delta\ \tilde{u}(t, x, \epsilon) + \mathcal{O}(\delta^2), \tag{A.3.17}$$

$$v_{p,2}\left(t, x, \frac{\epsilon}{1+\delta}\right) = v_{p,1}\left(t, x, \epsilon\right) + \delta\ \tilde{v}(t, x, \epsilon) + \mathcal{O}(\delta^2), \tag{A.3.18}$$

with $\tilde{\omega}, \tilde{b} \neq 0$*. Then, they have a zero-mode with homogeneous boundary conditions, namely a linear perturbation* (2.3.57) *with* $\lambda = 0$*.*

Poof

Suppose two families of TPSs $(u_{p,1}, v_{p,1}, \omega_1)$ and $(u_{p,2}, v_{p,2}, \omega_2)$ satisfying (A.3.1)-(A.3.3) with boundary conditions

$$u_{p,1,2}(t, x_f, \epsilon) = \epsilon\rho_{1,2}\cos(\omega_{1,2}(\epsilon)t), \tag{A.3.19}$$

$$v_{p,1,2}(t, x_f, \epsilon) = -\epsilon\omega_{1,2}(\epsilon)\rho_{1,2}\cos(\omega_{1,2}(\epsilon)t), \tag{A.3.20}$$

which are arbitrarily close $\rho_2 = \rho_1(1+\delta)$, with $|\delta| \ll 1$. In this situation taking ϵ for the the first family and $\epsilon' = \epsilon/(1+\delta)$ for the second one, they have the same boundary conditions. Therefore there are no corrections in powers of δ at the boundary. We also suppose that there exists ρ_1, ϵ such that

$$\omega_2\left(\frac{\epsilon}{1+\delta}\right) = \omega_1(\epsilon) + \delta^2\tilde{\omega}(\epsilon) + \mathcal{O}(\delta^3) = \omega_1(\epsilon) + \Omega(\epsilon, \delta), \tag{A.3.21}$$

$$u_{p,2}\left(t, x, \frac{\epsilon}{1+\delta}\right) = u_{p,1}\left(t, x, \epsilon\right) + \delta\ \tilde{u}(t, x, \epsilon) + \mathcal{O}(\delta^2), \tag{A.3.22}$$

$$v_{p,2}\left(t, x, \frac{\epsilon}{1+\delta}\right) = v_{p,1}\left(t, x, \epsilon\right) + \delta\ \tilde{v}(t, x, \epsilon) + \mathcal{O}(\delta^2), \tag{A.3.23}$$

with $\tilde{\omega}, \tilde{b} \neq 0$. In this case

$$u_{p,2}\left(t, x, \frac{\epsilon}{1+\delta}\right) =$$
$$\sum_{n=0}^{\infty} u_{n,2}\left(x, \frac{\epsilon}{1+\delta}\right)\left[\cos(n\omega_1(\epsilon)t)\cos(n\Omega(\epsilon,\delta)t) - \sin(n\omega_1(\epsilon)t)\sin(n\Omega(\epsilon,\delta)t)\right], \tag{A.3.24}$$
$$v_{p,2}\left(t, x, \frac{\epsilon}{1+\delta}\right) =$$
$$\sum_{n=0}^{\infty} v_{n,2}\left(x, \frac{\epsilon}{1+\delta}\right)\left[\sin(n\omega_1(\epsilon)t)\cos(n\Omega(\epsilon,\delta)t) + \cos(n\omega_1(\epsilon)t)\sin(n\Omega(\epsilon,\delta)t)\right]. \tag{A.3.25}$$

Then, expanding in δ at first order we obtain

$$u_{p,2}\left(t,x,\frac{\epsilon}{1+\delta}\right)-u_{p,1}\left(t,x,\epsilon\right)=\delta\sum_{n=0}^{\infty}\cos(n\omega_1(\epsilon)t)\sum_{k=0}^{\infty}k\epsilon^k u_{n,k,2}(x)+\mathcal{O}(\delta^2), \quad \text{(A.3.26)}$$

$$v_{p,2}\left(t,x,\frac{\epsilon}{1+\delta}\right)-v_{p,1}\left(t,x,\epsilon\right)=\delta\sum_{n=0}^{\infty}\sin(n\omega_1(\epsilon)t)\sum_{k=0}^{\infty}k\epsilon^k v_{n,k,2}(x)+\mathcal{O}(\delta^2). \quad \text{(A.3.27)}$$

These expressions at first order in δ are solutions of the linearized EOMs due to $(u_{p,1}, v_{p,1}, \omega_1)$ and $(u_{p,2}, v_{p,2}, \omega_2)$ are both solutions of the EOMs. Therefore (A.3.26)-(A.3.27) form a linear zero-mode with homogeneous boundary conditions of the form (A.3.10)-(A.3.10). This last relation is obtained by imposing $\lambda = 0$, $u_n^{(1)} = \sum k\epsilon^n u_{n,k,2}(x)$ $v_n^{(1)} = \sum k\epsilon^n v_{n,k,2}(x)$.

A.3.2 Propositions Resonant Systems

This appendix gathers the proofs and technical details of the results displayed in sections 3.1 and 3.2. Starting with the propositions given in sections 3.1.1-3.1.3 we introduce the following definitions:

$$S_{nmkl}\equiv\begin{cases} f_n f_m f_k f_l C_{nmkl} & n,m,k,l\geq 0,\\ 0 & \text{if any index is negative}\ , \end{cases} \quad \text{(A.3.28)}$$

$$g_p^{(n,m)}\equiv\sum_{k=0}^{n+m}k^p\frac{f_k f_{n+m-k}}{f_n f_m}C_{nmk,n+m-k}=\frac{1}{f_n^2 f_m^2}\sum_{k=0}^{n+m}k^p S_{nmk,n+m-k}, \quad \text{(A.3.29)}$$

$$F_p(x)\equiv\sum_{k=0}^{\infty}k^p f_k^2 x^k, \quad \text{(A.3.30)}$$

$$\beta\equiv C_{2020},\qquad \gamma\equiv\left(\frac{f_0 f_2}{f_1^2}\right)^2,\qquad G\equiv\frac{1}{2\gamma-1}, \quad \text{(A.3.31)}$$

Propositions 3.1.1.1 to 3.1.1.3 are formed by smaller propositions; therefore, we will provide them with their proofs instead proofs for Propositions 3.1.1.1 to 3.1.1.3.

Proposition 0.1: *if the interaction coefficients satisfy* (3.0.2),(3.1.1) *and*

$$g_0^{(n,m)}=1,\qquad g_2^{(n,m)}=c_2(n^2+m^2)+c_1 nm+c_0(n+m), \quad \text{(A.3.32)}$$

c_1, c_2, c_3 *are univocally determined:*

$$c_0=\frac{1-2\beta}{2},\qquad c_1=2\gamma(1-2\beta),\qquad c_2=\beta. \quad \text{(A.3.33)}$$

Poof

This can be seen by exploring $g_0^{(n,m)}$ and $g_2^{(n,m)}$ for low-lying values of n and m. First of all, $g_0^{(0,0)} = 1$ is identical to (3.1.1), which we have already assumed. Then, $g_0^{(0,1)} = 1$ enforces

$$C_{0101} = \frac{1}{2}. \tag{A.3.34}$$

Additionally, $g_0^{(1,1)} = 1$ and $g_0^{(2,0)} = 1$ enforce

$$2\sqrt{\gamma}\, C_{1120} + C_{1111} = 1, \qquad 2\beta + \frac{1}{\sqrt{\gamma}} C_{1120} = 1, \tag{A.3.35}$$

where we have introduced

$$\beta = C_{2020}, \qquad \gamma = \left(\frac{f_0 f_2}{f_1^2}\right)^2. \tag{A.3.36}$$

Computing $g_2^{(n,m)}$ at low-lying n and m from the above expressions, we obtain

$$g_2^{(0,1)} = g_2^{(1,0)} = \frac{1}{2}, \qquad g_2^{(0,2)} = g_2^{(2,0)} = 1 + 2\beta, \qquad g_2^{(1,1)} = 1 + 2\gamma(1 - 2\beta). \tag{A.3.37}$$

From this and (A.3.32),

$$g_2^{(n,m)} = \beta(n^2 + m^2) + 2\gamma(1 - 2\beta)nm + \frac{1 - 2\beta}{2}(n + m). \tag{A.3.38}$$

Proposition 0.2: *if* (3.0.2),(3.1.1) *and* (A.3.32) *are satisfied, then* f_n *is given by*

$$f_n = \begin{cases} \dfrac{1}{\sqrt{n!}} & \text{if } \gamma = \frac{1}{2}, \\ \sqrt{\dfrac{(G)_n}{n!}} & \text{if } \gamma > \frac{1}{2}, \end{cases} \tag{A.3.39}$$

where $(x)_n \equiv x(x+1)\cdots(x+n-1)$ *denotes the rising Pochhammer symbol.*

Poof

The idea behind the proof is that the summation identities (A.3.32) do not manifestly respect the symmetries of C, and imposing the symmetries of C produces extra conditions which, in particular, completely fix f_n. Due to the symmetries of C, and the corresponding symmetries of S inherited through (A.3.28), the following identity holds for any x:

$$\sum_{n+m=k+l} n^2 x^{(n+m+k+l)/2} S_{nmkl} = \sum_{n+m=k+l} k^2 x^{(n+m+k+l)/2} S_{nmkl}. \tag{A.3.40}$$

Equivalently,

$$\sum_{n,m=0}^{\infty} n^2 x^{n+m} \sum_{k=0}^{n+m} S_{nmk,n+m-k} = \sum_{n,m=0}^{\infty} x^{n+m} \sum_{k=0}^{n+m} k^2 S_{nmk,n+m-k}. \tag{A.3.41}$$

Then, from (A.3.29), (A.3.32) and (A.3.38),

$$\sum_{n,m=0}^{\infty} n^2 f_n^2 f_m^2 x^{n+m} = \sum_{n,m=0}^{\infty} f_n^2 f_m^2 x^{n+m} \left[\beta(n^2+m^2) + 2\gamma(1-2\beta)nm + \frac{1-2\beta}{2}(n+m) \right]. \tag{A.3.42}$$

Rewriting through (A.3.30),

$$F_0 F_2 - 2\gamma F_1^2 - F_0 F_1 = 0. \tag{A.3.43}$$

We note that

$$F_p = (x\partial_x)^p F_0, \tag{A.3.44}$$

which gives the following differential equation for F_0:

$$F_0\, \partial_x^2 F_0 - 2\gamma(\partial_x F_0)^2 = 0. \tag{A.3.45}$$

or

$$\partial_x(\partial_x F_0/F_0) - (2\gamma - 1)(\partial_x F_0/F_0)^2 = 0, \tag{A.3.46}$$

which is integrated to

$$\frac{\partial_x F_0}{F_0} = \frac{G}{h_1 - x}, \tag{A.3.47}$$

and then to

$$F_0 = h_2\,(h_1 - x)^{-G}, \tag{A.3.48}$$

where h_1 and h_2 are arbitrary integration constants. If $\gamma = 1/2$, then (A.3.46) is integrated to

$$F_0 = h_2\, e^{h_1 x}. \tag{A.3.49}$$

We note that if f_n has been used for defining the ansatz (A.3.53), then $\tilde{f}_n = d_1 d_2^n f_n$ with arbitrary d_1 and d_2 is equally good, since it simply amounts to a multiplicative rescaling of a, b and p. This freedom implies the possibility to arbitarily scale F_0 and x in (A.3.48)-(A.3.49) without essentially changing the ansatz (A.3.53), and in particlar one can set h_1 and h_2 to 1, which gives

$$F_0(x) = \begin{cases} e^x & \text{if } \gamma = \frac{1}{2}, \\ (1-x)^{-G} & \text{if } \gamma > \frac{1}{2}. \end{cases} \tag{A.3.50}$$

Expanding these expressions in powers of x reproduces (A.3.39). For $\gamma < 1/2$ (negative G) the Taylor coefficients of F_0 can be negative, and hence f_n can be imaginary. Since our construction assumes real f_n (and all known cases in the recent literature arising as resonant systems of the equations of mathematical physics are in this category), we shall simply discard such values of γ and restrict ourselves to $\gamma \geq 1/2$.

Proposition 0.3: $g_0^{(n,m)} = 1$ *implies*

$$g_1^{(n,m)} = \frac{n+m}{2}. \tag{A.3.51}$$

Poof

The expression for $g_1^{(n,m)}$ straightforwardy follows from the symmetry of S under permutation of the third and the fourth index:

$$g_1^{(n,m)} = \frac{1}{f_n^2 f_m^2}\sum_{k=0}^{n+m} kS_{nmk,n+m-k} = \frac{1}{2f_n^2 f_m^2}\left[\sum_{k=0}^{n+m} kS_{nmk,n+m-k} + \sum_{k=0}^{n+m}(n+m-k)S_{nm,n+m-k,k}\right]$$
$$= \frac{n+m}{2f_n^2 f_m^2}\sum_{k=0}^{n+m} S_{nmk,n+m-k} = \frac{n+m}{2} g_0^{(n,m)} = \frac{n+m}{2}. \tag{A.3.52}$$

Proposition 0.4: *if* (3.0.2),(3.1.1) *and* (A.3.32) *are obeyed, the ansatz*

$$\alpha_n(\tau) = f_n\,(b(\tau) + na(\tau))\,(p(\tau))^n, \tag{A.3.53}$$

is respected by (3.0.1)*, provided that three ordinary differential equations, are satisfied by* $a(t)$*,* $b(t)$ *and* $p(t)$*.*

Poof

Substitution of (A.3.53) into (3.0.1) results in

$$i\left(\dot{b} + \dot{a}n + (b+an)n\frac{\dot{p}}{p}\right) = \sum_{j=0}^{\infty} f_j^2 x^j(\bar{b}+\bar{a}j)\sum_{k=0}^{n+j}\frac{f_k f_{n+j-k}}{f_n f_j}C_{njk,n+j-k}(b+ak)(b+a(n+j-k)), \tag{A.3.54}$$

where we have defined

$$x = |p|^2. \tag{A.3.55}$$

The sum over k is evaluated using (A.3.32) and (A.3.51) which follows from (A.3.32), and it is a quadratic polynomial in n and m. Summation over j is then expressed in terms of F_p defined by (A.3.30) and given by (A.3.44) and (A.3.50). The remaining expression on the right-hand side of (A.3.54) is then a quadratic polynomial in n. The left-hand side of (A.3.54) is likewise a quadratic polynomial in n, and equating the three coefficients of the two polynomials produces three ordinary differential equations for the three functions a, b, p, as claimed.

Direct evaluation of the sums in (A.3.54) along the lines described above produces the following equations:

$$i\,\dot{b} = b^2(\bar{b}F_0 + \bar{a}F_1) + ab(\bar{b}F_1 + \bar{a}F_2) - \frac{1-2\beta}{2}a^2\Big[\bar{b}(F_1 - F_2) - \bar{a}(F_2 - F_3)\Big], \tag{A.3.56}$$

$$i\,\frac{\dot{a}}{a} = \frac{1+2\beta}{2}b(\bar{b}F_0 + \bar{a}F_1) + \frac{1}{2}a\bar{b}\Big[(2\beta-1)F_0 + (2-4\gamma+8\beta\gamma)F_1\Big] \tag{A.3.57}$$
$$+ \frac{1}{2}a\bar{a}\Big[(2\beta-1)F_1 + (2-4\gamma+8\beta\gamma)F_2\Big],$$

$$i\,\frac{\dot{p}}{p} = \frac{(1-2\beta)}{2}a(\bar{b}F_0 + \bar{a}F_1), \tag{A.3.58}$$

where F_p is understood as $F_p(x)$ in all expressions.

Proposition 0.5: *for all solutions of* (3.0.1) *restricted to* (A.3.53), $|\alpha_n|^2$ *is periodic in time and the quantity*

$$Z = \begin{cases} \sum_{n=0}^{\infty} \sqrt{(n+1)(n+G)}\, \bar{\alpha}_{n+1}\alpha_n & \text{if } \gamma > \frac{1}{2}, \\ \sum_{n=0}^{\infty} \sqrt{n+1}\, \bar{\alpha}_{n+1}\alpha_n & \text{if } \gamma = \frac{1}{2}. \end{cases} \tag{A.3.59}$$

is conserved.

Poof

Equations (A.3.56)-(A.3.58) must evidently respect the general conserved quantities of the resonant system given by (3.0.3), (3.0.4) and (3.0.5). Restricted to our ansatz, these quantities take the form

$$N = |b|^2 F_0 + (\bar{a}b + a\bar{b})F_1 + |a|^2 F_2, \tag{A.3.60}$$

$$J = |b|^2 F_1 + (\bar{a}b + a\bar{b})F_2 + |a|^2 F_3, \tag{A.3.61}$$

$$H = N^2 + 2\gamma\,(2\beta - 1)\,S^2, \tag{A.3.62}$$

where

$$S = |a|^2 \frac{F_1}{F_0}\,(F_0 + (2\gamma - 1)F_1)\,. \tag{A.3.63}$$

In verifying various conservation laws, one can conveniently use

$$\dot{F}_p = \frac{\dot{x}}{x} F_{p+1}. \tag{A.3.64}$$

It turns out that (A.3.56)-(A.3.58) admit an extra complex conserved quantity given by (A.3.59), which written in terms of a, b, p becomes

$$\begin{aligned} Z = {} & \bar{p}(|b|^2 + a\bar{b})\,(F_0 + (2\gamma - 1)F_1) \\ & + \bar{p}(|a|^2 + \bar{a}b + a\bar{b})\,(F_1 + (2\gamma - 1)F_2) + \bar{p}|a|^2\,(F_2 + (2\gamma - 1)F_3)\,. \end{aligned} \tag{A.3.65}$$

Note that at this point we make no claims about the conservation of this quantity by the full resonant system (3.0.1), though this will form the main topic of the next section.

We shall essentially follow the strategy of [75]. One starts by expressing $|a|^2$, $|b|^2$ and $\mathrm{Re}(\bar{a}b)$ in terms of x and the conserved quantities N, J and S:

$$|a|^2 = \frac{F_0}{F_1} \frac{1}{(F_0 + (2\gamma - 1)F_1)} S \tag{A.3.66}$$

$$|b|^2 = \frac{F_3 N - F_2 J}{F_1^2 - F_0 F_2} - \frac{F_3 F_1 - F_2^2}{(F_1^2 - F_0 F_2)^2} \left(F_1 N - F_0 J - S \frac{F_0}{F_1} \frac{F_2 F_1 - F_0 F_3}{F_0 + (2\gamma - 1)F_1} \right) \tag{A.3.67}$$

$$2\,\mathrm{Re}(\bar{a}b) = \frac{1}{F_1^2 - F_0F_2}\left(F_1N - F_0J - S\frac{F_0}{F_1}\frac{F_2F_1 - F_0F_3}{F_0 + (2\gamma-1)F_1}\right) \tag{A.3.68}$$

The equation of $\dot{x}$ can also be rewritten in terms of conserved quantities. First,

$$\frac{\dot{x}}{x} = (2\beta - 1)\,\mathrm{Im}(\bar{a}b)F_0. \tag{A.3.69}$$

Using $(\mathrm{Im}(\bar{a}b))^2 = |a|^2|b|^2 - (\mathrm{Re}(\bar{a}b))^2$, one expresses the square of the right-hand side through the conserved quantities and x. Finally, introducing

$$y = \frac{x}{1-x} \tag{A.3.70}$$

one obtains

$$\begin{aligned}\frac{\dot{y}^2}{(1-2\beta)^2} =& -\frac{1}{4}\left(N^2 + 8\gamma(2\gamma-1)S^2\right)y^2 \\ &+ \frac{1}{2}(2\gamma-1)\Big[S(N-4\gamma S) + J(N + 2(2\gamma-1)S)\Big]y - \frac{1}{4}(1-2\gamma)^2\,(J-S)^2\,.\end{aligned} \tag{A.3.71}$$

The last equation is simply in the form of energy conservation for an one-dimensional harmonic oscillator, hence all of its solutions are periodic and of the form

$$y = B + A\sin(\Omega t + \theta)\,, \qquad \Omega = \frac{1-2\beta}{2}\sqrt{N^2 + 8\gamma(2\gamma-1)S^2}, \tag{A.3.72}$$

where

$$A = -\frac{1}{\Omega}\sqrt{(\Omega B)^2 - \frac{(1-2\beta)^2}{4}(1-2\gamma)^2\,(J-S)^2}, \tag{A.3.73}$$

$$B = \frac{1}{2\Omega^2}\frac{(1-2\beta)^2}{2}(2\gamma-1)\,(S(N-4\gamma S) + J(N + 2(2\gamma-1)S))\,. \tag{A.3.74}$$

The periodicity of y is transferred to x through (A.3.70) and hence to $|\alpha_n|^2$ through (A.3.66)-(A.3.68) and

$$|\alpha_n|^2 = f_n^2x^n\left(|b|^2 + 2n\,\mathrm{Re}\,(\bar{a}b) + n^2|a|^2\right). \tag{A.3.75}$$

This is directly analogous to the periodic dynamics of the spectrum observed in specific cases in the literature [72, 73, 75, 76].

Proposition 0.6: (A.3.53) *contains a biparametric family of stationary solutions of the form*

$$p = qe^{-i\omega(q,c)\tau}, \qquad b = \beta(q,c)e^{-i\lambda(q,c)\tau}, \qquad a = \kappa(q,c)e^{-i\lambda(q,c)\tau}, \tag{A.3.76}$$

for which $Z = 0$.

Poof

From (A.3.55), (A.3.58) and (A.3.65), one finds

$$\frac{\dot{x}}{2\beta-1}=\frac{\mathrm{Im}(pZ)}{1+F_1/(GF_0)}. \tag{A.3.77}$$

For initial data with $Z=0$, x is constant, and hence so are $|b|^2$, $|a|^2$, $Re(a\bar{b})$ (see (A.3.66)-(A.3.68)) and the spectrum (A.3.75). Thus one has a family of stationary solutions of the form $p=qe^{-i\omega\tau}$, $b=\beta e^{-i\lambda\tau}$ and $a=\kappa e^{-i\lambda\tau}$, labelled by two parameters c and q, with real-valued

$$\kappa=-c(1-q^2), \tag{A.3.78}$$

$$\beta_\pm=\frac{c}{2}\left(1+(2G+1)q^2\pm\sqrt{1-(6+4G)q^2+q^4}\right), \tag{A.3.79}$$

$$\lambda_\pm=\frac{c^2}{4(1-q^2)^G}\Big((1-q^2)(2+q^2(G(2\beta-1)-2)) \pm(2+q^2(2+G(1-2\beta)))\sqrt{1-(6+4G)q^2+q^4}\Big), \tag{A.3.80}$$

$$\omega_\pm=c^2\frac{(2\beta-1)}{4(1-q^2)^{G-1}}\left(1+q^2\pm\sqrt{1-(6+4G)q^2+q^4}\right). \tag{A.3.81}$$

In the case of $\gamma=1/2$ there is also a stationary state for the initial data with $Z=0$:

$$\kappa=-c, \tag{A.3.82}$$

$$\beta_\pm=\frac{c}{2}\left(1+2q^2\pm\sqrt{1-4q^2}\right), \tag{A.3.83}$$

$$\lambda_\pm=\frac{c^2}{4}e^{q^2}\left(2+(2\beta-1)q^2\pm(2-(2\beta-1)q^2)\sqrt{1-4q^2}\right), \tag{A.3.84}$$

$$\omega_\pm=\frac{c^2}{4}e^{q^2}(2\beta-1)(1\pm\sqrt{1-4q^2}). \tag{A.3.85}$$

Proposition 0.7: *for a given resonant system* (3.0.1) *satisfying* (A.3.32), *the range of motion of* $|p|^2$, *defined by* $(1-p_-^2)/(1-p_+^2)$ *where* $p_+\equiv max(|p|)$ *and* $p_-\equiv min(|p|)$, *is uniformly bounded for all solutions within the ansatz* (A.3.53).

Poof

Again we follow the strategy developed in [75] for a particular special case of our present setup. We write

$$\frac{1+y_+}{1+y_-}=\frac{(1+y_+)^2}{(1+y_-)(1+y_+)}\leq\frac{(1+y_++y_-)^2}{1+y_-+y_++y_-y_+}. \tag{A.3.86}$$

The last expression has the advantage that y_++y_- and y_+y_- are expressible through the coefficients in (A.3.71), which are algebraically simpler than (A.3.73)-(A.3.74). More specifically,

$$\frac{(1+y_++y_-)^2}{1+y_-+y_++y_-y_+}=\frac{(N+2(2\gamma-1)S)^2\,(N+2(2\gamma-1)J)^2}{(N+(2\gamma-1)J+(2\gamma-1)S)^2\,(N^2+8\gamma(2\gamma-1)S^2)}$$

$$\leq \frac{4\left(N+2(2\gamma-1)S\right)^2}{(N^2+8\gamma(2\gamma-1)S^2)} \leq 4\left(1+2(2\gamma-1)\frac{S}{N}\right)^2. \tag{A.3.87}$$

Since

$$N = F_0\left|b+\frac{F_1}{F_0}a\right|^2 + S \geq S, \tag{A.3.88}$$

we conclude that

$$\frac{1+y_+}{1+y_-} \leq 4\left(4\gamma-1\right)^2. \tag{A.3.89}$$

Hence for a fixed resonant system (fixed γ) and fixed y_-, the maximal value of $|p|$ in (A.3.53) is bounded from above by a fixed number, irrespectively of other initial conditions.

Proposition 3.1.2.1: $\mathcal{D}_{nmkl} = 0$ *implies* (3.1.5). *Therefore, Propositions 3.1.1.1 to 3.1.1.3 apply to any resonant system satisfying this condition.*

Poof

Assume first $\gamma > 1/2$. Take $l = n+m-1-k$ in (3.1.11) and then sum over k from 0 to $n+m-1$, which gives

$$\sum_{k=0}^{n+m-1}\Big[(n-1+G)\,S_{n-1,mk,n+m-1-k} + (m-1+G)\,S_{n,m-1,k,n+m-1-k} \tag{A.3.90}$$
$$-(k+1)S_{nm,k+1,n+m-1-k} - (n+m-k)S_{nmk,n+m-k}\Big] = 0.$$

If one changes k to $k-1$ in the first term of the second line, the two terms in the second line can be effectively combined to yield

$$\sum_{k=0}^{n+m-1}\Big[(n-1+G)\,S_{n-1,mk,n+m-1-k} + (m-1+G)\,S_{n,m-1,k,n+m-1-k}\Big] \tag{A.3.91}$$
$$-(n+m)\sum_{k=0}^{n+m} S_{nmk,n+m-k} = 0.$$

Using (A.3.29), this is written as

$$(n-1+G)f_{n-1}^2 f_m^2 g_0^{(n-1,m)} + (m-1+G)f_n^2 f_{m-1}^2 g_0^{(n,m-1)} - (n+m)f_n^2 f_m^2 g_0^{(n,m)} = 0. \tag{A.3.92}$$

From (A.3.39),

$$\left(\frac{f_n}{f_{n+1}}\right)^2 = \frac{n+1}{n+G}, \tag{A.3.93}$$

hence

$$(n+m)g_0^{(n,m)} = ng_0^{(n-1,m)} + mg_0^{(n,m-1)}. \tag{A.3.94}$$

Since $C_{0000} = S_{0000} = 1$ by our choice of the time variable, $g_0^{(0,0)} = 1$. Furthermore, if either n or m is negative $g^{(n,m)} = 0$. First, fix $m = 0$, obtaining

$$g_0^{(n,0)} = g_0^{(n-1,0)} = \cdots = g_0^{(0,0)} = 1. \tag{A.3.95}$$

Analogously,

$$g_0^{(0,m)} = 1. \tag{A.3.96}$$

After that, the process can be repeated by fixing $m = 1$ and proving that

$$g_0^{(n,1)} = 1, \tag{A.3.97}$$

and further on by induction,

$$g_0^{(n,m)} = 1 \tag{A.3.98}$$

for all nonnegative n and m.

Analysis of $g_2^{(n,m)}$ proceeds in a similar fashion, and we shall be proving (A.3.38) directly. Multiply (3.1.11) by k^2, set $l = n + m - 1 - k$ and then sum over k from 1 to $n + m - 1$, which gives

$$\sum_{k=1}^{n+m-1} k^2 \Big[(n-1+G)\, S_{n-1,mk,n+m-1-k} + (m-1+G)\, S_{n,m-1,k,n+m-1-k} \tag{A.3.99}$$
$$- (k+1) S_{nm,k+1,n+m-1-k} - (n+m-k) S_{nmk,,n+m-k} \Big] = 0.$$

Replace k by $k - 1$ in the first term of the second line and combine the two terms of the second line into one sum:

$$\sum_{k=0}^{n+m-1} k^2 \Big[(n-1+G)\, S_{n-1,mk,n+m-1-k} + (m-1+G)\, S_{n,m-1,k,n+m-1-k} \Big] \tag{A.3.100}$$
$$- \sum_{k=0}^{n+m} \Big[(n+m-2)k^2 + k \Big] S_{nmk,n+m-k} = 0.$$

In terms of $g_p^{(n,m)}$, this is

$$(n-1+G) f_{n-1}^2 f_m^2 g_2^{(n-1,m)} + (m-1+G) f_n^2 f_{m-1}^2 g_2^{(n,m-1)} \tag{A.3.101}$$
$$- (n+m-2) f_n^2 f_m^2 g_2^{(n,m)} - f_n^2 f_m^2 g_1^{(n,m)} = 0.$$

Since we have already proved that $g_0^{(n,m)} = 1$, from Proposition 3.1.2.2, $g_1^{(n,m)} = (n+m)/2$. Then, by (A.3.93),

$$(n+m-2) g_2^{(n,m)} = n g_2^{(n-1,m)} + m g_2^{(n,m-1)} - \frac{n+m}{2}. \tag{A.3.102}$$

Since we have already proved (A.3.98), (A.3.37) holds, which (together with $g_2^{(n,m)} = 0$ for negative n or m) provides complete boundary conditions for solving (A.3.102).

We start with $m = 0$ in (A.3.102). The first order finite difference equation

$$(n-2)g_2^{(n,0)} = ng_2^{(n-1,0)} - \frac{n}{2} \tag{A.3.103}$$

has an unique solution matching $g_2^{(2,0)}$ given by (A.3.37), which is

$$g_2^{(n,0)} = \beta n^2 + \frac{1-2\beta}{2}n. \tag{A.3.104}$$

This manifestly agrees with (A.3.38).

The case $m = 1$ requires separate treatment, which we give explicitly for the sake of accuracy. (The proof for higher values of m will proceed inductively). One gets

$$(n-1)g_2^{(n,1)} = ng_2^{(n-1,1)} + \beta n^2 - \beta n - \frac{1}{2}. \tag{A.3.105}$$

The unique solution of this first order finite difference equation matching $g_2^{(1,1)}$ given by (A.3.37) is

$$g_2^{(n,1)} = \beta n^2 + n\left[2\gamma(1-2\beta) + \frac{1-2\beta}{2}\right] + \frac{1}{2}, \tag{A.3.106}$$

which agrees with (A.3.38).

Now assume that (A.3.38) holds for $m = M - 1$. By the symmetry of $g_2^{(n,m)}$ under permutation of n and m this also fixes

$$g_2^{(M-1,M)} = \beta((M-1)^2 + M^2) + 2\gamma(1-2\beta)M(M-1) + \frac{1-2\beta}{2}(2M+1), \tag{A.3.107}$$

which serves as the initial condition for solving

$$\begin{aligned}(n+M-2)g_2^{(n,M)} - ng_2^{(n-1,M)} \\ = M\Big[\beta(n^2 + (M-1)^2) + 2\gamma(1-2\beta)n(M-1) + \frac{1-2\beta}{2}(n+M-1)\Big] - \frac{n+M}{2}.\end{aligned} \tag{A.3.108}$$

The right hand side is a quadratic polynomial in n. The left hand side is a finite difference operator acting on g_2 so that for any polynomial g_2 it returns a polynomial of the same degree. Therefore, one can look for a particular solution in the form of quadratic polynomial by substituting a general polynomial in (A.3.108) and matching the coefficients. This gives

$$g_2^{(n,M)} = \beta(n^2 + M^2) + 2\gamma(1-2\beta)nM + \frac{1-2\beta}{2}(n+M), \tag{A.3.109}$$

which also happens to satisfy the initial condition (A.3.107). This means that (A.3.109) is the unique solution of the first order finite difference equation (A.3.108) satisfying (A.3.109). Hence, we have proved that $g_2^{(n,m)}$ still respects (A.3.38) at $m = M$. By

induction, this completes our proof of (A.3.32). The special case $\gamma = 1/2$ is treated similarly.

Proposition 3.1.2.2: *if the interaction coefficients satisfy $\mathcal{D}_{nmkl} = 0$, Z, defined in* (3.1.8)*, is a conserved quantity of the resonant system* (3.0.1).

Poof

From the resonant system (3.0.1), the time derivative of Z is given by

$$\dot{Z} \sim \sum_{n+m=k+l} \sqrt{(n+1)(n+G)}\, C_{nmkl} \bar{\alpha}_{n+1} \bar{\alpha}_m \alpha_k \alpha_l - \sum_{n+m+1=k+l} \sqrt{(n+1)(n+G)}\, C_{n+1,mkl} \bar{\alpha}_k \bar{\alpha}_l \alpha_m \alpha_n, \tag{A.3.110}$$

where the propotionality sign implies that we are omitting overall numerical factors.

It is convenient to re-express the above formula in terms of $\beta_n = \alpha_n / f_n$ and $S_{nkmj} = f_n f_k f_m f_j C_{nkmj}$. Using (A.3.93), this gives

$$\dot{Z} \sim \sum_{n+m=k+l} (n+G) S_{nmkl} \bar{\beta}_{n+1} \bar{\beta}_m \beta_k \beta_l - \sum_{n+m+1=k+l} (n+1) S_{n+1,mkl} \bar{\beta}_k \bar{\beta}_l \beta_m \beta_n. \tag{A.3.111}$$

We swap k with n and l with m in the second sum and redefine n to $n-1$ in the first sum (while remembering that S identically vanishes if any of its indices is negative). This gives

$$\dot{Z} \sim \sum_{n+m=k+l+1} \left[(n-1+G) S_{n-1,mkl} - (k+1) S_{nm,k+1,l}\right] \bar{\beta}_n \bar{\beta}_m \beta_k \beta_l. \tag{A.3.112}$$

Since both the summation and $\bar{\beta}_n \bar{\beta}_m \beta_k \beta_l$ are symmetric under permutations $(n \leftrightarrow m)$ and $(k \leftrightarrow l)$, in order for $\dot{Z}$ to vanish, it is sufficient to have the symmetric part of the expression in the square brackets with respect to the said permutations vanish. This is in fact identical to (3.1.11)-(3.1.12). The above argument is phrased for $\gamma > 1/2$. The proof for $\gamma = 1/2$ proceeds in a completely analogous fashion.

Proposition 3.1.2.3: *if $\mathcal{D}_{nmkl} = 0$, all solutions of* (3.1.7) *can be reached by acting on the stationary solutions* (3.1.9) *with symmetry transformations associated with the conserved quantities $N, J, \mathrm{Re}(Z), \mathrm{Im}(Z)$,* (3.0.4), (3.0.5), (3.1.8).

Poof

For systems that abide by the Z-conservations, the action of the associated symmetries must evidently be respected. The infinitesimal actions are constructed by computing the Poisson brackets of $\mathrm{Re}\, Z$ and $\mathrm{Im}\, Z$ with H given by (3.0.3), which produces two independent infenitesimal transformations, which can be compactly expressed in terms of $\beta_n = \alpha_n / f_n$ as

$$\delta\beta_n \sim \begin{cases} i\big(n\beta_{n-1} + (n+G)\beta_{n+1}\big) & \text{if } \gamma > \frac{1}{2}, \\ i\big(n\beta_{n-1} + \beta_{n+1}\big) & \text{if } \gamma = \frac{1}{2}, \end{cases} \tag{A.3.113}$$

and

$$\delta\beta_n \sim \begin{cases} n\beta_{n-1} - (n+G)\beta_{n+1} & \text{if } \gamma > \frac{1}{2}, \\ n\beta_{n-1} - \beta_{n+1} & \text{if } \gamma = \frac{1}{2}. \end{cases} \tag{A.3.114}$$

Within the ansatz (A.3.53) these infinitesimal transformations can be straightforwardly integrated to derive the following finite forms:

$$p \mapsto \frac{p - i\tanh\eta}{1 + ip\tanh\eta},, \tag{A.3.115}$$

$$a \mapsto \frac{ap}{(p\cosh\eta + i\sinh\eta)(\cosh\eta - ip\sinh\eta)^{G+1}}, \tag{A.3.116}$$

$$b \mapsto \frac{b(1+ip\tanh\eta) - iaG\tanh\eta}{(1+ip\tanh\eta)(\cosh\eta + ip\sinh\eta)^{G}}, \tag{A.3.117}$$

and

$$p \mapsto \frac{p + \tanh\xi}{1 + p\tanh\xi}, \tag{A.3.118}$$

$$a \mapsto \frac{ap}{(p\cosh\xi + \sinh\xi)(\cosh\xi + p\sinh\xi)^{G+1}}, \tag{A.3.119}$$

$$b \mapsto \frac{b(1+p\tanh\xi) - aG\tanh\xi}{(1+p\tanh\xi)(\cosh\xi + p\sinh\xi)^{G}}. \tag{A.3.120}$$

At $\gamma = 1/2$, these transformations can be written compactly in terms of one complex parameter ζ:

$$p \mapsto p + \zeta, \tag{A.3.121}$$

$$b \mapsto \left(b - ap\bar{\zeta}\right) e^{-p\bar{\zeta} - |\zeta|^2/2}, \tag{A.3.122}$$

$$a \mapsto \frac{ap}{p+\zeta} e^{-p\bar{\zeta} - |\zeta|^2/2}. \tag{A.3.123}$$

The above transformations can be used to generate dynamical solutions within the ansatz (A.3.53) from stationary solutions in a manner identical to the analysis of [73]. More specifically, starting with stationary solutions (A.3.76), displayed in (A.3.78)-(A.3.85), the parameter c allows choosing the overall scale of a and b, and q allows choosing the absolute value of p. Thereafter, applying (A.3.115)-(A.3.123) allows adjusting the magnitude and phase of a/b. Furthermore, the phase rotation symmetries $\alpha_n \mapsto e^{i\theta}\alpha_n$ and $\alpha_n \mapsto e^{i\theta n}\alpha_n$ can be used to arbitrarily adjust the common phase of a and b, and the phase of p, producing generic dynamical solutions within the ansatz (A.3.53).

Proposition 3.1.3.1: *the general solution of* (3.1.18), *subject to the symmetries inhered from* S_{nmkl} *and the regularity of* (3.1.16) *and its derivatives at the origin, is*

$$S(y,z,v,w) = \frac{\mathcal{F}\left(\ln\left[\frac{(1-vy)(1-wz)}{(1-vz)(1-wy)}\right]\right)}{\left[(1-vy)(1-vz)(1-wy)(1-wz)\right]^{G/2}}, \tag{A.3.124}$$

where $\mathcal{F}(x) = \mathcal{F}(-x)$ is an arbitrary symmetric function only restricted by regularity.

Poof

The general solutions of (3.1.18) can be constructed via the method of characteristics. Introduce ξ parameterizing the following curves

$$y = \frac{1}{\xi - \xi_y}, \qquad z = \frac{1}{\xi - \xi_z}, \qquad v = \xi, \qquad w = \xi - \xi_0. \tag{A.3.125}$$

The equation then becomes

$$\frac{d}{d\xi}\left((\xi - \xi_y)^G (\xi - \xi_z)^G S\right) = 0, \tag{A.3.126}$$

which is directly integrated as

$$(\xi - \xi_y)^G (\xi - \xi_z)^G S = A(\xi_y, \xi_z, \xi_0), \tag{A.3.127}$$

where A is an arbitrary function. Since ξ is simply v for our simple characteristics, it is convenient to eliminate it from the formulas in favor of v:

$$S = \frac{A(v - 1/y, v - 1/z, v - w)}{(yz)^G}. \tag{A.3.128}$$

Because of the symmetries of S, (3.1.18) must be obeyed as well after (y, z) is permuted with (v, w):

$$v(v\partial_v + G)S + w(w\partial_w + G)S - (\partial_y + \partial_z)S = 0. \tag{A.3.129}$$

By an argument identical to the one given above, we must have

$$S = \frac{B(y - 1/v, y - 1/w, y - z)}{(vw)^G}. \tag{A.3.130}$$

Finally, we can explore the compatibility condition of (3.1.18) and (A.3.129) by acting with $v(v\partial_v + a) + w(w\partial_w + a) - (\partial_y + \partial_z)$ on the former and $y(y\partial_y + a) + z(z\partial_z + a) - (\partial_v + \partial_w)$ on the latter and subtracting the results, which yields simply

$$(y\partial_y + z\partial_z - v\partial_v - w\partial_w)S = 0. \tag{A.3.131}$$

Hence,

$$S = C(yv, zv, yw, zw), \tag{A.3.132}$$

with some function C (the last of the four arguments is not independent of the first three, but it is convenient to present the dependences in this symmetric way). One can check that applying further commutation operations to (3.1.18), (A.3.129) and (A.3.131) does not result in any new compatibility conditions. It therefore remains to compare the three representations (A.3.128), (A.3.130) and (A.3.132).

We rewrite (A.3.128) as

$$S = \frac{\tilde{A}(v - 1/y, v - 1/z, v - w)}{(yz)^G \left[(1/y - v)(1/z - v)(1/y - v + (v - w))(1/z - v + (v - w))\right]^{G/2}}$$

$$= \frac{\tilde{A}(v-1/y, v-1/z, v-w)}{[(1-vy)(1-vz)(1-wy)(1-wz)]^{G/2}}. \tag{A.3.133}$$

Since the denominator only depends on vy, vz, wy and wz, and by (A.3.132), the entire S only depends on vy, vz, wy and wz, the newly introduced $\tilde{A}$ (whose arguments are explicitly indicated above) must also be expressible as a function of vy, vz, wy and wz only. By a similar argument from (A.3.130),

$$S = \frac{\tilde{B}(y-1/v, y-1/w, y-z)}{[(1-vy)(1-vz)(1-wy)(1-wz)]^{G/2}}, \tag{A.3.134}$$

where $\tilde{B}$ is a function that must be expressible both through the indicated variables and through vy, vz, wy and wz. Furthermore, by comparison with (A.3.133), it must also be expressible through $v-1/y$,$v-1/z$ and $v-w$. But there is only one combination of y, z, v, w that can be expressed through either (vy, vz, wy, wz) or $(v-1/y, v-1/z, v-w)$ or $(y-1/v, y-1/w, y-z)$, namely

$$\frac{(1-vy)(1-wz)}{(1-vz)(1-wy)}. \tag{A.3.135}$$

Thus, $\tilde{A}$ and $\tilde{B}$ must be functions of this ratio. Furthermore, since the interchange of y and z inverts this ratio while it should not change S, all of the constraints can be summarized by introducing an arbitrary even function $\mathcal{F}(x) = \mathcal{F}(-x)$ and writing the general S as

$$S(y,z,v,w) = \frac{\mathcal{F}\left(\ln\left[\frac{(1-vy)(1-wz)}{(1-vz)(1-wy)}\right]\right)}{[(1-vy)(1-vz)(1-wy)(1-wz)]^{G/2}}. \tag{A.3.136}$$

Proposition 3.1.3.2: *the general solution of* (3.1.19), *subject to the symmetries inhered from* S_{nmkl} *and the regularity of* (3.1.16) *and its derivatives at the origin, is*

$$S(y,z,v,w) = \mathcal{G}(y-z, v-w)e^{(y+z)(v+w)/2}, \tag{A.3.137}$$

where $\mathcal{G}$ *is non-singular at the origin, even in both arguments and symmetric under the permutation of the two arguments.*

Poof

The general solution of (3.1.19) is obtained by following the same procedure as for Proposition 3.1.3.1. It is

$$S = \mathcal{G}(y, z, v-w)e^{(y+z)(v+w)/2}, \tag{A.3.138}$$

with any $\mathcal{G}$. By symmetry under interchange of (y,z) and (v,w), $\mathcal{G}$ must depend on y and z only in combination $y-z$. We thus write

$$S(y,z,v,w) = \mathcal{G}(y-z, v-w)e^{(y+z)(v+w)/2}, \tag{A.3.139}$$

where $\mathcal{G}$ is non-singular at the origin, even in both arguments and symmetric under the permutation of the two arguments. Note that in this case the solution for S contains an arbitrary function of two variables rather than one variable as in (3.1.20). The smaller number of constraints on the solution in this case can already be seen at the level of (3.1.19), since this equation is automatically compatible with its counterpart obtained by interchanging (y, z) and (v, w), not resulting in any extra compatibility conditions.

Proposition 3.1.5.1: *If the summations* (3.1.4) *have the form*

$$g_l^{(n,m)} = \sum_{i=0}^{\kappa l+\delta} g_i n^i m^{\kappa l+\delta-i}, \tag{A.3.140}$$

with $\kappa, \delta \in \mathbb{N}$, $g_i \in \mathbb{R}$ *such that* $g_l^{(n,m)} = g_l^{(m,n)}$. *The ansatz* (3.1.31) *only closes in* (3.0.1), *leaving all the function* a_i *and* p *free, in the next situations*

$$g_l^{(n,m)} = \sum_{i=0}^{l} g_i n^i m^{l-i} \quad \text{and } N = 1 \tag{A.3.141}$$

$$g_l^{(n,m)} = \sum_{i=0}^{l+1} g_i n^i m^{l+1-i} \quad \text{and } N = 0 \tag{A.3.142}$$

Proof

For our purpose we will look at the powers of n on the LHS and RHS, if the highest powers are the same in both sides the ansatz has an opportunity. Nevertheless, if the highest powers are not the same, additional restrictions can be required (we will not study this situation).

Inserting the ansatz (3.1.31) in (3.0.1) and multiplying both the equation by $1/(f_n p^n)$ the LHS becomes a polynomial in n of degree $N+1$, while the RHS is written as

$$\frac{1}{f_n p^n} \sum_{m=0}^{\infty} \sum_{k=0} C_{nmkl} \bar{\alpha}_m \alpha_k \alpha_{n+m-k} = \sum_{l,i,j}^{N} \bar{a}_l a_i a_j \sum_{m=0}^{\infty} f_m^2 |p|^{2m} m^l \sum_{k=0} \frac{f_k f_{n+m-k}}{f_n f_m} C_{nmkl} k^i (n+m-k)^j. \tag{A.3.143}$$

Using the definition (A.3.29) and paying only attention n it can be written as

$$\sum_{l,i,j}^{N} \bar{a}_l a_i a_j \sum_{m=0}^{\infty} f_m^2 |p|^{2m} m^l g_{j+i}^{(n,m)} n^{N-j} A_j(m,k), \tag{A.3.144}$$

where $A_j(m,k)$ gathers the contributions of j, m, k. As the LHS is a polynomial in n the only possibility for the closure of (3.1.31) is that the summation identities $g_l^{(n,m)}$ are polynomials in n, m for $l = 0, 1, ..., 2N$. Note that negative powers are not allowed due to $g_l^{(n,m)}$ must be finite for $n = 0$ and we are requiring that (A.3.144) is a polynomial in n. At this point many possibilities can be imposed (taking into account that due to the

resonant condition any $g_{2l+1}^{(n,m)}$ is determined by the set $\{g_{2l}^{(n,m)}, g_{2l-2}^{(n,m)}, ..., g_{2}^{(n,m)}, g_{0}^{(n,m)}\}$). Our experience with different resonant models shows that the next election is suitable

$$g_l^{(n,m)} = \sum_{i=0}^{\kappa l+\delta} g_i n^i m^{\kappa l+\delta-i}, \tag{A.3.145}$$

with $\kappa = 1, 2, ...(\kappa = 0$ is discarded using Proposition 3.1.1.3: $g_1^{(n,m)} = (n+m)g_0^{(n,m)})$, $\delta = 0, 1, 2, ...,\ g_i \in \mathbb{R}$ such that $g_l^{(n,m)} = g_l^{(m,n)}$. With this supposition the highest power of the RHS becomes $n^{2\kappa N+\delta}$, while highest powers of the LHS is n^{N+L}. Finally, we obtain that the only possibilities for N to match both powers are $(\kappa, \delta, N):\ (1, 0, 1),\ (1, 0, 1)$.

Proposition 3.1.5.2: *if* (3.1.35) *is satisfied, the solutions of* (3.1.36) *are stationary states of the form*

$$\alpha_n(\tau) = Ae^{i(\lambda+n\omega)\tau}, \tag{A.3.146}$$

where A is the amplitude and the expressions for λ, ω can be found in the appendix A.3.2.

Proof

We suppose that the interaction coefficients satisfy the symmetries $C_{nmkl} = C_{mnkl} = C_{nmlk} = C_{klnm}$ and the summation property

$$g_0^{(n,m)} = \sum_{k=0}^{n+m} \frac{f_k f_{n+m-k}}{f_n f_m} C_{nmk(n+m-k)} = \eta + \sigma(n+m). \tag{A.3.147}$$

We will also use the conserved quantities (3.0.4)-(3.0.5). For the ansatz (3.1.36) they become

$$N = |b|^2 F_0, \qquad J = |b|^2 F_1. \tag{A.3.148}$$

Introducing (3.1.36) in the resonant equation (3.0.1), gathering terms with the same power of n and using (A.3.148) we obtain the equations

$$i\dot{b} = (\eta N + \sigma J)b, \tag{A.3.149}$$

$$i\dot{p} = \sigma N p. \tag{A.3.150}$$

Thus

$$b(\tau) = Be^{-i\lambda\tau}, \qquad p(\tau) = Ae^{-i\omega\tau}, \tag{A.3.151}$$

with

$$\lambda = (\eta N + \sigma J), \qquad \omega = \sigma N. \tag{A.3.152}$$

Proposition 3.2.1.1: *If the RHS of* (3.2.10) *does not contain solutions of the homogeneous equation (it is equivalent to $\Omega_{nkl} - 2C_{n0n0} \neq 0\ \forall n, l, k > 0$), hence its solution is*

$$q_n(\tau) = \sum_{l=0}^{n-1} \sum_{k=1}^{\mathcal{N}_{nl}} A_{nkl} e^{-i\Omega_{nkl}\tau}, \tag{A.3.153}$$

where $\mathcal{N}_{nl}$, Ω_{nkl} and A_{nkl} are integer, real and complex numbers respectively. The meaning of each component and the expressions of Ω_{nkl} can be found below, in (3.2.17)-(3.2.18) or in appendix A.3.2.

Poof

We are going to prove that (3.2.15) is solution of (3.2.10) with

$$\Omega_{nkl} = \sum_{j=1}^{n} a_{nj}\theta_j - l\theta_0, \tag{A.3.154}$$

where $\theta_0 = C_{0000}$, $\theta_{n>0} = 2C_{n0n0}$ and a_{nk} are the positive integer solutions of the constraints

$$\sum_{j=1}^{n} a_{nj}\ j = n \qquad \sum_{j=1}^{n} a_{nj} = l+1 \qquad 0 \le a \le n \qquad 0 \le l < n \tag{A.3.155}$$

The subscript k simply labels each possible solution (A.3.155) for fixed n, l and $\mathcal{N}_{nl}$ denotes the total number of these solutions. Note that for $l = 0$ there is only the solution $\Omega_{n10} = 2C_{n0n0}$ which corresponds with the solution of the homogeneous equation. If for any $0 < l < n$ exists k such that $\Omega_{nkl} = 2C_{n0n0}$, (3.2.10) has secular terms, (3.2.15) is not valid and the expansion (3.2.1) is invalidated at times $t \sim 1/\delta$.

A proof by induction fits very well this problem:

- n = 1:

  In this situation the RHS is $|q_0|^2 q_1 \sim e^{i\theta_1 \tau}$. From formulas (A.3.154) and (A.3.155) we obtain the same result $\Omega_{111} = \theta_1$.

- n:

  We claim that the frequencies satisfy:

$$\Omega_{nkl} = \sum_{j=1}^{n} a_{nj}\theta_j - l\theta_0 \tag{A.3.156}$$

$$\sum_{j=1}^{n} a_{nj}\ j = n \qquad \sum_{j=1}^{n} a_{nj} = l+1 \qquad 0 \le a \le n \qquad 0 \le l < n \tag{A.3.157}$$

- n + 1:

  We will consider first the terms of the RHS $\bar{q}_0 q_i q_{n+1-i}$ with $i \neq 0, (n+1)$. For them we can use (A.3.156) to obtain the frequencies

$$\Omega_{ik\hat{l}} + \Omega_{(n+1-i)k\tilde{l}} - \theta_0 = \sum_{j=1}^{i} \hat{a}_{ij}\theta_j + \sum_{j=1}^{n+1-i} \tilde{a}_{(n+1-i)j}\theta_j - \left(\hat{l} + \tilde{l} + 1\right)\theta_0 \tag{A.3.158}$$

Where the constraints are satisfied individually:

$$\sum_{j=1}^{i} \hat{a}_{ij}\ j = i \qquad \sum_{j=1}^{i} \hat{a}_{ij} = \hat{l} + 1 \qquad 0 \leq \hat{a} \leq k \qquad 0 \leq \hat{l} < i \tag{A.3.159}$$

$$\sum_{j=1}^{(n+1-i)} \tilde{a}_{(n+1-i)j}\ j = (n+1-i) \qquad \sum_{j=1}^{n+1-i} \tilde{a}_{(n+1-i)j} = \tilde{l} + 1$$

$$0 \leq \tilde{a} \leq (n+1-i) \quad 0 \leq \tilde{l} < (n+1-i) \tag{A.3.160}$$

For $\hat{a}_{ij}$ and $\tilde{a}_{(n+1-i)j}$ the index j runs from 1 to i and $(n+1-i)$ respectively. For our purpose we fill with zeros the components until covering j from 1 to n meaning that now (A.3.158) can be written as

$$\Omega_{ik\hat{l}} + \Omega_{(n+1-i)k\tilde{l}} - \theta_0 = \sum_{j=1}^{n+1} \left(\hat{a}_{ij} + \tilde{a}_{(n+1-i)j}\right) \theta_j - l\theta_0 \tag{A.3.161}$$

with $l \equiv \left(\hat{l} + \tilde{l} + 1\right)$. Note that $n+1$ is greater than i and $(n+1-i)$. However it is not a problem due to for each of them we filled additional values of j with zeros. Making the same with the constraints for $a = \hat{a} + \tilde{a}$ we obtain that

$$\sum_{j=1}^{n+1} \left(\hat{a}_{ij} + \tilde{a}_{(n+1-i)j}\right)\ j = n+1 \quad \sum_{j=1}^{n+1} \left(\hat{a}_{ij} + \tilde{a}_{(n+1-i)j}\right) = \hat{l} + \tilde{l} + 2 = l + 1 \tag{A.3.162}$$

$$0 \leq (\hat{a} + \tilde{a}) \leq (n+1) \quad 1 \leq \left(\hat{l} + \tilde{l} + 1\right) < (n+1)$$

This expression almost corresponds with (A.3.156) and (A.3.157) for $n+1$, except for $l = 0$ which is generated by $|q_0|^2 q_{n+1}$ and corresponds to the homogeneous equation. It has frequency $2C_{(n+1)0(n+1)0}$ that matches with $\Omega_{(n+1)10}$ as was explained at the beginning of this proof.

Proposition CF: (3.3.8) *satisfies* $\mathcal{D}_{nmkl} = 0$ *for* $n + m - k - l = 1$ *with* $G = 2$ *and* $\beta = 1/3$, *defined in* (3.1.2).

Proof

Taking the interaction coefficients (3.3.8) they trivially satisfy the symmetries (3.0.2).

Now we calculate S_{nmkl} from (3.3.8) using (A.3.28) and setting $G = 2$ in (A.3.39)

$$S_{nmkl} = \min(n, m, k, l) + 1. \tag{A.3.163}$$

Now we are ready to compute $\mathcal{D}_{nmkl}$ defined in (3.1.12). We can check by direct computation that for the resonant channel $n+m=k+l+1$, $\mathcal{D}_{nmkl}=0$ (remember that in this expression the resonant channel has this form). It can also be checked the relation

$$2\min(n,m,k,n+m-k)=n+m-|k-n|-|k-m|. \tag{A.3.164}$$

Proposition rGP: (3.3.22) *satisfies* $\mathcal{D}_{nmkl}=0$ *for* $n+m-k-l=1$ *with* $G=\mu+1$ *and* $\beta=3/8$, *defined in* (3.1.2).

Proof

We are going to show that the interaction coefficients (3.3.22) satisfy (3.1.11)-(3.1.12) provided that $n+m=k+l+1$, which are the only values of the indices in (3.1.11-3.1.12) for which the conditions constrain the interaction coefficients actually appearing in the resonant system (3.0.1).

Setting $G=\mu+1$ through (A.3.28)

$$S_{nmkl}=2\frac{\Gamma(\mu+1)\Gamma\left(\frac{1}{2}\right)}{\Gamma\left(\mu+\frac{1}{2}\right)}\int_0^\infty d\rho\, e^{-2\rho}\rho^{2\mu}L_n^\mu(\rho)L_m^\mu(\rho)L_k^\mu(\rho)L_l^\mu(\rho), \tag{A.3.165}$$

and therefore

$$\begin{aligned}\mathcal{D}_{nmkl}\sim\int_0^\infty d\rho\, e^{-2\rho}\rho^{2\mu}\big[&(n+\mu)L_{n-1}^\mu L_m^\mu L_k^\mu L_l^\mu+(m+\mu)L_n^\mu L_{m-1}^\mu L_k^\mu L_l^\mu \\ &-(k+1)L_n^\mu L_m^\mu L_{k+1}^\mu L_l^\mu-(l+1)L_n^\mu L_m^\mu L_k^\mu L_{l+1}^\mu\big].\end{aligned} \tag{A.3.166}$$

We now use

$$nL_n^\mu=(n+\mu)L_{n-1}^\mu-\rho L_{n-1}^{\mu+1} \tag{A.3.167}$$

in all four terms to rewrite the above as

$$\begin{aligned}\mathcal{D}_{nmkl}\sim\int_0^\infty d\rho\, e^{-2\rho}\rho^{2\mu}\big[&(n+m-k-l-2\mu-2)L_n^\mu L_m^\mu L_k^\mu L_l^\mu \\ &+\rho(L_{n-1}^{\mu+1}L_m^\mu L_k^\mu L_l^\mu+L_n^\mu L_{m-1}^{\mu+1}L_k^\mu L_l^\mu+L_n^\mu L_m^\mu L_k^{\mu+1}L_l^\mu+L_n^\mu L_m^\mu L_k^\mu L_l^{\mu+1})\big].\end{aligned} \tag{A.3.168}$$

Thereafter, we use $n+m-k-l=1$ in the first line and

$$L_n^\mu=L_n^{\mu+1}-L_{n-1}^{\mu+1} \tag{A.3.169}$$

in the last two terms of the second line to obtain

$$\begin{aligned}\mathcal{D}_{nmkl}\sim\int_0^\infty d\rho\, e^{-2\rho}\rho^{2\mu}\big[&(2\rho-2\mu-1)L_n^\mu L_m^\mu L_k^\mu L_l^\mu \\ &+\rho(L_{n-1}^{\mu+1}L_m^\mu L_k^\mu L_l^\mu+L_n^\mu L_{m-1}^{\mu+1}L_k^\mu L_l^\mu+L_n^\mu L_m^\mu L_{k-1}^{\mu+1}L_l^\mu+L_n^\mu L_m^\mu L_k^\mu L_{l-1}^{\mu+1})\big].\end{aligned} \tag{A.3.170}$$

Finally, we use

$$\partial_\rho L_n^\mu=-L_{n-1}^{\mu+1} \tag{A.3.171}$$

to obtain

$$\mathcal{D}_{nmkl} \sim \int_0^\infty d\rho\, e^{-2\rho}\rho^{2\mu}(2\rho - 2\mu - 1 - \rho\partial_\rho)L_n^\mu L_m^\mu L_k^\mu L_l^\mu, \tag{A.3.172}$$

which is the same as

$$\mathcal{D}_{nmkl} \sim \int_0^\infty d\rho\, \partial_\rho\Big[e^{-2\rho}\rho^{2\mu+1}L_n^\mu L_m^\mu L_k^\mu L_l^\mu\Big] = e^{-2\rho}\rho^{2\mu+1}L_n^\mu(\rho)L_m^\mu(\rho)L_k^\mu(\rho)L_l^\mu(\rho)\Big|_{\rho=0}^{\rho=\infty}, \tag{A.3.173}$$

which evidently equals 0.

Proposition xLL: (3.3.28) *satisfies* (3.1.11) *with* $\gamma = 1/2$ *and* $\beta = (3L-1)/4(2L-1)$, *defined in* (3.1.2).

Proof

We are going to prove that (3.3.27) satisfy (3.1.11)-(3.1.12) with $\gamma = 1/2$, provided that $n + m = k + l + 1$. We start by writing (A.3.28).

$$S_{nmkl} = \frac{2^{2L+1}(L!)^4}{(2L)!n!m!k!l!}\int_0^\infty d\rho\, e^{-2\rho}\rho^{n+m-2L}L_L^{n-L}(\rho)L_L^{m-L}(\rho)L_L^{k-L}(\rho)L_L^{l-L}(\rho), \tag{A.3.174}$$

and therefore

$$\begin{aligned} n!m!k!l!\mathcal{D}_{nmkl} \sim \int_0^\infty d\rho\, e^{-2\rho}\rho^{n+m-1-2L}\big[&nL_L^{n-1-L}L_L^{m-L}L_L^{k-L}L_L^{l-L} + mL_L^{n-L}L_L^{m-1-L}L_L^{k-L}L_L^{l-L} \\ &- \rho L_L^{n-L}L_L^{m-L}L_L^{k+1-L}L_L^{l-L} - \rho L_L^{n-L}L_L^{m-L}L_L^{k-L}L_L^{l+1-L}\big]. \end{aligned} \tag{A.3.175}$$

Applying (A.3.169) followed by (A.3.167) in the first line, and (A.3.169) in the second line, we get

$$\begin{aligned} \mathcal{D}_{nmkl} \sim \int_0^\infty d\rho\, e^{-2\rho}\rho^{n+m-1-2L}\big[&(n+m-2L-2\rho)L_L^{n-L}L_L^{m-L}L_L^{k-L}L_L^{l-L} \\ &- \rho(L_{L-1}^{n+1-L}L_L^{m-L}L_L^{k-L}L_L^{l-L} + L_L^{n-L}L_{L-1}^{m+1-L}L_L^{k-L}L_L^{l-L} \\ &+ L_L^{n-L}L_L^{m-L}L_{L-1}^{k+1-L}L_L^{l-L} + L_L^{n-L}L_L^{m-L}L_L^{k-L}L_{L-1}^{l+1-L})\big]. \end{aligned} \tag{A.3.176}$$

Due to (A.3.171), this is the same as

$$\begin{aligned} \mathcal{D}_{nmkl} \sim \int_0^\infty d\rho\, \partial_\rho\big[e^{-2\rho}\rho^{n+m-2L}L_L^{n-L}L_L^{m-L}L_L^{k-L}L_L^{l-L}\big] \\ = e^{-2\rho}\rho^{n+m-2L}L_L^{n-L}L_L^{m-L}L_L^{k-L}L_L^{l-L}\Big|_{\rho=0}^{\rho=\infty}, \end{aligned} \tag{A.3.177}$$

which evidently equals 0. (Note that $n + m = k + l + 1$, and the polynomials $L_L^{n-L}(\rho)$ do not include any powers of ρ below ρ^{L-n}, which ensures that the contribution at $\rho = 0$ vanishes.)

Proposition mrSd: *for* $d = 3$, (3.3.49) *satisfies* $\mathcal{D}_{nmkl} = 0$ *for* $n + m - k - l = 1$ *with* $G = 1$ *and* $\beta = 1/3$, *defined in* (3.1.2).

Proof

We are going to show that (3.3.49) for $d = 3$ satisfy (3.1.11) with $G = 1$ restricted to the resonant channel $n + m = k + l + 1$. First we calculate (A.3.28),

$$S_{nmkl} = \frac{1}{1 + n + m}. \tag{A.3.178}$$

Now the computation of $\mathcal{D}_{nmkl} = 0$ is straightforward.

Proposition mrAdS: (3.3.59) *satisfies* $\mathcal{D}_{nmkl} = 0$ *for* $n + m - k - l = 1$ *with* $G = \delta$ *and* $\beta = \frac{1}{2}\frac{\delta+1}{2\delta+1}$, *defined in* (3.1.2).

Proof

We are going to show that (3.3.59) satisfy (3.1.11) with $G = \delta$ restricted to the resonant channel $n + m = k + l + 1$. First we calculate (A.3.28),

$$S_{nmkl} = \frac{\Gamma(2\delta)}{\Gamma(\delta)^2}\frac{\Gamma(n+\delta)\Gamma(k+\delta)\Gamma(m+\delta)\Gamma(l+\delta)}{\Gamma(n+1)\Gamma(k+1)\Gamma(m+1)\Gamma(l+1)}\frac{\Gamma(n+m+1)}{\Gamma(n+m+2\delta)}. \tag{A.3.179}$$

Now the computation of $\mathcal{D}_{nmkl} = 0$ is straightforward.

Proposition nrAdS: (3.3.74) *satisfies* $\mathcal{D}_{nmkl} = 0$ *for* $n + m - k - l = 1$ *with* $G = 2$ *and* $\beta = \frac{3}{8}$, *defined in* (3.1.2).

Proof

This proof can be found in appendix B of [78].

Generating Function $G_L(s, \rho)$**:**

We start by establishing (3.3.32) as a consequence of (3.3.15):

$$\begin{aligned} G_L(s,\rho) = \sum_{n=0}^{\infty}\frac{s^n}{n!}L_L^{n-L}(\rho) &= \frac{1}{L!}\partial_t^L\sum_{n=0}^{\infty}\frac{s^n}{n!}\frac{e^{-\frac{t\rho}{1-t}}}{(1-t)^{n-L+1}}\bigg|_{t=0} \\ &= \frac{e^s}{L!}\partial_t^L\Big((1-t)^{L-1}e^{-\frac{t(\rho-s)}{1-t}}\Big)\Big|_{t=0} = \frac{e^s(s-\rho)^L}{L!}. \end{aligned} \tag{A.3.180}$$

The last equality can be obtained by first noticing that $\partial_t^L\big((1-t)^{L-1}e^{-\frac{tx}{1-t}}\big)$ at $t = 0$ is a polynomial of degree L in x. Computing its derivatives at $x = 0$ straightforwardly shows that the first $L - 1$ derivatives vanish, while the Lth derivative is $L!(-1)^L$. Hence the polynomial is simply $(-x)^L$, which gives the desired result.

Complex Plane Representation:

We are going to present the technical details in relation to the complex plane representation of resonant systems (3.0.1) satisfying (3.1.11). For brevity, we shall not be treating this special case here, and will concentrate on generic values of G ($\gamma > 1/2$). For this purpose we defined

$$\beta_n = \frac{\alpha_n}{f_n}, \qquad S_{nmkl} = f_n f_m f_k f_l C_{nmkl}. \tag{A.3.181}$$

The resonant system (3.3.116) can be expressed through β_n defined by (A.3.181) as

$$i\frac{(G)_n}{n!}\frac{d\beta_n}{dt} = \sum_{n+m=k+l} S_{nmkl}\bar{\beta}_m\beta_k\beta_l. \tag{A.3.182}$$

In order to take advantage of Propositions 3.1.3.1-3.1.3.2, we introduce the following generating functions for β_n:

$$u(t,z) = \sum_{n=0}^{\infty}\beta_n z^n, \qquad \tilde{u}(t,z) = \sum_{n=0}^{\infty}\frac{\bar{\beta}_n}{z^n}, \tag{A.3.183}$$

so that

$$\beta_n(t) = \frac{1}{2\pi i}\oint\frac{dz}{z^{n+1}}u(z,t), \qquad \bar{\beta}_n = \frac{1}{2\pi i}\oint dz\, z^{n-1}\tilde{u}(z,t). \tag{A.3.184}$$

Note that the integration contour for β_n must not enclose any singularities of u, while the integration contour for $\bar{\beta}_n$ must enclose all singularities of $\tilde{u}$. The tilde-conjugation can be understood as taking complex conjugates of the values of u on the unit circle, and then analytically continuing away from the unit circle to obtain $\tilde{u}$. One can also write

$$\tilde{u}(z) = \overline{u\,(1/\bar{z})}. \tag{A.3.185}$$

Substituting (A.3.184) to (A.3.182), multiplying with z^n and summing over n, one gets

$$\frac{i}{\Gamma(G)}\partial_t\partial_z^{G-1}(z^{G-1}u(t,z)) = \frac{1}{(2\pi i)^3}\oint\frac{ds}{s}\oint\frac{dv}{v}\oint\frac{dw}{w}S(z,s,1/v,1/w)\tilde{u}(t,s)u(t,v)u(t,w), \tag{A.3.186}$$

where we have used the fact that the constraint $n+m=k+l$ in the summation can be ignored since S_{nmkl} extracted from the generating function S automatically vanish unless this constraint is satisfied. The integration contours for v and w are outside the unit circle but do not enclose any singularities of u, while the integration contour for s is inside the unit circle and encloses all singularities of $\tilde{u}$. Note that to ensure convergence in the resummation of S according to Propositions 3.1.3.1-3.1.3.2, $|v|$ and $|w|$ must be greater than both $|z|$ and $|s|$. The fractional derivative $\partial_z^{(G-1)}$ is defined by its action on powers of z

$$\partial_z^a z^b = \frac{\Gamma(b+1)}{\Gamma(b-a+1)}z^{b-a}, \tag{A.3.187}$$

with Γ being the usual Euler's Γ-function. This simple-minded definition goes back to the very origins of the fractional calculus [212, 213]. In general, acting with fractional derivatives on integer powers of z produces fractional powers, which are not single-valued, which is a source of ambiguities in defining fractional calculus. Note, however, that applying $\partial_z^a z^a$ to an analytic function, which is the only operation we need for (A.3.186), always results in an analytic function, hence no subtleties occur in this case. The way (A.3.187) enters the complex plane representation of (3.1.25) is through the relation $\Gamma(n+G)/\Gamma(n+1) = \Gamma(G)\ (G)_n/n!$.

We note that the differentiation defined by (A.3.187) can be equally well implemented via a Cauchy-like complex contour formula for the operator $\partial_z^a z^a$ featured in (A.3.186) acting on a holomorphic function $f(z)$:

$$\partial_z^a (z^a f(z)) = \frac{\Gamma(a+1)}{2\pi i} \oint \frac{s^a\, f(s)\, ds}{(s-z)^{a+1}}. \tag{A.3.188}$$

Indeed, expanding $f(s)$ in terms of integer powers of s, we see that (A.3.188) acts on the individual powers in accordance with (A.3.187), as can be verified by evaluating the residue at $s = \infty$. (Note that, for noninteger a, there is a cut in the complex plane, but it only extends from $s = 0$ to $s = z$, without affecting the evaluation of the residue at $s = \infty$. The integration contour is defined to lie outside this cut.)

A representation of the form (A.3.186) has been previously obtained for the conformal flow [75], which corresponds in our present language to $G = 2$ (while the right-hand side integral can be further simplified due to particular factorization properties of S in the case of the conformal flow). Our present derivation has established this representation for the entire class of partially solvable resonant systems satisfying (3.1.11), of which the conformal flow is a representative. One can substitute (3.1.20) into (A.3.186) to obtain explicitly

$$\frac{i}{\Gamma(G)} \partial_t \partial_z^{G-1} (z^{G-1} u(t,z)) = \frac{1}{(2\pi i)^3} \oint \frac{ds\, dv\, dw}{s\,(vw)^{1-G}} \frac{\tilde{u}(t,s) u(t,v) u(t,w)\ \mathcal{F}\left(\ln\left[\frac{(v-s)(w-z)}{(v-z)(w-s)}\right]\right)}{[(v-s)(v-z)(w-s)(w-z)]^{G/2}}, \tag{A.3.189}$$

Note the emergence of the cross-ratio $(v-s)(w-z)/(v-z)(w-s)$, which is a conformally invariant combination of the coordinates of four points (z, s, v, w) on the complex plane [214].

Stationary States Bifurcating from the Lowest Mode:

We claim that

$$u(t,z) = \frac{e^{-i\lambda t}}{1-pz} \tag{A.3.190}$$

solves (A.3.186) for any complex value of p (and some p-dependent value of λ). Note that if one sends p to 0, one obtains $u(t,z) = e^{-i\lambda t}$, which does not depend on z and corresponds to $\alpha_{n\geq 0} = 0$, i.e., to the single-mode stationary states supported by mode 0. Thus, our family (A.3.190) bifurcates from mode 0, as anticipated in the title.

The LHS of (A.3.189) becomes simply

$$\frac{\lambda e^{-i\lambda t}}{(1-pz)^G}, \tag{A.3.191}$$

as one can easily see by applying (A.3.188) and evaluating the residue at $1/p$. For the RHS of (A.3.189), we first note that

$$\tilde{u}(t,z) = \frac{e^{i\lambda t}}{1-\bar{p}/z}. \tag{A.3.192}$$

Hence, the RHS of (A.3.189) may be written as

$$\frac{e^{-i\lambda t}}{(2\pi i)^3}\oint \frac{ds\,dv\,dw}{s\,(vw)^{1-G}}\frac{\mathcal{F}\left(\ln\left[\frac{(v-s)(w-z)}{(v-z)(w-s)}\right]\right)}{[(v-s)(v-z)(w-s)(w-z)]^{G/2}}\frac{1}{1-\bar{p}/s}\frac{1}{1-pv}\frac{1}{1-pw}, \tag{A.3.193}$$

Consider first the integral over v. There are branch cuts connecting $v=0$, $v=z$ and $v=s$, but all of these branch cuts are inside the integration contour, while the simple pole at $v=1/p$ is outside the contour. Thus, the integral can be evaluated as the residue at $v=1/p$. The same argument applies to the integral over w. Implementing these two operations, one gets:

$$\frac{1}{(1-pz)^G}\frac{e^{-i\lambda t}}{2\pi i}\oint \frac{ds}{(s-\bar{p})(1-sp)^G}. \tag{A.3.194}$$

Note that at $v=w=1/p$ the argument of $\mathcal{F}$ has turned into 0, while we have assumed $\mathcal{F}(0)=1$ by a choice of the time scale. The function $\mathcal{F}$ has thus dropped out from our expression at this stage. As far as the remaining integral over s is concerned, once again, there is a branch cut outside the integration contour, but inside there is only a simple pole, so one can express the result through the residue, obtaining

$$\frac{1}{(1-|p|^2)^G}\frac{e^{-i\lambda t}}{(1-pz)^G}. \tag{A.3.195}$$

This expression for the RHS of (A.3.189) manifestly matches the LHS given by (A.3.191). The equations of motion are thus satisfied by our family of stationary states (A.3.190) provided that

$$\lambda = \frac{1}{(1-|p|^2)^G}. \tag{A.3.196}$$

Note that this holds for every value of G, and irrespectively of the form of the arbitrary function $\mathcal{F}$ contained in the definition (3.1.21) of our class of resonant systems.

Stationary States Bifurcating from Higher Modes:

We now proceed with the stationary solutions bifurcating from mode number N. We claim that the relevant generating function $u(t,z)$ satisfies

$$u(t,z) = e^{-i\lambda t}u(z), \qquad \partial_z^{G-1}(z^{G-1}u(z)) = \frac{(\bar{p}-z)^N}{(1-pz)^{N+G}}. \tag{A.3.197}$$

Indeed, if $p = 0$, $\partial_z^{G-1}(z^{G-1}u)$ is proportional to z^N, and hence u itself is proportional to z^N, i.e., the only nonvanishing α_n is α_N. (The above formula, as well as (A.3.190), originated as a guess based on numerical experimentation, before being provided an analytic proof that we are about to present.)

We have specified $u(z)$ through the result of acting on it with $\partial_z^{G-1} z^{G-1}$. What about $u(z)$ itself? We can say that it is of the form

$$u(z) = \sum_{k=0}^{N} \frac{c_k}{(1-pz)^{k+1}}, \tag{A.3.198}$$

though we are not aware of simple explicit expressions for c_k. Differentiation of the individual terms in (A.3.198) follows the rule

$$\partial_z^{G-1} \frac{z^{G-1}}{(1-pz)^{k+1}} = \frac{\Gamma(G)}{2\pi i} \oint \frac{ds}{(s-z)^G} \frac{s^{G-1}}{(1-ps)^{k+1}} = \frac{\Gamma(G)}{(-p)^{k+1}} \partial_s^k \frac{s^{G-1}}{(s-z)^G}\bigg|_{s=1/p}. \tag{A.3.199}$$

The last expression is evidently a linear combination of terms of the form $1/(1-pz)^G$, $1/(1-pz)^{G+1}$, ..., $1/(1-pz)^{G+k}$. Hence, $\partial_z^{G-1}(z^{G-1}u(t,z))$ is a linear combinations of terms of the form $1/(1-pz)^G$, $1/(1-pz)^{G+1}$, ..., $1/(1-pz)^{G+N}$ with coefficients that are themselves linear combinations of c_0, c_1, ..., c_N. By tuning these $N+1$ coefficients, we can make $\partial_z^{G-1}(z^{G-1}u(t,z))$ equal $1/(1-pz)^{G+N}$ times an arbitrary polynomial of degree N in z, and in particular, we can make it equal (A.3.197).

With these preliminaries, the LHS of (A.3.186) is by construction

$$\frac{\lambda\, e^{-i\lambda t}}{\Gamma(G)} \frac{(\bar{p}-z)^N}{(1-pz)^{N+G}}, \tag{A.3.200}$$

and we have to prove that the RHS of (A.3.186), given by

$$\frac{e^{-i\lambda t}}{(2\pi i)^3} \oint \frac{ds\, dv\, dw}{s\,(vw)^{1-G}} \frac{\tilde{u}(s)u(v)u(w)\ \mathcal{F}\left(\ln\left[\frac{(v-s)(w-z)}{(v-z)(w-s)}\right]\right)}{[(v-s)(v-z)(w-s)(w-z)]^{G/2}}, \tag{A.3.201}$$

matches this form. Our proof will proceed in two steps. In step 1, we shall show that (A.3.201) must be of the form

$$\frac{Q_N(z)\, e^{-i\lambda t}}{(1-pz)^{N+G}}, \tag{A.3.202}$$

where $Q_N(z)$ is a polynomial of degree N in z. In step 2, we shall show that (A.3.201) and its first $N-1$ z-derivatives must vanish at $z = \bar{p}$, which means that (A.3.201) has a degree N zero at that point. Combined, these two facts imply that (A.3.201) is proportional to

$$e^{-i\lambda t} \frac{(\bar{p}-z)^N}{(1-pz)^{N+G}}, \tag{A.3.203}$$

The coefficient of proportionality simply fixes λ, and in view of (A.3.200), the equation of motion (A.3.189) is satisfied. We now proceed filling in the details of step 1 and step 2

required to complete the proof. In handling (A.3.201) below, we shall suppress the factor $e^{-i\lambda t}$ which is common to the entire expression (A.3.201) and already matches (A.3.200).

Step 1. With (A.3.198) in mind, the integrals over v and w in (A.3.201) can be evaluated in terms of residues as a linear combination of terms of the form

$$\frac{1}{2\pi i}\oint\frac{ds}{s}\tilde{u}(s)\;\partial_v^k\partial_w^l\left(\frac{\mathcal{F}\left(\ln\left[\frac{(v-s)(w-z)}{(v-z)(w-s)}\right]\right)}{(vw)^{1-G}\left[(v-s)(v-z)(w-s)(w-z)\right]^{G/2}}\right)\Bigg|_{v,w=1/p} \tag{A.3.204}$$

with

$$0\leq k,l\leq N. \tag{A.3.205}$$

Now, for any $\mathcal{G}$ that depends on the indicated argument,

$$\partial_v\mathcal{G}\left(\ln\left[\tfrac{(v-s)(w-z)}{(v-z)(w-s)}\right]\right)=\left(\frac{1}{v-s}-\frac{1}{v-z}\right)\mathcal{G}'\left(\ln\left[\tfrac{(v-s)(w-z)}{(v-z)(w-s)}\right]\right). \tag{A.3.206}$$

Applying such differentiations recursively, each v-derivative may produce either one extra factor of $1/(v-z)$ if it acts on the numerator in (A.3.204) or on the factor $1/(v-z)^{G/2}$, or it may produce one extra factor of $1/(v-s)$ in a similar manner, or it may produce simply extra factors of v if it acts on $1/v^{1-G}$ (such factors will be expressed through p only after one substitutes $v=1/p$ at the end, and are irrelevant for our present argument). Furthermore, in the process of differentiation, $\mathcal{F}$ may change into another function of the same argument. The situation with w-differentiations is, of course, directly parallel. We denote the number of extra factors of $1/(v-z)$ generated through such differentiations as k_1, the number of extra factors $1/(v-s)$ as k_2, the number of extra factors of $1/(w-z)$ as l_1, and the number of factors $1/(w-s)$ as l_2. Evidently, from the above description of differentiations,

$$k_1+k_2\leq k\quad\text{and}\quad l_1+l_2\leq l. \tag{A.3.207}$$

One concludes that $\partial_v^k\partial_w^l(\ldots)$ in (A.3.204) consists of terms of the form

$$\frac{\mathcal{G}\left(\ln\left[\frac{(v-s)(w-z)}{(v-z)(w-s)}\right]\right)}{(v-z)^{k_1+G/2}(v-s)^{k_2+G/2}(w-z)^{l_1+G/2}(w-s)^{l_2+G/2}}, \tag{A.3.208}$$

where we have omitted the (s,z)-independent prefactor, and $\mathcal{G}$ is some function expressed through $\mathcal{F}$ and its derivatives. Once $v=w=1/p$ have been substituted, the argument of $\mathcal{G}$ turns into 0, so it is just a number. At the end, once again ignoring (s,z)-independent factors, (A.3.204) is written as a linear combination of terms of the form

$$\frac{1}{(1-pz)^{G+k_1+l_1}}\frac{1}{2\pi i}\oint\frac{\tilde{u}(s)\,ds}{s\,(1-ps)^{G+k_2+l_2}}. \tag{A.3.209}$$

Now, with $\sigma=1/s$,

$$\frac{1}{2\pi i}\oint ds\frac{\tilde{u}(s)}{s\,(1-ps)^{G+k_2+l_2}}=\frac{1}{2\pi i}\oint d\sigma\frac{\sigma^{G+k_2+l_2-1}\tilde{u}(1/\sigma)}{(\sigma-p)^{G+k_2+l_2}}. \tag{A.3.210}$$

But $\sigma^{k_2+l_2}/(\sigma-p)^{k_2+l_2}$ can be written as a linear combination of terms of the form $1/(\sigma-p)^m$ with $0 \le m \le k_2+l_2$. Hence, (A.3.209) can be written as a linear combination of

$$\frac{1}{2\pi i}\oint d\sigma \frac{\sigma^{G-1}\tilde{u}(1/\sigma)}{(\sigma-p)^{G+m}} = \frac{1}{\Gamma(G+m)}\partial_\sigma^{G+m-1}\left(\sigma^{G-1}\tilde{u}(1/\sigma)\right)\Big|_{\sigma=p}. \tag{A.3.211}$$

By (A.3.185), $\tilde{u}(1/\sigma)$ is exactly the same as $u(z)$ with z replaced by σ and p replaced by $\bar{p}$. Therefore, from (A.3.197),

$$\partial_\sigma^{G-1}\left(\sigma^{G-1}\tilde{u}(1/\sigma)\right) = \frac{(p-\sigma)^N}{(1-\bar{p}\sigma)^{N+G}}, \tag{A.3.212}$$

which evidently has a degree N zero at $\sigma = p$. Hence, at least N further differentiations ($m \ge N$) must be applied in (A.3.211) in order for the result to be nonzero. So (A.3.209) can only be nonvanishing if $k_2 + l_2 \ge N$. But by (A.3.205) and (A.3.207) this implies $k_1 + l_1 \le N$. Thus, after evaluating of the s-integral in (A.3.209), the result is a linear combination of $1/(1-pz)^{G+n}$ with $0 \le n \le N$. Since all contributions to (A.3.201) are in the form (A.3.209), this property is inherited by (A.3.201), and hence the latter must then be expressible as (A.3.202).

Step 2. To pin down $Q_N(z)$ in (A.3.202), we shall compute the kth z-derivative of (A.3.201) at $z = \bar{p}$, and we shall start with performing the s-integral in (A.3.201). The structure of the argument is rather similar to step 1, but with the roles of (z, s) and (v, w) interchanged. The s-integral is evaluated through the residues of $\tilde{u}$. The following expression for $\tilde{u}$ follows from (A.3.198):

$$\tilde{u}(s) = \sum_{l=0}^{N}\frac{\bar{c}_l}{(1-\bar{p}/s)^{l+1}} = s\sum_{l=0}^{N}\frac{d_l}{(s-\bar{p})^{l+1}}, \tag{A.3.213}$$

where d_l are certain linear combinations of $\bar{c}_l$. Then the kth z-derivative of (A.3.201) at $z = \bar{p}$ consists of terms of the form

$$\frac{1}{(2\pi i)^2}\oint\frac{dv\,dw}{(vw)^{1-G}}\,u(v)u(w)\partial_z^k\partial_s^l\left(\frac{\mathcal{F}\left(\ln\left[\frac{(v-s)(w-z)}{(v-z)(w-s)}\right]\right)}{[(v-s)(v-z)(w-s)(w-z)]^{G/2}}\right)\Bigg|_{z,s=\bar{p}}. \tag{A.3.214}$$

The z- and s-differentiations are performed in a manner directly parallel to the v- and w-differentiations in step 1. One gets a collection of terms of the form

$$\frac{1}{(2\pi i)^2}\oint\frac{dv}{v}\oint\frac{dw}{w}\frac{u(v)u(w)}{v^{k_1+l_1}w^{k_2+l_2}(1-\bar{p}/v)^{G+k_1+l_1}(1-\bar{p}/w)^{G+k_2+l_2}}, \tag{A.3.215}$$

with $k_1 + k_2 = k$ and $l_1 + l_2 = l$, which can be rewritten as

$$\partial_v^{G-1+k_1+l_1}(v^{G-1}u(v))\,\partial_w^{G-1+k_2+l_2}(w^{G-1}u(w))\Big|_{v,w=\bar{p}}. \tag{A.3.216}$$

But by construction $\partial_z^{G-1}(z^{G-1}u(z))$ has a degree N zero at $z = \bar{p}$. Therefore, at least N extra differentiations must be applied in both factors above in order to make the result

nonvanishing, i.e., $k_1 + l_1 \geq N$ and $k_2 + l_2 \geq N$, while $l_1 + l_2 = l \leq N$ from (A.3.213), and hence $k = k_1 + k_2 \geq N$. In other words, if we apply fewer than N z-derivatives to (A.3.201) and evaluate the result at $z = \bar{p}$, all the terms identially vanish. That means that (A.3.201) has a degree N zero at $z = \bar{p}$. Since we already know that it is of the form (A.3.202), it must be proportional to (A.3.203), completing our proof that (A.3.197) satisfies the equations of motion (A.3.189). Note that the specific form of the arbitrary function $\mathcal{F}$ defining our resonant system does not affect the form of stationary solutions (A.3.197), though it may affect the relation of λ and p.

A.4 Interaction Coefficients for a Scalar Field in AdS$_{d+1}$

A.4.1 Massive Scalar Field in AdS$_{d+1}$

We shall consider a massive scalar field in AdS_{d+1} with boundary conditions $x^{\Delta-d}\phi(t,x)\big|_{x\to\pi/2} = 0$, where

$$\Delta = \frac{d}{2} + \sqrt{\left(\frac{d}{2}\right)^2 + m^2}, \tag{A.4.1}$$

which made an appearance in section 3.3.8. This model is also fully resonant and an approximation of the form (3.3.116) can be derived. The massless case was developed in [35]; the process is quite similar for the massive scalar, so we will only present the main results.

The model is governed by the action

$$S = \frac{1}{16\pi G}\int d^{d+1}x\sqrt{-g}\,(R - 2\Lambda) - \frac{1}{2}\int d^{d+1}x\sqrt{-g}\left(\partial_\mu\phi\partial^\mu\phi + m^2\phi^2\right). \tag{A.4.2}$$

Our ansatz for the metric is (3.3.103). Developing the time-averaging strategy described in the main text, or in [35, 36] which contain a more thorough discussion, we obtain the expressions for the interaction coefficients, after splitting them in three types according to the number of coincident indices, $T_l \equiv C_{llll}$, $R_{il} \equiv 2C_{ilil}$ for $i \neq l$ and $S_{ijkl} \equiv C_{ijkl}$ for $\{i,j\} \neq \{k,l\}$. Imposing $\delta(t,0) = 0$:

$$T_l = \frac{1}{2}\omega_l^2 X_{llll} + \frac{3}{2}Y_{llll} + 2\omega_l^4 W_{llll} + 2\omega_l^2 W^*_{llll} - \omega_l^2\left(A_{ll} + \omega_l^2 V_{ll}\right), \tag{A.4.3}$$

$$\begin{aligned} R_{il} =& \frac{1}{2}\left(\frac{\omega_i^2+\omega_l^2}{\omega_l^2-\omega_i^2}\right)\left(\omega_l^2 X_{illi} - \omega_i^2 X_{liil}\right) + 2\left(\frac{\omega_l^2 Y_{ilil} - \omega_i^2 Y_{lili}}{\omega_l^2-\omega_i^2}\right) + \left(\frac{\omega_i^2\omega_l^2}{\omega_l^2-\omega_i^2}\right)(X_{illi} - X_{lili}) \\ &+ \frac{1}{2}\left(Y_{iill} + Y_{llii}\right) + \omega_i^2\omega_l^2\left(W_{llii} + W_{iill}\right) + \omega_i^2 W^*_{llii} + \omega_l^2 W^*_{iill} - \omega_l^2\left(A_{ii} + \omega_i^2 V_{ii}\right), \end{aligned} \tag{A.4.4}$$

$$S_{ijkl} = -\frac{1}{4}\left(\frac{1}{\omega_i+\omega_j} + \frac{1}{\omega_i-\omega_k} + \frac{1}{\omega_j-\omega_k}\right)\left(\omega_i\omega_j\omega_k X_{lijk} - \omega_l Y_{iljk}\right)$$

$$
\begin{aligned}
&-\frac{1}{4}\left(\frac{1}{\omega_i+\omega_j}+\frac{1}{\omega_i-\omega_k}-\frac{1}{\omega_j-\omega_k}\right)(\omega_j\omega_k\omega_l X_{ijkl}-\omega_i Y_{jikl})\\
&-\frac{1}{4}\left(\frac{1}{\omega_i+\omega_j}-\frac{1}{\omega_i-\omega_k}+\frac{1}{\omega_j-\omega_k}\right)(\omega_i\omega_k\omega_l X_{jikl}-\omega_j Y_{ijkl})\\
&-\frac{1}{4}\left(\frac{1}{\omega_i+\omega_j}-\frac{1}{\omega_i-\omega_k}-\frac{1}{\omega_j-\omega_k}\right)(\omega_i\omega_j\omega_l X_{kijl}-\omega_k Y_{ikjl}),
\end{aligned}
\tag{A.4.5}
$$

where

$$X_{ijkl}=\int_0^{\pi/2} dx e_i'(x)e_j(x)e_k(x)e_l(x)\mu(x)^2\nu(x), \tag{A.4.6}$$

$$Y_{ijkl}=\int_0^{\pi/2} dx e_i'(x)e_j(x)e_k'(x)e_l'(x)\mu(x)^2\nu(x), \tag{A.4.7}$$

$$W_{ijkl}=\int_0^{\pi/2} dx e_i(x)e_j(x)\mu(x)\nu(x)\int_0^x dy e_k(y)e_l(y)\mu(y), \tag{A.4.8}$$

$$W^*_{ijkl}=\int_0^{\pi/2} dx e_i'(x)e_j'(x)\mu(x)\nu(x)\int_0^x dy e_k(y)e_l(y)\mu(y), \tag{A.4.9}$$

$$V_{ij}=\int_0^{\pi/2} dx e_i(x)e_j(x)\mu(x)\nu(x), \tag{A.4.10}$$

$$A_{ij}=\int_0^{\pi/2} dx e_i'(x)e_j'(x)\mu(x)\nu(x). \tag{A.4.11}$$

The interaction coefficients for the choice $\delta(t,\pi/2)=0$ are almost the same:

$$T_l^{(\delta(t,\pi/2)=0)}=T_l^{(\delta(t,0)=0)}+\omega_l^2\left(A_{ll}+\omega_l^2 V_{ll}\right), \tag{A.4.12}$$

$$R_{il}^{(\delta(t,\pi/2)=0)}=R_{il}^{(\delta(t,0)=0)}+\omega_l^2\left(A_{ii}+\omega_i^2 V_{ii}\right), \tag{A.4.13}$$

$$S_{ijkl}^{(\delta(t,\pi/2)=0)}=S_{ijkl}^{(\delta(t,0)=0)}. \tag{A.4.14}$$

Here, $e_n(x)$ and ω_n are the eigenmodes and their associated eigenvalues of the linear problem:

$$\ddot{\phi}_1-\mathcal{L}\phi_1=0 \qquad \text{with} \qquad \mathcal{L}=\frac{1}{\mu(x)}\partial_x\left(\mu(x)\partial_x\right)-\frac{m^2}{\cos^2 x}. \tag{A.4.15}$$

Their expressions are

$$e_n(x)=k_n\cos^{\Delta}x\,P_n^{\left(\frac{d}{2}-1,\ \Delta-\frac{d}{2}\right)}(\cos 2x), \qquad k_n=2\sqrt{\frac{(n+\Delta/2)\Gamma(n+1)\Gamma(n+\Delta)}{\Gamma(n+d/2)\Gamma(n+\Delta-d/2+1)}}, \tag{A.4.16}$$

and

$$\omega_n=\Delta+2n, \qquad n=0,1,\ldots, \tag{A.4.17}$$

where Δ is given in (A.4.1) and $P_n^{(a,b)}(x)$ are Jacobi polynomials. We have defined $\mu(x)$ and $\nu(x)$ as in (3.3.105).

In analogy with the explanation for the massless scalar field given in section 3.3.7, the current model has the resonant condition $\omega_n + \omega_m = \omega_k + \omega_l$, which through (A.4.17) is equivalent to $n + m = k + l$. However there could be two more resonant channels, $\omega_n = \omega_m + \omega_k + \omega_l$ and $\omega_n + \omega_m + \omega_k = \omega_l$, equivalent to $n = m + k + l + \Delta$ and $n = l - m - k - \Delta$, respectively. If Δ is integer these last two conditions can be satisfied and a priori two new terms must be included in the system of equations (3.3.116):

$$i\omega_n\dot{\alpha}_n = \sum_{\omega_n+\omega_m=\omega_k+\omega_l} C_{nmkl}\,\bar{\alpha}_m\alpha_k\alpha_l + \sum_{\omega_n=\omega_m+\omega_k+\omega_l} Q_{nmkl}\,\alpha_m\alpha_k\alpha_l + \sum_{\omega_n+\omega_m+\omega_k=\omega_l} U_{nmkl}\,\bar{\alpha}_m\bar{\alpha}_k\alpha_l. \tag{A.4.18}$$

In our situation we did not perform an analytic study of Q_{ijkl} and U_{ijkl} as in [36], where it was proven that for a massless scalar field ($\Delta = d$) these coefficients vanish, but numerical calculations suggest that they also vanish for nonzero masses. On the other hand, when Δ is not an integer, the conditions $n = m + k + l + \Delta$ and $n = l - m - k - \Delta$ are not satisfied for any combination of the indices. Therefore, these interaction channels disappear upon time-averaging. We thus see that, for any Δ, the relevant dynamics is governed by equation (3.3.116) through T_l, R_{il} and S_{ijkl}.

We note that the given expressions for T_l, R_{il} and S_{ijkl} are exactly the same as in [36], where all derivations are specialized to $m^2 = 0$. However, if we were to transform these integrals using integration by parts to the form of [35], the resulting expressions would have differed from those of [35] by additional terms with explicit dependence on m^2.

A.4.2 Analytic Formulas for a Massless Scalar Field in AdS_4

These formulas come from the integration of (A.4.3)-(A.4.5) with $d = 3$, $m^2 = 0$ and $\Delta = 3$. We have followed the strategy introduced in [56]. Therein, authors noted that the eigenfunctions e_n, e'_n can be written in the reduced form

$$e_n(x) = \frac{1}{\sqrt{\pi(n+1)(n+2)}}\frac{f_{n+1}(x)}{\sin x}, \qquad f_n(x) = (n+1)\sin(2nx) + n\sin(2(n+1)x), \tag{A.4.19}$$

$$e'_n(x) = \frac{3+2n}{\sqrt{\pi(n+1)(n+2)}}\frac{\cos x}{\sin^2 x}g_{n+1}(x), \quad g_n(x) = -(n+1)\sin(2nx) + n\sin(2(n+1)x). \tag{A.4.20}$$

These expressions are crucial for our evaluation of (A.4.3)-(A.4.5). Any eigenfunction is composed of the same number of trigonometric functions. In consequence, formulas (A.4.6)-(A.4.11) are reduced to a fixed number of integrals independently of the mode numbers. The final expressions are too long to be presented here, instead, we are going to write a list of nontrivial integrals which are necessary for these computations. The majority of these integrals were obtained by successive integrations by parts of integrals contained in [215].

- $n = 0, 1, 2, \ldots$

$$\int dx \frac{\cos((2n+1)x)}{\sin x} = 2\sum_{k=1}^{n} \frac{\cos 2kx}{2k} + \log(\sin x) \tag{A.4.21}$$

- $n = 0, 1, 2, \ldots$

$$\int dx \frac{\cos((2n)x)}{\sin x} = 2\sum_{k=1}^{n} \frac{\cos(2k-1)x}{2k-1} + \log\left(\tan\frac{x}{2}\right) \tag{A.4.22}$$

- $n = 0, 1, 2, \ldots$

$$\int dx \frac{\sin((2n+1)x)}{\sin x} = 2\sum_{k=1}^{n} \frac{\sin((2k)x)}{2k} + x \tag{A.4.23}$$

- $n = 0, 1, 2, \ldots$

$$\int dx \frac{\sin((2n)x)}{\sin x} = 2\sum_{k=1}^{n} \frac{\sin((2k-1)x)}{2k-1} \tag{A.4.24}$$

- $n = 0, 1, 2, \ldots$

$$\int dx \frac{\cos(2nx)}{\sin^2 x} = -2n\left(\sum_{k=1}^{n} \frac{\sin(2kx)}{k} + x\right) - \frac{\cos((2n+1)x)}{\sin x} \tag{A.4.25}$$

- $n = 0, 1, 2, \ldots$

$$\int dx \frac{\cos((2n+1)x)}{\sin^2 x} = -2(2n+1)\sum_{k=1}^{n} \frac{\sin((2k-1)x)}{2k-1} - \frac{\cos(2nx)}{\sin x} \tag{A.4.26}$$

- $n = 0, 1, 2, \ldots$

$$\int dx \frac{\sin(2nx)}{\sin^2 x} = 2n\left(\sum_{k=1}^{n} \frac{\cos(2kx)}{k} + \log(\sin x)\right) - \frac{\sin((2n+1)x)}{\sin x} \tag{A.4.27}$$

- $n = 0, 1, 2, \ldots$

$$\int dx \frac{\sin((2n+1)x)}{\sin^2 x} = (2n+1)\left(2\sum_{k=1}^{n} \frac{\cos((2k-1)x)}{2k-1} + \log\left(\tan\left(\frac{x}{2}\right)\right)\right) - \frac{\sin(2nx)}{\sin x} \tag{A.4.28}$$

- $n = 1, 2, \ldots$

$$\int dx \frac{1}{\sin^{2n} x} = -\frac{1}{2n-1}\frac{\cos x}{\sin^{2n-1} x}\left(1 + \sum_{k=1}^{n-1} 2^k \sin^{2k} x \frac{(n-1)!}{(n-k-1)!}\frac{(2n-2k-3)!!}{(2n-3)!!}\right) \tag{A.4.29}$$

- $n = 1, 2, \ldots$

$$\int dx \frac{1}{\sin^{2n+1} x} = -\frac{1}{2n}\frac{\cos x}{\sin^{2n} x}\left(1 + \sum_{k=1}^{n-1} \frac{\sin^{2k} x}{2^k}\frac{(2n-1)!!}{(2n-2k-1)!!}\frac{(n-k-1)!}{(n-1)!}\right) + \frac{(2n-1)!!}{2^n n!}\log\left(\tan\left(\frac{x}{2}\right)\right) \tag{A.4.30}$$

- $n = 0, 1, 2, \ldots$

$$\int dx \frac{\cos((2n+1)x)}{\cos x} = 2\sum_{k=1}^{n}(-1)^{n-k}\frac{\sin((2k)x)}{2k} + (-1)^n x \tag{A.4.31}$$

- $n = 0, 1, 2, \ldots$

$$\int dx \frac{\cos((2n)x)}{\cos x} = 2\sum_{k=1}^{n}(-1)^{n-k}\frac{\sin((2k-1)x)}{2k-1} + (-1)^n \log\tan\left(\frac{\pi}{4} + \frac{x}{2}\right) \tag{A.4.32}$$

- $n = 0, 1, 2, \ldots$

$$\int dx \frac{\sin((2n+1)x)}{\cos x} = 2\sum_{k=1}^{n}(-1)^{n-k+1}\frac{\cos(2kx)}{2k} + (-1)^{n+1}\log\cos x \tag{A.4.33}$$

- $n = 0, 1, 2, \ldots$

$$\int dx \frac{\sin(2nx)}{\cos x} = 2\sum_{k=1}^{n}(-1)^{n-k+1}\frac{\cos((2k-1)x)}{2k-1} \tag{A.4.34}$$

- $n = 0, 1, 2, \ldots$

$$\int dx \frac{\sin(2nx)}{\cos^2 x} = (-1)^n 2n\left(\sum_{k=1}^{n}(-1)^k\frac{\cos(2kx)}{k} + \log\left(\cos(x)\right)\right) - \frac{\cos((2n+1)x)}{\cos x} \tag{A.4.35}$$

- $n = 0, 1, 2, \ldots$

$$\int dx \frac{\sin((2n+1)x)}{\cos^2 x} = (-1)^{n+1}2(2n+1)\sum_{k=1}^{n}(-1)^k\frac{\cos((2k-1)x)}{2k-1} + \frac{\cos(2nx)}{\cos x} \tag{A.4.36}$$

- $n = 0, 1, 2, \ldots$

$$\int dx \frac{\cos(2nx)}{\cos^2 x} = (-1)^{n+1}2n\left(x + \sum_{k=1}^{n}(-1)^k\frac{\sin(2kx)}{k}\right) + \frac{\sin((2n+1)x)}{\cos x} \tag{A.4.37}$$

- $n = 0, 1, 2, \ldots$

$$\int dx \frac{\cos((2n+1)x)}{\cos^2 x} = (-1)^n (2n+1) \left(2 \sum_{k=1}^{n} (-1)^k \frac{\sin((2k-1)x)}{2k-1} + \log\left(\tan\left(\frac{\pi}{4} + \frac{x}{2} \right) \right) \right) - \frac{\sin(2nx)}{\cos x} \tag{A.4.38}$$

- $n = 1, 2, \ldots$

$$\int dx \frac{1}{\cos^{2n} x} = \frac{1}{2n-1} \frac{\sin x}{\cos^{2n-1} x} \left(1 + \sum_{k=1}^{n-1} 2^k \cos^{2k} x \frac{(n-1)!}{(n-k-1)!} \frac{(2n-2k-3)!!}{(2n-3)!!} \right) \tag{A.4.39}$$

- $n = 1, 2, \ldots$

$$\int dx \frac{1}{\cos^{2n+1} x} = \frac{1}{2n} \frac{\sin x}{\cos^{2n} x} \left(1 + \sum_{k=1}^{n-1} \frac{\cos^{2k} x}{2^k} \frac{(2n-1)!!}{(2n-2k-1)!!} \frac{(n-k-1)!}{(n-1)!} \right) + \frac{(2n-1)!!}{2^n n!} \log\left(\tan\left(\frac{\pi}{4} + \frac{x}{2} \right) \right) \tag{A.4.40}$$

Additional integrals of the form

$$\int dx \frac{\cos(nx)}{\sin^\alpha x}, \qquad \int dx \frac{\sin(nx)}{\sin^\alpha x}, \qquad \int dx \frac{\cos(nx)}{\cos^\alpha x}, \qquad \int dx \frac{\sin(nx)}{\cos^\alpha x}, \tag{A.4.41}$$

where n, α are integers, can be obtained by integrating by parts and using (A.4.29)-(A.4.30) or (A.4.39)-(A.4.40) to reduce the exponent α until we can apply the integrals presented above. Note that they are indefinite integrals. The computation of (A.4.6)-(A.4.11) requires the evaluation at 0 and $\pi/2$. We can observe that it involves divergences, nevertheless, they are cancelled once we gather all of them to calculate (A.4.6)-(A.4.11). Performing this explicit calculation we also find that logarithmic terms also vanish in the final expressions. In consequence, the coefficients πT_l, πR_{il} are rational numbers (note that for these coefficients the square roots in (A.4.19)-(A.4.20) are not present).

A.5 Periodically Driven Systems

In this appendix we are going to gather the technical details and equations of chapter 4.

A.5.1 A Scalar Field in Global AdS$_4$

For the numerical resolution of ansatz (4.1.15)-(4.1.16), the system of equations (4.1.5a)-(4.1.5b) must be rewritten in a form that matches the structure used in section 2.3. It is obtained through the introduction of

$$F \equiv f e^{-\delta}. \tag{A.5.1}$$

The equations take the new form

$$\begin{aligned}
\dot{\Phi} &= (F\Pi)', && \text{(A.5.2)}\\
\dot{\Pi} &= \frac{1}{\tan^2 x}(\tan^2 x F\Phi)', && \text{(A.5.3)}\\
\delta' &= -\sin x \cos x \left(\Phi^2 + \Pi^2\right), && \text{(A.5.4)}\\
F' &= \frac{1+2\sin x}{\sin x \cos x}(e^{-\delta} - F), && \text{(A.5.5)}
\end{aligned}$$

this set of equations matches the form of (2.3.28)-(2.3.28). In particular (A.5.5) is obtained by multiplying the first equation of (4.1.5b) by $e^{-\delta}$ and gathering the terms

$$F' = \left(f' e^{-\delta} - \delta' f e^{-\delta}\right). \tag{A.5.6}$$

Now, assuming perturbation around TPSs: $\phi_p, \Pi_p, \delta_p, F_p$ with the ansatz

$$\begin{aligned}
\phi(t,x) &= \phi_p(t,x) + \epsilon\tilde{\phi}(t,x), && \text{(A.5.7)}\\
\Pi(t,x) &= \Pi_p(t,x) + \epsilon\tilde{\Pi}(t,x), && \text{(A.5.8)}\\
\delta(t,x) &= \delta_p(t,x) + \epsilon\tilde{\delta}(t,x), && \text{(A.5.9)}\\
F(t,x) &= F_p(t,x) + \epsilon\tilde{F}(t,x). && \text{(A.5.10)}
\end{aligned}$$

The equations for the linear perturbations take the form

$$\begin{aligned}
\tilde{\phi} &= F_p\tilde{\Pi} + \tilde{F}\Pi_p, && \text{(A.5.11)}\\
\dot{\tilde{\Pi}} &= \frac{1}{\tan^2 x}\left[\tan^2 x \left(F_p\tilde{\phi}' + \tilde{F}\phi_p'\right)\right]', && \text{(A.5.12)}\\
\tilde{\delta}' &= -2\sin x \cos x \left(\phi_p'\tilde{\phi}' + \Pi_p\tilde{\Pi}\right), && \text{(A.5.13)}\\
\tilde{F}' &= -\frac{1+2\sin x}{\sin x \cos x}(\tilde{\delta}e^{-\delta_p} - \tilde{F}). && \text{(A.5.14)}
\end{aligned}$$

A.5.2 AdS Soliton

Here we are going to present the EOMs (4.2.4)-(4.2.7) after applying the transformation

$$r^2 = 1 - \frac{z}{z_0}, \tag{A.5.15}$$

(we have already set $z_0 = 1$). In terms of the following variables (where now $\dot{} \equiv \partial_t, {}' \equiv \partial_r$)

$$B(t,r) \equiv b'(t,r), \qquad P(t,r) \equiv \frac{e^{\delta(t,r)}}{f(t,r)}\dot{b}(t,r), \tag{A.5.16}$$

the system of equations is rewritten as

$$\dot{B} = \left(fe^{-\delta}P\right)' \tag{A.5.17}$$

$$\dot{P} = \frac{(1-r^2)^2}{4r}\left[\left(3 - \frac{((1-r^2)^3-1)B}{r(1-r^2)^2}\right)fe^{-\delta}\right]' \tag{A.5.18}$$

$$f' = \frac{24r}{3-6r^4+4r^6-r^8}(1-f) + \delta' f \tag{A.5.19}$$

$$\delta' = \frac{1}{2(3+3r^2-3r^4+r^6)}\left(6(r^2-1)^3B + r(-3+6r^2-4r^4+r^6)B^2 + 4r(r^2-1)P^2\right) \tag{A.5.20}$$

$$\dot{f} = \frac{(r^2-1)}{(3+3r^2-3r^4+r^6)}\left(3(r^2-1)^2 + r(3-3r^2+r^4)B\right)f^2e^{-\delta}P \tag{A.5.21}$$

For the construction of TPSs this system of equation is rewritten to allow a direct application of the methods of section 2.3.1.2. For this purpose we introduce

$$F \equiv fe^{-\delta}. \tag{A.5.22}$$

The EOMs take the form

$$\dot{b} = FP \tag{A.5.23}$$

$$\dot{P} = \frac{(1-r^2)^2}{4r}\left[\left(3 - \frac{((1-r^2)^3-1)B}{r(1-r^2)^2}\right)F\right]' \tag{A.5.24}$$

$$F' = \frac{24r}{3-6r^4+4r^6-r^8}(e^{-\delta} - F) \tag{A.5.25}$$

$$\delta' = \frac{1}{2(3+3r^2-3r^4+r^6)}\left(6(r^2-1)^3B + r(-3+6r^2-4r^4+r^6)B^2 + 4r(r^2-1)P^2\right) \tag{A.5.26}$$

The equations for linear perturbations are derived following the same procedure as in the case of the scalar field.

A.6 Programs

This section contains details about our codes of time evolution and construction of TPSs and their linear modes. Our main programming languages are C, C++ and Fortran90.

A.6.1 Program for Time Evolution

A.6.1.1 Implementation

In this section we are going to sketch the techniques used to numerically solve the systems of equations displayed in chapter 4. As the models contained in this chapters have a similar structure we will adopt a general discussion using $u(t,x), U(t,x), v(t,x)$ to denote: $\phi(t,x), \Phi(t,x), \Pi(t,x)$ (section 4.1) and $b(t,r), B(t,r), P(t,x)$ (section 4.2), where $x \in [0, x_f)$ with the origin (or tip) at $x = 0$ and the boundary at $x = x_f$.

Under the isotropic ansatz (4.1.2) and (4.2.1) the EOMs for both models belong to the family of systems (where $\dot{} \equiv \partial_t, {}' \equiv \partial_x$)

$$\dot{U}(t,x) = \left[f(t,x)e^{-\delta(t,x)}v(t,x)\right]', \tag{A.6.1}$$

$$\dot{v}(t,x) = \frac{1}{\mu(x)}\left[f(t,x)e^{-\delta(t,x)}\left(c_{v,1}(x) + c_{v,2}(x)u'(t,x)\right)\right]', \tag{A.6.2}$$

$$\delta'(t,x) = c_{\delta,1}(x)U(t,x) + c_{\delta,2}(x)U(t,x)^2 + c_{\delta,3}(x)v(t,x)^2. \tag{A.6.3}$$

$$f'(t,x) = c_f(x)\left(1 - f(t,x)\right) + \delta'(t,x)f(t,x), \tag{A.6.4}$$

$$\dot{f}(t,x) = \left(\tilde{c}_1(x) + \tilde{c}_2(x)U(t,x)\right)P(t,x)f(t,x)^2 e^{-\delta(t,x)} \tag{A.6.5}$$

Note that equation (A.6.1) can be replaced by $\dot{u} = fe^{-\delta}v$, nevertheless we have found more convenient working with U instead of u. The equations for f and δ can be rewritten in an integral form showing that this system of equations is fully determined at each time t by $U(t,x), v(t,x)$. The integral representation of f is obtained by taking

$$c_f(x) = \frac{g'(x)}{g(x)} \tag{A.6.6}$$

and gathering terms on the LHS of (A.6.4) to reach

$$\left(ge^{-\delta}f\right)' = g'e^{-\delta}. \tag{A.6.7}$$

After setting the limits of integration from 0 to x and integrating by parts we obtain

$$f(t,x) = 1 + \frac{e^{\delta(t,x)}}{g(t,x)}\left(g_0 e^{-\delta_0(t)}\left(f_0(t) - 1\right) + \int_0^x dy\; g(y)\delta'(t,y)e^{-\delta(t,y)}\right), \tag{A.6.8}$$

where $g_0 = g(0),\ f_0(t) = f(t,0),\ \delta_0(t) = \delta(t,0)$. The value f_0 is chosen to guarantee the regularity of $f(t,x)$ at $x = 0$. Therefore, given U and v at a particular time, the system of equation is evaluated starting with (A.6.3), once δ is determined we solve (A.6.8) to obtain f, after that the time derivatives of U and v can be evaluated through (A.6.1) and (A.6.2) respectively. Following this procedure we see that equation (A.6.5) is not required, nevertheless despite this fact we will make use of this relation to check the consistency of our codes.

For the numerical modelling of this system of equations we have followed the notions given in [216]. For a good balance between accuracy and manageability, the code was

implemented using a fourth order scheme. The evolution in time was performed through a fourth-order Runge-Kutta method, its details can be found in [217]. Spatial derivatives were discretized by employing a centered fourth-order finite difference scheme while integrations were performed by a specifically designed scheme, based on local polynomial interpolation. This kind of implementations suffers from high-frequency noise generated as consequence of the discretization approach. To avoid this situation we have incorporated Kreiss-Oliger dissipation. Major problems come from the origin and boundary. To preserve the regularity of our functions close to these points we implemented the l'Hopital trick used in [216]. It takes the form

$$\frac{q(x)}{p(x)} = \frac{q'(x)}{p'(x)} - \frac{p(x)}{p'(x)} \left(\frac{q(x)}{p(x)}\right)', \tag{A.6.9}$$

and although the LHS and RHS are analytically equivalent, numerically the RHS is more robust than the LHS. Suppose that functions $q(x)$ and $p(x)$ go to zero at x_0 as $q(x), p(x) \sim (x - x_0)^\gamma$, thereby their ratio $q(x_0)/p(x_0)$ remains finite. Despite this analytic property, numerically the quantity $q(x)/p(x)$ is not well behaved in the environment of x_0, it is $q(x)/p(x) \sim (x - x_0)^\gamma/(x - x_0)^\gamma$. The RHS of (A.6.9) has the nice property of reducing the order of these zeros to leave RHS$\sim (x - x_0)^{\gamma-1}/(x - x_0)^{\gamma-1}$, therefore if $\gamma = 1$ we have avoided potential problems. This numerical regularization was applied to a reduced number of points close to the origin and boundary; an excessive number produces instabilities in the code. On some occasion the dissipation must skip these points.

In addition to these methods of stabilization we also have to take into account the fact that for consecutive points to the origin (boundary), our centered scheme requires information beyond the limits of our current grid. In order to solve this problem we have used the information provided by the asymptotic expansions to enlarged the grid with the required number of points at each end (considering enough terms to preserve the order of the full scheme). Note that instead of this addition of points we could implement forward (backward) derivatives close to the origin (boundary), nevertheless we have found numerical instabilities coming from the transition between schemes.

Finally, after the application of all these techniques, with the election $\delta(t, x_f) = 0$ evolutions remain stable with a constant Courant factor $\alpha = 0.1$. The optimum balance between all these implementations was reached by trial and error.

Once the numerical modelling of our problems guaranteed the stability of simulations, it was adapted to use parallel techniques. It reported a significant speed-up as well as allowed increasing the density of our spatial grid up to $2^{18} + 1$ points. High densities were only required when the evolution is approaching the system to a black hole formation, and therefore our standard simulations with smooth profiles were performed with $2^{10} + 1$ or $2^{11} + 1$ points. In order to preserve the computational resources and avoid brute-force calculations, a global mesh refinement was included such that, if high gradients are generated, our code "doubles" the number of points from $2^N + 1$ to $2^{N+1} + 1$. In this kind of setups high gradients are concentrated in small spatial regions; in consequence, the majority of the grid deals with smooth functions. A smarter option would be the implementation of local mesh refinement. Nevertheless, our goals were not related to the

accurate study of gravitational collapse but with TPSs and the deviation from this state, therefore a sophisticated tool like this was not necessary.

In our studies we have employed two different parallel codes to cross-check the results: one in Fortran 90 (parallelized with MPI) and another one in C (parallelized in CUDA). Both codes have been run at CESGA.[1]

A.6.1.2 Tests

Once we have achieved stable numerical modellings for our systems, we must implement tests to ensure that they work properly. In this section we are going to present tests supporting our codes of time evolution. In this case we have performed three kinds of tests to verify our confidence in the results obtained from the code:

- Convergence test: we have corroborated that our code respects the fourth-order convergence of the implemented scheme. For this purpose the test consisted of evolving the same initial data three times using a spatial spacing Δx, $\Delta x/2$ and $\Delta x/4$. Taking a quantity $g(t,x)$, which we will denote by g_1, g_2 and g_4 respectively for our three grids, their difference has been measured with

$$\|g_n - g_m\|_n \equiv \left(\int_0^{x_f} dx \ (g_n - g_m)^2 \right)^{1/2}, \tag{A.6.10}$$

  where $\| \ \|_n$ denotes that the integration has been performed in the grid $\Delta x/n$. The measurement of the convergence is done through the quantity

$$Q_n = \frac{\|g_{4n} - g_{2n}\|_n}{\|g_{2n} - g_n\|_n}, \tag{A.6.11}$$

  which is $Q_n \sim 2^{-\alpha}$ where α is the true order of convergence.

- Energy density: in chapter 4 we saw that the systems studied there do not conserve energy, nevertheless this quantity satisfies a differential equation which rules how it evolves in time, (4.1.12) in section 4.1 and (4.2.13) in section 4.2. They have the form

$$\dot{m} = K\left(\dot{u}_0, u_3\right), \tag{A.6.12}$$

  with $u_n = 1/n! \partial_x^n u(t,x)|_{x=x_f}$ and K denotes the LHS of the equation. Therefore we use the quantity

$$\Delta_m \equiv \dot{m} - K\left(\dot{u}_0, u_3\right) \tag{A.6.13}$$

  to measure if the time evolution is consistent with the equations of our model.

[1] Centro de Supercomputación de Galicia, `http://www.cesga.es/`.

- Momentum Constraint: we have also observed that the time evolution is determined by (A.6.1)-(A.6.4), therefore we will use the additional equation (A.6.5) to check the consistency of our simulations. This measurement is done through the quantity

$$\Delta_{MC} \equiv \left(\int_0^{x_f} dx \ \left(\dot{f}(t,x) - (\tilde{c}_1(x) + \tilde{c}_2(x) U(t,x)) \, P(t,x) f(t,x)^2 e^{-\delta(t,x)} \right)^2 \right)^{1/2} \tag{A.6.14}$$

Fig. A.1 shows as our codes satisfy these tests confirming their robustness and providing confidence in the produced results.

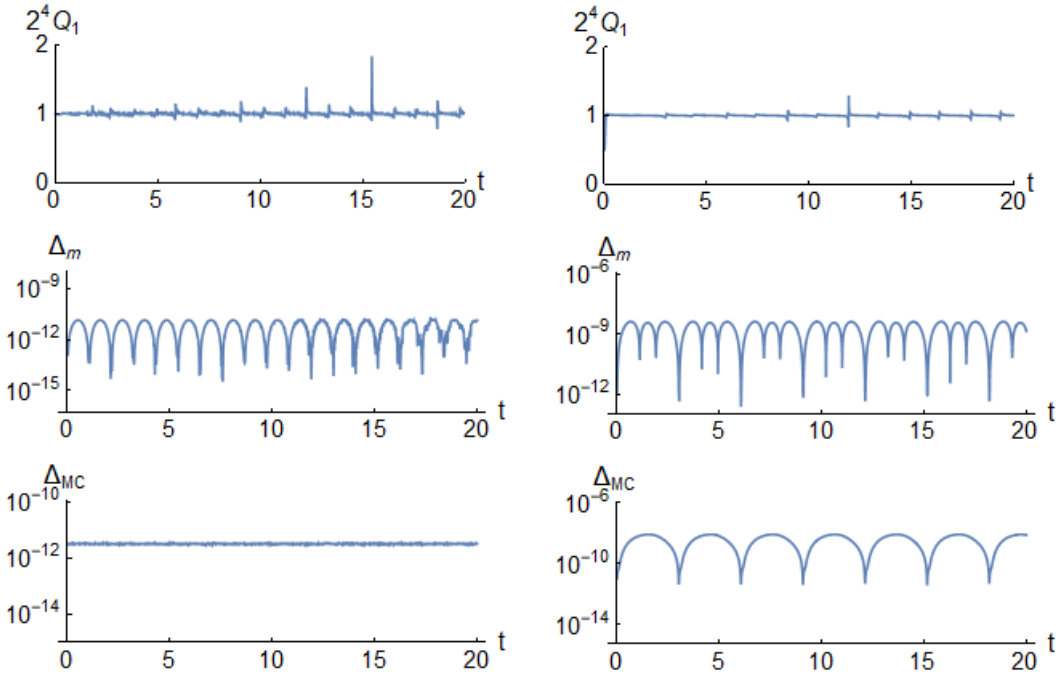

Figure A.1: These plots show the three tests introduced in the main text for our time evolution codes. Left: tests performed for our code of time evolution of a scalar field in global AdS_4 (section 4.1). Right: tests performed for our code of time evolution of gravitational fluctuation around the AdS soliton (section 4.2).

A.6.2 Programs for the Construction of TPSs and Floquet Modes

A.6.2.1 Implementation

These codes execute the numerical methods displayed in section 2.3 and in appendix A.1. Code for the construction of TPSs and their linear modes follow the same principles and therefore their implementation shares the main details, only minor modification are

needed. In this case we have used the programming language C. We have also developed a parallel version using OpenMP to reduce the high cost of time for large N and K. In the case of TPSs and Floquet modes for the model displayed in section 4.2 we have required the addition of multi-precision operations to guarantee the convergence of our results. This version was implemented after the analysis of section 4.1, it would be an excellent incorporation which could extend the scope of our code.

A.6.2.2 Tests

Now we are going to introduce tests for these codes. In this case our first test consists of measuring the consistency of the results. It is done by taking as reference a TPS and a Floquet mode obtained with large numbers of Chebyshev collocation points, N^*, and Fourier modes, K^*. After that we compare the same TPS and the Floquet mode obtained for lower values of N and K. If the code works properly and the solution exists, the results must converge with N, K approaching to N^*, K^*. In Fig. A.2 we can observe this situation, where we have used

$$\Delta\omega_K \equiv |\omega_K - \omega_{K^*}|, \qquad \Delta\lambda_K \equiv |\lambda_K - \lambda_{K^*}|. \tag{A.6.15}$$

The saturation of these quantities happens at the level of machine precision. To reach more accurate results our code must be implemented with higher numerical precision.

A second test for the construction of TPSs could consist of comparing the results of our spectral code with the time evolution of initial data obtained from its profiles. Nevertheless, there is a highly nontrivial check using adiabatic quenches. As we have seen in chapter 4 the independent construction of TPSs with the spectral code and with adiabatic quenches converges in the limit of $\beta \to \infty$, see Fig. A.3.

For Floquet modes, we have compared the spectral construction of these objects with fluctuations of a perturbed TPSs (initial conditions consist of (4.1.20) and (4.2.20)). Fig. A.4 shows a good agreement between our results, reporting confidence in our codes. In this case we also have a nontrivial test consisting of the unstable attractors for quenches with a duration β satisfying $|\beta - \beta_c| \ll 1$. It was found in sections 4.1 and 4.2 that this kind of quenches approaches the system to unstable TPSs perturbed with their exponentially growing mode with amplitude proportional to $|\beta - \beta_c|$, (see (4.1.25) and (4.2.24) for details). Therefore we can check if the exponential deviation of this process matches with the Floquet exponent obtained from the spectral code. Fig. A.5 represents particular examples of these quenches with $\beta < \beta_c$. We can appreciate there the exponential growing of the mass after reaching the plateau. In section 4.1 we obtained an excellent agreement between this analysis and the Floquet exponent obtained from the spectral code. In the case of section 4.2, TPSs displaying this effect remained unreachable for the spectral code impeding this corroboration.

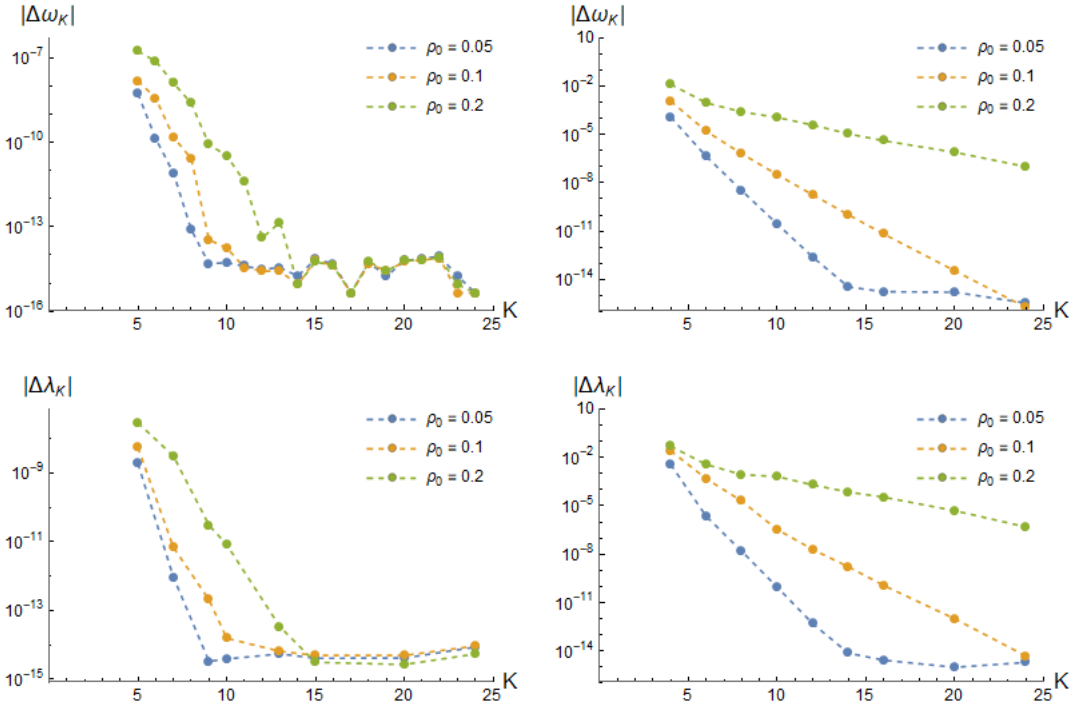

Figure A.2: These plots show the convergence of our codes for solutions constrained to $N = 2K$. The upper row corresponds to TPSs while the lower one to the lowest Floquet mode associated with these solutions. Results for a scalar field in AdS_4 are displayed on the left column and for the AdS soliton on the right one. They are subject to the reference solutions with $K^* = 25, 28$ respectively and $\rho = 0.001$ for both models. The saturation happens at the level of machine precision level.

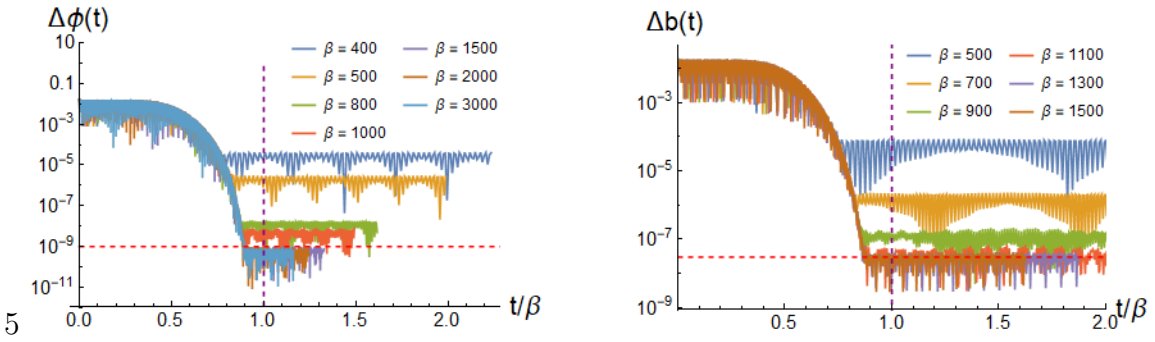

Figure A.3: Comparison of the TPS subject to (ρ_f, ω_f) with the states of the system through quenches of duration β from the static background to the final state with (ρ_f, ω_f). These measurements were performed with the quantities defined in (A.2.9). The purple dashed lined denotes the finalization of the quench while the red one denotes the level of numerical noise. Left: quenches from empty AdS_4 to $(\rho_f, \omega_f) = \left(10^{-3}, 2.9\right)$. Right: quenches from the AdS soliton to $(\rho_f, \omega_f) = \left(10^{-3}, 2.078\right)$. For further details see Fig. 4.11 and Fig. 4.19.

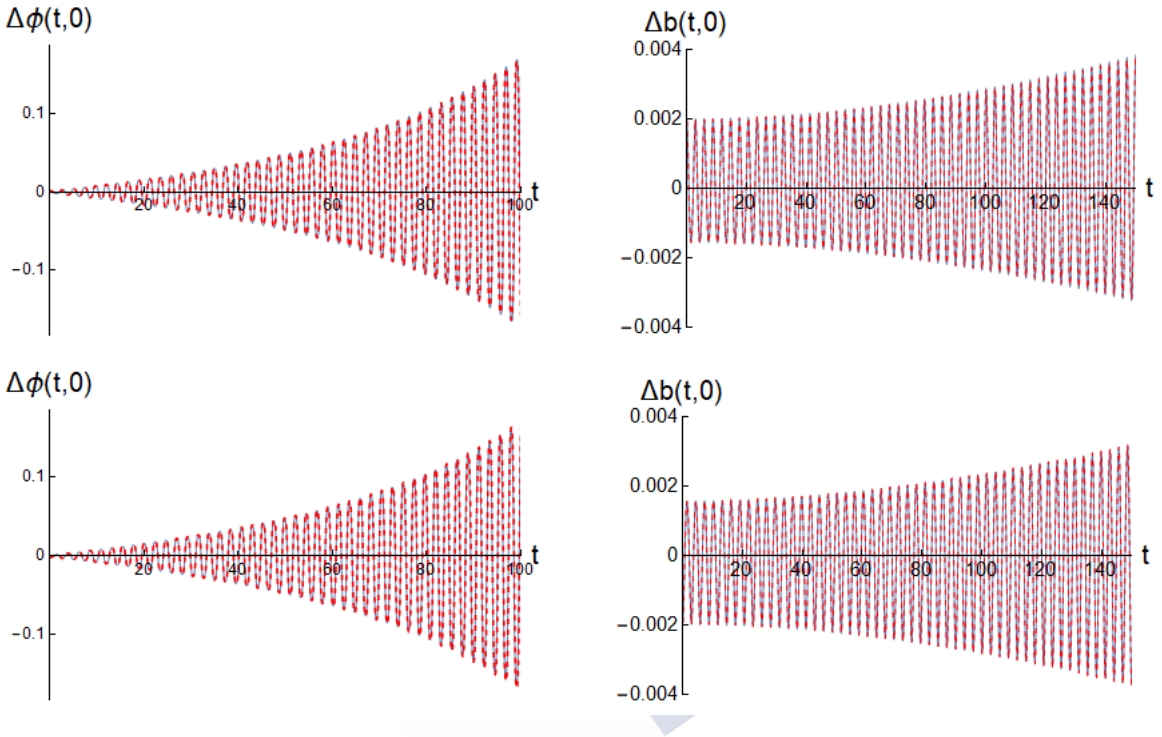

Figure A.4: Comparison between Floquet modes constructed with the spectral code (red dashed line) and fluctuations of TPSs, $\Delta\phi, \Delta b$, through the time evolution (blue solid line). These fluctuations were obtained by using $\Delta\phi(t,0) = \phi(t,0) - \phi_p(t,0)$ and $\Delta b(t,0) = b(t,0) - b_p(t,0)$, where ϕ_p, b_p correspond with the time evolution of TPSs and ϕ, b with the evolution of the same solutions perturbed with its Floquet modes following (4.1.20) and (4.2.20). We have selected the unstable TPSs because the effects of its exponentially growing mode can be easily distinguished from other fluctuations. The upper row contains the addition of Floquet modes to the TPS while the lower row contains the subtraction. Left: results for a scalar field in global AdS_4 (section 4.1). Right: results for gravitational fluctuations of the AdS soliton (section 4.2). Further details can be found in Fig. 4.8 and Fig. 4.18.

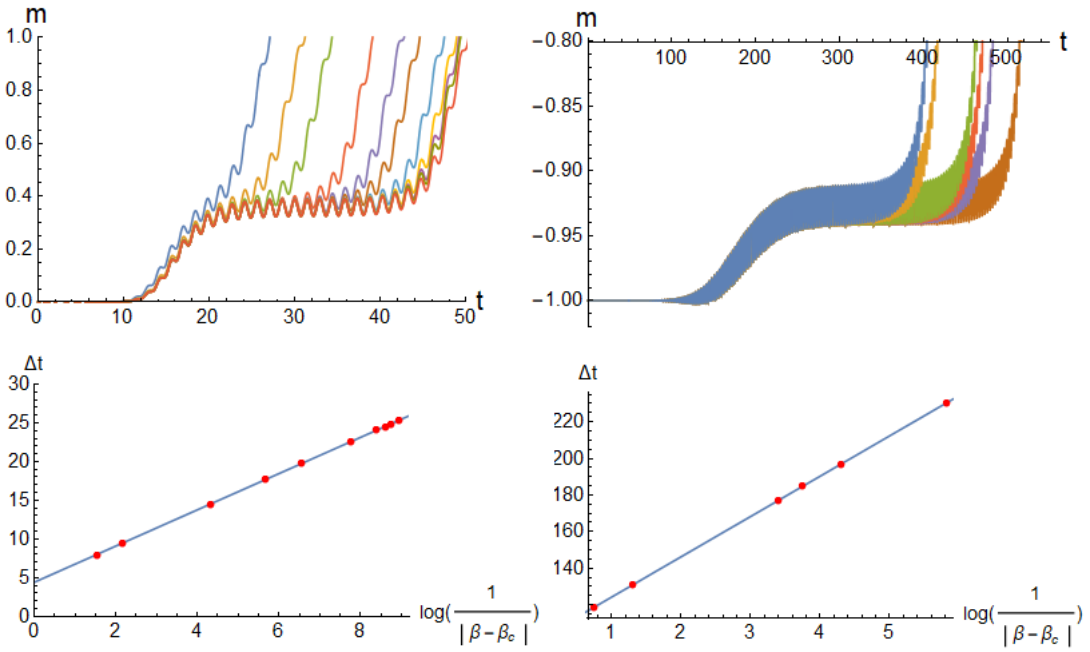

Figure A.5: Upper row: quenches in the amplitude ρ of duration $\beta < \beta_c$ from the static backgrounds, AdS_4 on the left and the AdS soliton on the right. Lower row: exponential deviation of the energy density from the plateau observed in the upper row ($20 < t < 40$ on the left and $200 < t < 400$ on the right). See Fig. 4.14, 4.15, 4.28 and 4.29 for further details.

USC
UNIVERSIDADE
DE SANTIAGO
DE COMPOSTELA

References

[1] S. Annenkov and V. Shrira, *Role of non-resonant interactions in evolution of nonlinear random water wave fields,* J. Fluid Mech. 561, 181?207 (2006).

[2] P. Janssen, *Ocean-Atmosphere Interaction*, Cambridge University Press, Cambridge (2004).

[3] S. Galtier, *Weak inertial-wave turbulence theory.* Phys. Rev. E 68, 015301 (2003).

[4] B. Bigot, S. Galtier and H. Politano, *An anisotropic turbulent model for solar coronal heating.* Astron. Astrophys. 490, 325?337 (2008).

[5] Y. Lvov, S. Nazarenko, and R. West, *Wave turbulence in Bose?Einstein condensates,* Physica D **184**, 333 (2003), arXiv:nlin/0507051v1.

[6] P. Bizoń and A. Rostworowski, *On weakly turbulent instability of anti-de Sitter space,* Phys. Rev. Lett. **107** (2011) 031102 arXiv:1104.3702 [gr-qc].

[7] S. Nazarenko, *Wave Turbulence*, Springer, (2011).

[8] D. Christodoulou, *The problem of a self-gravitating scalar field,* Commun. Math. Phys. **105** (1986) 337.

[9] D. Christodoulou, *Global Existence of Generalized Solutions of the Spherically Symmetric Einstein Scalar Equations in the Large,* Commun. Math. Phys. **106** (1986) 587.

[10] D. Christodoulou, *The Structure and Uniqueness of Generalized Solutions of the Spherically Symmetric Einstein Scalar Equations,* Commun. Math. Phys. **109** (1987) 591.

[11] D. Christodoulou, *A Mathematical Theory of Gravitational Collapse,* Commun. Math. Phys. **109** (1987) 613.

[12] D. Christodoulou, *The formation of black holes and singularities in spherically symmetric gravitational collapse,* Commun. Pure Appl. Math. **44** (1991) no.3, 339.

[13] M. W. Choptuik, *Universality and scaling in gravitational collapse of a massless scalar field,* Phys. Rev. Lett. **70** (1993) 9.

[14] D. Christodoulou and S. Klainerman, *The Global nonlinear stability of the Minkowski space,* Princeton University Press, Princeton, 1993.

[15] M. W. Choptuik, T. Chmaj and P. Bizon, *Critical behavior in gravitational collapse of a Yang-Mills field,* Phys. Rev. Lett. **77** (1996) 424.

[16] J. M. Maldacena, *The Large N limit of superconformal field theories and supergravity,* Int. J. Theor. Phys. **38** (1999) 1113, Adv. Theor. Math. Phys. **2** (1998) 231.

[17] F. Pretorius and M. W. Choptuik, *Gravitational collapse in (2+1)-dimensional AdS space-time,* Phys. Rev. D **62** (2000) 124012.

[18] D. Garfinkle, *An Exact solution for 2+1 dimensional critical collapse,* Phys. Rev. D **63** (2001) 044007.

[19] V. Husain and M. Olivier, *Scalar field collapse in three-dimensional AdS space-time,* Class. Quant. Grav. **18** (2001) L1.

[20] G. Clement and A. Fabbri, *Analytical treatment of critical collapse in (2+1)-dimensional AdS space-time,* Class. Quant. Grav. **18** (2001) 3665.

[21] D. Birmingham, *Choptuik scaling and quasinormal modes in the AdS / CFT correspondence,* Phys. Rev. D **64** (2001) 064024.

[22] C. Gundlach, *Critical phenomena in gravitational collapse,* Phys. Rept. **376** (2003) 339.

[23] J. Jalmuzna, A. Rostworowski and P. Bizon, *A Comment on AdS collapse of a scalar field in higher dimensions,* Phys. Rev. D **84** (2011) 085021

[24] P. Bizoń, *Is AdS stable?,* Gen. Rel. Grav. **46** (2014) no.5, 1724.

[25] M. T. Anderson, *On the uniqueness and global dynamics of AdS spacetimes,* Class. Quant. Grav. **23** (2006) 6935, arXiv:hep-th/0605293.

[26] O. J. C. Dias, G. T. Horowitz and J. E. Santos, *Gravitational Turbulent Instability of Anti-de Sitter Space,* Class. Quant. Grav. **29** (2012) 194002, arXiv:1109.1825 [hep-th].

[27] O. J. C. Dias, G. T. Horowitz, D. Marolf and J. E. Santos, *On the Nonlinear Stability of Asymptotically Anti-de Sitter Solutions,* Class. Quant. Grav. **29** (2012) 235019, arXiv:1208.5772 [gr-qc].

[28] M. Maliborski and A. Rostworowski, *Time-Periodic Solutions in an Einstein AdS-Massless-Scalar-Field System,* Phys. Rev. Lett. **111** (2013) 051102, arXiv:1303.3186 [gr-qc].

[29] A. Buchel, S. L. Liebling and L. Lehner, *Boson stars in AdS spacetime,* Phys. Rev. D **87** (2013) no.12, 123006, arXiv:1304.4166 [gr-qc].

[30] M. Maliborski and A. Rostworowski, *A comment on "Boson stars in AdS,"* arXiv:1307.2875 [gr-qc].

[31] F. V. Dimitrakopoulos, B. Freivogel, M. Lippert and I. S. Yang, *Position space analysis of the AdS (in)stability problem,* JHEP **1508** (2015) 077 arXiv:1410.1880 [hep-th].

[32] N. Kim, *Time-periodic solutions of massive scalar fields in dynamical AdS background: perturbative constructions,* Phys. Lett. B **742** (2015) 274 arXiv:1411.1633 [hep-th].

[33] N. Deppe and A. R. Frey, *Classes of stable initial data for massless and massive scalars in Anti-de Sitter spacetime,* JHEP **1512**, 004 (2015) arXiv:1508.02709 [hep-th].

[34] V. Balasubramanian, A. Buchel, S. R. Green, L. Lehner and S. L. Liebling, *Holographic thermalization, stability of anti-de Sitter space, and the Fermi-Pasta-Ulam paradox,* Phys. Rev. Lett. **113** (2014) 071601 arXiv:1403.6471 [hep-th].

[35] B. Craps, O. Evnin and J. Vanhoof, *Renormalization group, secular term resummation and AdS (in)stability,* JHEP **1410** (2014) 48 arXiv:1407.6273 [gr-qc].

[36] B. Craps, O. Evnin and J. Vanhoof, *Renormalization, averaging, conservation laws and AdS (in)stability,* JHEP **1501** (2015) 108 arXiv:1412.3249 [gr-qc].

[37] I-S. Yang, *Missing top of the AdS resonance structure,* Phys. Rev. D **91** (2015) 065011 arXiv:1501.00998 [hep-th].

[38] O. Evnin and R. Nivesvivat, *AdS perturbations, isometries, selection rules and the Higgs oscillator,* JHEP **1601** (2016) 151 arXiv:1512.00349 [hep-th].

[39] P. Basu, C. Krishnan and A. Saurabh, *A stochasticity threshold in holography and the instability of AdS,* Int. J. Mod. Phys. A **30** (2015) 1550128 arXiv:1408.0624 [hep-th].

[40] A. Buchel, S. R. Green, L. Lehner and S. L. Liebling, *Conserved quantities and dual turbulent cascades in anti-de Sitter spacetime,* Phys. Rev. D **91** (2015) 064026 arXiv:1412.4761 [gr-qc].

[41] P. Bizoń, M. Maliborski and A. Rostworowski, *Resonant Dynamics and the Instability of Anti-de Sitter Spacetime,* Phys. Rev. Lett. **115** (2015) no.8, 081103, arXiv:1506.03519 [gr-qc].

[42] B. Craps and O. Evnin, *AdS (in)stability: an analytic approach,* Fortsch. Phys. **64** (2016) 336, arXiv:1510.07836 [gr-qc].

[43] P. Bizoń and A. Rostworowski, *Gravitational Turbulent Instability of AdS_5,* Acta Phys. Polon. B **48** (2017) 1375, arXiv:1710.03438 [gr-qc].

[44] O. Dias and J. E. Santos, *AdS nonlinear instability: moving beyond spherical symmetry,* Class. Quant. Grav. **33** (2016) no.23, 23LT01, arXiv:1602.03890 [hep-th].

[45] H. Bantilan, P. Figueras, M. Kunesch and P. Romatschke, *Nonspherically Symmetric Collapse in Asymptotically AdS Spacetimes,* Phys. Rev. Lett. **119** (2017) no.19, 191103, arXiv:1706.04199 [hep-th].

[46] G. Moschidis, A proof of the instability of AdS for the Einstein–null dust system with an inner mirror, arXiv:1704.08681 [gr-qc].

[47] G. Moschidis, *The Einstein–null dust system in spherical symmetry with an inner mirror: structure of the maximal development and Cauchy stability,* arXiv:1704.08685 [gr-qc].

[48] D. Garfinkle, L. A. Pando Zayas and D. Reichmann, *On Field Theory Thermalization from Gravitational Collapse,* JHEP **1202** (2012) 119, arXiv:1110.5823 [hep-th].

[49] A. Buchel, L. Lehner and S. L. Liebling, *Scalar Collapse in AdS,* Phys. Rev. D **86** (2012) 123011, arXiv:1210.0890 [gr-qc].

[50] P. Bizoń and J. Jalmuzna, *Globally regular instability of AdS_3,* Phys. Rev. Lett. **111** (2013) no.4, 041102, arXiv:1306.0317 [gr-qc].

[51] J. Jalmuzna, *Three-dimensional Gravity and Instability of AdS_3,* Acta Phys. Polon. B **44** (2013) no.12, 2603 doi:10.5506/APhysPolB.44.2603 arXiv:1311.7409 [gr-qc].

[52] H. Friedrich, *On the AdS stability problem,* Class. Quant. Grav. **31** (2014) 105001, arXiv:1401.7172 [gr-qc].

[53] M. Maliborski and A. Rostworowski, *What drives AdS spacetime unstable?,* Phys. Rev. D **89** (2014) no.12, 124006, arXiv:1403.5434 [gr-qc].

[54] V. Balasubramanian, A. Buchel, S. R. Green, L. Lehner and S. L. Liebling, *Holographic Thermalization, Stability of Anti-de Sitter Space, and the Fermi-Pasta-Ulam Paradox,* Phys. Rev. Lett. **113** (2014) no.7, 071601, arXiv:1403.6471 [hep-th].

[55] J. Mas and A. Serantes, *Oscillating Shells in Anti-de Sitter Space,* Int. J. Mod. Phys. D **24** (2015) no.09, 1542003, arXiv:1507.01533 [gr-qc].

[56] S. R. Green, A. Maillard, L. Lehner and S. L. Liebling, *Islands of stability and recurrence times in AdS,* Phys. Rev. D **92** (2015) no.8, 084001, arXiv:1507.08261 [gr-qc].

[57] B. Craps, O. Evnin and J. Vanhoof, *Ultraviolet asymptotics and singular dynamics of AdS perturbations,* JHEP **1510** (2015) 079, arXiv:1508.04943 [gr-qc].

[58] B. Craps, O. Evnin, P. Jai-akson and J. Vanhoof, *Ultraviolet asymptotics for quasiperiodic AdS_4 perturbations,* JHEP **1510** (2015) 080, arXiv:1508.05474 [gr-qc].

[59] R. Arias, J. Mas and A. Serantes, *Stability of charged global AdS_4 spacetimes,* JHEP **1609** (2016) 024, arXiv:1606.00830 [hep-th].

[60] O. Evnin and C. Krishnan, *A Hidden Symmetry of AdS Resonances,* Phys. Rev. D **91** (2015) no.12, 126010, arXiv:1502.03749 [hep-th].

[61] E. Fermi, J. Pasta, and S. Ulam, *Studies of the nonlinear problems I,* Los Alamos Report LA-1940, (1955), reprinted in *Collected Papers of Enrico Fermi*, ed. E. Segre, Vol. II (University of Chicago Press, 1965).

[62] G. P. Berman and F. M. Izrailev, *The Fermi-Pasta-Ulam problem: 50 years of progress,* Chaos **15** (2005) 015104 arXiv:nlin/0411062.

[63] M. Maliborski, *Instability of Flat Space Enclosed in a Cavity,* Phys. Rev. Lett. **109** (2012) 221101, arXiv:1208.2934 [gr-qc].

[64] P. Gérard and S. Grellier, *The cubic Szegö equation,* Ann. Scient. Éc. Norm. Sup. **43** (2010) 761 arXiv:0906.4540 [math.CV].

[65] P. Gérard and S. Grellier, *Effective integrable dynamics for a certain nonlinear wave equation,* Anal. PDE **5** (2012) 1139 arXiv:1110.5719 [math.AP].

[66] P. Gérard and S. Grellier, *An explicit formula for the cubic Szegö equation,* Trans. Amer. Math. Soc. **367** (2015) 2979 arXiv:1304.2619 [math.AP].

[67] P. Gérard and S. Grellier, *The cubic Szegő equation and Hankel operators*, arXiv:1508.06814 [math.AP].

[68] P. Germain, Z. Hani and L. Thomann, *On the continuous resonant equation for NLS: I. Deterministic analysis,* J. Math. Pur. App. **105** (2016) 131 arXiv:1501.03760 [math.AP].

[69] P. Germain and L. Thomann, *On the high frequency limit of the LLL equation*, Quart. Appl. Math. **74** (2016) 633 arXiv:arXiv:1509.09080 [math.AP].

[70] P. Gérard, P. Germain and L. Thomann, *On the cubic lowest Landau level equation,* Arch. Rational Mech. Anal. **231** (2019) 1073 arXiv:1709.04276 [math.AP].

[71] A. F. Biasi, J. Mas and A. Paredes, *Delayed collapses of BECs in relation to AdS gravity,* Phys. Rev. E **95** (2017) 032216 arXiv:1610.04866 [nlin.PS].

[72] A. Biasi, P. Bizoń, B. Craps and O. Evnin, *Exact lowest-Landau-level solutions for vortex precession in Bose-Einstein condensates,* Phys. Rev. A **96** (2017) 053615 arXiv:1705.00867 [cond-mat.quant-gas].

[73] A. Biasi, P. Bizoń, B. Craps and O. Evnin, *Two infinite families of resonant solutions for the Gross-Pitaevskii equation,* Phys. Rev. E **98** (2018) 032222 arXiv:1805.01775 [cond-mat.quant-gas].

[74] B. Craps, M. De Clerck, O. Evnin and S. Khetrapal, *Energy level splitting for weakly interacting bosons in a harmonic trap,* arXiv:1903.04974 [cond-mat.quant-gas].

[75] P. Bizoń, B. Craps, O. Evnin, D. Hunik, V. Luyten and M. Maliborski, *Conformal flow on S^3 and weak field integrability in AdS_4,* Comm. Math. Phys. **353** (2017) 1179 arXiv:1608.07227 [math.AP].

[76] B. Craps, O. Evnin and V. Luyten, *Maximally rotating waves in AdS and on spheres,* JHEP **1709** (2017) 059 arXiv:1707.08501 [hep-th].

[77] A. Biasi, P. Bizon and O. Evnin, *Solvable cubic resonant systems,* Commun. Math. Phys. (2019), arXiv:1805.03634 [nlin.SI].

[78] P. Bizon, O. Evnin and F. Ficek, *A nonrelativistic limit for AdS perturbations,* JHEP **1812** (2018) 113 arXiv:1810.10574 [gr-qc].

[79] A. Biasi, P. Bizon and O. Evnin, *Complex plane representations and stationary states in cubic and quintic resonant systems,* arXiv:1904.09575 [math-ph].

[80] O. Evnin and W. Piensuk, *Quantum resonant systems, integrable and chaotic,* J. Phys. A **52** (2019) no.2, 025102, arXiv:1808.09173 [math-ph].

[81] A. Biasi, B. Craps and O. Evnin, *Energy returns in global AdS_4,* arXiv:1810.04753 [hep-th].

[82] P. Carracedo, J. Mas, D. Musso and A. Serantes, *Adiabatic pumping solutions in global AdS,* JHEP **1705** (2017) 141, arXiv:1612.07701 [hep-th].

[83] A. V. Ramallo, *Introduction to the AdS/CFT correspondence,* Springer Proc. Phys. **161** (2015) 411, arXiv:1310.4319 [hep-th].

[84] M. Ammon and J. Erdmenger, *Gauge/gravity duality : Foundations and applications,* Cambridge University Press, (2015).

[85] A. Eckardt, *Colloquium: Atomic quantum gases in periodically driven optical lattices,* Reviews of Modern Physics, vol. 89, no. 1, p. 011004, 2017.

[86] T. Oka and S. Kitamura, *Floquet Engineering of Quantum Materials,* Annual Review of Condensed Matter Physics, 2018.

[87] M. Bukov, L. D'Alessio, and A. Polkovnikov, *Universal high-frequency behavior of periodically driven systems: from dynamical stabilization to floquet engineering,* Advances in Physics, vol. 64, no. 2, pp. 139–226, 2015.

[88] P. Weinberg, M. Bukov, L. D′Alessio, A. Polkovnikov, S. Vajna, and M. Kolodrubetz, *Adiabatic perturbation theory and geometry of periodically-driven systems,* Physics Reports, vol. 688, pp. 1–35, 2017.

[89] L. D'Alessio and M. Rigol, *Long-time behavior of isolated periodically driven interacting lattice systems,* Physical Review X, vol. 4, no. 4, p. 041048, 2014.

[90] A. Lazarides, A. Das, and R. Moessner, *Equilibrium states of generic quantum systems subject to periodic driving,* Physical Review E, vol. 90, no. 1, p. 012110, 2014.

[91] P. Ponte, A. Chandran, Z. Papić, and D. A. Abanin, *Periodically driven ergodic and many-body localized quantum systems, Annals of Physics*, vol. 353, pp. 196–204, 2015.

[92] V. Novicenko, E. Anisimovas, G. Juzeliunas, *Floquet analysis of a quantum system with modulated periodic driving*, Phys. Rev. A 95, 023615 (2017).

[93] J. Cayssol, B. Dóra, F. Simon, R. Moessner, *Floquet topological insulators*, Phys. Status Solidi RRL, 7, 101-108 (2013).

[94] P. L. Kapitza. *Dynamic stability of a pendulum when its point of suspension vibrates.* Soviet Phys. JETP, 21:588?592, (1951).

[95] P. L. Kapitza. *Pendulum with a vibrating suspension*. Usp. Fiz. Nauk, 44:7?15, (1951).

[96] H. W. Broer, I. Hoveijn, M. van Noort, C. Sim, G. Vegter, *Journal of Dynamics and Differential Equations*, 16, 897 (2004).

[97] F. Wilczek, *Quantum Time Crystals,* Phys. Rev. Lett. **109** (2012). arXiv:1202.2539 [quant-ph].

[98] N. Y. Yao, C. Nayak, *Time crystals in periodically driven systems*, Physics Today **71**, 9, 40 (2018).

[99] A. Chandran and S. L. Sondhi, *Interaction-stabilized steady states in the driven $o(n)$ model,* Phys. Rev. B, vol. 93, p. 174305, May 2016.

[100] S. A. Weidinger and M. Knap, *Floquet prethermalization and regimes of heating in a periodically driven, interacting quantum system,* Scientific reports, vol. 7, p. 45382, 2017.

[101] N. Bao, X. Dong, E. Silverstein and G. Torroba, *Stimulated superconductivity at strong coupling,* JHEP **1110** (2011) 123, arXiv:1104.4098 [hep-th].

[102] W. J. Li, Y. Tian and H. b. Zhang, *Periodically Driven Holographic Superconductor,* JHEP **1307** (2013) 030, arXiv:1305.1600 [hep-th].

[103] T. Ishii and K. Murata, *Floquet superconductor in holography*, *Phys. Rev.*, vol. D98, no. 12, p. 126005, 2018.

[104] K. Hashimoto, S. Kinoshita, K. Murata, and T. Oka, *Holographic Floquet states I: a strongly coupled Weyl semimetal, JHEP*, vol. 05, p. 127, 2017.

[105] R. Auzzi, S. Elitzur, S. B. Gudnason, and E. Rabinovici, *On periodically driven ads/cft, Journal of High Energy Physics*, vol. 2013, no. 11, p. 16, 2013.

[106] S. Kinoshita, K. Murata, and T. Oka, *Holographic Floquet states II: Floquet condensation of vector mesons in nonequilibrium phase diagram*, *JHEP*, vol. 06, p. 096, 2018.

[107] M. Rangamani, M. Rozali, and A. Wong, *Driven holographic CFTs, Journal of High Energy Physics*, vol. 2015, no. 4, p. 93, 2015.

[108] M. Haack, D. Sarkar, and A. Yarom, *Probing anomalous driving, arXiv preprint arXiv:1812.08210*, 2018.

[109] C. Chin, R. Grimm, P. Julienne and E. Tiesinga, *Feshbach resonances in ultracold gases*, Rev. Mod. Phys. **82** (2010) 1225 arXiv:arXiv:0812.1496 [cond-mat.other].

[110] J. A. Murdock, *Perturbations: Theory and Methods*, SIAM (1987).

[111] J. Kevorkian and J. D. Cole. *Multiple Scale and Singular Perturbation*, Methods. Springer, 1996.

[112] M. Maliborski, *Dynamics of Nonlinear Waves on Bounded Domains,* arXiv:1603.00935 [gr-qc].

[113] A. Biasi, P. Carracedo, J. Mas, D. Musso and A. Serantes, *Floquet Scalar Dynamics in Global AdS,* JHEP **1804** (2018) 137, arXiv:1712.07637 [hep-th].

[114] A. Biasi, J. Mas and A. Serantes, *Gravitational wave driving of a gapped holographic system,* arXiv:1903.05618 [hep-th].

[115] J. P. Boyd, *Chebyshev and Fourier Spectral Methods*, Second Revised Edition (Dover Publications, 2001).

[116] G. Floquet, *Sur les équations différentielles linéaries á coefficients périodique*, Ann. École Norm. Sup., 12 (1883), pp. 47-88.

[117] F. Bloch, *Über die Quantenmechanik der Electronen in Kristallgittern*, Z. Phys., 52 (1928), pp. 555-600.

[118] F. M. Arscott, *Periodic Differential Equations*, Macmillan, NY (1964).

[119] M. S. P. Eastham, *The spectral theory of periodic differential equations*, Scottish Acad. Press, Edinburgh-London (1973).

[120] P. A. Kuchment, *Floquet Theory for Partial Differential Equations*, RUSS MATH SURV, (1982), 37 (4), 1-60.

[121] V. I. Yudovich, *The linearization method in hydrodynamical stability theory*, American Mathematical Society, (1989).

[122] C. Godreche, P. Manneville. *Hydrodynamics and Nonlinear Instabilities*, Cambridge University Press, (1998).

[123] N. Turbe, *Applications of Bloch expansions to periodic elastic and viscoelastic media*, Math. Meth. in Appl. Sci. 4(1982), 433-449.

[124] R. M. Christensen, *Theory of viscoelasticity*, Academic Press, New York and London, (1971).

[125] J. B. Griffiths and J. Podolsky, *Exact Space-Times in Einstein's general Relativity*, Cambridge University Press, Cambridge (2009).

[126] G. 't Hooft, *Dimensional reduction in quantum gravity,* Conf. Proc. C **930308** (1993) 284, arXiv:9310026 [gr-qc].

[127] L. Susskind, *The World as a hologram,* J. Math. Phys. **36** (1995) 6377, arXiv:9409089 [hep-th].

[128] M. Van Raamsdonk, *Lectures on Gravity and Entanglement,* arXiv:1609.00026 [hep-th].

[129] H. Nastase, *Introduction to AdS-CFT,* arXiv:0712.0689 [hep-th].

[130] M. Natsuume, *AdS/CFT Duality User Guide,* Vol. 903. Lecture Notes in Physics. Berlin; Tokyo: Springer Verlag (2015).

[131] C. Fefferman and C. R. Graham, *Conformal invariants*, in Elie Cartan et les Mathématiques d'aujourd'hui (Astérisque, 1985) **95**.

[132] C. Fefferman and C. R. Graham, *The ambient metric,* Ann. Math. Stud. **178** (2011) 1 arXiv:0710.0919 [math.DG].

[133] K. Skenderis, *Lecture notes on holographic renormalization,* Class. Quant. Grav. **19** (2002) 5849, arXiv:hep-th/0209067.

[134] S. S. Gubser, I. R. Klebanov and A. M. Polyakov, *Gauge theory correlators from noncritical string theory,* Phys. Lett. B **428** (1998) 105, arXiv:hep-th/9802109.

[135] E. Witten, *Anti-de Sitter space and holography,* Adv. Theor. Math. Phys. **2** (1998) 253, arXiv:hep-th/9802150.

[136] S. de Haro, S. N. Solodukhin and K. Skenderis, *Holographic reconstruction of space-time and renormalization in the AdS/CFT correspondence,* Commun. Math. Phys. **217** (2001) 595, arXiv:hep-th/0002230.

[137] G. W. Gibbons and S. W. Hawking, *Action integrals and partition functions in quantum gravity.* Phys. Rev., **D15**, 2752-2756, (1977).

[138] P. Breitenlohner and D. Z. Freedman, *Positive Energy in anti-De Sitter Backgrounds and Gauged Extended Supergravity,* Phys. Lett., vol. B115, pp. 197-201, 1982.

[139] P. Breitenlohner and D. Z. Freedman, *Stability in Gauged Extended Supergravity,* Annals Phys., vol. 144, p. 249, 1982.

[140] O. Fierro, D. Narbona, J. Oliva, C. Quijada and G. Rubilar, *Scalars on asymptotically locally AdS wormholes with $\mathcal{R}^2$ terms,* arXiv:1812.02089 [hep-th].

[141] A. Anabalon, J. Oliva and C. Quijada, *Fully resonant scalars on asymptotically AdS wormholes,* arXiv:1903.08239 [hep-th].

[142] P. Bizoń, D. Hunik-Kostyra and D. Pelinovsky, *Ground state of the conformal flow on S^3*, Comm. Pure Appl. Math. **72** (2019) 1123 arXiv:1706.07726 [math.AP];

[143] S. A. Fulling, *Aspects of Quantum Field Theory in Curved Space-time,* London Math. Soc. Student Texts **17** (1989).

[144] G. P. Agrawal, *Nonlinear fiber optics.* Academic press (2007).

[145] B. A. Malomed, D. Mihalache, F. Wise, and L. Torner, *Spatiotemporal optical solitons,* J. Opt. B: Quantum Semiclass. Opt. bf 7, R53, (2005).

[146] V. E. Zakharov, V. S. L'vov, and G. Falkovich, *Kolmogorov spectra of turbulence I: Wave turbulence*. Springer Science & Business Media (2012).

[147] H.-Y. Schive, T. Chiueh, and T. Broadhurst, *Cosmic structure as the quantum interference of a coherent dark wave,* Nat. Phys. **10**, 496 (2014).

[148] A. Paredes and H. Michinel, *Interference of dark matter solitons and galactic offsets,* Phys. Dark Univ. **12**, 50 (2016).

[149] F. Dalfovo, S. Giorgini, L. P. Pitaevskii, and S. Stringari, *Theory of Bose-Einstein condensation in trapped gases,* Rev. Mod. Phys. **71**, 463 (1999).

[150] R. Carretero-González, D. Frantzeskakis, and P. Kevrekidis, *Nonlinear waves in Bose–Einstein condensates: physical relevance and mathematical techniques,* Nonlinearity **21**, R139 (2008).

[151] I. Bloch, J. Dalibard and W. Zwerger, *Many-body physics with ultracold gases*, Rev. Mod. Phys. **80** (2008) 885 arXiv:arXiv:0704.3011 [cond-mat.other].

[152] N. R. Cooper, *Rapidly rotating atomic gases*, Adv. Phys. 57 (2008) 539 arXiv:arXiv:0810.4398 [cond-mat.mes-hall].

[153] A. L. Fetter, *Rotating trapped Bose-Einstein condensates*, Rev. Mod. Phys. **81** (2009) 647 arXiv:arXiv:0801.2952 [cond-mat.stat-mech].

[154] C. Sulem and P.-L. Sulem, *The nonlinear Schrödinger equation: self-focusing and wave collapse*, vol. 139. Springer Science & Business Media (2007).

[155] Y. Kagan, E. L. Surkov, and G. V. Shlyapnikov, *Evolution and global collapse of trapped Bose condensates under variations of the scattering length,* Phys. Rev. Lett. **79**, 2604 (1997).

[156] Y. Kagan, A. E. Muryshev, and G. V. Shlyapnikov, *Collapse and Bose-Einstein condensation in a trapped Bose gas with negative scattering length,* Phys. Rev. Lett. **81**, 933 (1998).

[157] L. Santos and G.V. Shlyapnikov, *Collapse dynamics of trapped Bose-Einstein condensates,* Phys. Rev. A **66**, 011602 (2002).

[158] J. M. Gerton, D. Strekalov, I. Prodan, and R. G. Hulet, *Direct observation of growth and collapse of a Bose–Einstein condensate with attractive interactions,* Nature, **408**, 692 (2000).

[159] J. L. Roberts, N. R. Claussen, S. L. Cornish, E. A. Donley, E. A. Cornell, and C. E. Wieman, *Controlled collapse of a Bose-Einstein condensate,* Phys. Rev. Lett. **86**, 4211 (2001).

[160] E. A. Donley, N. R. Claussen, S. L. Cornish, J. L. Roberts, E. A. Cornell, and C. E. Wieman, *Dynamics of collapsing and exploding Bose–Einstein condensates,* Nature **412**, 295 (2001).

[161] C. Eigen, A. L. Gaunt, A. Suleymanzade, N. Navon, Z. Hadzibabic, and R. P. Smith, *Observation of weak collapse in a Bose-Einstein condensate,* arXiv:1609.00352 (2016).

[162] H. Saito and M. Ueda, *Intermittent implosion and pattern formation of trapped Bose-Einstein condensates with an attractive interaction,* Phys. Rev. Lett. **86**, 1406 (2001).

[163] H. Saito and M. Ueda, *Power laws and collapsing dynamics of a trapped Bose-Einstein condensate with attractive interactions,* Phys. Rev. A **63**, 043601 (2001).

[164] S. K. Adhikari, *Mean-field description of collapsing and exploding Bose-Einstein condensates,* Phys. Rev. A **66**, 013611 (2002).

[165] C.M. Savage, N.P. Robins, and J.J. Hope, *Bose-Einstein condensate collapse: A comparison between theory and experiment,* Phys. Rev. A **67**, 014304 (2003).

[166] M. Ueda and H. Saito, *A consistent picture of a collapsing Bose-Einstein condensate,* J. Phys. Soc. Jpn. **72**, 127 (2003).

[167] L. M. Pismen and J. Rubinstein, *Motion of vortex lines in the Ginzburg-Landau model*, Physica D **47** (1991) 353.

[168] B. Jackson, J. F. McCann and C. S. Adams, *Vortex line and ring dynamics in trapped Bose-Einstein condensates*, Phys. Rev. A **61** (1999) 013604 arXiv:cond-mat/9907325 [cond-mat.stat-mech].

[169] J. Tempere and J. T. Devreese, *Vortex dynamics in a parabolically confined Bose-Einstein condensate*, Solid State Comm. **113** (2000) 471.

[170] A. L. Fetter and A. A. Svidzinsky, *Vortices in a trapped dilute Bose-Einstein condensate*, J. Phys. Cond. Matt. **13** (2001) R135 arXiv:cond-mat/0102003 [cond-mat.stat-mech].

[171] N. Parker, *Numerical studies of vortices and dark solitons in atomic Bose-Einstein condensates*, chapter 7, University of Durham Ph.D. thesis (2004), online at massey.dur.ac.uk.

[172] L. Bergé, *Wave collapse in physics: principles and applications to light and plasma waves,* Phys. Rep. **303**, 259 (1998).

[173] G. Fibich, *The nonlinear Schrödinger equation.* Springer (2015).

[174] L. O. Baksmaty, S. J. Woo, S. Choi, N. P. Bigelow, *Tkachenko Waves in Rapidly Rotating Bose-Einstein Condensates*, Phys. Rev. Lett., **92**, 160405, (2004), arXiv:0307368 [cond-mat.soft].

[175] J. P. Dahl and W. P. Schleich, *State operator, constants of the motion, and Wigner functions: The two-dimensional isotropic harmonic oscillator*, Phys. Rev. A **79** (2009) 024101.

[176] S. Kuksin and A. Maiocchi, *The effective equation method*, in *New Approaches to Nonlinear Waves*, Springer (2016) arXiv:1501.04175 [math-ph].

[177] P. G. Kevrekidis, D. J. Frantzeskakis and R. Carretero-González (eds), *Emergent nonlinear phenomena in Bose-Einstein condensates*, Springer (2008).

[178] D. E. Pelinovsky and P. G. Kevrekidis, *Periodic oscillations of dark solitons in parabolic potentials,* AMS Cont. Math. **473** (2008) 159 arXiv:0705.1016 [cond-mat.other].

[179] W. Wang, P. G. Kevrekidis, R. Carretero-González and D. J. Frantzeskakis, *Dark spherical shell solitons in three-dimensional Bose-Einstein condensates: Existence, stability and dynamics*, Phys. Rev. A **93** (2016) 023630 arXiv:1601.02176 [cond-mat.quant-gas].

[180] D. J. Frantzeskakis, *Dark solitons in atomic Bose-Einstein condensates: from theory to experiments,* J. Phys. A **43** (2010) 213001 arXiv:1004.4071 [quant-ph].

[181] T. Kapitula, P. G. Kevrekidis and R. Carretero-González, *Rotating matter waves in Bose-Einstein condensates,* Physica D **233** (2007) 112.

[182] E. G. Charalampidis, P. G. Kevrekidis and P. E. Farrell, *Computing stationary solutions of the two-dimensional Gross-Pitaevskii equation with deflated continuation,* Comm. Nonlin. Sci. Num. Sim. 54 (2018) 482 arXiv:1612.08145 [nlin.PS].

[183] A. Klein, D. Jaksch, Y. Zhang and W. Bao, *Dynamics of vortices in weakly interacting Bose-Einstein condensates,* Phys. Rev. A **76** (2007) 043602 arXiv:0709.2132 [quant-ph].

[184] W. Li, M. Haque and S. Komineas, *A vortex dipole in a trapped two-dimensional Bose-Einstein condensate,* Phys. Rev. A **77** (2008) 053610 arXiv:0712.4217 [cond-mat.other].

[185] P. J. Torres, R. Carretero-González, S. Middelkamp, P. Schmelcher, D. J. Frantzeskakis and P. G. Kevrekidis, *Vortex interaction dynamics in trapped Bose-Einstein condensates,* Comm. Pur. App. Analysis **10** (2011) 1589.

[186] J. A. Seman, E. A. L. Henn, M. Haque, R. F. Shiozaki, E. R. F. Ramos, M. Caracanhas, C. Castelo Branco, P. E. S. Tavares, F. J. Poveda-Cuevas, G. Roati, K. M. F. Magalhães and V. S. Bagnato, *Three-vortex configurations in trapped Bose-Einstein condensates,* Phys. Rev. A **82** (2010) 033616 arXiv:0907.1584 [cond-mat.quant-gas].

[187] C. Sulem, P.-L. Sulem and H. Frisch, *Tracing complex singularities with spectral methods,* J. Comput. Phys. **50** (1983) 138.

[188] D. Pelinovsky, D. Hunik-Kostyra and P. Bizoń, *Stationary states of the cubic conformal flow on S^3*, arXiv:1807.00426 [math-ph].

[189] J. Eisert, M. Friesdorf and C. Gogolin, *Quantum many-body systems out of equilibrium*, Nature Physics. 11. 10.1038/nphys3215, (2014).

[190] L. F. Cugliandolo, *Out-of-equilibrium dynamics of classical and quantum complex systems,* Comptes Rendus Phys., 14, 685?699, (2013).

[191] G. Franzese, I. Latella and J. Rubi, . *Nonequilibrium Phenomena in Confined Systems*, Entropy. 19. 507. 10.3390/e19090507, (2017).

[192] W. Kohn, *Periodic thermodynamics,* Journal of Statistical Physics, vol. 103, no. 3, pp. 417–423, 2001.

[193] A. Lazarides, A. Das, and R. Moessner, *Periodic thermodynamics of isolated quantum systems,* Physical review letters, vol. 112, no. 15, p. 150401, 2014.

[194] P. Calabrese, J. Cardy, *Time dependence of correlation functions following a quantum quench*, Phys. Rev. Lett. 96, 136801 (2006).

[195] C. Kollath, A. Lauchli, E. Altman, *Quench dynamics and non equilibrium phase diagram of the Bose-Hubbard model*, Phys. Rev. Lett. 98, 180601, (2007).

[196] M. Rigol, V. Dunjko, V. Yurovsky, M. Olshanii, *Relaxation in a completely integrable many-body quantum system: An ab initio study of the dynamics of the highly excited states of 1D lattice hard-core bosons*, Phys. Rev. Lett. 98, 050405 (2007).

[197] W. Berdanier, M. Kolodrubetz, R. Vasseur and J. E. Moore, *Floquet Dynamics of Boundary-Driven Systems at Criticality,* Phys. Rev. Lett. **118** (2017) no.26, 260602, arXiv:1701.05899 [cond-mat.str-el].

[198] V. Khemani, A. Lazarides, R. Moessner, and S. L. Sondhi, *Phase structure of driven quantum systems,* Physical review letters, vol. 116, no. 25, p. 250401, 2016.

[199] R. Citro, E. G. Dalla Torre, L. D'Alessio, A. Polkovnikov, M. Babadi, T. Oka, and E. Demler, *Dynamical stability of a many-body Kapitza pendulum*, Annals of Physics, 360, pp.694-710, (2015).

[200] P. Bizon and T. Chmaj, *First order phase transitions in gravitational collapse*, *Acta Phys. Polon.*, vol. B29, p. 1071, 1998.

[201] R. C. Myers, *Stress tensors and Casimir energies in the AdS / CFT correspondence*, Phys. Rev., vol. D60, p. 046002, 1999.

[202] D. N. Page, *Phase transitions for gauge theories on tori from the AdS / CFT correspondence*, JHEP, vol. 09, p. 037, 2008.

[203] A. Belin, J. de Boer, J. Kruthoff, B. Michel, E. Shaghoulian, and M. Shyani, *Universality of sparse $d > 2$ conformal field theory at large N*, JHEP, vol. 03, p. 067, 2017.

[204] P. Bueno and W. Witczak-Krempa, *Holographic torus entanglement and its renormalization group flow*, Phys. Rev., vol. D95, no. 6, p. 066007, 2017.

[205] B. Craps, E. J. Lindgren and A. Taliotis, *Holographic thermalization in a top-down confining model,* JHEP **1512**, 116 (2015), arXiv:1511.00859 [hep-th].

[206] M. Choptuik, J. E. Santos and B. Way, *Charting Islands of Stability with Multioscillators in anti?de Sitter space,* Phys. Rev. Lett. **121** (2018) no.2, 021103, arXiv:1803.02830 [hep-th].

[207] J. Cardy, *Quantum Revivals in Conformal Field Theories in Higher Dimensions,* J. Phys. A **49** (2016) no.41, 415401, arXiv:1603.08267 [cond-mat.stat-mech].

[208] B. Freivogel, J. McGreevy and S. J. Suh, *Exactly Stable Collective Oscillations in Conformal Field Theory,* Phys. Rev. D **85** (2012) 105002, arXiv:1109.6013 [hep-th].

[209] C. Ecker, A. Mukhopadhyay, F. Preis, A. Rebhan and A. Soloviev, *Time evolution of a toy semiholographic glasma,* JHEP **1808** (2018) 074, arXiv:1806.01850 [hep-th].

[210] L. N. Trefethen, *Approximation Theory and Approximation Practice*, SIAM, 2013.

[211] J. Berrut and L. N. Trefethen, *Barycentric Lagrange Interpolation*, SIAM Rev. **46**, 501?517 (2004).

[212] S. G. Samko, A. A. Kilbas and O. I. Marichev, *Fractional integrals and derivatives* (Gordon and Breach, 1993).

[213] S. Das, *Functional fractional calculus for system identification and controls* (Springer, 2008).

[214] P. H. Ginsparg, *Applied conformal field theory,* lectures at Les Houches Summer School 1988: *Fields, strings, critical phenomena*, arXiv:hep-th/9108028.

[215] I. S. Gradshteyn and I. M. Ryzhik. *Table of Integrals, Series, and Products*. Academic Press, New York, 6th edition, 2000.

[216] M. Maliborski and A. Rostworowski, *Lecture Notes on Turbulent Instability of Anti-de Sitter Spacetime,* Int. J. Mod. Phys. A **28** (2013) 1340020, arXiv:1308.1235 [gr-qc].

[217] W. H. Press, S. A. Teukolsky, W. T. Vetterling and B. P. Flannery, *Numerical Recipes. The Art of Scientific Computing*, 3rd Edition, 2007.